NUMERICAL SOLUTION FOR TURBULENT FILM CONDENSATION FROM VAPOR-GAS MIXTURES IN VERTICAL TUBES

BY

MEGHAN K. GROFF

A Thesis
Presented to the Faculty of Graduate Studies
In Partial Fulfillment of the Requirements for the Degree of

MASTER OF SCIENCE

Department of Mechanical and Manufacturing Engineering
University of Manitoba
Winnipeg, Manitoba

THE UNIVERSITY OF MANITOBA

FACULTY OF GRADUATE STUDIES

*****

COPYRIGHT PERMISSION PAGE

Numerical Solution for Turbulent Film Condensation from

Vapor-Gas Mixtures in Vertical Tubes

BY

Meghan K. Groff

A Thesis/Practicum submitted to the Faculty of Graduate Studies of The University

of Manitoba in partial fulfillment of the requirements of the degree

of

MASTER OF SCIENCE

ABSTRACT

The numerical model presented in this thesis deals with condensation in a vertical tube in the presence of a non-condensable gas. A vapor-gas mixture enters a tube of radius r_o with a specified velocity u_{in}, pressure P_{in}, gas mass fraction W_{in}, and temperature difference ΔT_{in} between the inlet and the wall. The temperature of the tube wall is maintained lower than the inlet temperature resulting in steam condensation and a liquid film of thickness δ forming along the wall. The model is capable of handling both turbulent and laminar flow conditions.

The model was derived from the full set of Navier-Stokes equations and the energy equation applied to both the core and the liquid film. The *r-z* coordinate system defining the problem was transformed into an η–χ coordinate system such that $\eta = 0$ at the centerline of the tube, $\eta = 1$ at the mixture-liquid interface, and $\eta = 2$ at the tube wall. The transformed governing equations were discretized using a finite volume method and solved in a fully-coupled manner using a block tri-diagonal matrix algorithm. In order to predict turbulence across both the core and the film, three different turbulence models were used and were tested and compared with one another. Model 1 used a mixing length model in both the core and the film, model 2 used a low Reynolds number k-ε model in both the core and the film, and model 3 used the k-ε model in the core and the mixing length model in the film.

Laminar results for steam-air mixtures were presented through velocity, temperature, and gas mass fraction cross-sectional profiles, as well as film thickness and Nusselt number axial distributions. A parametric study was done to determine the effects of inlet pressure P_{in}, inlet Reynolds number Re_{in}, inlet gas mass fraction W_{in}, and temperature difference ΔT_{in} on both the film thickness, and the local Nusselt number. From this study it was found that the film thickness increased when either ΔT_{in} or Re_{in} increased or when W_{in} or P_{in} decreased and the Nusselt number increased with increasing Re_{in} or decreasing ΔT_{in} or W_{in}.

For the case of turbulent flow, the local heat transfer coefficients resulting from the three turbulence models were compared with the experimental results of Goodykoontz and Dorsch (1966), Siddique (1992), and Kuhn (1995). Both models 2 and 3 compared well with all three experiments but the best agreement was found when comparing model 2 with Kuhn's data. In this case, 98% of the numerical results were within ± 30% of Kuhn's experimental results.

Turbulent results were obtained for a variety of inlet conditions and a parametric study was completed to determine the effects of the inlet parameters on both the film thickness and the local Nusselt number. Results showed similar trends as those found for laminar flow with the exception of the effect of inlet Reynolds number on the dimensionless film thickness.

ACKNOWLEDGEMENTS

I would like to thank my advisors, Dr. H.M. Soliman and Dr. S.J. Ormiston, for giving me the opportunity to work on this research project, and also for their valuable guidance. Also deserving recognition and thanks are NSERC, the Faculty of Graduate Studies and the Department of Mechanical and Manufacturing Engineering for their financial support. I would also like to gratefully thank my family and my fiancé Brendan, for their endless patience, love, support, and encouragement.

TABLE OF CONTENTS

LIST OF FIGURES

LIST OF TABLES

NOMENCLATURE

a, b	coefficients of discretized equations
A, B, E, F, X	block matrices
C_p	specific heat [J kg^{-1} K^{-1}]
D	diffusion coefficient [m^2 s^{-1}]
D^*	damping function
D^t	turbulent diffusion coefficient [m^2 s^{-1}]
Fr	Froude number ($u_{in}^2/(2\,g\,r_o)$)
g	gravitational acceleration [m s^{-2}]
h_{fg}	latent heat of vaporization [J kg^{-1}]
h_z	local heat transfer coefficient [W m^{-2} K^{-1}]
i, j_L, j_M	nodal index
J	mass flow rate at control volume faces in the η direction [kg s^{-1}]
J''	mass flux at control volume faces in the η direction [kg m^{-2} s^{-1}]
Ja	Jakob number ($C_p\Delta T / h_{fg}$)
k	turbulent kinetic energy [m^2 s^{-2}]
L	length [m]
ℓ	mixing length [m]
$\dot{m}$	total mass flow rate [kg s^{-1}]
NL	number of grid subdivisions in the η-direction in the liquid
NM	number of grid subdivisions in the η-direction in mixture
Nu_z	local Nusselt number ($h_z\,2r_o/\lambda_L$)

$\overline{Nu_z}$	average Nusselt number
NZ	number of grid subdivisions in the χ-direction
P	pressure [N m^{-2}]
P'	pressure gradient (dP/dz) [Pa m^{-1}]
P^*	dimensionless pressure $(P-P_{in})/(1/2\rho_{in}u_{in}^2)$
Pe	Peclet number (Re Pr)
Pr	Prandtl number $(\mu C_P/\lambda)$
Pr^t	turbulent Prandtl number $(\mu^t C_P/\lambda^t)$
r	radial coordinate [m]
r^*	dimensionless radial coordinate normal to tube walls (r/r_o)
r_o	radius of tube [m]
Δr	grid spacing in the r direction
Re_{in}	inlet Reynolds number $(\rho_{in}\, u_{in}\, 2r_o/\mu_{in})$
Sc	Schmidt number $(\rho D/\mu)$
Sc^t	turbulent Schmidt number $(\rho D^t/\mu^t)$
T	temperature [K]
ΔT	inlet-to-wall temperature difference [K] (T_{in}-T_{wall})
T^*	dimensionless temperature $(T-T_{wall})/(T_{in}-T_{wall})$
u	velocity in the z-direction [m s^{-1}]
u^*	dimensionless velocity in the z-direction (u/u_{in})
u_τ	friction velocity [m s^{-1}] ($\sqrt{\tau/\rho}$)
v	velocity in the r-direction [m s^{-1}]

v^*	dimensionless velocity in the r-direction (v/u_{in})
W	gas mass fraction ($\dot{m}_g / \dot{m}$)
z	axial coordinate [m]
z^*	dimensionless axial coordinate ($z/2r_o$)
Δz	grid spacing in the z direction

Subscripts

c	centerline
cw	cooling water
e	east face of control volume
ec	end of condensation path
eff	effective
E	neighboring control volume at the east side
g	gas
i	interface
in	tube inlet
L	liquid
M	vapor-gas mixture
n	north face of control volume
N	neighboring control volume at the north side
P	control volume center
s	south face of control volume
sb	bulk saturation

S	neighboring control volume at the south side
sat	saturated condition
sb	bulk saturation
v	vapor
w	west face of a control volume
W	neighboring control volume at the west side
wall	tube wall

Superscripts

"	flux, per unit area
l	laminar
n	current iteration
o	previous iteration
t	turbulent

Greek Symbols

α	convection weighting factor
β	diffusion weighting factor
χ	transformed coordinate along the tube
$\Delta\chi$	grid spacing in the χ direction
δ	thickness of condensate layer [m]

δ^*	dimensionless film thickness (δ/r_o)
δ_{BL}	boundary layer thickness [m]
ε	dissipation rate [$m^2\ s^{-3}$]
γ	relative error
η	transformed coordinate in the r direction
$\Delta\eta$	grid spacing in the η direction
φ	general variable used to represent dependent variables
λ	thermal conductivity [$W\ m^{-1}\ K^{-1}$]
λ^t	turbulent thermal conductivity [$W\ m^{-1}\ K^{-1}$]
μ	dynamic viscosity [$N\ s\ m^{-2}$]
ν	kinematic viscosity [$m^2\ s^{-1}$]
ρ	density [$kg\ m^{-3}$]
τ	shear stress [$N\ m^{-2}$]
ψ	relaxation factor

CHAPTER 1

INTRODUCTION

Condensation is defined as the process of changing from a vapor to a liquid phase and this process occurs when the temperature of the vapor is reduced below its saturation temperature. This process often occurs when a vapor is brought into contact with a cool surface resulting in either dropwise or filmwise condensation. The more common of the two and the most relevant to this thesis is filmwise condensation. This occurs when a condensed liquid film covers the entire surface and flows along the surface due to the forces of gravity and vapor shear. The condensate film provides a resistance to heat transfer between the vapor and the wall and therefore, a thinner film is more desirable to promote heat transfer.

The study of film condensation is important due to its relevance in many industries including refrigeration, chemical processing, and thermal power generation. The process of condensation has been studied since 1916 when Nusselt developed an analytical solution for vapor condensation along a vertical surface. Since then there have been numerous studies done on both internal and external condensation for various geometries. These studies range from simple correlations to advanced numerical and experimental models. More recently, for the case of internal film condensation, research has been done to study the effects of a non-condensable gas on vapor condensation. It has been found that the condensation rate drops substantially even when a small concentration of gas is present.

The topic of steam condensation in the presence of gas is important to the nuclear industry in the application of Passive Containment Cooling Systems (PCCS). In a PCCS, steam is discharged into a containment building filled with gases during a loss of coolant accident in a nuclear reactor. In order to condense this steam and reduce the pressure in the containment building, it is important to be able to predict how the gases will affect the condensation rate. The majority of theoretical studies on internal flow vapor condensation with the effect of a non-condensing gas have been made with simplified models while only a few were made with a detailed model based on the governing differential equations.

The purpose of the present study was to develop a numerical model from the full set of governing equations for vapor condensation in a vertical tube in the presence of a gas. In order to produce results for turbulent flow conditions, three different turbulence models were employed and compared with each other. This thesis is an extension of the work done by Siow (2001) who developed a numerical model for laminar film condensation inside a two-dimensional, parallel plate channel in the presence of a gas. Siow's model was adapted such that a cylindrical coordinate system was used instead of a Cartesian coordinate system. In addition to adjusting the geometry in the model, turbulence models were added to both the core and the film.

CHAPTER 2

LITERATURE REVIEW

2.1 Overview

The topic of film condensation has been studied since the beginning of the 19th century. Nusselt (1916) analyzed film condensation of a pure vapor on a vertical surface and developed solutions for the local and average Nusselt numbers. This was done by neglecting the shear stress at the liquid-vapor interface, neglecting the advection terms in both the momentum and energy equations, and assuming no pressure variation in the y direction (perpendicular to the plate). The resulting equation for the average Nusselt number on a plate of length L was:

$$\overline{\mathrm{Nu}}_{\mathrm{L}} = 0.943\left[\frac{\rho_{\mathrm{L}} g(\rho_{\mathrm{L}} - \rho_{\mathrm{v}}) h_{\mathrm{fg}} L^3}{\mu_{\mathrm{L}} \lambda_{\mathrm{L}} (T_{\mathrm{sat}} - T_{\mathrm{wall}})}\right]^{1/4} \tag{2.1}$$

Following his work, both external and internal flows with condensation have been studied extensively for various geometries and vapors. In addition to pure vapor condensation, numerous investigations have been done on the effect of a non-condensable gas on the rate of condensation. A review of theoretical studies of laminar film condensation on plates and tubes was reported by Rose (1988). For the purpose of this thesis, the focus will be on condensation in vertical tubes with and without a non-condensable gas present. This chapter will be separated into five sections: (1) numerical studies on pure vapor condensation in vertical tubes, (2) numerical studies on

condensation with a non-condensable gas in vertical tubes, (3) experimental studies on condensation in vertical tubes, (4) numerical models developed at the University of Manitoba, and (5) a review of turbulence models.

2.2 Numerical Studies on Pure Vapor Condensation in Vertical Tubes

There have been a large number of techniques proposed to predict the heat transfer coefficient for pure vapor condensation in vertical tubes. These techniques range from simple empirical correlations to solutions involving a full set of governing equations.

Shaw (1979) developed a simple empirical correlation to predict the heat transfer coefficient for forced convection condensation inside pipes. This correlation was based on his earlier work for saturated boiling heat transfer and is capable of predicting the heat transfer coefficient for a wide range of parameters. The correlation was developed by analyzing data from horizontal, vertical up-flow, and vertical down-flow orientations and finding an equation that applied to all these cases. Chen (1987) developed a general correlation that can be used for both the case of a quiescent vapor (as in Nusselt's solution) and a vapor under forced convection conditions (as in Shaw's correlation). Chen's correlation, based on analytical and experimental results, includes the effects of interfacial shear stress, interfacial waviness and turbulent transport in the condensate film. More recently, Kim and No (2000) developed a model for larger diameter tubes. This model was based on the similarity between the single-phase turbulent convective heat transfer and annular film condensation heat transfer.

In addition to the semi-empirical correlations discussed above, there have been several solutions developed from approximations of the governing equations including conservation of mass, momentum, and energy. Dobran and Thorsen (1980) modeled laminar flow in both the vapor core and the liquid film. They performed an integral analysis on the governing equations while assuming parabolic velocity and temperature profiles across the film and a parabolic velocity profile in the core. Their focus was to study the effect of the Froude-to-Reynolds number ratio, the Buoyancy number, the vapor-to-liquid viscosity ratio, the liquid Prandtl number, and the Subcooling number. Pohner and Desai (1989) developed a model for either a turbulent or a laminar vapor core and a laminar film. Closure was obtained by assuming velocity and temperature profiles in each phase. For the case of a turbulent core, the interfacial shear stress was defined using a turbulent friction factor and the interfacial heat flux was evaluated using a modified form of the Dittus-Boelter equation. Their turbulent core/laminar film model showed good agreement with experimental results. Chen and Ke (1993) modeled turbulent flow in the vapor with a laminar film near the entrance developing into a turbulent film once a certain film Reynolds number was reached. The contribution of their work was in proposing a new eddy viscosity model which was divided into three regions: the inner region in the liquid condensate near the wall, the interface region including both the liquid and the vapor, and the outer region for the vapor core. Bellinghausen and Renz (1992) developed a model based on the conservation equations of mass, momentum, and energy. The low Reynolds number k-ε model of Jones and Launder (1972) was applied to both the vapor and liquid film regions. In order to predict

the transition from laminar to turbulent film flow, a minimum value for the kinetic energy was set to avoid a complete damping of turbulence.

Panday (2003) proposed a model for pure vapor condensation with turbulence in both the liquid film and the core. In this model, Panday solved a full-set of parabolic governing equations including the conservation of mass, momentum, and energy in both the liquid film and the vapor core. Axial diffusion was neglected and the pressure gradient in the radial direction was assumed to be zero. Turbulence was modeled in both regions using Pletcher's mixing length model for boundary layer flow with transpiration.

In a recent model proposed by Oh and Revankar (2005a), a simple condensation model was developed to analyze complete condensation in a passive containment cooling system condenser. The liquid film was assumed laminar with a parabolic velocity profile and a linear temperature profile. The interfacial shear was determined from single-phase friction factor correlations. They assumed two different forms for the local heat transfer coefficient, h_z, using ideas proposed by previous investigators; these correlations for h_z require knowledge of the film thickness. An iterative solution procedure was used to calculate the film thickness along the tube and consequently the local heat transfer coefficient. They compared their results with their own experimental data and concluded that the agreement was good.

2.3 Numerical Studies on Condensation in the Presence of a Gas in Vertical Tubes

The presence of a non-condensable gas during vapor condensation has been found to greatly reduce the condensation rate. This is due to the buildup of non-condensable gas concentration at the mixture-liquid interface which decreases the partial pressure of the vapor and thus the interface temperature.

For theoretical analyses of condensation of vapor in the presence of a non-condensable gas, one of two techniques is usually employed: boundary layer analysis or heat and mass transfer analogy. For the boundary layer analysis, the governing conservation equations are solved in both the liquid film and the vapor-gas mixture and are linked together with interfacial boundary conditions. These equations are solved using an integral approach, assuming similarity, or via another numerical method. The heat and mass transfer analogy is based on a heat balance at the liquid-mixture interface where the heat transferred from the mixture is equated to the heat transferred through the condensate film. The heat transfer from the mixture phase is made up of sensible heat and the latent heat given off when the vapor condenses.

Several solutions have been developed based on the heat and mass transfer analogy. Wang and Tu (1988) used this method and included the effects of interfacial shear and pressure drop but neglected the sensible heat transfer from the gas phase. From their results, they found that with small amounts of gas (W = 1%), the heat transfer was reduced by 15-30% while with larger amounts of gas (W = 10%), the heat transfer was reduced by 60%. They also showed that the presence of gas had a larger effect on the

heat transfer for lower mixture velocities. Siddique et al. (1993) studied the effects of air or a lighter gas such as hydrogen or helium on steam condensation in vertical tubes. They modeled the gas-steam mixture using the analogy between heat and mass transfer and the liquid phase was modeled as heat conduction across a falling film. From their investigation, they determined that for the same gas mass fraction, hydrogen and helium have a more inhibiting effect on heat transfer when compared with air. They also found that the film roughness effects were negligible for gas mixtures with low Schmidt number ($Sc < 1.0$). Dehbi and Guentay (1997) developed a model that included the heat transfer to the coolant in addition to the heat transfer in the condenser. This allowed for a solution to be reached without the specification of a wall temperature. Their model used the heat and mass transfer analogy in the mixture along with a Nusselt-type solution in the liquid film. From their results they showed that the heat transfer coefficient was reduced by increasing the inlet gas mass fraction, reducing the inlet mass flow rate, increasing the inlet temperature (this reduced the flow rate), and using lighter gases such as hydrogen or helium. No and Park (2002) also used the heat and mass transfer analogy and proposed a non-iterative condensation model for steam condensation in the presence of a non-condensable gas. Their predictions showed good agreement with experimental data.

Ghiaasiaan et al. (1995) modeled condensation in a vertical tube based on the two-phase flow conservation equations and using the 'stagnant film model'. In the stagnant film model, a quasi-steady, stagnant gaseous film is assumed to separate the liquid-gas interface from the bulk gas and heat and mass transfer are assumed to take place through

this film by diffusion. They proved that the stagnant film model was capable of predicting the correct data trend over a wide range of parameters.

There have been very few solutions developed based on a complete boundary layer analysis for vapor condensation in vertical tubes in the presence of a gas. Yuann (1993) solved the complete set of governing equations including the conservation of mass, momentum, energy, and species concentration for both the liquid film and the vapor-gas mixture. Turbulence was modeled by employing the two equation low Reynolds k-ε model of Jones and Launder (1972) in both the mixture and the liquid film and using an empirical correlation to account for waves at the interface. Their model was validated by comparing with the experimental results of Vierow (1990), Siddique (1992), and Kuhn (1995). More recently, Revankar and Pollock (2004) developed a model based on these same governing equations. Several assumptions were made in their analysis including constant properties, locally self similar velocity profiles and a linear temperature profile across the liquid film. In addition an empirical correlation was used for the friction factor, a mixing length model was applied to the mixture region to account for turbulence, and the liquid film was assumed laminar.

2.4 Experimental Studies on Condensation in Vertical Tubes

Several experiments have been performed for condensation both with and without non-condensable gases. Some of these experiments are reviewed below.

Goodykoontz and Dorsch (1966, 1967) performed experiments on pure steam condensation in both a 15.9-mm diameter vertical tube and a 7.44-mm diameter tube for the NASA Lewis Research Centre. For the smaller diameter tube, a lower range of inlet velocities was tested resulting in a negligible pressure drop along the tube. For the larger diameter tube, high inlet vapor velocities were tested and static pressure rises were obtained for conditions of high heat flux. In both cases, the heat transfer coefficient was highest near the inlet and dropped along the condenser until complete condensation occurred.

To support General Electric's Passive Containment Cooling System (PCCS), Vierow (1990) constructed an experimental facility to study the effects of a non-condensable gas on steam condensation. The focus of this work was on presenting data on the local heat transfer coefficient and on understanding how non-condensable gas affects the condensation rate.

Siddique (1992) and Siddique et al. (1993) conducted an experimental investigation at the Massachusetts Institute of Technology (MIT) for steam condensation in the presence of air or helium flowing downward inside a 46-mm diameter vertical tube. The experiments for steam-air covered mixture inlet temperatures of 100, 120 and 140 ^{o}C, inlet air mass fractions of 10-35 %, and inlet Reynolds numbers of 5,000-22,700. For the steam-helium tests, the same inlet temperatures were tested while the inlet helium mass fractions ranged from 2 to 10 % and the inlet Reynolds numbers ranged from 5,000-11,400. Following this, Hasanein et al. (1996), also from MIT, extended the work of Siddique to cover a

wider range of inlet Reynolds numbers and gas mass fractions for the steam-helium experiments. In addition, they measured the local heat transfer coefficients of steam and the simultaneous presence of air and helium.

Kuhn (1995) and Kuhn et al. (1997) found that heat transfer coefficients from previous experiments did not agree with one another and believed that this may be caused by turbulence perturbations or by developing flow entrance effects in the cooling annulus which are influenced by the method used to determine the coolant bulk temperature. Therefore, Kuhn's objective was to develop a new test section and method to minimize these problems. A wide range of cases were run for steam condensation with either air or helium and three different correlations were developed: one implementing the degradation factor method, one using the diffusion layer theory, and one using a mass transfer conductance model. To prove that their test section was producing accurate and consistent results, several tests were repeated to demonstrate the level of reproducibility of the experimental data.

Park and No (1999) from the Korea Advanced Institute of Science and Technology performed experiments on condensation in the presence of air in a vertical tube of the passive containment cooling system of the CP-1300 to show the parametric effects on condensation heat transfer and to develop an empirical correlation. Also from this same institute, Kim and No (2000) performed pure steam condensation experiments at pressures as high as 7.5 MPa. Heat transfer coefficients were calculated and the two-phase pressure drops were measured.

More recently, Oh and Revankar (2005b) performed experiments on pure vapor condensation for turbulent flow in a 26.6-mm inside diameter vertical tube. In these experiments, complete condensation of steam was obtained by submerging a condenser tube in a pool of water where heat from the condenser tube was removed by boiling the water in the pool. From these experiments, they presented results for the overall heat transfer coefficient as a function of system pressure and temperature difference between the core and the wall. The data collected from these experiments showed that for a given steam flow rate, the pressure in the system adjusted itself to ensure complete condensation; for a large steam flow rate, the pressure in the system increased to condense all the steam. The condensation heat transfer rate was found to increase with pressure while the condensation heat transfer coefficient decreased with pressure. Oh and Revankar (2005c) also performed experiments to study the effects of a non-condensable gas (air) on steam condensation. From these experiments, they presented results for the overall heat transfer coefficient as a function of system pressure, inlet mass flow rate, and gas mass fraction (up to 10%). They found that the condensation heat transfer coefficient decreases with an increase in the amount of gas or an increase in pressure, while it increases with increasing inlet mass flow rate.

2.5 Numerical Models Developed at the University of Manitoba

The first study done at the University of Manitoba on vapor condensation in the presence of non-condensable gases was that by Chin (1995) and Chin et al. (1998). Chin modeled laminar film condensation on isothermal vertical and inclined plates using the complete two-phase boundary layer equations. Various vapor-gas mixtures were used including

steam-air, sodium-argon, and glycerine-bromine. The objective of this study was to examine the effects of either the inertia terms or the energy convection and subcooling terms on heat transfer. For sodium-argon mixtures it was found that the inertia effects were significant for non-wavy laminar flow and decreased as the gas mass fraction increased. For the glycerine-bromine mixtures, the effect of energy convection and subcooling was found to be significant for all values of gas mass fraction.

Srzic (1997) and Srzic et al. (1999) extended the work of Chin by studying the effects of a lighter gas on the heat transfer. His model solved the governing equations up to the separation point. It was found that the lighter gas resulted in a larger reduction in the heat transfer than heavier gases.

Groff et al. (2002) developed a numerically based algebraic correlation for Nusselt number during laminar film condensation from steam-air and steam-hydrogen mixtures on isothermal horizontal plates. Good agreement was obtained between the correlation and the numerical results with a root mean square deviation of about 1.7% for both vapor-gas mixtures.

Siow (2001) and Siow et al. (2002) modified the model further to study film condensation inside a parallel-plate channel in the presence of a non-condensable gas. In addition, Siow also re-developed the solution method such that the governing equations were solved simultaneously using an advanced matrix algorithm instead of the segregated solution method used in Chin and Srzic's work. Siow studied the effects of the inlet gas

mass fraction, the inlet velocity, the inlet pressure, and the temperature difference between the inlet and the wall on the heat transfer. In addition, the effect of a downward inclination on condensation was studied and it was found that the film thickness decreased substantially due to the gravitational acceleration. Siow also analyzed condensation of R134a-air mixtures and found that a lower heat transfer and higher pressure drop were obtained compared with the steam-air mixtures.

2.6 Turbulence Modeling

When modeling turbulent flow, the governing equations are the same as those for laminar flow, with the exception of the laminar stresses ($\mu \partial u / \partial y$) being increased by additional stresses known as Reynolds stresses. Turbulence models have been developed to calculate these stresses and thus close the system of equations. Boussinesq (1877) proposed a method for modeling the turbulent Reynolds stresses called the eddy viscosity concept. Analogous to the definition of the laminar shear stresses ($\tau = \mu \partial u / \partial y$), the Reynolds stress was defined as follows:

$$\tau^t = \mu^t \frac{\partial u}{\partial y} = \frac{v^t}{\rho} \frac{\partial u}{\partial y} \tag{2.2}$$

In this definition, μ^t is the eddy viscosity and is often modeled as being a function of either the mean velocity, or additional turbulence fields such as the turbulent kinetic energy (k) and dissipation rate (ε). Turbulence models are classified based on the number of transport equations used for the turbulence quantities. The two classes of

turbulence models that will be reviewed here are the zero equation models and the two equation models.

The zero equation models are relatively simple models that are easy and inexpensive to implement. Prandtl (1925) developed a mixing length theorem that received even more respect than the eddy viscosity concept mentioned above. This theorem was based on the idea that in turbulent flow, the fluid particles will join together to form lumps that move together as a unit. These lumps of fluid would retain their momentum in the x-direction for a distance ℓ in the y-direction. Prandtl defined this distance ℓ as the mixing length and defined the Reynolds stresses in terms of this mixing length as follows:

$$\tau^t = \rho \ell^2 \left|\frac{d\bar{u}}{dy}\right| \frac{du}{dy} \tag{2.3}$$

Comparing Equation (2.3) with the Boussinesq hypothesis shown by Equation (2.2) gives the following equation for the turbulent viscosity:

$$\mu^t = \rho \ell^2 \left|\frac{d\bar{u}}{dy}\right| \tag{2.4}$$

The physical interpretation of the mixing length was defined by Schlichting (1968) as "The distance in the transverse direction which must be covered by an agglomeration of fluid particles traveling with its original mean velocity in order to make the difference

between its velocity and the velocity in the new lamina equal to the mean transverse fluctuation in turbulent flow."

Von Karman (1939) speculated that near the wall, the mixing length may be proportional to the distance from the wall:

$$\ell = \kappa y \tag{2.5}$$

In the above equation, κ is the von Karman constant, and y is the distance from the wall. With this equation, the turbulent viscosity goes to zero at the wall.

Van Driest (1956) tried to improve the mixing length model for the region near the wall by including a term for viscous damping. The mixing length was defined as:

$$\ell = \kappa y\left(1-\exp\left(\frac{-y+}{A_o^{+}}\right)\right) \text{ where } A_o^{+} = 26 \text{ and } y+ = \frac{\rho y u_\tau}{\mu} \tag{2.6}$$

There have been several models based on the van Driest model. The one that will be reviewed here is Pletcher's (1974) mixing length model which was used in Panday's (2003) work to model pure vapor condensation in vertical tubes. Pletcher proposed a generalization of the van Driest damping function to handle flows in which the shear stress near the wall varies significantly. This turbulence model is suitable for flows with

transpiration and was used for both the liquid film and the vapor core in Panday's model. The equations defining this model will be discussed in the following chapter.

Two equation models use two partial differential equations to model turbulence quantities. In these models, the length scale is determined from a transport equation. This length scale is often expressed in terms of the dissipation rate, ε, but is sometimes expressed in terms of the specific dissipation rate, ω. This review will focus on the length scale being expressed in terms of ε. The most well known version of the k-ε model is that by Jones and Launder (1972). They proposed both a high Reynolds number model and a low Reynolds number model. The high Reynolds number model is given by the following equations:

Eddy Viscosity:

$$\nu^{t} = C_{\mu} k^{2} / \varepsilon \tag{2.7}$$

Turbulent Kinetic Energy:

$$\frac{\partial k}{\partial t} + U_{j} \frac{\partial k}{\partial x_{j}} = \tau_{i,j} \frac{\partial U_{i}}{\partial x_{j}} - \varepsilon + \frac{\partial}{\partial x_{j}} \left[\left(\nu + \frac{\nu^{t}}{\sigma_{k}} \frac{\partial k}{\partial x_{j}} \right) \right] \tag{2.8}$$

Dissipation Rate:

$$\frac{\partial \varepsilon}{\partial t} + U_{j} \frac{\partial \varepsilon}{\partial x_{j}} = C_{\varepsilon 1} \frac{\varepsilon}{k} \tau_{i,j} \frac{\partial U_{i}}{\partial x_{j}} - C_{\varepsilon 2} \frac{\varepsilon^{2}}{k} + \frac{\partial}{\partial x_{j}} \left[\left(\nu + \frac{\nu^{t}}{\sigma_{\varepsilon}} \frac{\partial \varepsilon}{\partial x_{j}} \right) \right] \tag{2.9}$$

Coefficients:

$$C_{\varepsilon 1} = 1.44, \quad C_{\varepsilon 2} = 1.92, \quad C_{\mu} = 0.09, \quad \sigma_k = 1.0, \text{ and } \quad \sigma_{\varepsilon} = 1.3 \tag{2.10}$$

For wall bounded flows, this high Reynolds number k-ε model cannot be used in the vicinity of the wall since it neglects the effects of viscosity. For this reason, empirical wall functions are often employed to connect the turbulent core to the solid boundary. More recently, low Reynolds number models have been developed which include a wall damping effect in the empirical constants of the transport equations. These models therefore allow integration of the transport equations for the turbulent kinetic energy and dissipation rate right up to the wall. There have been several reviews done comparing various low Reynolds number k-ε models including Patel et al. (1984), Hrenya et al. (1995), and Thakre and Joshi (2000). Depending on the flow conditions, each review found different conclusions in terms of which model best predicts the experimental results.

In the second model proposed by Jones and Launder (1972), viscous modifications were added to the k-ε model in order to adapt it for low-Reynolds-number regions close to the wall. This model was used by Yuann (1993) in modeling vapor condensation in the presence of a gas in vertical tubes and also in Bellinghausen and Renz (1992). The equations and coefficients defining this model will be discussed in the following chapter.

2.7 Summary

From this review it was found that the majority of numerical work done on condensation in vertical tubes in the presence of gas used the heat and mass transfer analogy. The only author who used the full set of governing equations for vapor-gas mixtures without profile assumptions was Yuann (1993). The purpose of this research was to develop a model based on the full set of governing equations for turbulent convection steam condensation in the presence of a gas. The equations in Siow's (2001) numerical model will be changed from Cartesian to radial coordinates and the geometry will be modified to model a vertical tube. In addition, turbulence models will be added to both the liquid film and the mixture core to allow for a solution for turbulent flow conditions.

The goal is to compare different turbulence models including a mixing length model and a two-equation model and evaluate their performance. The numerical model will be compared with experimental results using the different turbulence models and a parametric study will be done to analyze the effects of the various independent parameters on condensation.

CHAPTER 3

MODEL DESCRIPTION

3.1 Problem Statement and Assumptions

A diagram of the problem being considered is shown in Figure 3.1. A mixture of a saturated vapor and a non-condensable gas enters a vertical tube of radius r_o, with a uniform temperature profile, T_{in}, a uniform velocity profile, u_{in}, a uniform pressure P_{in}, and a uniform gas mass fraction, W_{in}. The temperature of the tube wall is maintained lower than that of the inlet mixture resulting in vapor condensation and a liquid film of thickness δ developing along the length of the tube. The mixture entering the tube is either laminar for cases of low inlet Reynolds numbers, or turbulent, for cases of high inlet Reynolds numbers. The liquid film is laminar near the inlet and can become turbulent at a sufficiently large value of liquid Reynolds number. The vertical orientation of the tube results in an axi-symmetric flow which allows the problem to be modeled as two-dimensional.

The following assumptions were made when formulating the governing equations:

- The flow is steady state – All the properties and flow conditions are assumed to be independent of time and therefore, variation with respect to time will not be considered.
- The liquid-mixture interface is smooth.

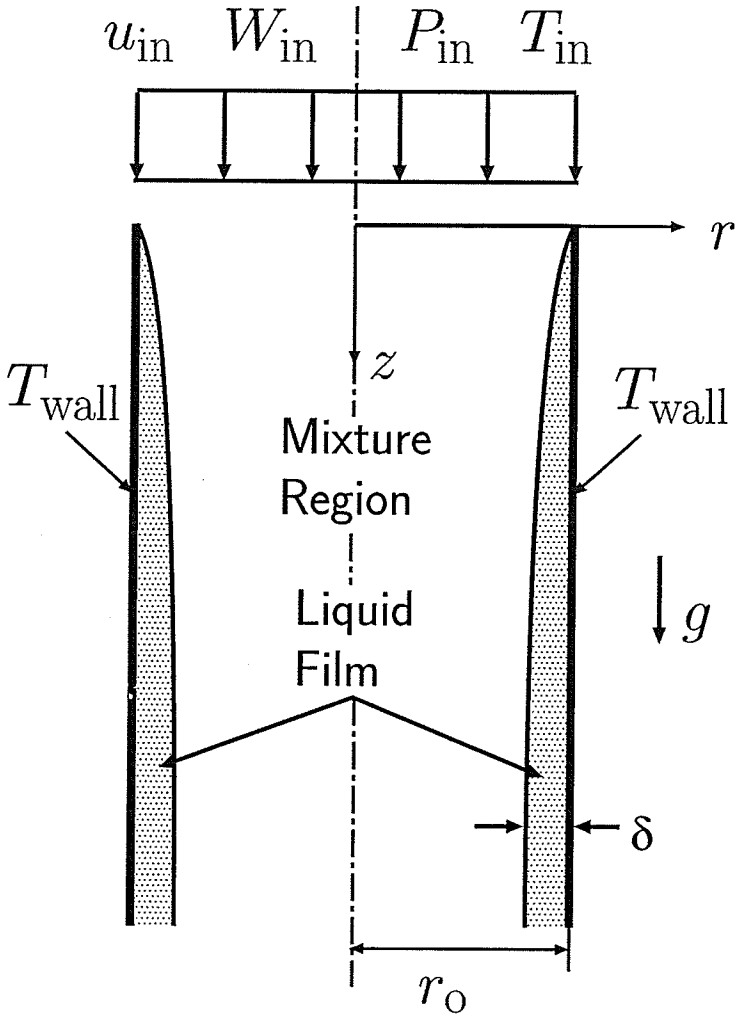

Figure 3.1 Physical model

- Both the liquid and the mixture are Newtonian fluids – The shear stresses in both phases are assumed to vary linearly with the strain rate, $\tau = \mu \partial u / \partial r$.
- The vapor-gas mixture is treated as an ideal gas mixture – The mixture is treated as a binary mixture of two ideal gases. The density is determined

from the ideal gas law and the total pressure is the sum of the partial pressures of the gases.

- Saturation conditions are assumed at the liquid-mixture interface – For condensation to occur, the vapor must be saturated; therefore, the interface temperature will equal the saturation temperature corresponding to the partial pressure of the vapor.
- The pressure is assumed uniform in the radial direction – Pressure variation across the tube is expected to be small therefore; $dP/dr = 0$. However, the pressure is allowed to vary in the axial (z) direction.
- Axial diffusion of heat, momentum, and mass are negligible – This is a valid assumption since the radial diffusion is much larger than the axial diffusion.

3.2 Mathematical Model

The liquid film and the mixture core were each defined by a set of governing equations in the r-z coordinate system and were connected by interfacial boundary conditions. For high liquid film Reynolds numbers, one of two turbulence models was included in the analysis: Pletcher's (1974) mixing length model or the low Reynolds number k-ε model of Jones and Launder (1972). All the properties in the equations are allowed to vary and are determined by methods that will be discussed in Section 3.3.

3.2.1 Liquid Phase Governing Equations

The liquid region was defined by the following equations for conservation of mass, momentum, and energy.

Liquid Continuity Equation:

$$\frac{\partial}{\partial z}(\rho_{\mathrm{L}} u_{\mathrm{L}}) + \frac{1}{r}\frac{\partial}{\partial r}(r\rho_{\mathrm{L}} v_{\mathrm{L}}) = 0 \tag{3.1}$$

Liquid Momentum Equation:

$$\frac{\partial}{\partial z}(\rho_{\mathrm{L}} u_{\mathrm{L}} u_{\mathrm{L}}) + \frac{1}{r}\frac{\partial}{\partial r}(r\rho_{\mathrm{L}} u_{\mathrm{L}} v_{\mathrm{L}}) = \frac{1}{r}\frac{\partial}{\partial r}\left(r\mu_{\mathrm{L,eff}}\frac{\partial u_{\mathrm{L}}}{\partial r}\right) + \rho_{\mathrm{L}} g - \frac{dP}{dz} \tag{3.2}$$

Liquid Energy Equation:

$$\frac{\partial}{\partial z}(\rho_{\mathrm{L}} u_{\mathrm{L}} C_{P,\mathrm{L}} T_{\mathrm{L}}) + \frac{1}{r}\frac{\partial}{\partial r}(r\rho_{\mathrm{L}} v_{\mathrm{L}} C_{P,\mathrm{L}} T_{\mathrm{L}}) = \frac{1}{r}\frac{\partial}{\partial r}\left(r\lambda_{\mathrm{L,eff}}\frac{\partial T_{\mathrm{L}}}{\partial r}\right) \tag{3.3}$$

In the above equations, $\mu_{\mathrm{L,eff}}$ and $\lambda_{\mathrm{L,eff}}$ are the effective viscosity and thermal conductivity, respectively, and are defined as:

$\mu_{\mathrm{L,eff}} = \mu_{\mathrm{L}} + \mu_{\mathrm{L}}^{\mathrm{t}}$ where $\mu_{\mathrm{L}}^{\mathrm{t}}$ is the turbulent viscosity in the liquid (3.4)

$\lambda_{\mathrm{L,eff}} = \lambda_{\mathrm{L}} + \lambda_{\mathrm{L}}^{\mathrm{t}}$ where λ_{L}^{t} is the turbulent thermal conductivity in the liquid (3.5)

with $\lambda_{\mathrm{L}}^{\mathrm{t}} = \dfrac{\mu_{\mathrm{L}}^{\mathrm{t}} C_{P,\mathrm{L}}}{\mathrm{Pr}_{\mathrm{L}}^{\mathrm{t}}}$ (3.6)

The liquid turbulent Prandtl number $\mathrm{Pr}_{\mathrm{L}}^{\mathrm{t}}$ was set to unity and the turbulent viscosity will be defined in Section 3.2.3. When the film is laminar, the turbulent viscosity and turbulent thermal conductivity are zero resulting in: $\mu_{\mathrm{L,eff}} = \mu_{\mathrm{L}}$ and $\lambda_{\mathrm{L,eff}} = \lambda_{\mathrm{L}}$.

3.2.2 Mixture Phase Governing Equations

Similar to the liquid region, the mixture region is also defined by the conservation of mass, momentum, and energy. In addition to these three equations, an extra equation is required for the conservation of gas.

Mixture Continuity Equation:

$$\frac{\partial}{\partial z}\left(\rho_{\mathrm{M}} u_{\mathrm{M}}\right)+\frac{1}{r}\frac{\partial}{\partial r}\left(r\rho_{\mathrm{M}} v_{\mathrm{M}}\right)=0 \tag{3.7}$$

Mixture Momentum Equation:

$$\frac{\partial}{\partial z}\left(\rho_{\mathrm{M}} u_{\mathrm{M}} u_{\mathrm{M}}\right)+\frac{1}{r}\frac{\partial}{\partial r}\left(r\rho_{\mathrm{M}} u_{\mathrm{M}} v_{\mathrm{M}}\right)=\frac{1}{r}\frac{\partial}{\partial r}\left(r\mu_{\mathrm{M,eff}}\frac{\partial u_{\mathrm{M}}}{\partial r}\right)+\rho_{\mathrm{M}} g-\frac{dP}{dz} \tag{3.8}$$

Mixture Energy Equation:

$$\begin{aligned}\frac{\partial}{\partial z}\left(\rho_{\mathrm{M}} u_{\mathrm{M}} C_{P,\mathrm{M}} T_{\mathrm{M}}\right)+\frac{1}{r}\frac{\partial}{\partial r}\left(r\rho_{\mathrm{M}} v_{\mathrm{M}} C_{P,\mathrm{M}} T_{\mathrm{M}}\right)= \\ \frac{1}{r}\frac{\partial}{\partial r}\left(r\lambda_{\mathrm{M,eff}}\frac{\partial T_{\mathrm{M}}}{\partial r}\right)+\frac{1}{r}\frac{\partial}{\partial r}\left(r\rho_{\mathrm{M}} D_{\mathrm{eff}}\left(C_{P,\mathrm{g}}-C_{P,\mathrm{v}}\right)\frac{\partial W}{\partial r}T_{\mathrm{M}}\right)\end{aligned} \tag{3.9}$$

Mixture Mass-Diffusion Equation:

$$\frac{\partial}{\partial z}\left(\rho_{\mathrm{M}} u_{\mathrm{M}} W\right)+\frac{1}{r}\frac{\partial}{\partial r}\left(r\rho_{\mathrm{M}} v_{\mathrm{M}} W\right)=\frac{1}{r}\frac{\partial}{\partial r}\left(r\rho_{\mathrm{M}} D_{\mathrm{eff}}\frac{\partial W}{\partial r}\right) \tag{3.10}$$

The effective viscosity $\mu_{\mathrm{M,eff}}$, the thermal conductivity $\lambda_{\mathrm{M,eff}}$, and the diffusion coefficient D_{eff} are defined as:

$$\mu_{\mathrm{M,eff}} = \mu_{\mathrm{M}} + \mu_{\mathrm{M}}^{\mathrm{t}} \quad \text{where } \mu_{\mathrm{M}}^{\mathrm{t}} \text{ is the turbulent viscosity in the mixture} \tag{3.11}$$

$$\lambda_{\mathrm{M,eff}} = \lambda_{\mathrm{M}} + \lambda_{\mathrm{M}}^{\mathrm{t}} \quad \text{where } \lambda_{M}^{t} \text{ is the turbulent thermal conductivity in the mixture} \tag{3.12}$$

$$\text{with } \lambda_{\mathrm{M}}^{\mathrm{t}} = \frac{\mu_{\mathrm{M}}^{\mathrm{t}} C_{P,\mathrm{M}}}{\mathrm{Pr}_{\mathrm{M}}^{\mathrm{t}}} \text{ and } \mathrm{Pr}_{\mathrm{M}}^{\mathrm{t}} = 1 \tag{3.13}$$

$$D_{\mathrm{eff}} = D + D^{\mathrm{t}} \tag{3.14}$$

$$\text{where } D^{\mathrm{t}} = \frac{\mu_{\mathrm{M}}^{\mathrm{t}}}{\rho_{\mathrm{M}}\,\mathrm{Sc}_{\mathrm{M}}^{\mathrm{t}}} \text{ and } \mathrm{Sc}_{\mathrm{M}}^{\mathrm{t}} = 1 \tag{3.15}$$

The last term of Equation (3.9) represents the energy transfer due to mass diffusion. When there is no gas, this term goes to zero. Equation (3.10) ensures that the amount of gas is conserved across a control volume.

3.2.3 Turbulence Models

One of two turbulence models was used to determine the turbulent viscosity for both the liquid and mixture regions in the above momentum equations: Pletcher's (1974) mixing length model or the Jones and Launder (1972) low Reynolds number k-ε model.

3.2.3.1 Mixing Length Model

Pletcher's mixing length model is based on the damping function proposed by van Driest (1956) and was developed for turbulent boundary layer flow with transpiration. The turbulent viscosity for both the liquid and the mixture regions is determined with the following equation:

$$\mu^{t} = \rho \ell^{2} \left| \frac{\partial u}{\partial r} \right| \tag{3.16}$$

where, ℓ is the mixing length defined by :

$$\ell = 0.41 D^{*} \quad \text{for} \quad y \leq \frac{0.089 \delta_{BL}}{0.41 D^{*}} \tag{3.17}$$

$$\ell = 0.89 \delta_{BL} \quad \text{for} \quad y > \frac{0.089 \delta_{BL}}{0.41 D^{*}} \tag{3.18}$$

For the liquid region, y is the distance measured from the wall, and for the mixture region, y is the distance measured from the interface. The boundary layer thickness (δ_{BL}) is defined as the value of y for which $u_{relative} = 0.99\ u_e$. In the mixture region, $u_{relative}$ is the mixture velocity relative to the velocity at the interface ($u_{relative} = u_M - u_i$) and u_e is the centerline velocity relative to the velocity at the interface ($u_e = u_c - u_i$). In the liquid region, $u_{relative}$ is the liquid velocity relative to the velocity at the wall and u_e is the

velocity at the interface relative to the velocity at the wall; since the velocity at the wall is zero, $u_{relative} = u_L$ and $u_e = u_i$. The damping function, D^* is given by:

$$D^* = 1 - \exp\left[\frac{-\rho_o y}{26\mu_o}\left(\frac{\tau\,\tau_{ft}}{\rho_o \tau_o}\right)^{1/2}\right] \tag{3.19}$$

The subscript o in the above equation refers to the wall for the liquid region and the interface for the mixture region. The shear stress τ is defined by:

$$\tau = \tau_o\left(1 + V_o^+ U^+ + P^+ y^+\right) \tag{3.20}$$

In this equation,

$$V_o^+ = \frac{v_o}{u_\tau} \tag{3.21}$$

$$U^+ = \frac{u}{u_\tau} \tag{3.22}$$

$$P^+ = \left(\frac{\mu}{\rho^2 u_\tau^{\,3}}\right)\frac{dP}{dz} \tag{3.23}$$

$$y^+ = \frac{\rho y u_\tau}{\mu} \tag{3.24}$$

$$u_\tau = \sqrt{\tau_o / \rho_o} \tag{3.25}$$

τ_{ft} is the shear stress for fully developed turbulent region and is evaluated at $y^+ = 26$.

3.2.3.2. Low Reynolds Number k-ε Model

In the Jones and Launder low Reynolds number k-ε model, the turbulent viscosity is determined from the solution of the transport equations for the turbulent kinetic energy and dissipation rate. One of the benefits of this model is that it is valid in the viscous sub-layer and therefore it can be applied right up to the wall in the liquid region and to the interface in the mixture region.

The turbulent kinetic energy and dissipation equations are identical in both the liquid film and the mixture region and will therefore only be shown only once for the liquid region:

Kinetic Energy:

$$\frac{\partial}{\partial z}(\rho_L u_L k_L)+\frac{1}{r}\frac{\partial}{\partial r}(r\rho_L v_L k_L)=\frac{1}{r}\frac{\partial}{\partial r}\left[r\left(\mu_L+\frac{\mu_L^t}{\sigma_k}\right)\frac{\partial k_L}{\partial r}\right] + \mu_L^t\left(\frac{\partial u_L}{\partial r}\right)^2-\rho_L\varepsilon_L-2\mu_L\left(\frac{\partial\sqrt{k_L}}{\partial r}\right)^2 \tag{3.26}$$

Dissipation Rate:

$$\frac{\partial}{\partial z}(\rho_L u_L \varepsilon_L)+\frac{1}{r}\frac{\partial}{\partial r}(r\rho_L v_L \varepsilon_L)=\frac{1}{r}\frac{\partial}{\partial r}\left[r\left(\mu_L+\frac{\mu_L^t}{\sigma_\varepsilon}\right)\frac{\partial \varepsilon_L}{\partial r}\right] + C_{\varepsilon 1}\frac{\varepsilon_L}{k_L}\mu_L^t\left(\frac{\partial u_L}{\partial r}\right)^2-C_{\varepsilon 2}f_2\rho_L\frac{\varepsilon_L^{\,2}}{k_L}+2\frac{\mu_L\mu_L^t}{\rho_L}\left(\frac{\partial^2 u_L}{\partial r^2}\right)^2 \tag{3.27}$$

The constants in the above equations are:

$$\sigma_k = 1.0 \qquad \sigma_\varepsilon = 1.3$$

$$C_{\varepsilon 1} = 1.55 \qquad C_{\varepsilon 2} = 2.0\left(1 - 0.3\exp\left(-\mathrm{Re}_{\mathrm{L}}^{\mathrm{t}\,2}\right)\right) \tag{3.28}$$

$$\text{where } \mathrm{Re}_{\mathrm{L}}^{\mathrm{t}} = \frac{\rho_{\mathrm{L}} k_{\mathrm{L}}^{\ 2}}{\mu_{\mathrm{L}} \varepsilon_{\mathrm{L}}} \tag{3.29}$$

The turbulent viscosity is determined from the following:

$$\mu_{\mathrm{L}}^{\mathrm{t}} = C_\mu f_\mu \rho_{\mathrm{L}} k_{\mathrm{L}}^{\ 2} / \varepsilon_{\mathrm{L}} \tag{3.30}$$

$$\text{where } C_\mu = 0.09 \quad \text{and} \quad f_\mu = \exp(-2.5/(1 + \mathrm{Re}_{\mathrm{L}}^{\mathrm{t}}/50)) \tag{3.31}$$

3.2.4 Boundary Conditions

Boundary conditions were defined at the tube wall, at the interface, at the centerline, and at the tube inlet.

At the tube wall ($r = r_{\mathrm{o}}$)

$$u_{\mathrm{L}} = 0 \tag{3.32}$$

$$v_{\mathrm{L}} = 0 \tag{3.33}$$

$$T_{\mathrm{L}} = T_{\mathrm{wall}} \tag{3.34}$$

$$k_{\mathrm{L}} = \varepsilon_{\mathrm{L}} = 0 \tag{3.35}$$

Equations (3.32) and (3.33) represent the no slip boundary condition at the wall. The temperature at the wall is set to T_{wall}, which is either constant along the length of the tube

or varies according to a prescribed profile taken from experimental results. When using the Jones and Launder k-ε model to define the turbulent parameters, the k and ε boundary conditions were both set to zero, which were the required values for this specific model.

At the interface ($r = r_o - \delta$)

$$u_L = u_M \tag{3.36}$$

$$T_L = T_M = T_{sat} \tag{3.37}$$

$$\mu_{L,eff} \frac{\partial u_L}{\partial r} = \mu_{M,eff} \frac{\partial u_M}{\partial r} \tag{3.38}$$

$$\rho_L v_L + \rho_L u_L \frac{d\delta}{dz} = \rho_M v_M + \rho_M u_M \frac{d\delta}{dz} = J''_{int} \tag{3.39}$$

$$\lambda_{L,eff} \frac{\partial T_L}{\partial r} = \lambda_{M,eff} \frac{\partial T_M}{\partial r} - J''_{int} h_{fg} \tag{3.40}$$

$$J''_{int} W - \rho_M D_{eff} \frac{\partial W}{\partial r} = 0 \tag{3.41}$$

$$k_L = \varepsilon_L = 0 \tag{3.42}$$

A zero-width control volume is used at the interface such that the velocity and temperature of the liquid at the interfacial node are set equal to those of the mixture (Equations (3.36) and (3.37)). Equations (3.38) to (3.40) balance the shear stress, the mass flux, and the heat transfer across the interface, respectively, and Equation (3.41) states that no gas will cross the interface. Finally, the last boundary condition sets the kinetic energy and dissipation at the interface to zero. The selection of this boundary condition will be discussed in Section 5.4.4.

At the centerline ($r = 0$)

$$\frac{\partial u_{\mathrm{M}}}{\partial r} = 0 \tag{3.43}$$

$$v_{\mathrm{M}} = 0 \tag{3.44}$$

$$\frac{\partial T_{\mathrm{M}}}{\partial r} = 0 \tag{3.45}$$

$$\frac{\partial W}{\partial r} = 0 \tag{3.46}$$

$$\frac{\partial k_{\mathrm{M}}}{\partial r} = 0 \tag{3.47}$$

$$\frac{\partial \varepsilon_{\mathrm{M}}}{\partial r} = 0 \tag{3.48}$$

The centerline acts as an axis of symmetry and therefore, the gradients of the axial velocity, temperature, gas mass fraction, kinetic energy, and the dissipation rate are all zero and the radial velocity is zero.

At the inlet ($z = 0$)

$$u_{\mathrm{L}} = 0 \tag{3.49}$$

$$u_{\mathrm{M}} = u_{\mathrm{in}} \tag{3.50}$$

$$v_{\mathrm{L}} = v_{\mathrm{M}} = 0 \tag{3.51}$$

$$T_{\mathrm{L}} = T_{\mathrm{wall}} \tag{3.52}$$

$$T_{\mathrm{M}} = T_{\mathrm{in}} \tag{3.53}$$

$$W = W_{\mathrm{in}} \tag{3.54}$$

$$k_L = \varepsilon_L = 0 \tag{3.55}$$

$$k_M = 1.5 I^2 u_{in}{}^2 \text{ where } I \text{ is the turbulence intensity and is set to } I = 0.037 \tag{3.56}$$

$$\varepsilon_M = \frac{k_M{}^{3/2}}{0.6 r_o} \tag{3.57}$$

$$\delta = 0 \tag{3.58}$$

In addition to the above governing equations, turbulence models, and boundary conditions, one other equation is required to completely define the problem: the global mass conservation equation. This equation states that the total amount of mass in both the liquid and mixture regions is conserved along the tube:

$$\int_0^{r_o-\delta} \rho_M u_M r dr + \int_{r_o-\delta}^{r_o} \rho_L u_L r dr = \frac{\dot{m}_{in}}{2\pi} \tag{3.59}$$

This equation is necessary for determining the axial pressure gradient *dP/dz*.

3.3 Properties

For the purpose of this study, the vapor-gas mixture entering the vertical tube consists of steam as the vapor and air as the gas. Both the mixture and the liquid properties were evaluated at each node at the local temperature and pressure corresponding to that node. All the equations used to determine the properties are presented in Appendix A of Siow (2001).

The specific heat, viscosity and thermal conductivity for both the vapor and the liquid water were taken from the steam-water tables given in Incropera and Dewitt (1996). In order to determine the properties at the exact local temperatures, interpolation between the table values was required. The liquid density, latent heat and steam saturation temperature and pressures were calculated using correlations from Irvine and Liley (1984).

The steam and the air were treated as ideal gases and therefore the densities for both fluids were determined by using the ideal gas law. The specific heat, viscosity, and thermal conductivity of the air were calculated using correlations from Irvine and Liley (1984).

With the vapor and air properties known, the mixture properties could be determined. The mixture viscosity, thermal conductivity and diffusion coefficient were calculated using equations from Reid et al. (1977). The density of the mixture was taken as the sum of the individual densities of the vapor and gas and the specific heat is the sum of the individual specific heats multiplied by their corresponding mass fractions.

CHAPTER 4

NUMERICAL SOLUTION METHOD

4.1 Introduction

A numerical solution was developed based on Equations (3.1) to (3.59). These equations were first transformed from an *r-z* coordinate system into an η–χ coordinate system. Following this, the transformed equations were discretized using a finite volume method and solved using a combination of an advanced matrix algorithm to solve for *u, J, W,* δ, and *dP/dz* and a separate solver for the turbulent viscosity. This chapter covers the detailed steps involved in developing the numerical model - from transforming the governing equations to arriving at a final converged solution.

4.2 Transformation of Coordinates

The *r-z* coordinate system was transformed into an η–χ coordinate system such that the centerline is at $\eta = 0$, the liquid-mixture interface is at $\eta = 1$ and the wall is at $\eta = 2$. The equations that relate the η–χ coordinate system to the *r-z* coordinate system are:

$$\chi = z \qquad \text{for } z \geq 0 \tag{4.1}$$

$$\eta = 2 - \frac{r_o - r}{\delta} \qquad \text{for } (r_o - \delta) \leq r \leq r_o \tag{4.2}$$

$$\eta = \frac{r}{(r_o - \delta)} \qquad \text{for } 0 \leq r \leq (r_o - \delta) \tag{4.3}$$

With the new coordinate system, the mixture region is now clearly defined as $0 \leq \eta \leq 1$ and the liquid region is defined as $1 \leq \eta \leq 2$. Although the film thickness is increasing in the z direction, the interface is always located at $\eta = 1$. The domain was divided into a certain number of stations NZ, that expand geometrically in the χ direction and a certain number of control volumes NL in the η direction in the liquid region, and NM in the η direction in the mixture region. The grid spacing in the liquid region remains constant while the control volumes in the mixture region expand geometrically towards the centerline. The reason for this is that the largest gradients in the mixture region occur near the interface and therefore a fine grid is required there. This new coordinate system will ensure that the number of nodes in the liquid and mixture regions remains constant with z and that the two regions are always separated by a zero width control volume at the interface.

Figure 4.1 shows a simplified grid for $NZ = 9$, $NL = 4$ and $NM = 6$ in the η-χ coordinate system. Each rectangle represents a control volume with a node at the center, where indexing is applied. The index i is used to label the station number in the χ direction, j_M is used to label the nodes in the η direction in the mixture region (starting at the centerline) and j_L is used to label the nodes in the η direction in the liquid region (starting at the interface). The control volumes at the centerline ($j_M = 1$), at the interface ($j_M = NM$), at the wall ($j_L = NL$), and at the inlet ($i = 1$) are all zero width; they were formed to prescribe the boundary conditions. Field variables such as u, T and W are stored at the nodal points, while J is stored at the north faces of the control volumes. The parameters δ and $dP/d\chi$ (or P') are scalar variables and each have a single value at every axial station.

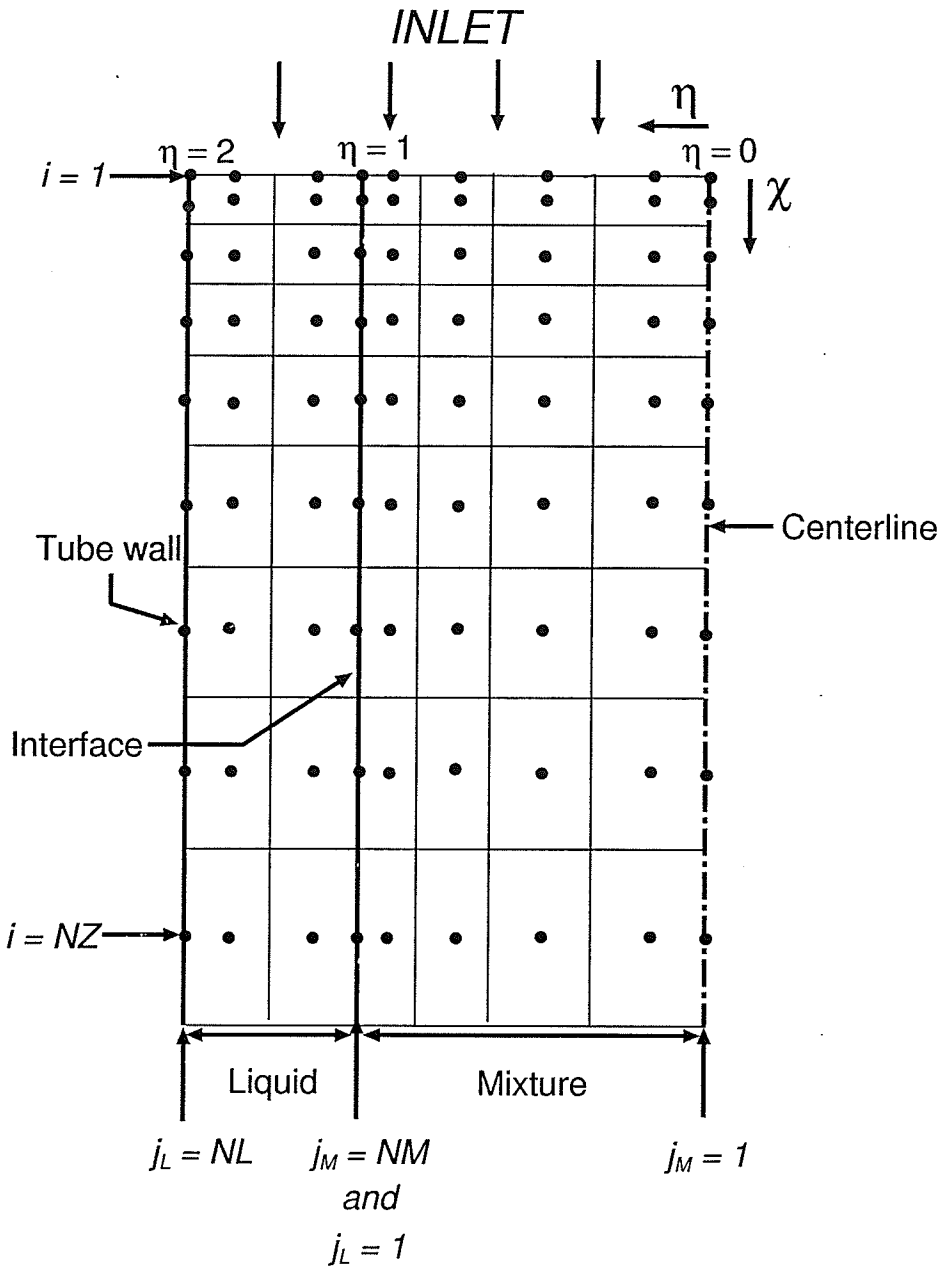

Figure 4.1 Grid in the η–χ coordinate system

Figure 4.2 represents the actual domain in the *r*-*z* coordinate system, showing the film thickness starting at $z = 0$ and growing along the channel.

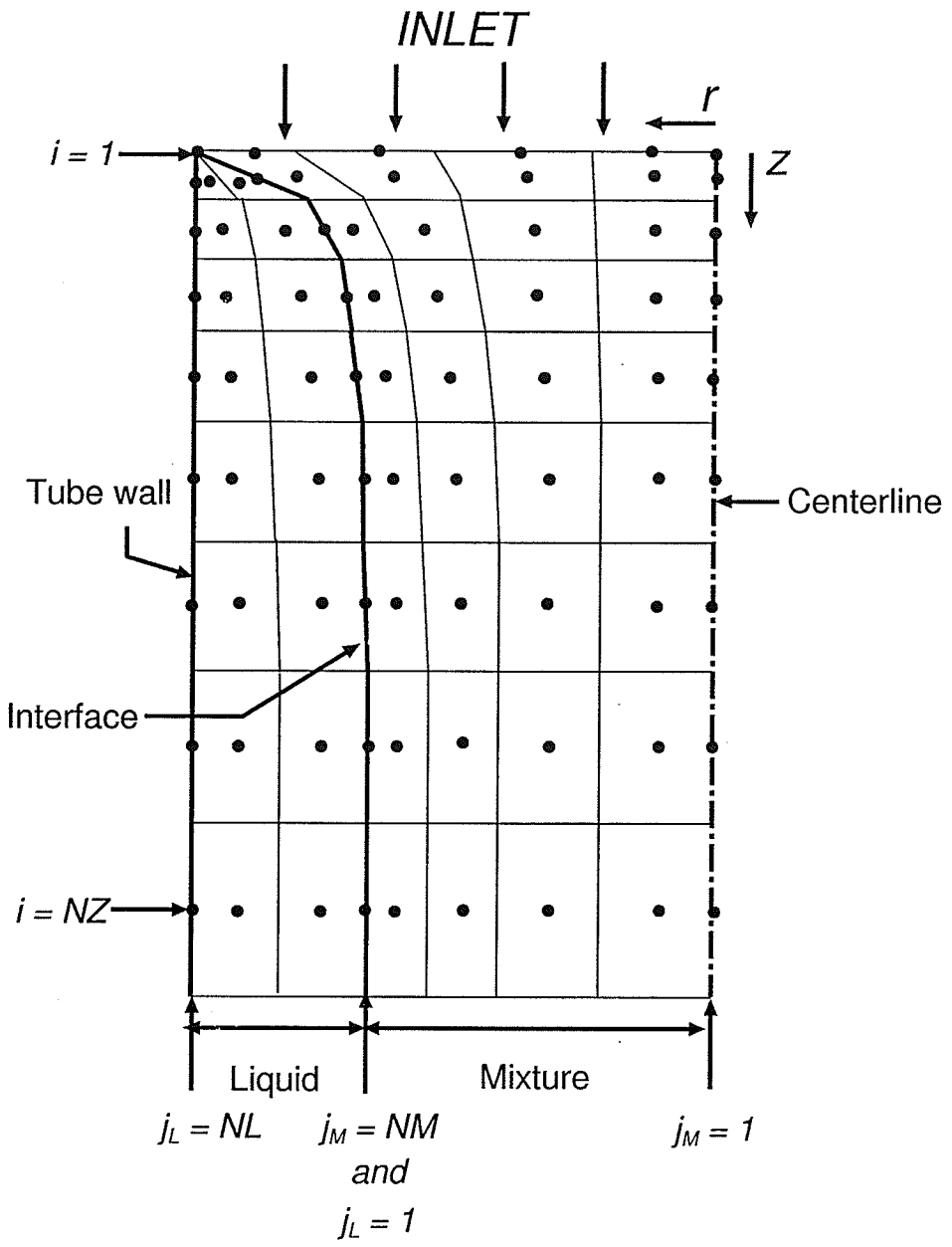

Figure 4.2 Grid in the *r-z* coordinate system

The governing equations and boundary conditions were transformed into the new coordinate system using Equations (4.1) to (4.3) above. The v-velocity component was substituted with the mass flux J'', which is defined by the boundary condition given by

Equation (3.39) and is perpendicular to the η-axis. The transformed governing equations are shown below. The derivation of these equations is shown in Appendix A.

Liquid Continuity:

$$\frac{1}{r\delta}\frac{\partial}{\partial\chi}\left(r\delta\rho_{\mathrm{L}}u_{\mathrm{L}}\right)+\frac{1}{r\delta}\frac{\partial}{\partial\eta}\left(rJ_{\mathrm{L}}''\right)=0 \tag{4.4}$$

Liquid Momentum:

$$\frac{1}{r\delta}\frac{\partial}{\partial\chi}\left(r\delta\rho_{\mathrm{L}}u_{\mathrm{L}}u_{\mathrm{L}}\right)+\frac{1}{r\delta}\frac{\partial}{\partial\eta}\left(rJ_{\mathrm{L}}''u_{\mathrm{L}}\right)=\frac{1}{r\delta}\frac{\partial}{\partial\eta}\left(\frac{r\mu_{\mathrm{L,eff}}}{\delta}\frac{\partial u_{\mathrm{L}}}{\partial\eta}\right)+\rho_{\mathrm{L}}g-\frac{dP}{d\chi} \tag{4.5}$$

Liquid Energy:

$$\frac{1}{r\delta}\frac{\partial}{\partial\chi}\left(r\delta\rho_{\mathrm{L}}u_{\mathrm{L}}C_{P,\mathrm{L}}T_{\mathrm{L}}\right)+\frac{1}{r\delta}\frac{\partial}{\partial\eta}\left(rJ_{\mathrm{L}}''C_{P,\mathrm{L}}T_{\mathrm{L}}\right)=\frac{1}{r\delta}\frac{\partial}{\partial\eta}\left(\frac{r\lambda_{\mathrm{L,eff}}}{\delta}\frac{\partial T_{\mathrm{L}}}{\partial\eta}\right) \tag{4.6}$$

Liquid Kinetic Energy Equation:

$$\begin{aligned}&\frac{1}{r\delta}\frac{\partial}{\partial\chi}\left(r\delta\rho_{\mathrm{L}}u_{\mathrm{L}}k_{\mathrm{L}}\right)+\frac{1}{r\delta}\frac{\partial}{\partial\eta}\left(rJ_{\mathrm{L}}''k_{\mathrm{L}}\right)=\\&\frac{1}{r\delta}\frac{\partial}{\partial\eta}\left[\frac{r}{\delta}\left(\mu_{\mathrm{L}}+\frac{\mu_{\mathrm{L}}^{\mathrm{t}}}{\sigma_k}\right)\frac{\partial k_{\mathrm{L}}}{\partial\eta}\right]+\mu_{\mathrm{L}}^{\mathrm{t}}\left[\frac{1}{\delta}\frac{\partial u_L}{\partial\eta}\right]^2-\rho_{\mathrm{L}}\varepsilon_{\mathrm{L}}-2\mu_{\mathrm{L}}\left(\frac{1}{\delta}\frac{\partial\sqrt{k_{\mathrm{L}}}}{\partial\eta}\right)^2\end{aligned} \tag{4.7}$$

Liquid Dissipation Equation:

$$\frac{1}{r\delta}\frac{\partial}{\partial\chi}\left(r\delta\rho_{\mathrm{L}}u_{\mathrm{L}}\varepsilon_{\mathrm{L}}\right)+\frac{1}{r\delta}\frac{\partial}{\partial\eta}\left(rJ_{\mathrm{L}}''\varepsilon_{\mathrm{L}}\right)=\frac{1}{r\delta}\frac{\partial}{\partial\eta}\left[\frac{r}{\delta}\left(\mu_{\mathrm{L}}+\frac{\mu_{\mathrm{L}}^{\mathrm{t}}}{\sigma_{\varepsilon}}\right)\frac{\partial\varepsilon_{\mathrm{L}}}{\partial\eta}\right]$$
$$+C_{\varepsilon 1}\frac{\varepsilon_{\mathrm{L}}}{k_{\mathrm{L}}}\mu_{\mathrm{L}}^{\mathrm{t}}\left[\frac{1}{\delta}\frac{\partial u_{L}}{\partial\eta}\right]^{2}-\rho_{\mathrm{L}}C_{\varepsilon 2}\frac{\varepsilon_{\mathrm{L}}^{\ 2}}{k_{\mathrm{L}}}+\frac{2\mu_{\mathrm{L}}\mu_{\mathrm{L}}^{\mathrm{t}}}{\rho_{\mathrm{L}}\delta^{2}}\left(\frac{\partial^{2}u_{\mathrm{L}}}{\partial\eta}\right)^{2} \tag{4.8}$$

Mixture Continuity:

$$\frac{1}{r(r_{\mathrm{o}}-\delta)}\frac{\partial}{\partial\chi}\left(r(r_{\mathrm{o}}-\delta)\rho_{\mathrm{M}}u_{\mathrm{M}}\right)+\frac{1}{r(r_{\mathrm{o}}-\delta)}\frac{\partial}{\partial\eta}\left(rJ_{\mathrm{M}}''\right)=0 \tag{4.9}$$

Mixture Momentum:

$$\frac{1}{r(r_{\mathrm{o}}-\delta)}\frac{\partial}{\partial\chi}\left(r(r_{\mathrm{o}}-\delta)\rho_{\mathrm{M}}u_{\mathrm{M}}u_{\mathrm{M}}\right)+\frac{1}{r(r_{\mathrm{o}}-\delta)}\frac{\partial}{\partial\eta}\left(rJ_{\mathrm{M}}''u_{\mathrm{M}}\right)$$
$$=\frac{1}{r(r_{\mathrm{o}}-\delta)}\frac{\partial}{\partial\eta}\left(\frac{r\mu_{\mathrm{M,eff}}}{(r_{\mathrm{o}}-\delta)}\frac{\partial u_{\mathrm{M}}}{\partial\eta}\right)+\rho_{\mathrm{M}}g-\frac{dP}{d\chi} \tag{4.10}$$

Mixture Energy:

$$\frac{1}{r(r_{\mathrm{o}}-\delta)}\frac{\partial}{\partial\chi}\left(r(r_{\mathrm{o}}-\delta)\rho_{\mathrm{M}}u_{\mathrm{M}}C_{P,\mathrm{M}}T_{\mathrm{M}}\right)+\frac{1}{r(r_{\mathrm{o}}-\delta)}\frac{\partial}{\partial\eta}\left(rJ_{\mathrm{M}}''C_{P,\mathrm{M}}T_{\mathrm{M}}\right)=$$
$$\frac{1}{r(r_{\mathrm{o}}-\delta)}\frac{\partial}{\partial\eta}\left(\frac{r\lambda_{\mathrm{M,eff}}}{(r_{\mathrm{o}}-\delta)}\frac{\partial T_{\mathrm{M}}}{\partial\eta}\right)+\frac{1}{r(r_{\mathrm{o}}-\delta)}\frac{\partial}{\partial\eta}\left(\frac{r\rho_{\mathrm{M}}D_{\mathrm{eff}}\left(C_{P,\mathrm{g}}-C_{P,\mathrm{v}}\right)T_{\mathrm{M}}}{(r_{\mathrm{o}}-\delta)}\frac{\partial W}{\partial\eta}\right) \tag{4.11}$$

Mixture Mass Diffusion:

$$\frac{1}{r(r_{\mathrm{o}}-\delta)}\frac{\partial}{\partial\chi}\left(r(r_{\mathrm{o}}-\delta)\rho_{\mathrm{M}}u_{\mathrm{M}}W\right)+\frac{1}{r(r_{\mathrm{o}}-\delta)}\frac{\partial}{\partial\eta}\left(rWJ_{\mathrm{M}}''\right)$$
$$=\frac{1}{r(r_{\mathrm{o}}-\delta)}\frac{\partial}{\partial\eta}\left(\frac{r\rho_{\mathrm{M}}D_{\mathrm{eff}}}{(r_{\mathrm{o}}-\delta)}\frac{\partial W}{\partial\eta}\right) \tag{4.12}$$

Overall Mass Conservation:

$$\int_0^1 \rho_M u_M \eta (r_o - \delta)^2 d\eta + \int_1^2 \rho_L u_L \delta(\delta(\eta - 2) + r_o) d\eta = \frac{\dot{m}_{in}}{2\pi} \tag{4.13}$$

Mixture Kinetic Energy Equation:

$$\begin{aligned} &\frac{1}{r(r_o - \delta)} \frac{\partial}{\partial \chi} \left(r(r_o - \delta) \rho_M u_M k_M \right) + \frac{1}{r(r_o - \delta)} \frac{\partial}{\partial \eta} \left(r J''_M k_M \right) = \\ &\frac{1}{r(r_o - \delta)} \frac{\partial}{\partial \eta} \left[\frac{r}{(r_o - \delta)} \left(\mu_M + \frac{\mu_M^t}{\sigma_k} \right) \frac{\partial k_M}{\partial \eta} \right] + \mu_M^t \left[\frac{1}{(r_o - \delta)} \frac{\partial u_M}{\partial \eta} \right]^2 \\ &- \rho_M \varepsilon_M - 2\mu_M \left(\frac{1}{(r_o - \delta)} \frac{\partial \sqrt{k_M}}{\partial \eta} \right)^2 \end{aligned} \tag{4.14}$$

Mixture Dissipation Equation:

$$\begin{aligned} &\frac{1}{r(r_o - \delta)} \frac{\partial}{\partial \chi} \left(r(r_o - \delta) \rho_M u_M \varepsilon_M \right) + \frac{1}{r(r_o - \delta)} \frac{\partial}{\partial \eta} \left(r J''_M \varepsilon_M \right) = \\ &\frac{1}{r(r_o - \delta)} \frac{\partial}{\partial \eta} \left[\frac{r}{(r_o - \delta)} \left(\mu_M + \frac{\mu_M^t}{\sigma_\varepsilon} \right) \frac{\partial \varepsilon_M}{\partial \eta} \right] + C_{\varepsilon 1} \frac{\varepsilon_M}{k_M} \mu_M^t \left[\frac{1}{(r_o - \delta)} \frac{\partial u_M}{\partial \eta} \right]^2 \\ &- C_{\varepsilon 2} \rho_M \frac{{\varepsilon_M}^2}{k_M} + \frac{2\mu_M \mu_M^t}{\rho_M (r_o - \delta)^2} \frac{\partial^2 u_M}{\partial \eta^2} \end{aligned} \tag{4.15}$$

Boundary Conditions:

At the wall, $\eta = 2$

$$u_L = 0 \tag{4.16}$$

$$J''_L = 0 \tag{4.17}$$

$$T_L = T_{wall} \tag{4.18}$$

$$k_L = 0 \tag{4.19}$$

$$\varepsilon_{\mathrm{L}} = 0 \tag{4.20}$$

At the interface, $\eta = 1$

$$u_{\mathrm{L}} = u_{\mathrm{M}} \tag{4.21}$$

$$\frac{\mu_{\mathrm{L,eff}}}{\delta}\frac{\partial u_{\mathrm{L}}}{\partial \eta} = \frac{\mu_{\mathrm{M,eff}}}{(r_{\mathrm{o}} - \delta)}\frac{\partial u_{\mathrm{M}}}{\partial \eta} \tag{4.22}$$

$$J''_{\mathrm{L}} = J''_{\mathrm{M}} \tag{4.23}$$

$$T_{\mathrm{L}} = T_{\mathrm{M}} = T_{\mathrm{sat}} \tag{4.24}$$

$$J''_{\mathrm{M}} W - \frac{\rho_{\mathrm{M}} D_{\mathrm{eff}}}{(r_{\mathrm{o}} - \delta)}\frac{\partial W}{\partial \eta} = 0 \tag{4.25}$$

$$\frac{\lambda_{\mathrm{L,eff}}}{\delta}\frac{\partial T_{\mathrm{L}}}{\partial \eta} = \frac{\lambda_{\mathrm{M,eff}}}{(r_{\mathrm{o}} - \delta)}\frac{\partial T_{\mathrm{M}}}{\partial \eta} - J''_{\mathrm{M}} h_{\mathrm{fg}} \tag{4.26}$$

$$k_{\mathrm{L}} = k_{\mathrm{M}} = 0 \tag{4.27}$$

$$\varepsilon_{\mathrm{L}} = \varepsilon_{\mathrm{M}} = 0 \tag{4.28}$$

At the centerline, $\eta = 0$

$$\frac{\partial u_{\mathrm{M}}}{\partial \eta} = 0 \tag{4.29}$$

$$\frac{\partial T_{\mathrm{M}}}{\partial \eta} = 0 \tag{4.30}$$

$$\frac{\partial W}{\partial \eta} = 0 \tag{4.31}$$

$$J''_{\mathrm{M}} = 0 \tag{4.32}$$

$$\frac{\partial k_M}{\partial \eta} = 0 \tag{4.33}$$

$$\frac{\partial \varepsilon_M}{\partial \eta} = 0 \tag{4.34}$$

4.3 Discretization

4.3.1 Introduction

The transformed equations above were integrated across a control volume of thickness $d\eta$ and length $d\chi$.

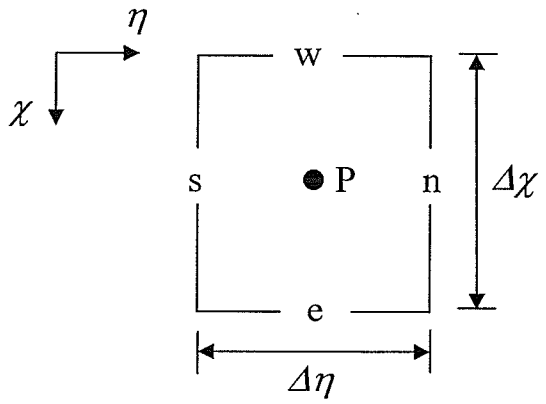

Figure 4.3 Control volume

The integration of the governing equations of motion, energy conservation, and turbulence quantities over a typical control volume as shown in Figure 4.3 above used a finite volume method and resulted in a set of algebraic equations. The resulting equations required north, south, east, and west face values for all the variables and properties. In addition, a Newton Raphson Linearization was used for all the non-linear terms. The

details of the methods followed in discretizing the governing equations and boundary conditions will be discussed throughout this chapter.

4.3.2 Face Values for Variables

The u velocity, temperature, gas mass fraction, kinetic energy, and dissipation (these fields will be represented in general by φ hereafter) at the east and west faces of a control volume were defined using the upwind differencing scheme such that:

$$\varphi_e = \varphi_P \qquad \text{and} \qquad \varphi_w = \varphi_W \tag{4.35}$$

At the north and south faces, an exponential differencing scheme was applied:

$$\varphi_n = (RNP + \alpha_n)\varphi_P + (RNN - \alpha_n)\varphi_N \tag{4.36}$$

$$\varphi_s = (RSS + \alpha_s)\varphi_S + (RSP - \alpha_s)\varphi_P \tag{4.37}$$

where, $RNP = \dfrac{\Delta\eta_N}{\Delta\eta_N + \Delta\eta_P}$ $\qquad RNN = \dfrac{\Delta\eta_P}{\Delta\eta_N + \Delta\eta_P}$

$$RSS = \frac{\Delta\eta_P}{\Delta\eta_S + \Delta\eta_P} \qquad RSP = \frac{\Delta\eta_S}{\Delta\eta_S + \Delta\eta_P} \tag{4.38}$$

The exponential differencing scheme is also used to determine the derivatives at the north and south faces:

$$\frac{\partial \varphi}{\partial \eta_{\mathrm{n}}} = \beta_{\mathrm{n}} \frac{\phi_{\mathrm{N}} - \varphi_{\mathrm{P}}}{\eta_{\mathrm{N}} - \eta_{\mathrm{P}}} \quad , \qquad \text{and} \qquad \frac{\partial \varphi}{\partial \eta_{s}} = \beta_{s} \frac{\phi_{\mathrm{P}} - \varphi_{\mathrm{S}}}{\eta_{\mathrm{P}} - \eta_{\mathrm{S}}} \tag{4.39}$$

$$\text{where } \alpha_{\mathrm{n}} = \frac{0.5 Pe_{\mathrm{n}}{}^{2}}{0.5 + Pe_{\mathrm{n}}{}^{2}}, \qquad \alpha_{\mathrm{s}} = \frac{0.5 Pe_{\mathrm{s}}{}^{2}}{0.5 + Pe_{\mathrm{s}}{}^{2}} \tag{4.40}$$

$$\beta_{\mathrm{n}} = \frac{1 + 0.005 Pe_{\mathrm{n}}{}^{2}}{1 + 0.05 Pe_{\mathrm{n}}{}^{2}}, \qquad \beta_{\mathrm{s}} = \frac{1 + 0.005 Pe_{\mathrm{s}}{}^{2}}{1 + 0.05 Pe_{\mathrm{s}}{}^{2}} \tag{4.41}$$

For the mixture region ($0 \leq \eta \leq 1$):

$$Pe_{\mathrm{n}} = \frac{(r_{\mathrm{o}} - \delta) J_{\mathrm{n}}^{''} (\eta_{\mathrm{N}} - \eta_{\mathrm{P}})}{\Gamma_{\mathrm{n}}}, \quad Pe_{s} = \frac{(r_{\mathrm{o}} - \delta) J_{s}^{''} (\eta_{\mathrm{P}} - \eta_{\mathrm{S}})}{\Gamma_{\mathrm{s}}} \tag{4.42}$$

For the liquid film ($1 \leq \eta \leq 2$):

$$Pe_{\mathrm{n}} = \frac{\delta J_{\mathrm{n}}^{''} (\eta_{\mathrm{N}} - \eta_{\mathrm{P}})}{\Gamma_{\mathrm{n}}}, \qquad Pe_{\mathrm{s}} = \frac{\delta J_{\mathrm{s}}^{''} (\eta_{\mathrm{P}} - \eta_{\mathrm{S}})}{\Gamma_{\mathrm{s}}} \tag{4.43}$$

The diffusion coefficient for all the variables is shown in Table 4.1.

Table 4.1 – Diffusion coefficients

Variable	Γ_n	Γ_s
u_L or u_M	$\mu_n + \mu_n^t$	$\mu_s + \mu_s^t$
T_L or T_M	$\lambda_n/C_{P,n} + \mu_n^t/\mathrm{Pr}^t$	$\lambda_s/C_{P,s} + \mu_s^t/\mathrm{Pr}^t$
W	$\rho_n D_n + \mu_n^t/\mathrm{Sc}^t$	$\rho_n D_s + \mu_s^t/\mathrm{Sc}^t$
k_L or k_M	$\mu_n + \mu_n^t/\sigma_k$	$\mu_s + \mu_s^t/\sigma_k$
ε_L or ε_M	$\mu_n + \mu_n^t/\sigma_\varepsilon$	$\mu_s + \mu_s^t/\sigma_\varepsilon$

The normal mass flow rate, J, was stored at the north face of each control volume:

$$J_n = J_P \qquad \text{and} \qquad J_s = J_S \tag{4.44}$$

The film thickness was assumed to vary linearly across a station:

$$\delta_e = 2\delta_P - \delta_w \tag{4.45}$$

4.3.3 Face Values for Properties

The east and west face values for the properties (ρ, μ, k, C_p and D) were determined using the upwind differencing scheme shown by Equation (4.35). The north and south face values were evaluated using a harmonic mean on a uniform mesh:

$$\varphi_n = \frac{\varphi_P \varphi_N}{f_n \varphi_P + (1 - f_n)\varphi_N} \qquad \varphi_s = \frac{\varphi_S \varphi_P}{f_s \varphi_S + (1 - f_s)\varphi_P} \tag{4.46}$$

where $f_n = \dfrac{\eta_N - \eta_n}{\eta_N - \eta_P}$ and $f_s = \dfrac{\eta_P - \eta_s}{\eta_P - \eta_S}$ (4.47)

4.3.4 Newton Raphson Linearization

If $\Psi = f(\varphi_1, \varphi_2, \varphi_3)$

$\varphi_1 = \{u_L, J_L, T_L, u_M, J_{M,} T_M, W, \delta, P'\}$

And $\varphi_2 = \{u_L, J_L, T_L, u_M, J_{M,} T_M, W, \delta, P'\}$

$\varphi_3 = \{u_L, J_L, T_L, u_M, J_{M,} T_M, W, \delta, P'\}$

Then the general Newton Raphson Linearization would give the following:

$$\Psi^n = \Psi^o + \frac{\partial \Psi^o}{\partial \varphi_1}\left(\varphi_1^n - \varphi_1^o\right) + \frac{\partial \Psi^o}{\partial \varphi_2}\left(\varphi_2^n - \varphi_2^o\right) + \frac{\partial \Psi^o}{\partial \varphi_3}\left(\varphi_3^n - \varphi_3^o\right)$$

The subscript 'n' refers to the current iteration and 'o' refers to the previous iteration.

4.3.5 Discretization Steps

The following steps were taken in discretizing Equations (4.4) to (4.34) above:

1. The equation was integrated across a control volume of thickness $\Delta\eta$ and length $\Delta\chi$, as shown by the following example for the liquid continuity equation (Equation (4.4)): $2\pi \int_w^e \int_s^n \left[\frac{1}{r\delta}\frac{\partial}{\partial \chi}\left(r\delta\rho_L u_L\right) + \frac{1}{r\delta}\frac{\partial}{\partial \eta}\left(rJ_L''\right)\right] r\, d\eta\, d\chi = 0$

2. The upwind differencing scheme given by Equation (4.34) was applied to all the east and west variables and properties, Equation (4.44) was applied to the east and

west film thicknesses and Equation (4.43) was applied to the north and south face mass fluxes.

3. The Newton Raphson Linearization discussed above was applied to all the non-linear terms.
4. The exponential differencing scheme was applied to all the variables and derivatives at the north and south faces.
5. The dependent variables were factored out and grouped into separate terms.

Detailed steps will be shown in Section 4.3.6 below for discretizing the mixture momentum equation.

The coefficients of the resulting algebraic equations can be found in Appendices B, C and D and are represented as follows:

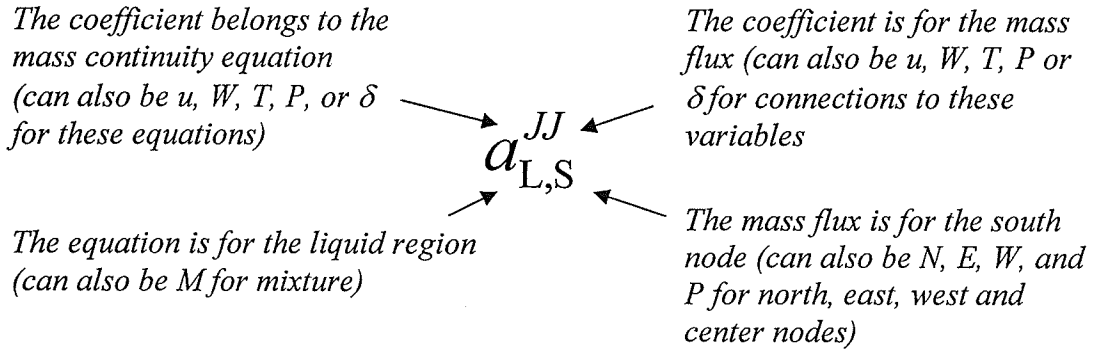

4.3.6 Discretized Governing Equations

Liquid continuity equation:

$$a^{JJ}_{L,S} J_{L,S} + a^{Ju}_{L,P} u_{L,P} + a^{JJ}_{L,P} J_{L,P} + a^{J\delta}_{L,P} \delta_P = b^{J}_{L,P} \qquad (4.48)$$

Liquid momentum equation:

$$a_{\mathrm{L,S}}^{uu}u_{\mathrm{L,S}} + a_{\mathrm{L,S}}^{uJ}J_{\mathrm{L,S}} + a_{\mathrm{L,P}}^{uu}u_{\mathrm{L,P}} + a_{\mathrm{L,P}}^{uJ}J_{\mathrm{L,P}} + a_{\mathrm{L,N}}^{uu}u_{L,N} + a_{\mathrm{L,P}}^{u\delta}\delta_P + a_{\mathrm{L,P}}^{uP}P_{\mathrm{P}}^{'} = b_{\mathrm{L,P}}^{u} \tag{4.49}$$

Liquid energy equation:

$$a_{\mathrm{L,S}}^{TJ}J_{\mathrm{L,S}} + a_{\mathrm{L,S}}^{TT}T_{\mathrm{L,S}} + a_{\mathrm{L,P}}^{Tu}u_{\mathrm{L,P}} + a_{\mathrm{L,P}}^{TJ}J_{\mathrm{L,P}} + a_{\mathrm{L,P}}^{TT}T_{\mathrm{L,P}} + a_{\mathrm{L,N}}^{TT}T_{\mathrm{L,N}} + a_{\mathrm{L,P}}^{T\delta}\delta_{\mathrm{P}} = b_{\mathrm{L,P}}^{T} \tag{4.50}$$

Mixture continuity equation:

$$a_{\mathrm{M,S}}^{JJ}J_{\mathrm{M,S}} + a_{\mathrm{M,P}}^{Ju}u_{\mathrm{M,P}} + a_{\mathrm{M,P}}^{JJ}J_{\mathrm{M,P}} + a_{\mathrm{M,P}}^{J\delta}\delta_{\mathrm{P}} = b_{\mathrm{M,P}}^{J} \tag{4.51}$$

Mixture momentum equation:

1. Multiply Equation (4.10) by $2\pi r(r_o-\delta)$ and integrate:

$$2\pi\int_{\mathrm{w}}^{\mathrm{e}}\int_{\mathrm{s}}^{\mathrm{n}}\frac{\partial}{\partial\chi}\left(\eta(r_{\mathrm{o}}-\delta)^2\rho_{\mathrm{M}}u_{\mathrm{M}}u_{\mathrm{M}}\right)d\eta\,d\chi + 2\pi\int_{\mathrm{w}}^{\mathrm{e}}\int_{\mathrm{s}}^{\mathrm{n}}\frac{\partial}{\partial\eta}\left(\eta(r_{\mathrm{o}}-\delta)J_{\mathrm{M}}^{''}u_{\mathrm{M}}\right)d\eta\,d\chi$$
$$= 2\pi\int_{\mathrm{w}}^{\mathrm{e}}\int_{\mathrm{s}}^{\mathrm{n}}\frac{\partial}{\partial\eta}\left(\eta\mu_{\mathrm{M,eff}}\frac{\partial u_{\mathrm{M}}}{\partial\eta}\right)d\eta\,d\chi + 2\pi\int_{\mathrm{w}}^{\mathrm{e}}\int_{\mathrm{s}}^{\mathrm{n}}\eta(r_{\mathrm{o}}-\delta)^2\rho_{\mathrm{M}}g\,d\eta\,d\chi$$
$$- 2\pi\int_{\mathrm{w}}^{\mathrm{e}}\int_{\mathrm{s}}^{\mathrm{n}}\eta(r_{\mathrm{o}}-\delta)^2P'd\eta\,d\chi$$

$$2\pi\int_{\mathrm{w}}^{\mathrm{e}}\frac{\partial}{\partial\chi}\left(\eta(r_{\mathrm{o}}-\delta)^2\rho_{\mathrm{M}}u_{\mathrm{M}}u_{\mathrm{M}}\right)\Delta\eta\,d\chi +$$
$$2\pi\int_{\mathrm{w}}^{\mathrm{e}}\left(\eta_{\mathrm{n}}(r_o-\delta)J_{\mathrm{M,n}}^{''}u_{\mathrm{M,n}} - \eta_{\mathrm{s}}(r_{\mathrm{o}}-\delta)J_{\mathrm{M,s}}^{''}u_{\mathrm{M,s}}\right)d\chi =$$
$$2\pi\int_{\mathrm{w}}^{\mathrm{e}}\left(\eta_{\mathrm{n}}\mu_{\mathrm{M,n,eff}}\left.\frac{\partial u_{\mathrm{M}}}{\partial\eta}\right|_{\mathrm{n}} - \eta_{\mathrm{s}}\mu_{\mathrm{M,s,eff}}\left.\frac{\partial u_{\mathrm{M}}}{\partial\eta}\right|_{\mathrm{s}}\right)d\chi + 2\pi\int_{\mathrm{w}}^{\mathrm{e}}\eta(r_{\mathrm{o}}-\delta)^2\rho_{\mathrm{M}}g\Delta\eta\,d\chi$$
$$- 2\pi\int_{\mathrm{w}}^{\mathrm{e}}\eta(r_{\mathrm{o}}-\delta)^2P'\Delta\eta\,d\chi$$

$$2\pi\left(\eta_P\left(r_o-\delta_e\right)^2\rho_{M,e}u_{M,e}u_{M,e}-\eta_P\left(r_o-\delta_w\right)^2\rho_{M,w}u_{M,w}u_{M,w}\right)\Delta\eta$$
$$+2\pi\left(\eta_n\left(r_o-\delta_P\right)J''_{M,n}u_{M,n}-\eta_s\left(r_o-\delta_P\right)J''_{M,s}u_{M,s}\right)\Delta\chi=$$
$$2\pi\left(\eta_n\mu_{M,n,eff}\left.\frac{\partial u_M}{\partial\eta}\right|_n-\eta_s\mu_{M,s,eff}\left.\frac{\partial u_M}{\partial\eta}\right|_s\right)\Delta\chi+2\pi\eta_P\left(r_o-\delta_P\right)^2\rho_{M,P}g\Delta\eta\Delta\chi$$
$$-2\pi\eta_P\left(r_o-\delta_P\right)^2P'_P\Delta\eta\Delta\chi$$

2. Use the upwind differencing scheme on all the east and west face variables and properties, Equation (4.45) on the east face film thickness and Equation (4.44) on the north and south face mass fluxes.

$$2\pi\left(\eta_P\left(r_o-\left(2\delta_P-\delta_w\right)\right)^2\rho_{M,P}u_{M,P}u_{M,P}-\eta_P\left(r_o-\delta_w\right)^2\rho_{M,W}u_{M,W}u_{M,W}\right)\Delta\eta$$
$$+\left(J_{M,P}u_{M,n}-J_{M,S}u_{M,s}\right)\Delta\chi=2\pi\left(\eta_n\mu_{M,n,eff}\left.\frac{\partial u_M}{\partial\eta}\right|_n-\eta_s\mu_{M,s,eff}\left.\frac{\partial u_M}{\partial\eta}\right|_s\right)\Delta\chi$$
$$+2\pi\eta_P\left(r_o-\delta_P\right)^2\rho_{M,P}g\Delta\eta\Delta\chi-2\pi\eta_P\left(r_o-\delta_P\right)^2P'_P\Delta\eta\Delta\chi$$

Expand the above equation to get the following:

$$2\pi\eta_P\Delta\eta\left(r_o^{\,2}+\delta_w^{\,2}+2\delta_w r_o\right)\rho_{M,P}u_{M,P}u_{M,P}+8\pi\eta_P\Delta\eta\delta_P^{\,2}\rho_{M,P}u_{M,P}u_{M,P}$$
$$-8\pi\eta_{M,P}\Delta\eta\delta_P\left(r_o+\delta_w\right)\rho_{M,P}u_{M,P}u_{M,P}-2\pi\eta_P\Delta\eta\left(r_o-\delta_w\right)^2\rho_{M,W}u_{M,W}u_{M,W}$$
$$+J_{M,P}u_{M,n}\Delta\chi-J_{M,S}u_{M,s}\Delta\chi=2\pi\eta_n\mu_{M,n,eff}\left.\frac{\partial u_M}{\partial\eta}\right|_n\Delta\chi-2\pi\eta_s\mu_{M,s,eff}\left.\frac{\partial u_M}{\partial\eta}\right|_s\Delta\chi$$
$$+2\pi\eta r_o^{\,2}\rho_M g\Delta\eta\Delta\chi-4\pi\eta r_o\delta_P\rho_M g\Delta\eta\Delta\chi+2\pi\eta\delta_P^{\,2}\rho_M g\Delta\eta\Delta\chi$$
$$-2\pi\eta r_o^{\,2}P'_P\Delta\eta\Delta\chi+4\pi\eta r_o\delta_P P'_P\Delta\eta\Delta\chi-2\pi\eta\delta_P^{\,2}P'_P\Delta\eta\Delta\chi$$

3. Use Newton Raphson Linearization on all the non-linear terms:

$$
\begin{aligned}
&2\pi\eta_P\Delta\eta\left(r_o^{\,2}+\delta_w^{\,2}+2\delta_w r_o\right)\rho_{M,P}\left(2u^o_{M,P}u^n_{M,P}-u^o_{M,P}u^o_{M,P}\right)\\
&+8\pi\eta_P\Delta\eta\rho_{M,P}\left(2\delta_P^{o\,2}u^o_{M,P}u^n_{M,P}+2u^o_{M,P}{}^2\delta^n_P\delta^o_P-3u^o_{M,P}{}^2\delta_P^{o\,2}\right)\\
&-8\pi\eta_P\Delta\eta\left(r_o+\delta_w\right)\rho_{M,P}\left(2\delta^o_P u^o_{M,P}u^n_{M,P}+\delta^n_P u^o_{M,P}{}^2-2\delta^o_P u^o_{M,P}u^o_{M,P}\right)\\
&-2\pi\eta_P\Delta\eta\left(r_o-\delta_w\right)^2\rho_{M,W}u_{M,W}u_{M,W}\\
&+\left(J^n_{M,P}u^o_{M,n}+J^o_{M,P}u^n_{M,n}-J^o_{M,P}u^o_{M,n}\right)-\left(J^n_{M,S}u^o_{M,s}+J^o_{M,S}u^n_{M,s}-J^o_{M,S}u^o_{M,s}\right)\\
&=2\pi\eta_n\mu_{M,n,eff}\left.\frac{\partial u_M}{\partial\eta}\right|_n\Delta\chi-2\pi\eta_s\mu_{M,s,eff}\left.\frac{\partial u_M}{\partial\eta}\right|_s\Delta\chi+2\pi\eta r_o^{\,2}\rho_{M,P}g\Delta\eta\Delta\chi
\end{aligned}
$$

$$
\begin{aligned}
&-4\pi\eta_P r_o\delta^n_P\rho_{M,P}g\Delta\eta_M\Delta\chi+2\pi\eta_P\rho_{M,P}g\Delta\eta\Delta\chi\left(2\delta^o_P\delta^n_P-\delta_P^{o\,2}\right)-2\pi\eta_P r_o^{\,2}\left.\frac{dP}{d\chi}\right|^n_P\Delta\eta\Delta\chi\\
&+4\pi\eta_P r_o\left(\delta^n_P P'^o_P+\delta^o_P P'^n_P-\delta^o_P P'^o_P\right)\Delta\eta\Delta\chi\\
&-2\pi\eta_P\left(2\delta^n_P\delta^o_P P'^o_P+\delta_P^{o\,2}P'^n_P-2\delta_P^{o\,2}P'^o_P\right)\Delta\eta\Delta\chi
\end{aligned}
$$

4. Use the exponential differencing scheme on the current ('n') north and south face variables and the north and south derivatives:

$$
\begin{aligned}
&2\pi\eta_P\Delta\eta\left(r_o^{\,2}+\delta_w^{\,2}+2\delta_w r_o\right)\rho_{M,P}\left(2u^o_{M,P}u^n_{M,P}-u^o_{M,P}u^o_{M,P}\right)\\
&+8\pi\eta_P\Delta\eta\rho_{M,P}\left(2\delta_P^{o\,2}u^o_{M,P}u^n_{M,P}+2u^o_{M,P}{}^2\delta^n_P\delta^o_P-3u^o_{M,P}{}^2\delta_P^{o\,2}\right)\\
&-8\pi\eta_P\Delta\eta\left(r_o+\delta_w\right)\rho_{M,P}\left(2\delta^o_P u^o_{M,P}u^n_{M,P}+\delta^n_P u^o_{M,P}{}^2-2\delta^o_P u^o_{M,P}u^o_{M,P}\right)\\
&-2\pi\eta_P\Delta\eta\left(r_o-\delta_w\right)^2\rho_{M,W}u_{M,W}u_{M,W}\\
&+\left(J^n_{M,N}u^o_{M,n}+J^o_{M,N}\left(\left(RNP+\alpha^u_n\right)u^n_{M,P}+\left(RNN-\alpha^u_n\right)u^n_{M,N}\right)-J^o_{M,N}u^o_{M,n}\right)\\
&-\left(J^n_{M,S}u^o_{M,s}+J^o_{M,S}\left(\left(RSS+\alpha^u_s\right)u^n_{M,S}+\left(RSP-\alpha^u_s\right)u^n_{M,P}\right)-J^o_{M,S}u^o_{M,s}\right)\\
&=2\pi\eta_n\mu_{M,n,eff}\left(\beta^u_n\frac{u^n_{M,N}-u^n_{M,P}}{\eta_N-\eta_P}\right)\Delta\chi-2\pi\eta_s\mu_{M,s,eff}\left(\beta^u_s\frac{u^n_{M,P}-u^n_{M,S}}{\eta_P-\eta_S}\right)\Delta\chi\\
&+2\pi\eta_P r_o^{\,2}\rho_{M,P}g\Delta\eta\Delta\chi-4\pi\eta_P r_o\delta^n_P\rho_{M,P}g\Delta\eta\Delta\chi+2\pi\eta_P\rho_{M,P}g\Delta\eta\Delta\chi\left(2\delta^o_P\delta^n_P-\delta_P^{o\,2}\right)\\
&-2\pi\eta_P r_o^{\,2}P'^n_P\Delta\eta\Delta\chi+4\pi\eta_P r_o\left(\delta^n_P P'^o_P+\delta^o_P P'^n_P-\delta_P{}^o P'^o_P\right)\Delta\eta\Delta\chi\\
&-2\pi\eta_P\left(2\delta^n_P\delta^o_P P'^o_P+\delta_P^{o\,2}P'^n_P-2\delta_P^{o\,2}P'^o_P\right)\Delta\eta\Delta\chi
\end{aligned}
$$

5. Now factor out the dependent variables and group them together

$$\left[-\left(RSS+\alpha_s^u\right)J_{M,S}^o-2\pi\eta_s\mu_{M,s,eff}\left(\frac{\beta_s^u}{\eta_P-\eta_S}\right)\Delta\chi\right]u_{M,S}^n-J_{M,S}^n u_{M,s}^o$$

$$\left[\begin{array}{l}4\pi\eta_P\Delta\eta\left(r_o-2\delta_P+\delta_w\right)^2\rho_{M,P}u_{M,P}^o\\+\left(RNP+\alpha_n^u\right)J_{M,P}^o-\left(RSP-\alpha_s^u\right)J_{M,S}^o\\+2\pi\eta_n\mu_{M,n,eff}\left(\frac{\beta_n^u}{\eta_N-\eta_P}\right)\Delta\chi+2\pi\eta_s\mu_{M,s,eff}\left(\frac{\beta_s^u}{\eta_P-\eta_S}\right)\Delta\chi\end{array}\right]u_{M,P}^n+J_{M,P}^n u_{M,n}^o$$

$$+\left[\left(RNN-\alpha_n^u\right)J_{M,P}^o-2\pi\eta_n\mu_{M,n,eff}\left(\frac{\beta_n^u}{\eta_N-\eta_P}\right)\Delta\chi\right]u_{M,N}^n$$

$$+\left[\begin{array}{l}-8\pi\eta_P\Delta\eta\left(r_o-2\delta_P^o+\delta_w\right)\rho_{M,P}{u_{M,P}^o}^2\\+4\pi\eta_P\rho_{M,P}g\Delta\eta\Delta\chi(r_o-\delta_P^o)-4\pi\eta_P P_P'^o\Delta\eta\Delta\chi(r_o-\delta_P^o)\end{array}\right]\delta_P^n$$

$$+2\pi\eta_P\Delta\eta\Delta\chi(r_o-\delta_P^o)^2P_P'^n=2\pi\eta_P\Delta\eta\left(r_o-\delta_e^o\right)^2\rho_{M,P}u_{M,P}^o u_{M,P}^o$$

$$-8\pi\eta_P\Delta\eta\rho_{M,P}{u_{M,P}^o}^2\left(r_o-\delta_e^o\right)\delta_P^o+2\pi\eta_P\Delta\eta\left(r_o-\delta_w\right)^2\rho_{M,W}{u_{M,W}}^2$$

$$+2\pi\eta_P\rho_{M,P}g\Delta\eta\Delta\chi({r_o}^2-{\delta_P^o}^2)+4\pi\eta_p\delta_P^o P_P'^o\Delta\eta\Delta\chi(r_o-\delta_P^o)+J_{M,P}^o{u_{M,n}}^o-J_{M,S}^o u_{M,s}^o$$

Where *RSP*, *RSS*, *RNP*, and *RNN* are defined by Equation (4.38).

The resulting equation takes the following form:

$$a_{M,S}^{uu}u_{M,S}+a_{M,S}^{uJ}J_{M,S}+a_{M,P}^{uu}u_{M,P}+a_{M,P}^{uJ}J_{M,P}+a_{M,N}^{uu}u_{M,N}+a_{M,P}^{u\delta}\delta_P+a_{M,P}^{uP}P_P'=b_{M,P}^u \qquad (4.52)$$

where,

$$a_{M,S}^{uu}=-\left(RSS+\alpha_s^u\right)J_{M,S}^o-2\pi\eta_s\frac{\beta_{M,s}^u\mu_{M,s,eff}\Delta\chi}{\left(\eta_P-\eta_S\right)}$$

$$a_{M,S}^{uJ}=-u_{M,s}^o$$

$$a_{\mathrm{M,P}}^{uu} = 4\pi\left(r_{\mathrm{o}} - \delta_{\mathrm{e}}^{\mathrm{o}}\right)^2 \rho_{\mathrm{M,P}} u_{\mathrm{M,P}}^{\mathrm{o}} \eta_{\mathrm{P}} \Delta\eta + \left(RNP + \alpha_{\mathrm{n}}^{u}\right) J_{\mathrm{M,P}}^{\mathrm{o}} - \left(RSP - \alpha_{\mathrm{s}}^{u}\right) J_{\mathrm{M,S}}^{\mathrm{o}}$$
$$+ 2\pi\eta_{\mathrm{n}} \mu_{\mathrm{M,n,eff}} \left(\frac{\beta_{\mathrm{n}}^{u}}{\eta_{\mathrm{N}} - \eta_{\mathrm{P}}}\right) \Delta\chi + 2\pi\eta_{\mathrm{s}} \mu_{\mathrm{M,s,eff}} \left(\frac{\beta_{\mathrm{s}}^{u}}{\eta_{\mathrm{P}} - \eta_{\mathrm{S}}}\right) \Delta\chi$$

$$a_{\mathrm{M,P}}^{uJ} = u_{\mathrm{M,n}}^{\mathrm{o}}$$

$$a_{\mathrm{M,N}}^{uu} = \left(RNN - \alpha_{\mathrm{n}}^{u}\right) J_{\mathrm{M,P}}{}^{\mathrm{o}} - 2\pi\eta_{\mathrm{n}} \frac{\beta_{\mathrm{n}}^{u} \mu_{\mathrm{M,n,eff}} \Delta\chi}{\left(\eta_{\mathrm{N}} - \eta_{\mathrm{P}}\right)}$$

$$a_{\mathrm{M,P}}^{u\delta} = -8\pi\eta_{\mathrm{P}} \Delta\eta \left(r_{\mathrm{o}} - \delta_{\mathrm{e}}^{\mathrm{o}}\right) \rho_{\mathrm{M,P}} u_{\mathrm{M,P}}^{\mathrm{o}}{}^2$$
$$+ 4\pi\eta_{\mathrm{P}} \rho_{\mathrm{M,P}} g \Delta\eta \Delta\chi (r_{\mathrm{o}} - \delta_{\mathrm{P}}^{\mathrm{o}}) - 4\pi\eta_{\mathrm{P}} P_{\mathrm{P}}'^{\mathrm{o}} \Delta\eta \Delta\chi (r_{\mathrm{o}} - \delta_{\mathrm{P}}^{\mathrm{o}})$$

$$a_{M,P}^{up} = 2\pi\left(r_{\mathrm{o}} - \delta_{\mathrm{P}}^{\mathrm{o}}\right)^2 \eta_{\mathrm{P}} \Delta\eta \Delta\chi$$

$$b_{\mathrm{M,P}}^{u} = 2\pi\eta_{\mathrm{P}} \Delta\eta \left(r_{\mathrm{o}} - \delta_{\mathrm{e}}^{\mathrm{o}}\right)^2 \rho_{\mathrm{M,P}} u_{\mathrm{M,P}}^{\mathrm{o}} u_{\mathrm{M,P}}^{\mathrm{o}} - 8\pi\eta_{\mathrm{P}} \Delta\eta \rho_{\mathrm{M,P}} u_{\mathrm{M,P}}^{\mathrm{o}}{}^2 \left(r_{\mathrm{o}} - \delta_{\mathrm{e}}^{\mathrm{o}}\right) \delta_{\mathrm{P}}^{\mathrm{o}}$$
$$+ 2\pi\eta_{\mathrm{P}} \Delta\eta \left(r_{\mathrm{o}} - \delta_{\mathrm{w}}\right)^2 \rho_{\mathrm{M,W}} u_{\mathrm{M,W}}{}^2 + 2\pi\eta_{\mathrm{P}} \rho_{\mathrm{M,P}} g \Delta\eta \Delta\chi (r_{\mathrm{o}}{}^2 - \delta_{\mathrm{P}}^{\mathrm{o}2})$$
$$+ 4\pi\eta_{\mathrm{P}} \delta_{\mathrm{P}}{}^{\mathrm{o}} P_{\mathrm{P}}'^{\mathrm{o}} \Delta\eta \Delta\chi (r_{\mathrm{o}} - \delta_{\mathrm{P}}{}^{\mathrm{o}}) + J_{\mathrm{M,P}}^{\mathrm{o}} u_{\mathrm{M,n}}^{\mathrm{o}} - J_{\mathrm{M,S}}^{\mathrm{o}} u_{\mathrm{M,s}}^{\mathrm{o}}$$

Mixture energy equation:

$$a_{\mathrm{M,S}}^{TJ} J_{\mathrm{M,S}} + a_{\mathrm{M,S}}^{TT} T_{\mathrm{M,S}} + a_{M,S}^{TW} W_{\mathrm{S}} + a_{\mathrm{M,P}}^{Tu} u_{\mathrm{M,P}} + a_{\mathrm{M,P}}^{TJ} J_{\mathrm{M,P}} +$$
$$a_{\mathrm{M,P}}^{TT} T_{\mathrm{M,P}} + a_{\mathrm{M,P}}^{TW} W_{\mathrm{P}} + a_{\mathrm{M,N}}^{TT} T_{\mathrm{M,N}} + a_{\mathrm{M,N}}^{TW} W_{\mathrm{N}} + a_{\mathrm{M,P}}^{T\delta} \delta_{\mathrm{P}} = b_{\mathrm{M,P}}^{T} \tag{4.53}$$

Mixture mass diffusion equation:

$$a_{\mathrm{M,S}}^{WJ} J_{\mathrm{M,S}} + a_{\mathrm{M,S}}^{WW} W_{\mathrm{S}} + a_{\mathrm{M,P}}^{Wu} u_{\mathrm{M,P}} + a_{\mathrm{M,P}}^{WJ} J_{\mathrm{M,P}} + a_{\mathrm{M,P}}^{WW} W_{\mathrm{P}} + a_{M,N}^{WW} W_{N} + a_{\mathrm{M,P}}^{W\delta} \delta_{\mathrm{P}} = b_{\mathrm{M,P}}^{W} \tag{4.54}$$

4.3.7 Discretized *k-ε* Equations

Liquid kinetic energy equation:

$$a_{\mathrm{L,S}}^{kk} k_{\mathrm{L,S}} + a_{\mathrm{L,N}}^{kk} k_{\mathrm{L,N}} + a_{\mathrm{L,P}}^{kk} k_{\mathrm{L,P}} = b_{\mathrm{L,P}}^{k} \tag{4.55}$$

Liquid dissipation equation:

$$a_{\mathrm{L,S}}^{\varepsilon\varepsilon}\varepsilon_{\mathrm{L,S}} + a_{\mathrm{L,N}}^{\varepsilon\varepsilon}\varepsilon_{\mathrm{L,N}} + a_{\mathrm{L,P}}^{\varepsilon\varepsilon}\varepsilon_{\mathrm{L,P}} = b_{\mathrm{L,P}}^{\varepsilon} \tag{4.56}$$

Mixture kinetic energy equation:

$$a_{\mathrm{M,S}}^{kk}k_{\mathrm{M,S}} + a_{\mathrm{M,N}}^{kk}k_{\mathrm{M,N}} + a_{\mathrm{M,P}}^{kk}k_{\mathrm{M,P}} = b_{\mathrm{M,P}}^{k} \tag{4.57}$$

Mixture dissipation equation:

$$a_{\mathrm{M,S}}^{\varepsilon\varepsilon}\varepsilon_{\mathrm{M,S}} + a_{\mathrm{M,N}}^{\varepsilon\varepsilon}\varepsilon_{\mathrm{M,N}} + a_{\mathrm{M,P}}^{\varepsilon\varepsilon}\varepsilon_{\mathrm{M,P}} = b_{\mathrm{M,P}}^{\varepsilon} \tag{4.58}$$

4.3.8 Discretized Boundary Conditions

At the tube wall ($\eta = 2$)

$$J_{\mathrm{L,P}} = 0 \tag{4.59}$$

$$u_{\mathrm{L,P}} = 0 \tag{4.60}$$

$$T_{\mathrm{L,P}} = T_{\mathrm{wall}} \tag{4.61}$$

At the interface ($\eta = 1$)

Mass continuity at the interface:

$$a_{\mathrm{I,S}}^{JJ}J_{M,S} + a_{\mathrm{I,P}}^{JJ}J_{\mathrm{L,P}} = b_{\mathrm{I,P}}^{J} \tag{4.62}$$

Equating shear stresses at the interface:

$$a_{\mathrm{I,S}}^{uu}u_{\mathrm{M,S}} + a_{\mathrm{I,P}}^{uu}u_{\mathrm{L,P}} + a_{\mathrm{I,N}}^{uu}u_{\mathrm{L,N}} + a_{\mathrm{I,P}}^{u\delta}\delta_{\mathrm{P}} = b_{\mathrm{I,P}}^{u} \tag{4.63}$$

Saturated temperature at the interface:

$$a_{\mathrm{I,P}}^{TT} T_{\mathrm{M,P}} + a_{\mathrm{I,P}}^{TW} W_{\mathrm{P}} + a_{\mathrm{I,P}}^{TP} P_{\mathrm{P}}^{'} = b_{\mathrm{I,P}}^{T} \tag{4.64}$$

Impermeability at the interface:

$$a_{\mathrm{I,S}}^{WJ} J_{\mathrm{M,S}} + a_{\mathrm{I,P}}^{WW} W_{\mathrm{P}} + a_{\mathrm{I,S}}^{WW} W_{\mathrm{S}} + a_{\mathrm{I,P}}^{u\delta} \delta_{\mathrm{P}} = b_{\mathrm{I,P}}^{W} \tag{4.65}$$

Energy conservation at the interface:

$$a_{\mathrm{I,S}}^{\delta T} T_{\mathrm{M,S}} + a_{\mathrm{I,P}}^{\delta J} J_{\mathrm{L,P}} + a_{\mathrm{I,P}}^{\delta T} T_{\mathrm{L,P}} + a_{\mathrm{I,N}}^{\delta T} T_{\mathrm{L,N}} + a_{\mathrm{I,P}}^{\delta\delta} \delta_{\mathrm{P}} = b_{\mathrm{I,P}}^{\delta} \tag{4.66}$$

At the centerline ($\eta = 0$)

$$J_{\mathrm{M,P}} = 0 \tag{4.67}$$

$$u_{\mathrm{M,P}} = u_{\mathrm{M,N}} \tag{4.68}$$

$$T_{\mathrm{M,P}} = T_{\mathrm{M,N}} \tag{4.69}$$

$$W_{\mathrm{P}} = W_{\mathrm{N}} \tag{4.70}$$

Finally, the discretized mass balance equation results in the following algebraic equation:

$$\sum_{jm-1}^{NM-1} a_{\mathrm{M},jm}^{Pu} u_{\mathrm{M},jm} + \sum_{jl-1}^{NL} a_{\mathrm{L},jl}^{Pu} u_{\mathrm{L},jl} + a_{\mathrm{P}}^{P\delta} \delta_{\mathrm{P}} = b_{\mathrm{P}}^{P} \tag{4.71}$$

4.4 Solving the Discretized Conservation Equations

A computer code was developed in-house to solve the above set of discretized equations.

The algorithm on which this code was based is described in the following sections.

4.4.1 Construction of the Matrix

Starting at the first station, a matrix was constructed using the linearized, discretized governing Equations (4.48) to (4.50) for the liquid film and (4.53 to 4.56) for the mixture, the boundary conditions and the overall mass conservation equation (4.71). The turbulent kinetic energy and dissipation equations were not included in this matrix; they were calculated separately using a Tri-Diagonal Matrix Algorithm (TDMA). This will be discussed in Section 4.5.

The unknowns in the matrix are the mass flux, J, the velocity, u, the temperature, T, the gas mass fraction, W, the film thickness, δ, and the pressure gradient, P'. The four variables, J, u, T, and W make up a block matrix for each control volume and row of the matrix. The continuity equation was used to solve for J, the momentum equation for u, the energy equation for T, and the mass diffusion equation for W. These block matrices are followed by the two scalar variables δ and P'. The interfacial energy equation is used to solve for δ and the global mass balance equation for P'. Equation (4.72) below shows how the matrix was set up. The first row of the matrix represents the node at the tube centerline ($j_M = 1$), row NM represents the node at the interface ($j_M = NM$, $j_L = 1$) and row $NM + NL$ represents the node at the wall ($j_L = NL$). The last two rows in the matrix are for calculating the film thickness and the pressure gradient respectively. More details on the individual matrix entries are shown in Appendix E.

$$\begin{bmatrix} A_{M,P} & A_{M,N} & & & & & & & \vdots \\ 1 & 1 & & & & & & & \\ A_{M,S} & A_{M,P} & A_{M,N} & & & & & & \\ 2 & 2 & 2 & & & & & & \\ & \ddots & \ddots & \ddots & & & & & \\ & & A_{M,S} & A_{M,P} & A_{M,N} & & & & \\ & & NM-1 & NM-1 & NM-1 & & & & \\ & & & A_{I,S} & A_{I,P} & A_{I,N} & & & E_2 \\ & & & & A_{L,S} & A_{L,P} & A_{L,N} & & \\ & & & & 2 & 2 & 2 & & \\ & & & & & \ddots & \ddots & \ddots & \\ & & & & & & A_{L,S} & A_{L,P} & A_{L,N} \\ & & & & & & NL-1 & NL-1 & NL-1 \\ & & & & & & & A_{L,S} & A_{L,P} \\ & & & & & & & NL & NL \\ \cdots & & & & E_1 & & & \cdots & E_3 \end{bmatrix} \begin{bmatrix} \vdots \\ \\ \\ \\ \\ X_1 \\ \\ \\ \\ \vdots \\ X_2 \end{bmatrix} \begin{bmatrix} \vdots \\ \\ \\ \\ \\ B_1 \\ \\ \\ \\ \vdots \\ B_2 \end{bmatrix} \quad (4.72)$$

4.4.2 Solving the Matrix

From Equation (4.72) above it can be seen that the off-diagonal entries of the bordered block matrix are mainly zeroes. For this reason, it would be very inefficient to solve this matrix using a conventional solver such as Gauss elimination. In order to reduce the computation effort, a direct solver was developed based on the bordered matrix algorithm discussed by Behie et al. (1985) and the standard block-tridiagonal matrix algorithm (BTDMA).

Equation (4.72) can be written as:

$$\begin{bmatrix} \mathbf{A}_{BTDM} & \mathbf{E}_2 \\ \mathbf{E}_1 & \mathbf{E}_3 \end{bmatrix} \begin{bmatrix} \mathbf{X}_1 \\ \mathbf{X}_2 \end{bmatrix} = \begin{bmatrix} \mathbf{B}_1 \\ \mathbf{B}_2 \end{bmatrix} \quad (4.73)$$

where, $\mathbf{A}_{BTDM}$: block-tridiagonal matrix of size $(N \times N)$

$\mathbf{E}_1$: $(2 \times N)$ block matrix

$\mathbf{E}_2$: $(N \times 2)$ block matrix

$\mathbf{E}_3$: (2×2) block matrix

$\mathbf{B}_1, \mathbf{X}_1$: $(N \times 1)$ vector

$\mathbf{B}_2, \mathbf{X}_2$: (2×1) vector

$N = 4(NL + NM - 1)$

Equation (4.73) can be transformed into:

$$\begin{bmatrix} \mathbf{A}_{BTDM} & \mathbf{O} \\ \mathbf{E}_1 & \mathbf{I} \end{bmatrix} \begin{bmatrix} \mathbf{I} & \mathbf{A}_{BTDM}^{-1}\mathbf{E}_2 \\ \mathbf{O} & \mathbf{E}_3 - \mathbf{E}_1\mathbf{A}_{BTDM}^{-1}\mathbf{E}_2 \end{bmatrix} \begin{bmatrix} \mathbf{X}_1 \\ \mathbf{X}_2 \end{bmatrix} = \begin{bmatrix} \mathbf{B}_1 \\ \mathbf{B}_2 \end{bmatrix}$$

or,
$$\begin{bmatrix} \mathbf{A}_{BTDM} & \mathbf{O} \\ \mathbf{E}_1 & \mathbf{I} \end{bmatrix} \begin{bmatrix} \mathbf{F}_1 \\ \mathbf{F}_2 \end{bmatrix} = \begin{bmatrix} \mathbf{B}_1 \\ \mathbf{B}_2 \end{bmatrix} \tag{4.74}$$

where,
$$\begin{bmatrix} \mathbf{F}_1 \\ \mathbf{F}_2 \end{bmatrix} = \begin{bmatrix} \mathbf{I} & \mathbf{A}_{BTDM}^{-1}\mathbf{E}_2 \\ \mathbf{O} & \mathbf{E}_3 - \mathbf{E}_1\mathbf{A}_{BTDM}^{-1}\mathbf{E}_2 \end{bmatrix} \begin{bmatrix} \mathbf{X}_1 \\ \mathbf{X}_2 \end{bmatrix} \tag{4.75}$$

Equation (4.74) can be written as the combination of two matrix equations:

$$\mathbf{A}_{BTDM}\ \mathbf{F}_1 = \mathbf{B}_1 \tag{4.76}$$

and
$$\mathbf{E}_1\ \mathbf{F}_1 + \mathbf{F}_2 = \mathbf{B}_2 \tag{4.77}$$

$\mathbf{F}_1$ of Equation (4.76) was determined using the BTDMA method. Since $\mathbf{A}_{BTDM}$ is an ($N \times N$) matrix and $\mathbf{B}_1$ is a ($N \times 1$) vector, the result $\mathbf{F}_1$ is also a ($N \times 1$) vector. Next, $\mathbf{F}_2$ was calculated from Equation (4.77) and it is a (2×1) vector.

Let $\mathbf{F}_3 = \mathbf{A}_{BTDM}^{-1} \mathbf{E}_2$ (4.78)

or, $\mathbf{A}_{BTDM}\ \mathbf{F}_3 = \mathbf{E}_2$ (4.79)

Equation (4.78) can be solved using BTDMA. Since $\mathbf{E}_2$ is an ($N \times 2$) matrix, BTDMA has to be applied twice to get $\mathbf{F}_3$. Block $\mathbf{F}_3$ is another ($N \times 2$) matrix. Equation (4.79) was substituted into Equation (4.75), which becomes:

$$\mathbf{X}_1 + \mathbf{F}_3\ \mathbf{X}_2 = \mathbf{F}_1 \quad (4.80)$$

and $$(\mathbf{E}_3 - \mathbf{E}_1\ \mathbf{F}_3)\ \mathbf{X}_2 = \mathbf{F}_2 \quad (4.81)$$

The result of ($\mathbf{E}_3 - \mathbf{E}_1\ \mathbf{F}_3$) is a ($2 \times 2$) matrix and thus Equation (4.81) can be easily solved using Cramer's rule to obtain $\mathbf{X}_2$. Finally, $\mathbf{X}_1$ was calculated from Equation (4.80).

Because of non-linearities, an iterative approach was needed to arrive at a solution. An initial guess for mass flux, velocity, temperature, gas mass fraction, pressure gradient, film thickness and turbulent viscosity was required before calculating the coefficients in the matrix. The new solution obtained from the matrix calculation was compared with the value from the previous iteration. If the convergence criterion was not met, the

coefficients were re-calculated with the new results and the matrix was re-solved. The convergence criteria are discussed in Section 4.6.

4.5 Turbulence Model Calculation

The turbulence model equations were solved once a converged solution was achieved for mass flux, velocity, temperature, gas mass fraction, film thickness and pressure gradient. When the mixing length model was employed, the turbulent viscosity was calculated in one step. Once a new turbulent viscosity was obtained, the matrix discussed in Section 4.4 was resolved until convergence. This loop continued until the turbulent viscosity and the matrix convergence set had both converged.

When the k-ε model was used, a different iterative procedure was required. The kinetic energy and dissipation rate equations were solved in a segregated manner, each using a tri-diagonal matrix algorithm. The kinetic energy equation was first solved, followed by the dissipation rate equation. The coefficients of both the kinetic energy and the dissipation equation contain old values of kinetic energy, dissipation and turbulent viscosity; therefore, several iterations were required before a solution was reached. After each k and ε calculation, a new turbulent viscosity was obtained. The calculations of the two equations were repeated until a converged solution was obtained for k and ε. The value of turbulent viscosity calculated from these k and ε fields was then used to re-calculate the matrix coefficients discussed in Section 4.4 above. The matrix calculation was then repeated until a new converged solution was reached. Iterations of the matrix

followed by iterations of the k-ε model continued until an overall converged solution was achieved.

4.6 Convergence Criteria

4.6.1 Convergence Criteria for *u, J, W, T, δ, dP/dz*

After each matrix calculation, the solution for velocity, mass flux, temperature, gas mass fraction, film thickness and pressure gradient was compared with the previous calculation. The relative error was calculated as follows:

$$\gamma = \left| \frac{\varphi^{n} - \varphi^{o}}{\varphi^{n}} \right| \tag{4.82}$$

Once $\gamma < 1 \times 10^{-7}$ was achieved for all the nodal values in all the fields, the matrix was said to have converged. This converged solution however is with old values of turbulent viscosity. The turbulent viscosity must therefore be re-calculated with the new converged matrix solution.

4.6.2 Convergence Criteria for k and ε

When the k-ε model was employed, a convergence check was performed after each calculation of k and ε. Since these parameters have a very wide range of values and the kinetic energy is very small near a wall or interface, a better error calculation for this case is a range-normalized relative difference:

$$\gamma = \left| \frac{\varphi^{n} - \varphi^{o}}{Range(\varphi^{n})} \right| \qquad \text{where} \quad Range(\varphi^{n}) = \varphi^{n}_{max} - \varphi^{n}_{min} \tag{4.83}$$

Once $\gamma < 1 \times 10^{-7}$ was achieved at all nodes across a station, the k and ε equations were said to have converged and the matrix calculation was repeated with the new turbulent viscosity.

4.6.3 Overall Convergence Check

An overall convergence check was required once a converged matrix solution was obtained followed by a converged turbulent viscosity solution. When the k-ε model was employed, the overall convergence check was done by comparing the old converged k and ε values (those used in the previous matrix calculation) with the new converged k and ε values. This check was done using Equation (4.83). Once $\gamma < 1 \times 10^{-7}$ was achieved at all nodes, the solution was said to have converged at that station and the solution was marched to the next station.

When the mixing length model was employed, the overall convergence check was done by comparing the old turbulent viscosities at each node (those used in the previous matrix calculation) with the new turbulent viscosities. This check was done using Equation (4.82). Once $\gamma < 1 \times 10^{-5}$ was achieved at all nodes, the solution was said to have converged and the solution was marched to the next station to repeat calculations.

4.7 Relaxation Factors

After each matrix calculation, if the convergence criterion was not met, a relaxation factor (ψ) was applied to all the variables before the next iteration:

$$\varphi_{\text{relaxed}} = \varphi^{\circ} + \psi_{\varphi}(\varphi^{n} - \varphi^{\circ}) \tag{4.84}$$

where $\varphi = \left\{u, J, T, W, \delta, \frac{dP}{dz}\right\}$

The typical values used for the relaxation factors for these variables are as follows:

$\psi_u = 0.6$ $\qquad$ $\psi_W = 1$

$\psi_J = 0.6$ $\qquad$ $\psi_\delta = 0.1$

$\psi_T = 0.1$ $\qquad$ $\psi_{\frac{dP}{dz}} = 0.2$

4.8 Flow Reversal

The solution was advanced in the χ direction, station by station, until either a specified length L was reached or flow reversal occurred. Flow reversal occurred when the solution converged and resulted in a negative velocity at one or more nodal points across the tube (in either the liquid or the mixture regions). The numerical model is invalid for negative velocities due to the parabolic approach taken in the solution method. For this reason, when a negative velocity was obtained, the program was terminated. Flow reversal most often occured for the case of pure vapor when the condensation rate was large, and also when a fully developed inlet velocity profile was set (this is discussed in the following chapter).

CHAPTER 5

VALIDATION TESTS

5.1 Introduction

To ensure that the numerical model was producing accurate results, several validation tests were done for both laminar and turbulent flow. These validation tests included grid independence tests and comparisons with analytical, numerical and experimental results. All the results presented in this chapter correspond to steam as the condensing vapor and air as the non-condensable gas, unless otherwise stated.

5.2 Grid Independence

The grid independence tests consisted of running the code using various grid sizes and comparing the results to determine the optimum control volume size such that further reduction would not substantially change the results. The case chosen for this test was one with a large condensation rate since this would require the finest mesh; run 3 of Goodykoontz and Dorsch (1966) was chosen for this test. The range of values used for the number of control volumes in the liquid region, NL, the mixture region, NM, and the number of stations, NZ, were as follows: $40 < NL < 100$, $60 < NM < 120$, and $2000 < NZ < 5000$ for 2.2 metres of tube length. Table 5.1 shows the maximum percent difference in the velocity and temperature profiles at four different z locations (z = 0.34 m, 0.69 m, 1.26 m, and 2.2 m) when the number of control volumes in the liquid region was increased from 40 to 100.

Table 5.1 Maximum difference in u and T profiles at $z = 0.34$ m, 0.69 m, 1.26 m, and 2.2 m when NL is increased from 40 to 100 ($NM = 100$, $NZ = 4000$)

NL	**Maximum % Difference in *u* and *T* profiles**
40 vs. 60	0.2002%
60 vs. 80	0.1225%
80 vs. 100	0.0771%

From the above table it can be seen that when increasing the number of control volumes in the liquid region from 80 to 100, the velocity and temperature profiles changed by less than 0.1 %. Therefore, grid independence was achieved at $NL = 80$.

Table 5.2 shows the maximum percent difference in velocity and temperature profiles when the number of control volumes in the mixture region was increased from 60 to 120.

Table 5.2 Maximum difference in u and T profiles at $z = 0.34$ m, 0.69 m, 1.26 m, and 2.2 m when NM is increased from 60 to 120 ($NL = 80$, $NZ = 4000$)

NM	**Maximum % Difference in *u* and *T* profiles**
60 vs. 80	0.2497%
80 vs. 100	0.1300%
100 vs. 120	0.0806%

From this table it can be observed that the maximum percent difference in the velocity and temperature profiles was less than 0.1% when increasing the number of control volumes from 100 to 120. The solution was therefore considered grid independent for this case when $NM = 100$.

For run 3 of Goodykoontz and Dorsch, the total length of the tube was 2.2 m. The minimum number of stations required for the solution to converge for this length of tube was approximately 2000. Starting with $NZ = 2000$, the number of stations was increased until the maximum percent difference in δ, dP/dz and Nu_z was less than 0.1%. Table 5.3 shows the maximum percent difference when increasing the number of stations from 2000 to 5000.

Table 5.3 Maximum difference in δ, dP/dz and Nu_z when NZ is increased from 2000 to 5000 ($NL = 80$, $NM = 100$)

NZ	**Maximum % Difference in δ**	**Maximum % Difference in *dP/dz***	**Maximum % Difference in Nu_z**
2000 vs. 3000	0.0225%	0.2889%	0.0286%
3000 vs. 4000	0.0105%	0.1372%	0.0137%
4000 vs. 5000	0.0061%	0.0794%	0.0079%

Table 5.3 shows that the pressure gradient, dP/dz, has the largest percent difference when increasing the number of stations. When the number of stations was increased from 4000

to 5000 the results changed by less than 0.1 % for all three distributions. Therefore, 4000 stations were sufficient for a length of 2.2 m.

5.3 Validation of the Laminar Model

5.3.1 Introduction

In order to validate the laminar model, three different comparisons were made: two for pure vapor condensation and one for vapor-gas mixtures. The comparisons made for pure vapor were with Nusselt's analytical solution for condensation on a flat plate and with Dobran and Thorsen's (1980) analytical and numerical results for condensation in vertical tubes. No previous work could be found for the case of laminar condensation of vapor in the presence of gas. For this reason, an analytical solution was developed for the location in the pipe where virtually complete condensation has occurred (termed "end of condensation").

5.3.2 Comparison with Nusselt (1916)

As mentioned previously in the literature review, Nusselt (1916) developed an analytical solution for laminar film condensation of a pure saturated, quiescent vapor on a vertical, isothermal surface. Included in his solution was an equation for the film thickness δ as a function of distance z along the length of the plate:

$$\delta(z) = \left[\frac{4\lambda_L \mu_L (T_{sat} - T_{wall}) z}{g\rho_L (\rho_L - \rho_v) h_{fg}} \right]^{1/4} \tag{5.1}$$

In order to emulate the conditions of Nusselt's solution, a large tube radius (r_o = 1 m) and a low inlet Reynolds number (Re_{in} = 50) were used. Figure 5.1 shows a comparison of the present numerical solution with Equation (5.1). As can be seen with this figure, excellent agreement was obtained. Aside from the first couple of stations (a very small distance near the inlet), the present results for film thickness were within 1 % of Nusselt's solution, with a deviation of less than 0.3 % for the majority of the stations.

5.3.3 Comparison with Dobran and Thorsen (1980)

The only published work available for laminar forced convection condensation in a vertical tube is that of Dobran and Thorsen (1980). They presented both an analytical

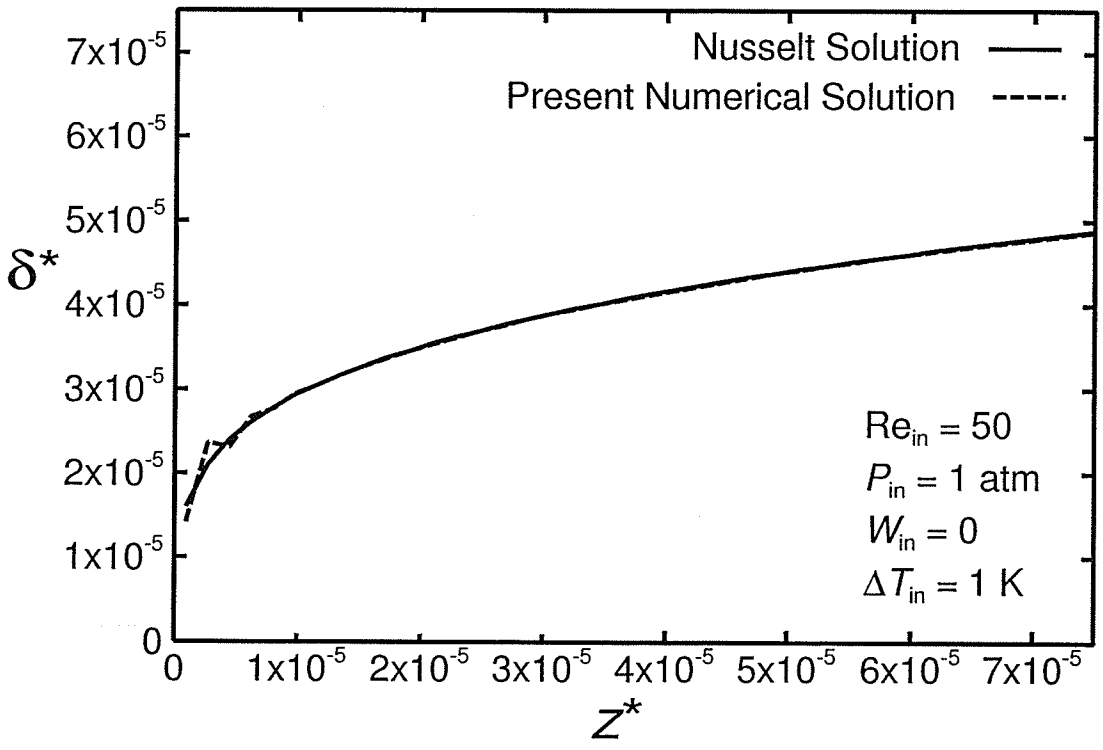

Figure 5.1 Film thickness comparison with Nusselt's (1916) analytical solution

solution, which neglects inertia effects and assumes constant inter-phase shear, and a numerical solution. Their numerical solution was obtained starting with the full set of governing equations and using an integral analysis and profile assumptions for the velocity in both the liquid and the vapor regions. They presented results for Nusselt number and film thickness at a location defined as L^*, where all the vapor had condensed. In the present model, flow reversal often occurred before all the vapor was condensed, and therefore L^* was defined as the length at which flow reversal occurred. For the purpose of this comparison, a fully developed inlet velocity profile was used to match the conditions of Dobran and Thorsen. Table 5.4 compares the present results with Dobran and Thorsen's numerical (DTN) and analytical (DTA) results.

Table 5.4 Comparison with Dobran and Thorsen (1980) for $Fr_{in}/Re_{in} = 0.01$ and $\rho_v/\rho_L = 0.05$

				$\delta^*\|_{L^*}$			$Nu_z\|_{L^*}$			
Case	Pr_L	μ_v/μ_L	Ja	Present	DTN	DTA	Present	DTN	DTA	$\dot{m}_L / \dot{m}_{in}$
1	2	0.04	0.05	0.168	0.1703	0.153	10.68	10.78	13.06	0.96
2	2	2	0.05	0.092	0.098	0.088	20.78	19.55	22.74	0.87
3	0.005	0.04	0.001	0.172	0.169	0.153	10.57	10.76	13.06	0.7
4	0.005	0.04	0.005	0.268	0.187	0.153	6.43	9.61	13.06	0.7

In cases 1 and 2, the present results compare well with DTN and DTA, falling between the two results. For cases 3 and 4, corresponding to low liquid Prandtl numbers, the dimensionless film thickness at the condensation length was higher than both DTN and

DTA results while the Nusselt numbers for these cases were lower. The last column in the table indicates the amount of vapor remaining in the core when flow reversal occurred. In cases 3 and 4, 30% of the inlet mass still remained when the flow reversed.

Several tests were done to determine why flow reversal was occurring so early when a fully developed inlet velocity profile was used in the comparisons with Dobran and Thorsen. Figures 5.2 and 5.3 show the velocity profile when flow reversal occurs for a uniform and a fully developed inlet velocity profile, respectively.

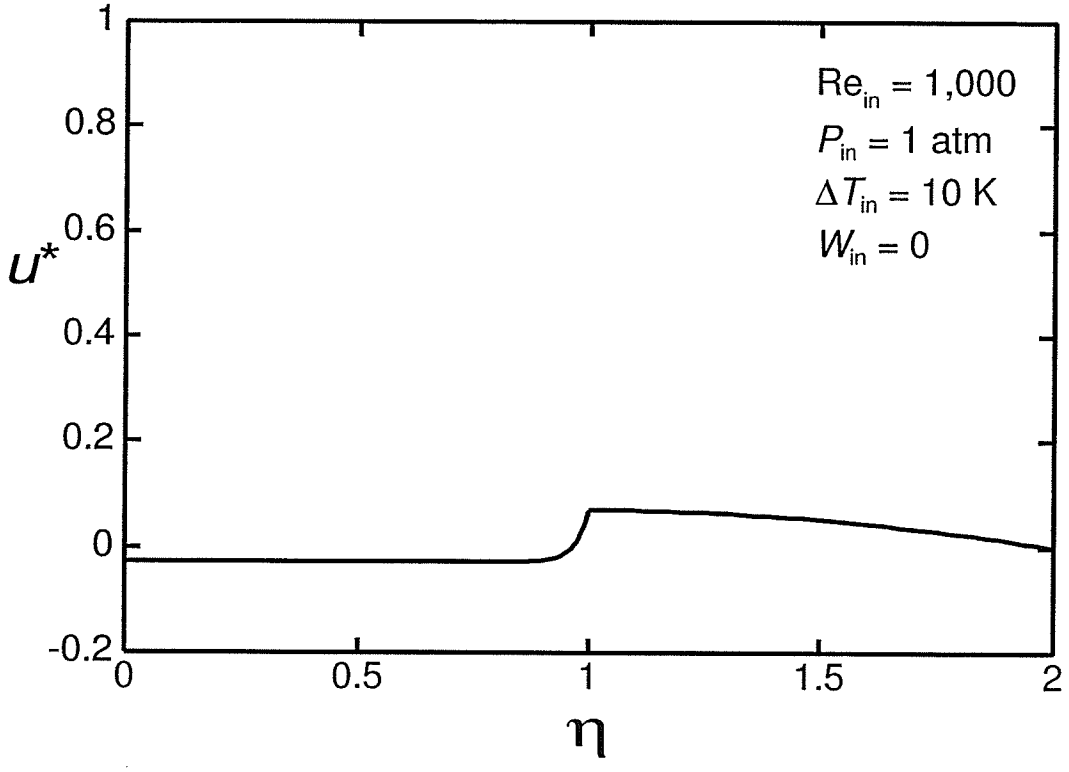

Figure 5.2 Velocity profile at flow reversal (z^* = 4.86 cm) with a uniform inlet velocity

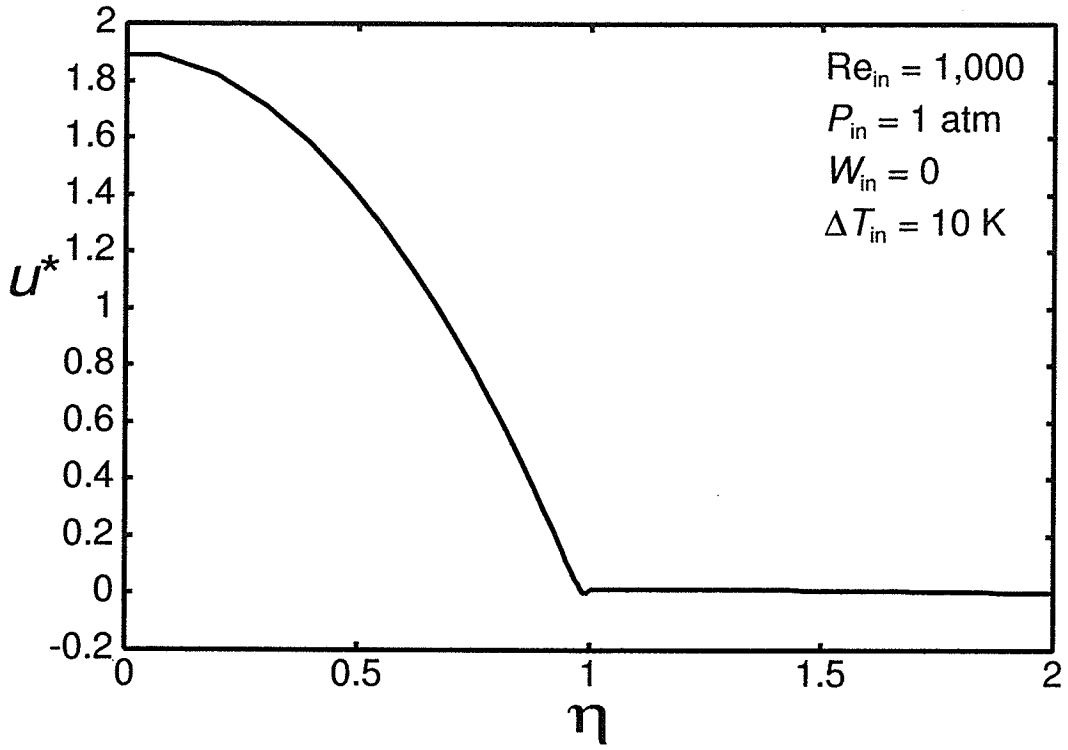

Figure 5.3 Velocity profile at flow reversal ($z^* = 0.26$ cm) with a fully developed inlet velocity

Both of these profiles correspond to the following dimensionless inlet conditions: $Pr_L = 1.87$, $\rho_v/\rho_L = 0.0006$, $\mu_v/\mu_L = 0.04$, $Fr_{in}/Re_{in} = 0.005$, and $Ja = 0.018$. From Figure 5.2 it can be seen that with a uniform inlet profile, flow reversal does not occur until almost all the vapor has condensed. In addition it can be seen that at separation, the velocity at the centerline is slightly negative. In the case of a fully developed inlet profile (shown in Figure 5.3), separation occurs in the mixture region near the interface when there is still a relatively large vapor velocity at the centerline. In Dobran and Thorsen's model, they assumed a parabolic velocity profile that could never resemble the profile shown in Figure 5.3; this could explain why flow reversal did not occur in their model until 100% of the vapor had condensed. The separation near the interface can be explained by comparing the pressure gradient distribution along the length of the tube as

well as the amount of mass condensed for the two different inlet profiles. From Figure 5.4 it can be seen that for the case of fully developed inlet, the adverse pressure gradient was larger than for the case of a uniform inlet. In Schlichting's "Boundary Layer Theory" (1968), he stated that a laminar boundary layer can support only very small adverse pressure gradients without the occurrence of separation. This could explain why, for the case of a fully developed inlet profile where the adverse pressure gradient was large, separation occurred. In addition, Schlichting also explained how boundary layer suction helps to stabilize the flow by removing the decelerated particles before they are given a change to cause separation. Figure 5.5 compares the amount of mass condensed for both inlet profiles. It can be observed that the amount of vapor condensed was smaller for the case of a fully developed inlet and is therefore less stable and more likely to separate.

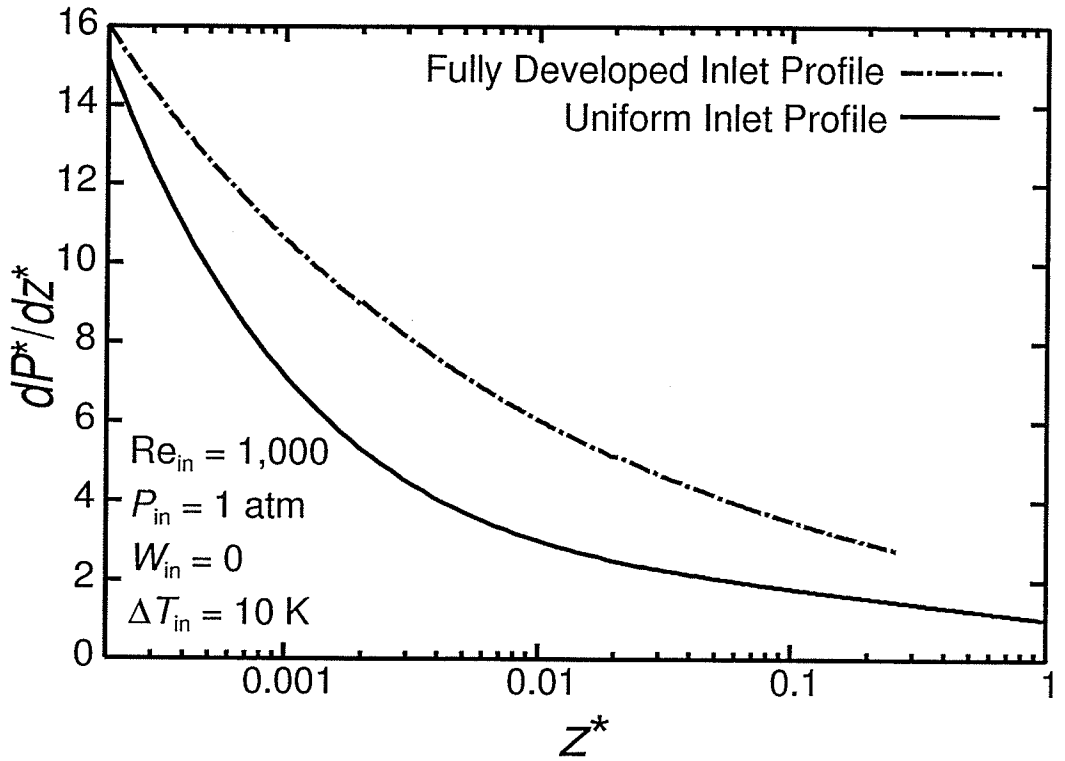

Figure 5.4 Dimensionless pressure gradient comparison between a fully developed and a uniform inlet velocity profile

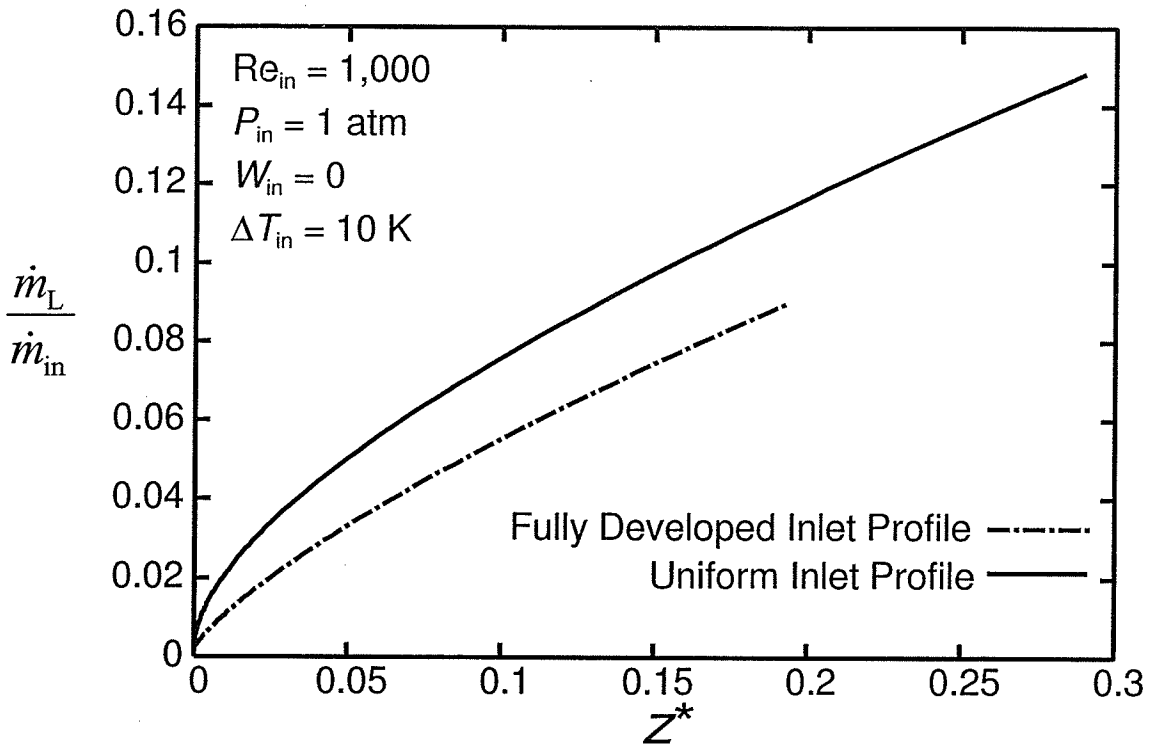

Figure 5.5 Comparison between a fully developed and a uniform inlet velocity profile in terms of $\dot{m}_L / \dot{m}_{in}$

5.3.4 End of Condensation Solution

While condensation occurs along the length of the tube, the velocity profile, temperature profile and gas mass fraction profile are continuously changing. Eventually, the mixture composition reduces to a gas fully saturated with vapor and the condensation process shuts off. At this point, the temperature in the liquid and mixture is T_{wall}, and the gas mass fraction and velocity profiles no longer vary with z. This situation is referred to here as the 'end of condensation'. The fully developed conditions greatly simplify the governing equations and therefore, an analytical solution can easily be obtained.

The following conditions, which are valid in the end-of-condensation region, were applied to the governing equations:

- $v_L = 0$ (5.2)

- $v_M = 0$ (5.3)
- $\frac{\partial u_L}{\partial z} = \frac{\partial u_M}{\partial z} = 0$ (5.4)
- $T_L = T_M = T_{wall}$ (5.5)
- Uniform W and physical properties

The governing equations reduce to:

$$\frac{\mu_L}{r}\frac{d}{dr}\left[r\frac{du_L}{dr}\right] = \left(\frac{dP}{dz}\right)_{ec} - \rho_L g \tag{5.6}$$

$$\frac{\mu_M}{r}\frac{d}{dr}\left[r\frac{du_M}{dr}\right] = \left(\frac{dP}{dz}\right)_{ec} - \rho_M g \tag{5.7}$$

These equations were non-dimensionalized using the following dimensionless groups:

$$P^* = \frac{P - P_{in}}{\frac{1}{2}\rho_{in}u_{in}^2} \qquad z^* = \frac{z}{2r_o}$$

$$\mathrm{Re}_{in} = \frac{\rho_{in}u_{in}2r_o}{\mu_{in}} \qquad r^* = \frac{r}{r_o}$$

$$\mathrm{Fr} = \frac{u_{in}^2}{g2r_o} \qquad \delta^* = \frac{\delta}{r_o}$$

$$u^* = \frac{u}{u_{in}}$$

The resulting non-dimensional equations are:

$$\frac{1}{r^*}\frac{d}{dr^*}\left[r^*\frac{du_L{}^*}{dr^*}\right]=\frac{1}{8}\mathrm{Re}_{in}\left(\frac{\mu_{in}}{\mu_L}\right)\frac{dP^*}{dz^*}-\frac{1}{4}\frac{\mathrm{Re}_{in}}{\mathrm{Fr}}\left(\frac{\rho_L}{\rho_{in}}\right)\left(\frac{\mu_{in}}{\mu_L}\right) \tag{5.8}$$

$$\frac{1}{r^*}\frac{d}{dr^*}\left[r^*\frac{du_M{}^*}{dr^*}\right]=\frac{1}{8}\mathrm{Re}_{in}\left(\frac{\mu_{in}}{\mu_M}\right)\frac{dP^*}{dz^*}-\frac{1}{4}\frac{\mathrm{Re}_{in}}{\mathrm{Fr}}\left(\frac{\rho_M}{\rho_{in}}\right)\left(\frac{\mu_{in}}{\mu_M}\right) \tag{5.9}$$

Integrating the above equations results in velocity profiles for the liquid and mixture region:

$$u^*_{L,ec}=\left[\frac{1}{32}\mathrm{Re}_{in}\left(\frac{\mu_{in}}{\mu_L}\right)\frac{dP^*}{dz^*}-\frac{1}{16}\frac{\mathrm{Re}_{in}}{\mathrm{Fr}}\left(\frac{\rho_L}{\rho_{in}}\right)\left(\frac{\mu_{in}}{\mu_L}\right)\right]r^{*2}+C_1\ln r^*+C_2 \tag{5.10}$$

$$u^*_{M,ec}=\left[\frac{1}{32}\mathrm{Re}_{in}\left(\frac{\mu_{in}}{\mu_M}\right)\frac{dP^*}{dz^*}-\frac{1}{16}\frac{\mathrm{Re}_{in}}{\mathrm{Fr}}\left(\frac{\rho_M}{\rho_{in}}\right)\left(\frac{\mu_{in}}{\mu_M}\right)\right]r^{*2}+C_3\ln r^*+C_4 \tag{5.11}$$

The constants C_1, C_2, C_3, and C_4 were evaluated by applying the following boundary conditions:

- No slip at the tube wall:

$$u_L{}^*=0 \text{ at } r^*=1 \tag{5.12}$$

- No shear stress at the centerline:

$$\frac{du_{\mathrm{M}}^{*}}{dr^{*}} = 0 \text{ at } r^{*} = 0 \tag{5.13}$$

- Velocity continuity at the interface:

$$u_{\mathrm{L,ec}}^{*} = u_{\mathrm{M,ec}}^{*} \text{ at } r^{*} = \delta_{\mathrm{ec}}^{*} \tag{5.14}$$

- Shear continuity at the interface:

$$\left(\frac{\mu_{\mathrm{L}}}{\mu_{\mathrm{in}}}\right)\frac{du_{\mathrm{L}}{}^{*}}{dr^{*}} = \left(\frac{\mu_{\mathrm{M}}}{\mu_{\mathrm{in}}}\right)\frac{du_{\mathrm{M}}{}^{*}}{dr^{*}} \text{ at } r^{*} = \delta_{\mathrm{ec}}^{*} \tag{5.15}$$

With these boundary conditions, the constants were calculated as:

$$C_1 = \frac{\delta_{\mathrm{ec}}^{*}}{2}\left[\frac{1}{4}\frac{\mathrm{Re_{in}}}{\mathrm{Fr}}\left(\frac{\mu_{\mathrm{in}}}{\mu_{\mathrm{L}}}\right)\left(\frac{\rho_{\mathrm{L}} - \rho_{\mathrm{M}}}{\rho_{\mathrm{in}}}\right)\right] \tag{5.16}$$

$$C_2 = \frac{1}{16}\frac{\mathrm{Re_{in}}}{\mathrm{Fr}}\left(\frac{\rho_{\mathrm{L}}}{\rho_{\mathrm{in}}}\right)\left(\frac{\mu_{\mathrm{in}}}{\mu_{\mathrm{L}}}\right) - \frac{1}{32}\mathrm{Re_{in}}\left(\frac{\mu_{\mathrm{in}}}{\mu_{\mathrm{L}}}\right)\frac{dP^{*}}{dz^{*}} \tag{5.17}$$

$$C_3 = 0 \tag{5.18}$$

$$\begin{aligned} C_4 = \frac{\delta_{\mathrm{ec}}^{*}}{4}\Bigg[&\frac{1}{8}\mathrm{Re_{in}}\frac{dP^{*}}{dz^{*}}\left(\frac{\mu_{\mathrm{in}}}{\mu_{\mathrm{L}}} - \frac{\mu_{\mathrm{in}}}{\mu_{\mathrm{M}}}\right) - \frac{1}{4}\frac{\mathrm{Re_{in}}}{\mathrm{Fr}}\left(\frac{\rho_{\mathrm{L}}\mu_{\mathrm{in}}}{\rho_{\mathrm{in}}\mu_{\mathrm{L}}} - \frac{\rho_{\mathrm{M}}\mu_{\mathrm{in}}}{\rho_{\mathrm{in}}\mu_{\mathrm{M}}}\right) \\ &+ 2\ln\delta_{\mathrm{ec}}^{*}\left[\frac{1}{4}\frac{\mathrm{Re_{in}}}{\mathrm{Fr}}\left(\frac{\mu_{\mathrm{in}}}{\mu_{\mathrm{L}}}\right)\left(\frac{\rho_{\mathrm{L}} - \rho_{\mathrm{M}}}{\rho_{\mathrm{in}}}\right)\right]\Bigg] - \frac{1}{32}\mathrm{Re_{in}}\left(\frac{\mu_{\mathrm{in}}}{\mu_{\mathrm{L}}}\frac{dP^{*}}{dz^{*}}\right) \\ &+ \frac{1}{16}\frac{\mathrm{Re_{in}}}{\mathrm{Fr}}\left(\frac{\rho_{\mathrm{L}}}{\rho_{\mathrm{in}}}\right)\left(\frac{\mu_{\mathrm{in}}}{\mu_{\mathrm{L}}}\right) \end{aligned} \tag{5.19}$$

There are two unknowns in the above equations, δ_{ec}* and dP^*/dz^*. To determine these unknowns, the following conservation of mass equations can be applied:

$$\dot{m}_{L,ec} = \rho_L \int_{\delta_{ec}}^{r_o} u_{L,ec} 2\pi r_o dr = \dot{m}_{in}\left(1 - \frac{W_{in}}{W_{ec}}\right) \tag{5.20}$$

$$\dot{m}_{M,ec} = \rho_M \int_{\delta_{ec}}^{r_o} u_{M,ec} 2\pi r_o dr = \dot{m}_{in}\left(\frac{W_{in}}{W_{ec}}\right) \tag{5.21}$$

The above equations state that the mass flow rate of the mixture at the inlet must equal the mass flow rate of the condensate at the end of condensation plus the mass flow rate of the mixture at the end of condensation. The gas concentration, W_{ec} can be determined by assuming the gas at the end of condensation is fully saturated with vapor at T_{wall} and taking the total pressure from the numerical solution. The equation used to determine W_{ec} is:

$$W_{ec} = 1 - 0.6219\frac{P_{sat}}{P_{ec} - P_{sat}} \tag{5.22}$$

Where P_{sat} is the saturation pressure at T_{wall}.

In dimensionless form, Equations (5.20) and (5.21) become:

$$\int_{\delta_{ec}^*}^{1} u_{L,ec}^* r^* dr^* = \frac{1}{2}\left(\frac{\rho_{in}}{\rho_L}\right)\left(1 - \frac{W_{in}}{W_{ec}}\right) \tag{5.23}$$

$$\int_0^{\delta_{ec}^*} u_{M,ec}^* r^* dr^* = \frac{1}{2}\left(\frac{\rho_{in}}{\rho_M}\right)\left(\frac{W_{in}}{W_{ec}}\right) \tag{5.24}$$

Substituting the velocity distribution for the liquid (Equation (5.10)) into Equation (5.23) and the velocity distribution for the mixture (Equation (5.11)) into Equation (5.24) results in the following two equations:

$$\frac{\mu_{in}}{\mu_L}\frac{1}{8}\mathrm{Re}_{in}\frac{dP^*}{dz^*} = \left\{\frac{1}{4}\frac{\mathrm{Re}_{in}}{\mathrm{Fr}}\frac{\mu_{in}}{\mu_L}\left[\frac{(\delta_{ec}^*)\ln\delta_{ec}^*}{4}\left(\frac{\rho_L-\rho_M}{\rho_{in}}\right)+\frac{(\delta_{ec}^*)}{8}\left(\frac{2\rho_L-\rho_M}{\rho_{in}}\right)\right.\right. \tag{5.25}$$

$$\left.\left.-\frac{(\delta_{ec}^*)^4}{16}\left(\frac{3\rho_L-2\rho_M}{\rho_{in}}\right)-\frac{\rho_L}{16\rho_{in}}\right]+\frac{1}{2}\frac{\rho_{in}}{\rho_L}\left(1-\frac{W_{in}}{W_{ec}}\right)\right\}\Bigg/\left\{-\frac{1}{16}+\frac{(\delta_{ec}^*)^2}{8}-\frac{(\delta_{ec}^*)^4}{16}\right\}$$

$$\frac{\mu_{in}}{\mu_L}\frac{1}{8}\mathrm{Re}_{in}\frac{dP^*}{dz^*} = \left\{\frac{1}{4}\frac{\mathrm{Re}_{in}}{\mathrm{Fr}}\frac{\mu_{in}}{\rho_{in}}\left[\frac{(\delta_{ec}^*)^4\ln\delta_{ec}^*}{4}\left(\frac{\rho_M-\rho_L}{\mu_L}\right)+\frac{(\delta_{ec}^*)}{16}\left(\frac{2\rho_L}{\mu_L}-\frac{\rho_M}{\mu_M}\right)\right.\right.$$

$$\left.\left.-\frac{(\delta_{ec}^*)^2}{8}\left(\frac{\rho_L}{\mu_L}\right)\right]+\frac{1}{2}\frac{\rho_{in}}{\rho_M}\left(\frac{W_{in}}{W_{ec}}\right)\right\}\Bigg/\left\{\frac{(\delta_{ec}^*)^4}{16}\left(2-\frac{\mu_L}{\mu_M}\right)-\frac{(\delta_{ec}^*)^2}{8}\right\} \tag{5.26}$$

Equating the left hand sides of Equations (5.25) and (5.26) results in one equation with one unknown (δ_{ec}^*). Once δ_{ec}^* is obtained, dP^*/dz^* can be found from either Equation (5.25) or (5.26). The coefficients needed for the velocity profiles can then be evaluated using the known values for δ_{ec}^* and dP^*/dz^*.

The results from the numerical solution were compared with the analytical solution discussed above. The inlet conditions used for this comparison were Re_{in} =1000, P_{in} = 1 atm, W_{in} = 0.2, and ΔT_{in} = 20 K. Comparisons of the film thickness and pressure gradient distribution, and the u velocity profiles with the end of condensation solution are plotted in Figures 5.6 to 5.9. From these plots it can be seen that the results from the numerical solution reach the end of condensation analytical solution at large values of z^*.

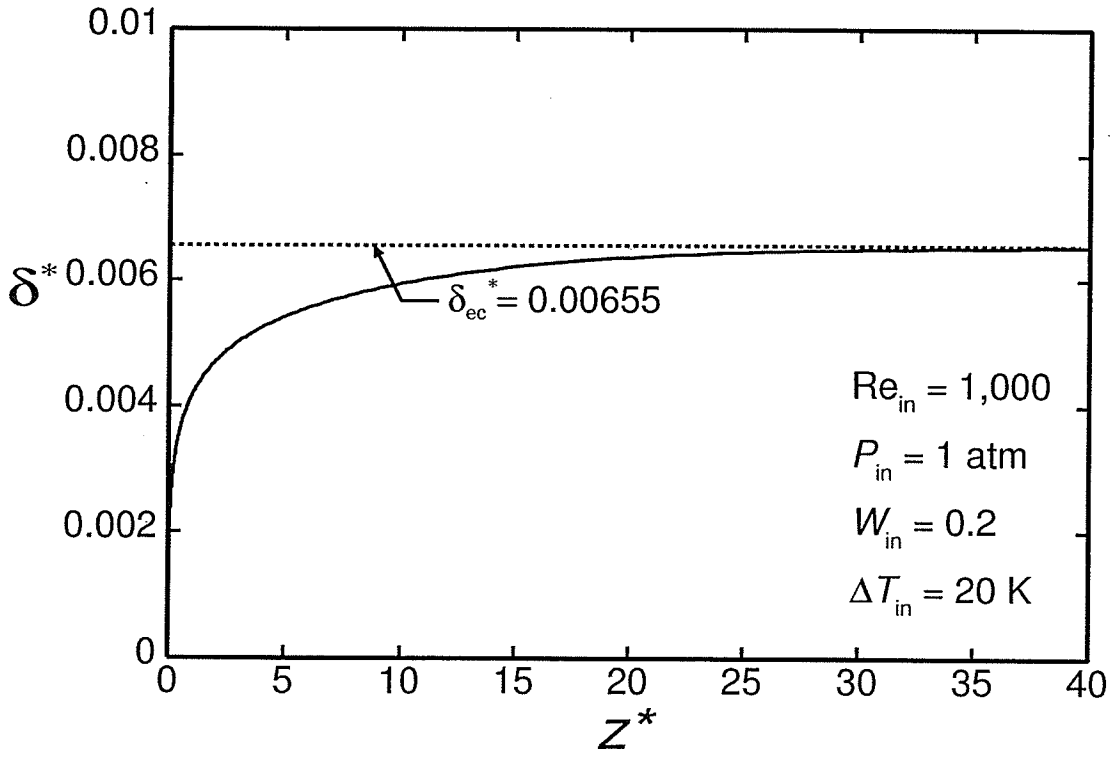

Figure 5.6 Dimensionless film thickness distribution

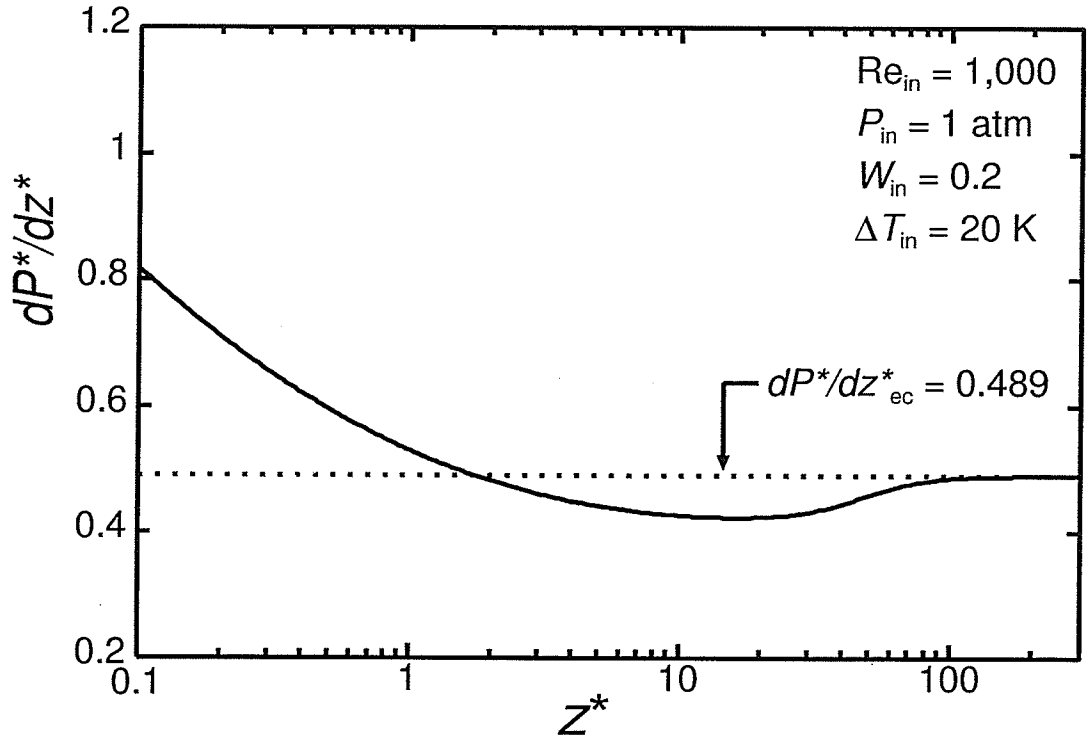

Figure 5.7 Dimensionless pressure gradient distribution

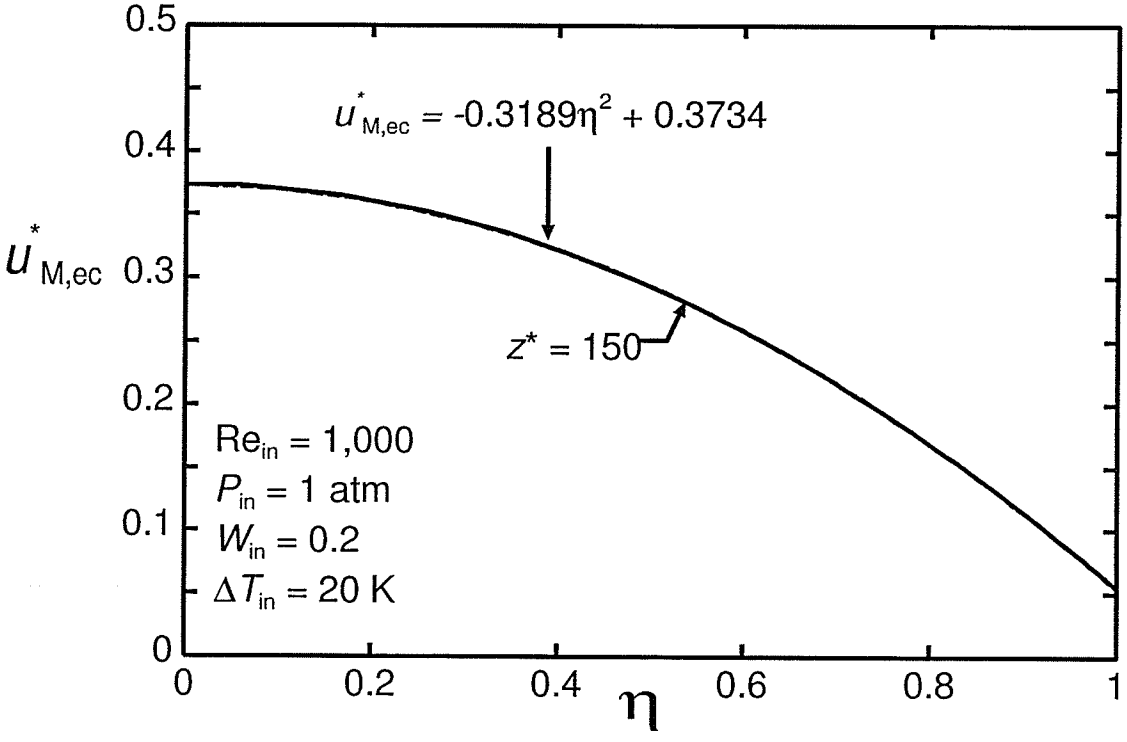

Figure 5.8 End of condensation velocity profile in the mixture

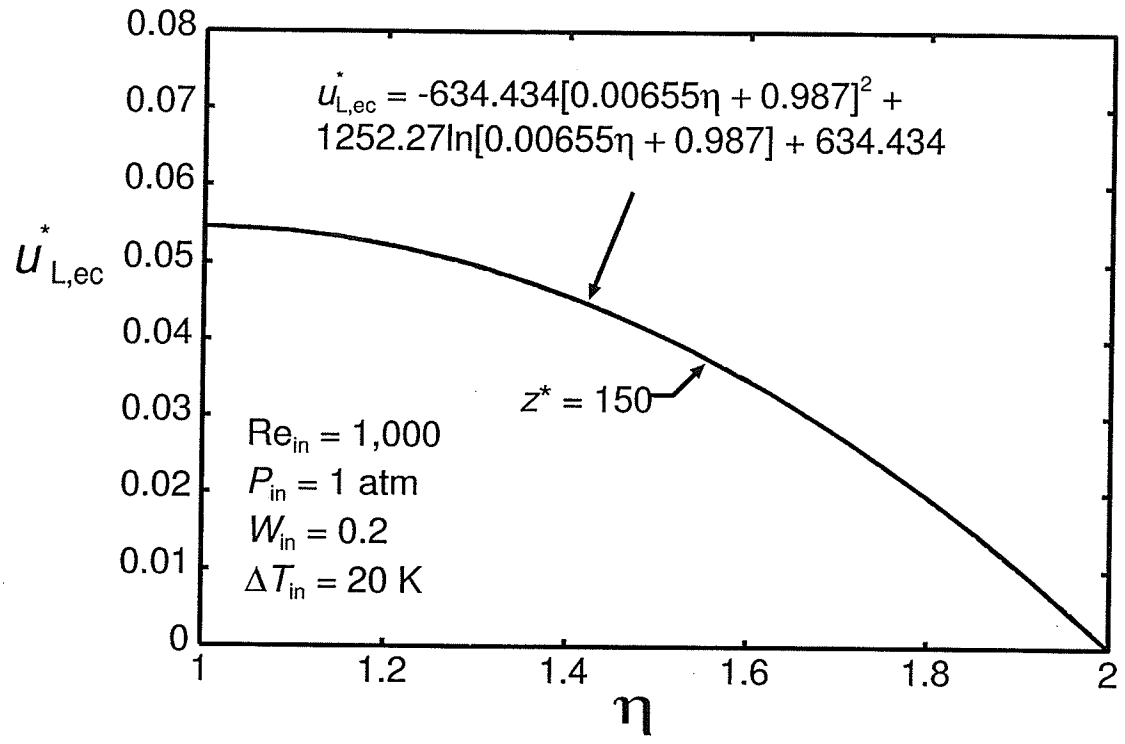

Figure 5.9 – End of condensation velocity profile in the liquid

5.4 Validation of the Turbulence Models

5.4.1 Introduction

Both the mixing length and the k-ε low Reynolds number turbulence models were validated to ensure that they were being applied correctly to the model. First the mixing length model was applied to both the liquid film and the core regions and results were compared with Panday's numerical results. Following this, the k-ε model was applied to the core region and results were compared with single phase pipe flow. Finally, the k-ε model was validated in the liquid film.

5.4.2 Mixing Length Model

As was previously discussed in the literature review, Panday (2003) developed a numerical model from the same equations and boundary conditions that were used in the present model. The difference in the present model is that it includes the presence of gas during condensation while Panday's model is for pure vapor. The mixing length model chosen for the present solution was the one used in Panday's work and was developed by Pletcher (1974).

Panday (2003) presented results for pure steam condensation in a 24-mm diameter tube with inlet velocities from 20 to 50 m/s, an inlet temperature of 117 °C, and a wall temperature of 107 °C. In Panday's paper, results of the Nusselt number were compared with a correlation from Chen (1987) for velocities of 20 and 50 m/s. Figures 5.10 and 5.11 compare the present model with both Panday and Chen's results for local Nusselt number for these two inlet velocities. Figure 5.10 shows the local Nusselt number distribution for an inlet velocity of 20 m/s. From this figure it can be observed that the present model agrees very well with both Panday and Chen's results for $z^* > 20$. For $z^* < 20$, there is a large deviation between Chen and Panday with the present results falling in between. Figure 5.11 shows the local Nusselt number distribution for an inlet velocity of 50 m/s. In this plot, Panday's results are considerably higher than the other two in the region $z^* < 150$. The present results agree with Chen's for $z^* > 50$ and fall between the other two sets of results for $z^* < 50$. The results of this comparison indicate that the mixing length model is producing reasonable results.

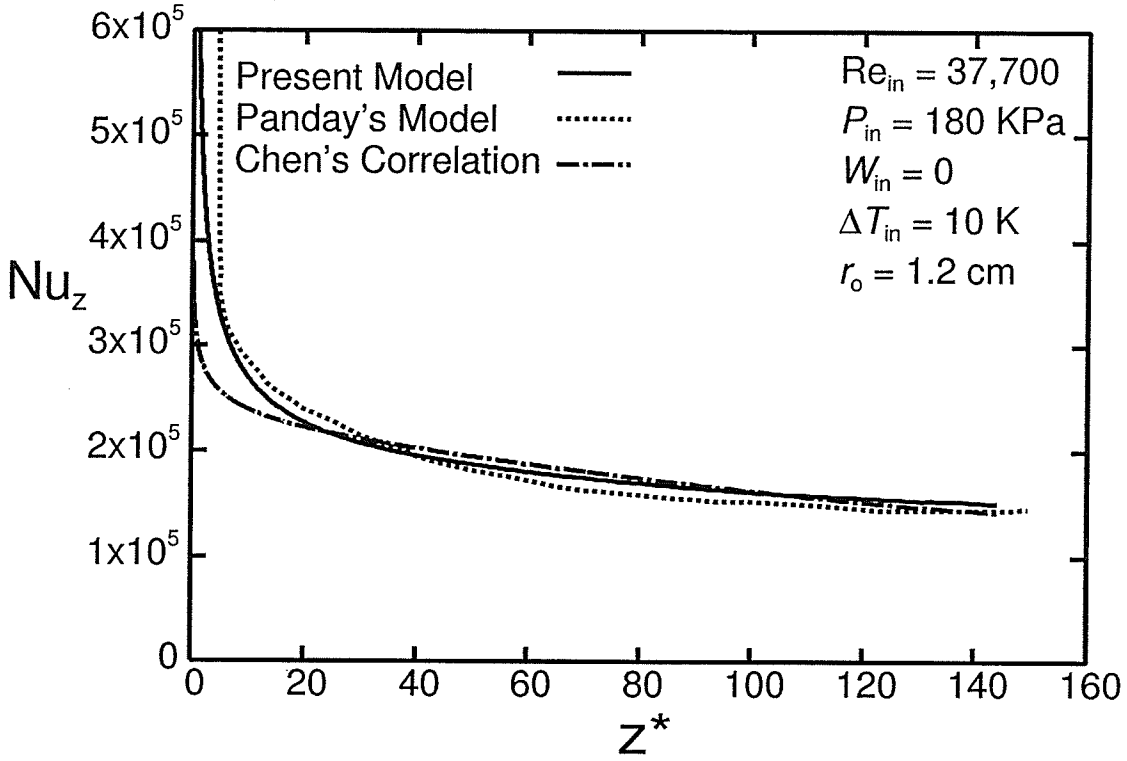

Figure 5.10 Local Nusselt number comparison with Panday (2003) and Chen (1987) for Re_{in} = 37,700

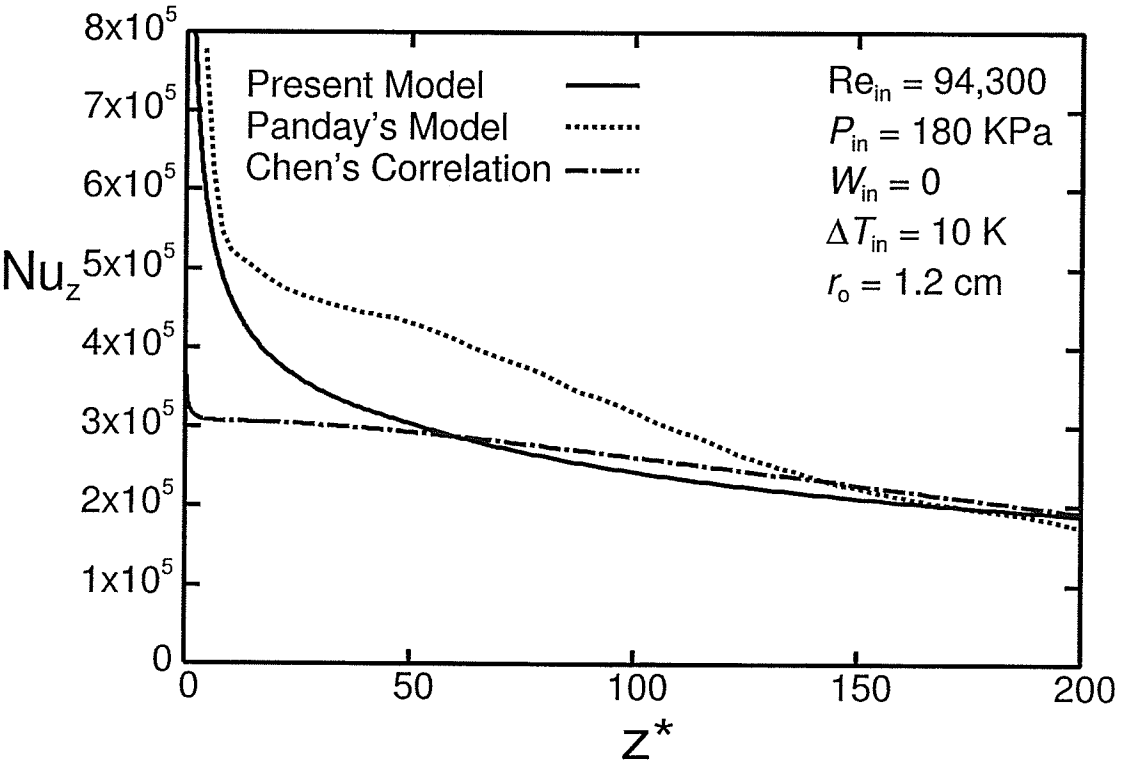

Figure 5.11 Local Nusselt number comparison with Panday (2003) and Chen (1987) for Re_{in} = 94,300

5.4.3 k-ε Model in the Core

To validate the Jones and Launder low Reynolds number k-ε model in the core, the model was set up to approximate single-phase flow in a tube and results were compared with single-phase pipe flow results. In order to model single-phase pipe flow, the condensation rate must be negligible and the interface must act as a wall. To ensure a low condensation rate, the temperature difference across the film was set to a low value (either 0.01 or 0.1 K), the inlet gas mass fraction was set to 0.9, and the latent heat was set to 22.25 GJ/kg. In addition to this, the velocity at the interface was set to zero such that the no slip boundary condition was applied at the interface. The resulting fully developed velocity profiles for 3 different cases were compared with experimental results from Nikuradse (1932). Figures 5.12 to 5.14 show the resulting fully developed velocity profiles for inlet Reynolds numbers of 4,000, 23,000, and 110,000, respectively. In these figures, u_c is the centerline velocity. From these plots it can be seen that the present model agrees reasonably well with the results from Nikuradse and that as the inlet Reynolds number increases, the agreement improves.

In addition to comparing velocity profiles, the kinetic energy profiles were plotted to ensure that the k-ε equations were producing the correct trends. Figures 5.15 to 5.17 show these plots for the three different Reynolds numbers mentioned above. These profiles show that the kinetic energy increases from the centerline to the interface and reaches its peak value between $y/r_o = 0$ and 0.2 followed by a sharp drop to zero at the interface. Previous results on single phase turbulent pipe flow show this same trend (Wilcox, 2002).

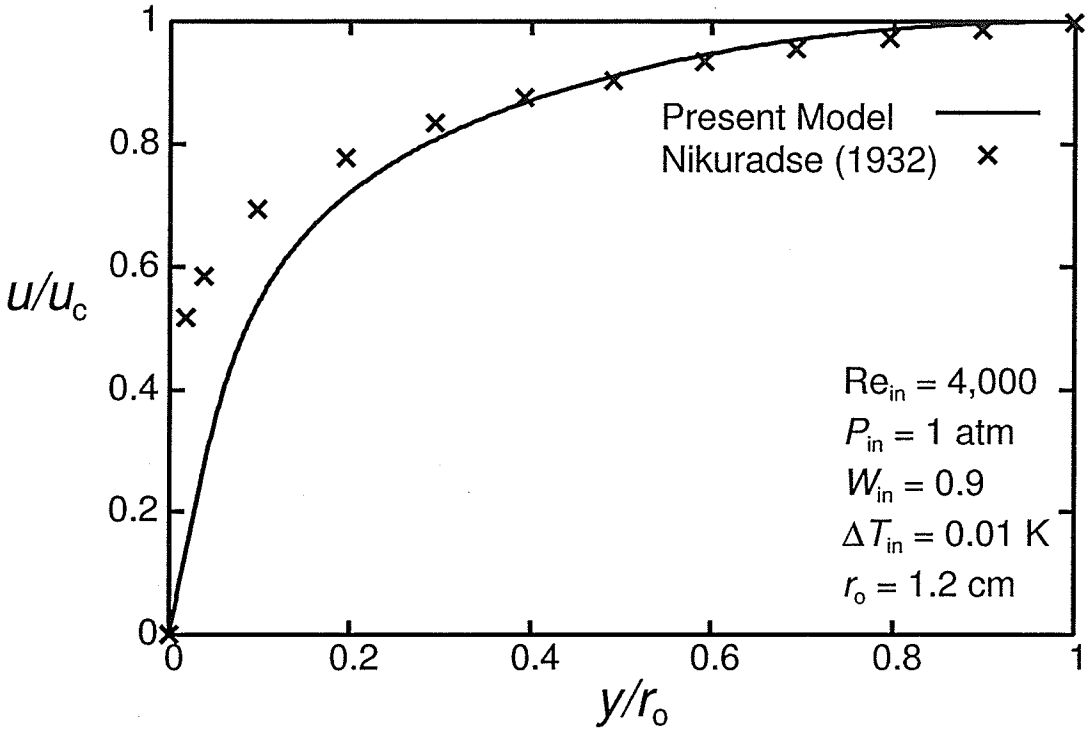

Figure 5.12 Single-phase velocity profile comparison with Nikuradse (1932) for Re_{in} = 4,000 ($\dot{m}_L / \dot{m}_{v,in} = 6.6 \times 10^{-5}$)

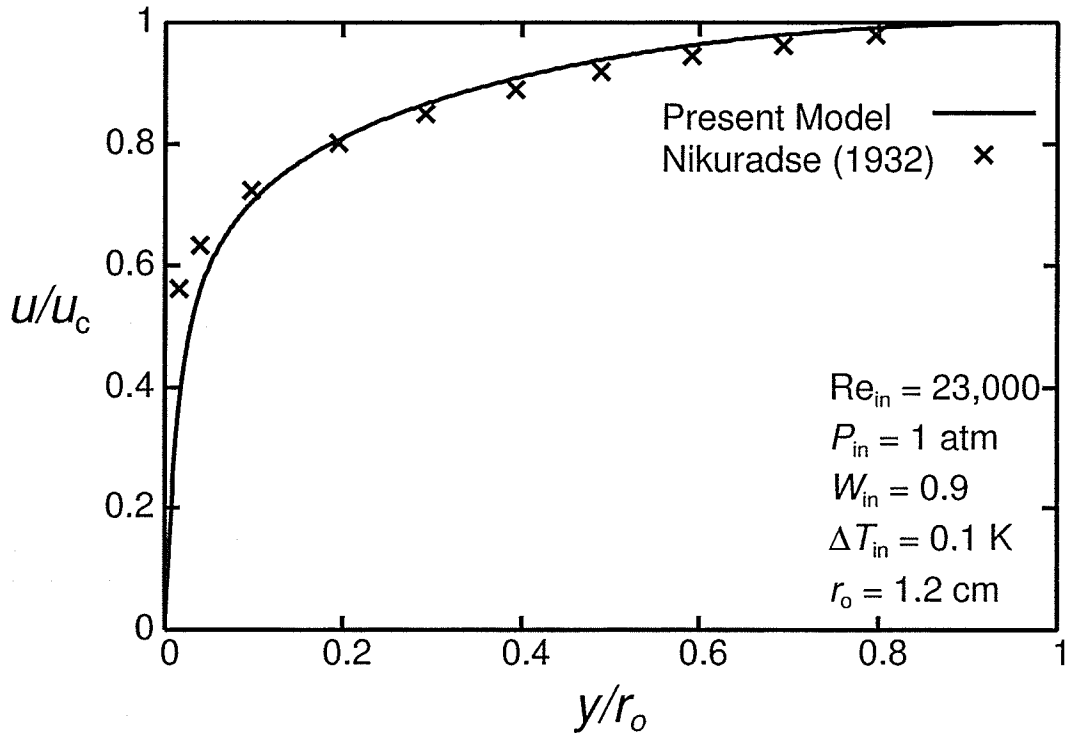

Figure 5.13 Single-phase velocity profile comparison with Nikuradse (1932) for Re_{in} = 23,000 ($\dot{m}_L / \dot{m}_{v,in} = 4.1 \times 10^{-5}$)

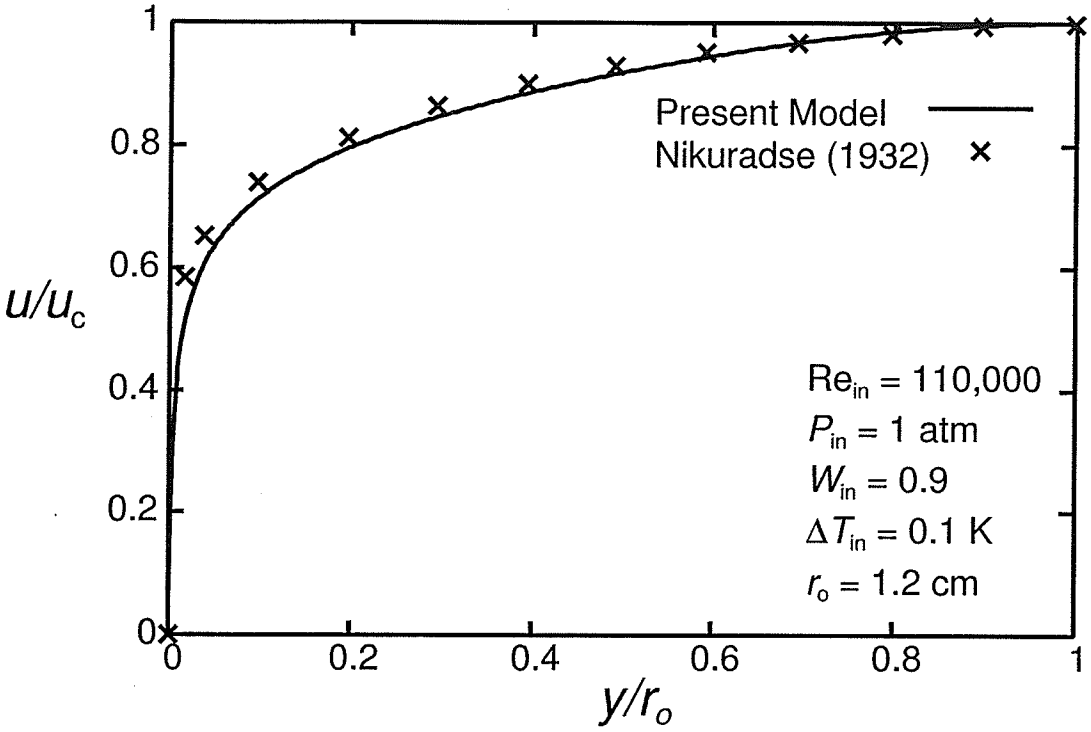

Figure 5.14 Single-phase velocity profile comparison with Nikuradse (1932) for $Re_{in} = 110{,}000$ ($\dot{m}_L / \dot{m}_{v,in} = 1.1 \times 10^{-7}$)

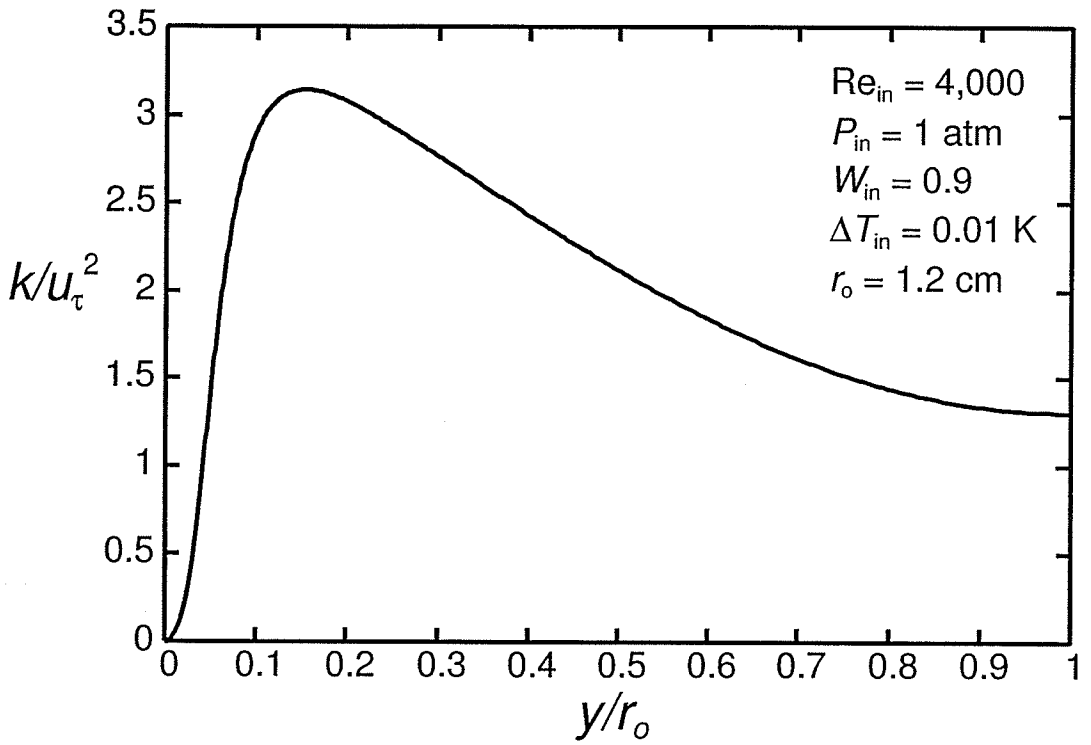

Figure 5.15 Single-phase turbulent kinetic energy pofile for $Re_{in} = 4{,}000$ ($\dot{m}_L / \dot{m}_{v,in} = 6.6 \times 10^{-5}$)

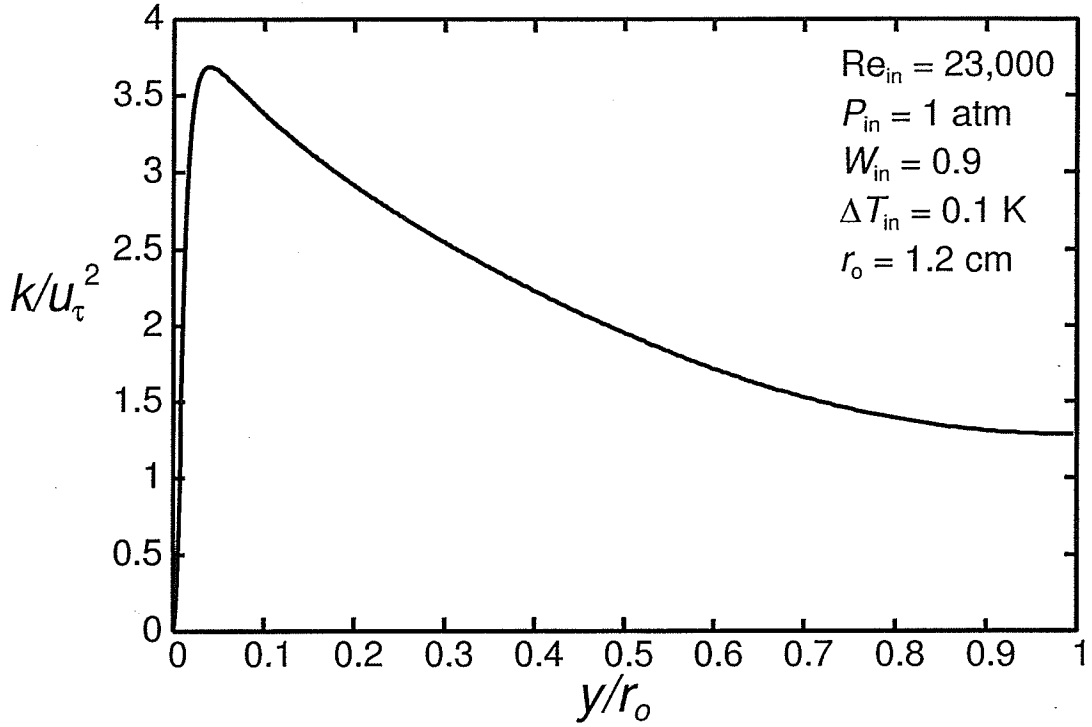

Figure 5.16 Single-phase turbulent kinetic energy profile for $Re_{in} = 23{,}000$ ($\dot{m}_L / \dot{m}_{v,in} = 4.1 \times 10^{-5}$)

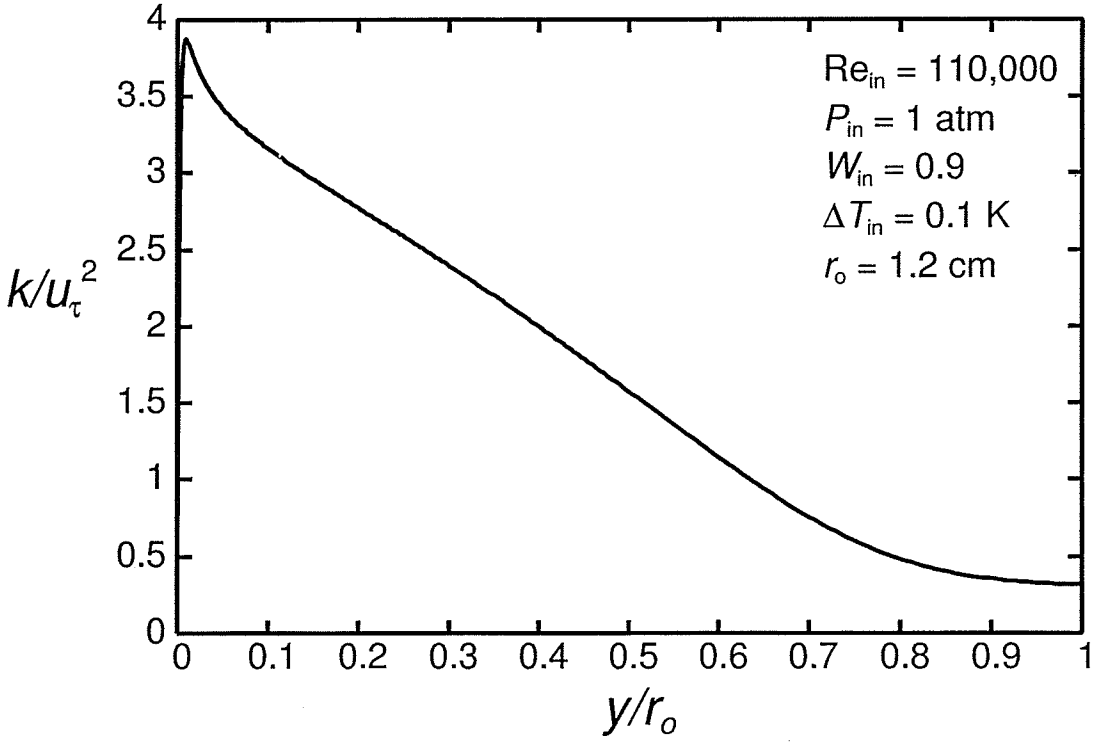

Figure 5.17 Single-phase turbulent kinetic energy profile for $Re_{in} = 110{,}000$ ($\dot{m}_L / \dot{m}_{v,in} = 1.1 \times 10^{-7}$)

5.4.4 k-ε Model in the Film

Only two published articles were found on condensation in vertical tubes using the Jones and Launder low Reynolds number k-ε model in the liquid film: Yuann (1993) and Bellinghausen and Renz (1992). Yuann used this model in both the core and the film and set k and ε to zero at both the wall and the interface. Yuann found that the k-ε model never predicted turbulence in the liquid region; the turbulent viscosity was negligible across the entire film. Bellinghausen and Renz also used this low Reynolds number k-ε model in the liquid. Their boundary conditions are unknown as they were not stated in their paper. They found that a minimum value for μ^t was required for the k-ε model to predict turbulence: $\mu^t_{min} = 0.5\mu$.

The boundary conditions in the present model for k and ε were set to zero at both the interface and the wall. Several authors have justified this choice of boundary condition for the interface. Rodi (1993), Akai et al. (1981), Issa (1988), and Newton and Behnia (2000) developed models for two-phase stratified flow. These authors assumed that for the case of a smooth stratified flow, the interface could be treated as a moving wall and therefore applied the same boundary conditions at the interface as they applied at the wall.

In the present model, when the interface is treated as a wall, the same behavior occurs as did for Yuann; the turbulent viscosity is completely dampened. In order to initiate turbulence in the liquid, attempts were made to set a minimum μ^t as was done in Bellinghausen and Renz (1992). It was found that this did help initiate turbulence at a

certain axial station but the turbulent viscosity was immediately dampened back to zero. In addition to the minimum turbulent viscosity used in Bellinghausen and Renz ($\mu^t_{min} = 0.5\mu$), several other values were tested including $\mu^t_{min} = 0.1\mu$ and $\mu^t_{min} = 0.9\mu$; the turbulent viscosity was still dampened for both these cases. Since no details were given in Bellinghausen and Renz, it was difficult to predict what boundary conditions and methods were used. It was concluded that the low Reynolds number k–ε model would never produce turbulence across a thin film when the boundary conditions are set to zero at the inlet, the wall and the interface.

5.4.5 Comparisons with Yuann (1993)

Yuann (1993) developed a numerical model for condensation from a vapor-gas mixture in vertical tubes using the same governing equations that were used in the present model. In addition, he used the low-Reynolds-number k-ε turbulence model of Jones and Launder (1972) in both the mixture and the liquid regions. Therefore, another test used to validate the k-ε turbulence model in both the liquid and mixture regions was to compare the present numerical results with Yuann's.

Three cases were chosen for comparison from Yuann's results that included conditions with the minimum and the maximum gas mass fraction as well as a low and a high value for inlet pressure. Unfortunately, Yuann did not present tabulated results for various inlet mass flow rates so comparisons could not be made for various $\dot{m}_{in}$; all these results corresponded to $\dot{m}_{in}$ = 40 kg/h. Figures 5.18 to 5.23 show the film-thickness and the heat-transfer-coefficient distributions for the three selected cases. The heat transfer

coefficient in these plots is calculated as $h_{L,z} = \frac{q''_{wall}}{(T_{int} - T_{wall})}$. It must be noted that $h_{L,z}$ used by Yuann was based on the temperature difference, T_{int}-T_{wall}, while h_z that will be used in the present study uses T_{in}-T_{wall} as the temperature difference.

From these figures it can be seen that the largest differences correspond to the case of W_{in} = 0.4, P_{in} = 276 kPa, and ΔT_{in} = 2.13 K (Figures 5.20 and 5.21) while in the other 2 cases, the present numerical results agree reasonably well with Yuann. There are several possible reasons for the differences between the two sets of results.

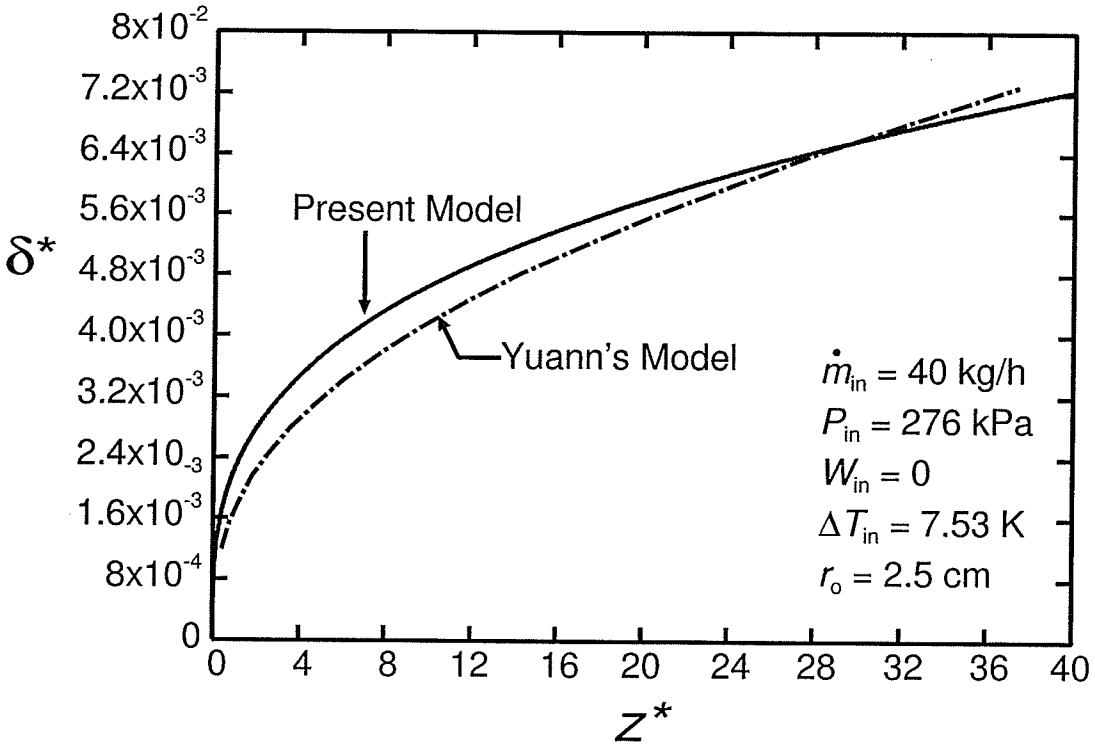

Figure 5.18 Dimensionless film thickness comparison with Yuann (1993) for P_{in} = 276 kPa, W_{in} = 0, and ΔT_{in} = 7.53 K

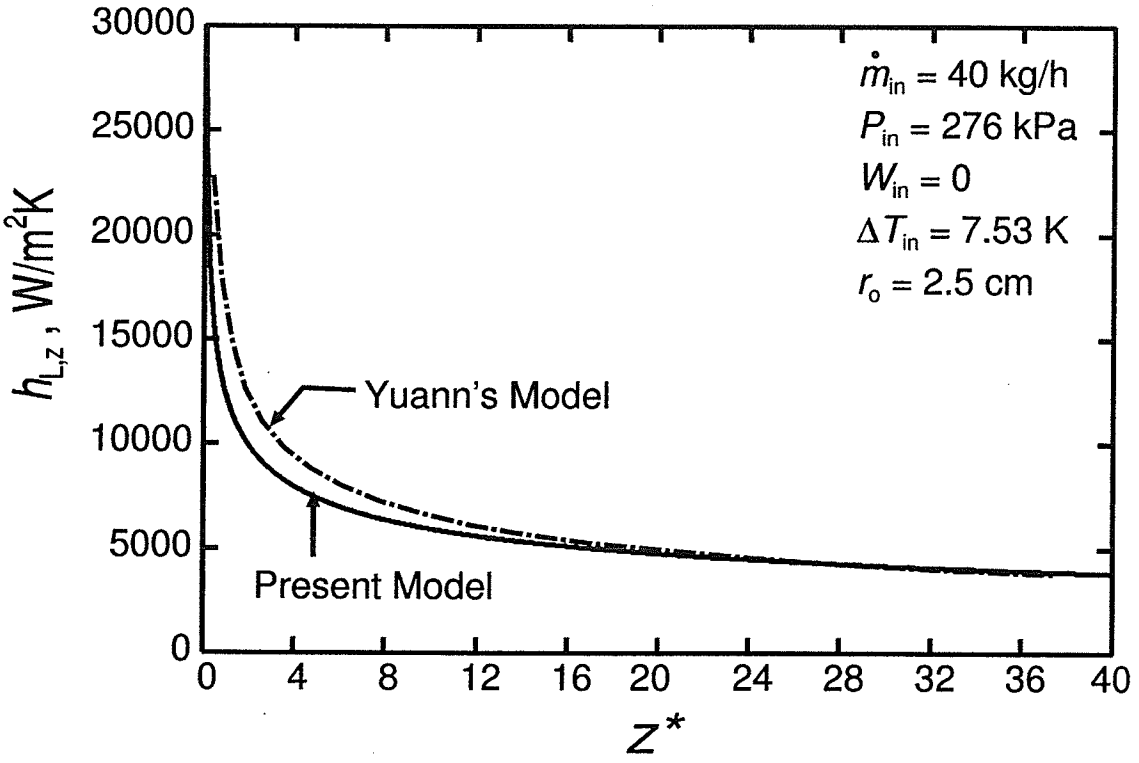

Figure 5.19 Heat transfer coefficient comparison with Yuann (1993) for P_{in} = 276 kPa, W_{in} = 0, and ΔT_{in} = 7.53 K

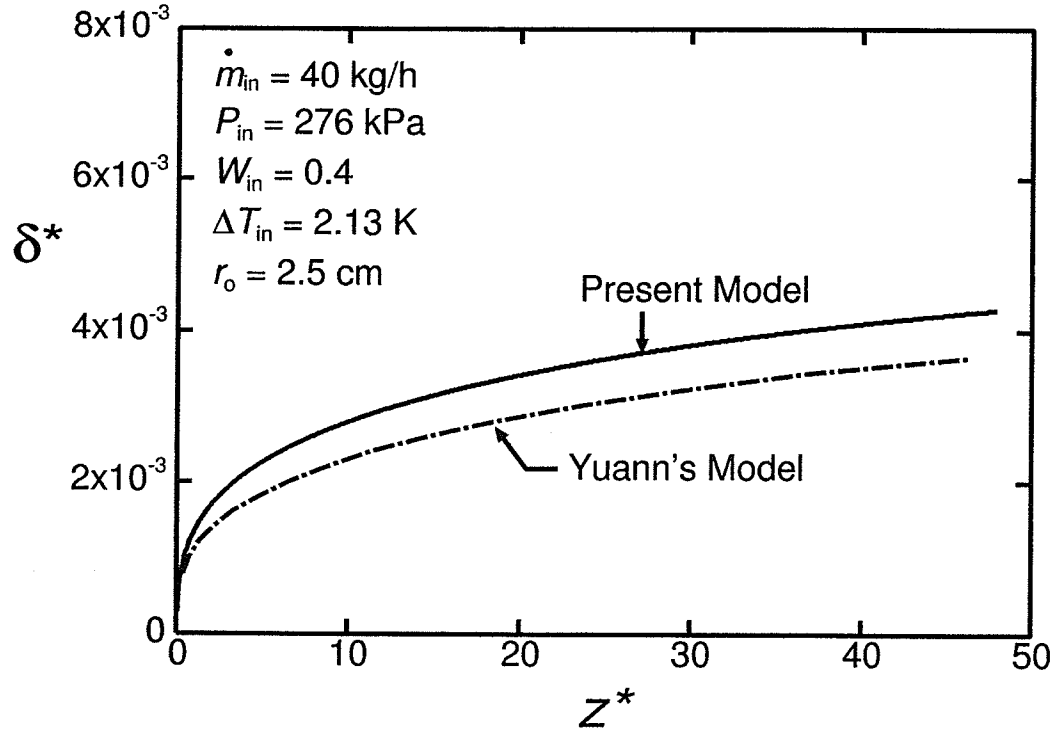

Figure 5.20 Dimensionless film thickness comparison with Yuann (1993) for P_{in} = 276 kPa, W_{in} = 0.4, and ΔT_{in} = 2.13 K

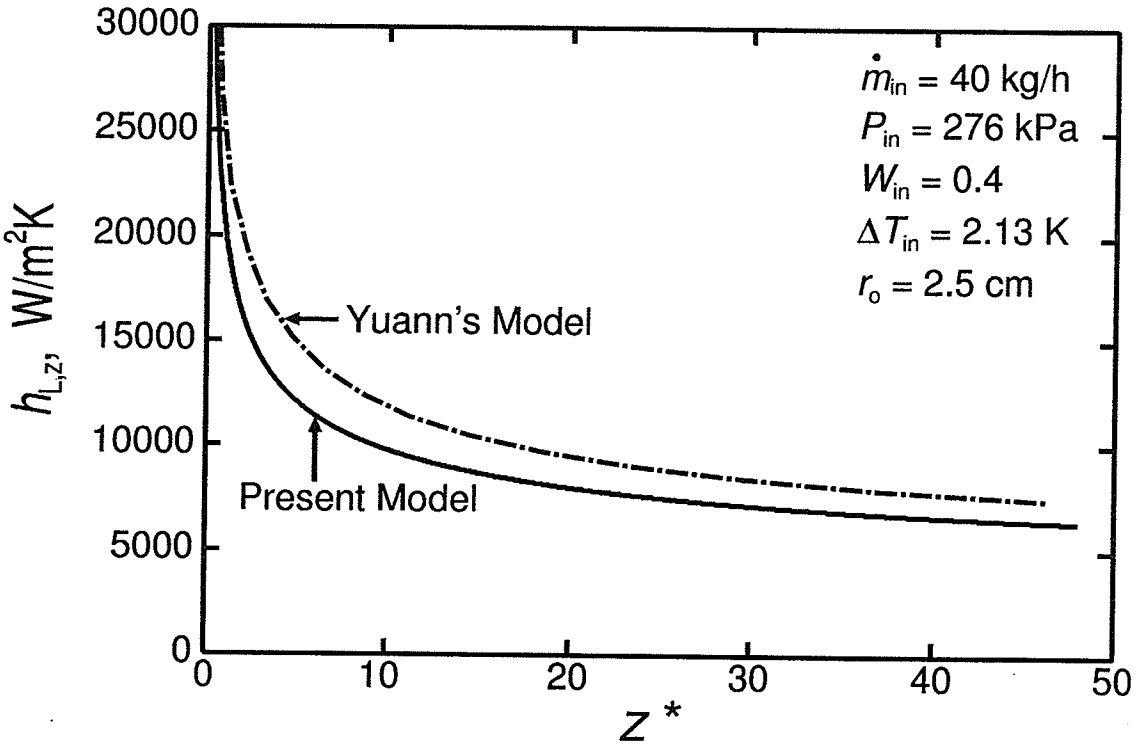

Figure 5.21 Heat transfer coefficient comparison with Yuann (1993) for P_{in} = 276 kPa, W_{in} = 0.4, and ΔT_{in} = 2.13 K

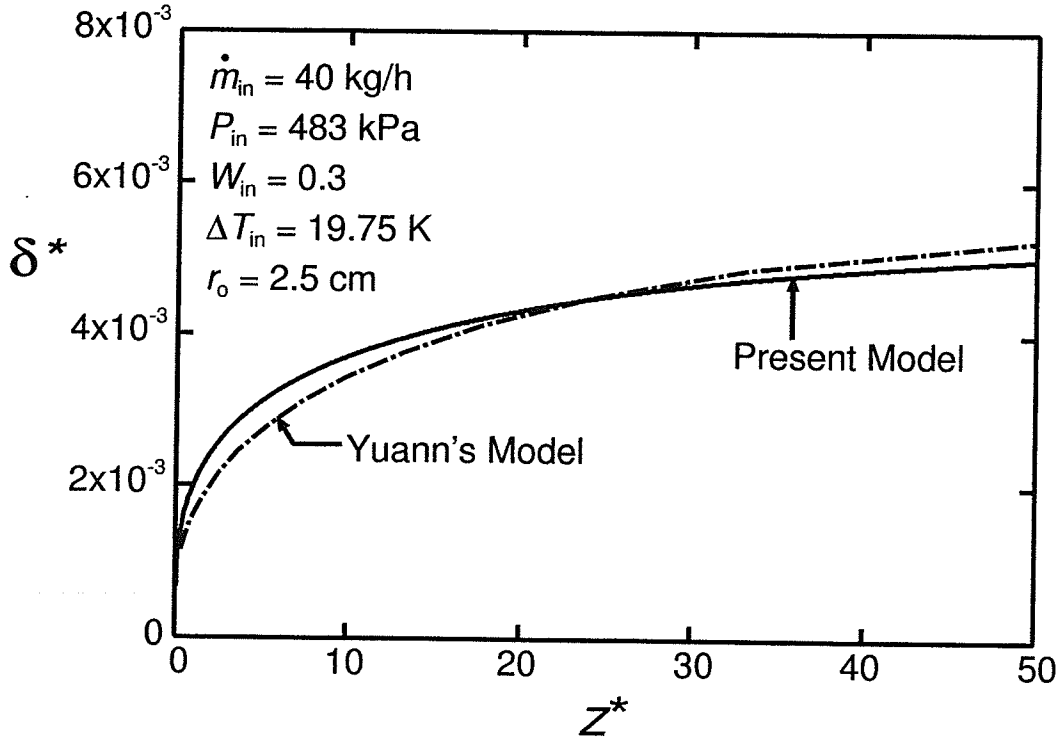

Figure 5.22 Dimensionless film thickness comparison with Yuann (1993) for P_{in} = 483 kPa, W_{in} = 0.3, and ΔT_{in} = 19.75 K

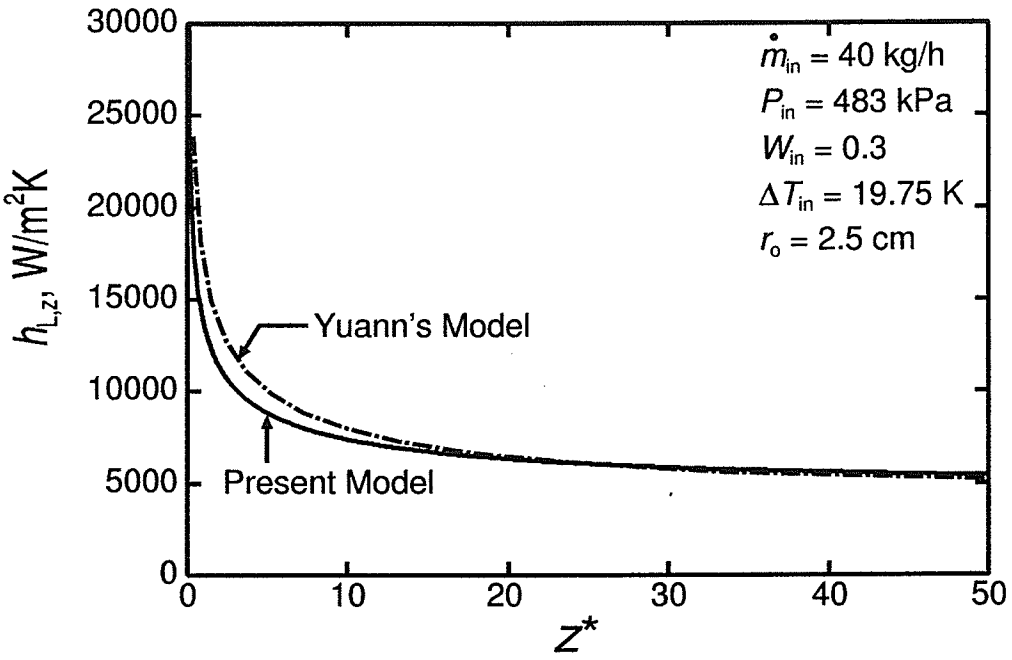

5.23 Heat transfer coefficient comparison with Yuann (1993) for P_{in} = 483 kPa, W_{in} = 0.3, and ΔT_{in} = 19.73 K

One discrepancy that was found between the present results and Yuann's was that although the conditions of inlet mass flow rate, inlet temperature, inlet pressure, and the tube diameter were set to match Yuann's, the calculated value of Re_{in} from the present model did not always agree with his. It was found that the present value of Re_{in} agreed closely with Yuann's for cases of pure steam; however, for cases with steam-air mixtures, Yuann's values of Re_{in} were higher than the present values and the discrepancy increased with increasing W_{in}. The formulae used by Yuann for calculating the mixture properties are identical to the formulae used in the present study; therefore, differences in the values of the viscosity of air are the only possible reason for the discrepancy in Re_{in}. In order to ensure that our property values were correct, the viscosity of air used in the present analysis was compared with the values from Incropera and DeWitt (1996) for temperatures from 250 K to 600 K and deviations were always less than 1 %.

Another major difference between Yuann's work and the present analysis is that he used the *r-z* coordinate system in discretizing the flow domain, while the $\eta-\chi$ coordinate system was used in the present work. There are several advantages in using the $\eta-\chi$ coordinate system. In the *r-z* coordinate system, the number of control volumes in the film was increased from one axial station to the next, while in the $\eta-\chi$, a fixed number of control volumes in the film was used at all axial stations. Another advantage in using the $\eta-\chi$ coordinates is that the control-volume faces are orthogonal everywhere in the domain, while in the *r-z* coordinate system, the control-volume faces are non-orthogonal at the interface. Finally, the last advantage that will be mentioned here is that in the $\eta-\chi$ coordinate system used in the present model, the spacing between the nodes in the radial direction remains constant when advancing from one station to the next; however, in the *r-z* coordinate system the spacing is more complicated. In Yuann's thesis, advancing the mesh from one station to another in the liquid film was clearly explained, while advancing the mesh in the mixture region from one station to the next was not elaborated on. There are several complications that arise when using the *r-z* coordinate system for this problem that were eliminated when the $\eta-\chi$ coordinate system was used.

In addition to the above differences between Yuann's approach and the present approach, there are several other differences that were found between the present analysis and Yuann's; these differences are listed below:

1. For the $v-$ velocity boundary condition at the centerline, Yuann used $\partial v/\partial r = 0$ while in the present model the *v*-velocity was set to zero. The radial velocity must

vanish at the centerline otherwise there will be a mass source or sink at the centerline.

2. In Yuann's model, the film thickness was calculated from an energy balance across the entire liquid film while in the present model, the film thickness was calculated from an energy balance at the interface.
3. Yuann used a completely segregated approach in his solution method while the present model uses a fully coupled approach.
4. Yuann included an empirical correlation to account for surface waviness at the interface. The addition of this correlation resulted in a thinner film and a larger heat transfer coefficient, as seen in Figures 5.18 to 5.23.

The above figures and discussion show that for the most part, the present model agrees reasonably well with Yuann's results and the discrepancies found are likely due to the different methods used in the numerical models.

CHAPTER 6

LAMINAR FLOW RESULTS

6.1 Introduction

In order to obtain laminar results from the model, the turbulent viscosity was set to zero and the equations of the turbulence model were not solved. In this chapter, the velocity, temperature and gas mass fraction profiles will be analyzed as well as the film thickness and Nusselt number distributions. In addition, the effect of varying the independent parameters on the film thickness and Nusselt number will be studied. Results were obtained for steam-air mixtures entering the tube with inlet Reynolds numbers between 500 and 2000, inlet gas mass fractions between 0 and 0.8, inlet pressures from 0.5 atm to 2 atm, and temperature differences from 5 to 20 K. These results have been reported in a recent publication by Groff et al. (2004).

6.2 Velocity, Temperature and Gas Mass Fraction

The results presented in Figures 6.1 to 6.3 are profiles of dimensionless velocity, dimensionless temperature, and gas mass fraction at various axial stations along the tube. The conditions used for these results are an inlet pressure of 1 atm, an inlet Reynolds number of 1000, a temperature difference of 20 K, and an inlet gas mass fraction of 0.2. The mixture region corresponds to $\eta = 0$ to 1 and the liquid film region corresponds to $\eta = 1$ to 2. From the dimensionless velocity profile in Figure 6.1, it can be observed that as z^* increases to 25, the velocity in the mixture decreases, while the velocity in the liquid film increases. This trend is due to the transfer of mass from the mixture to the liquid.

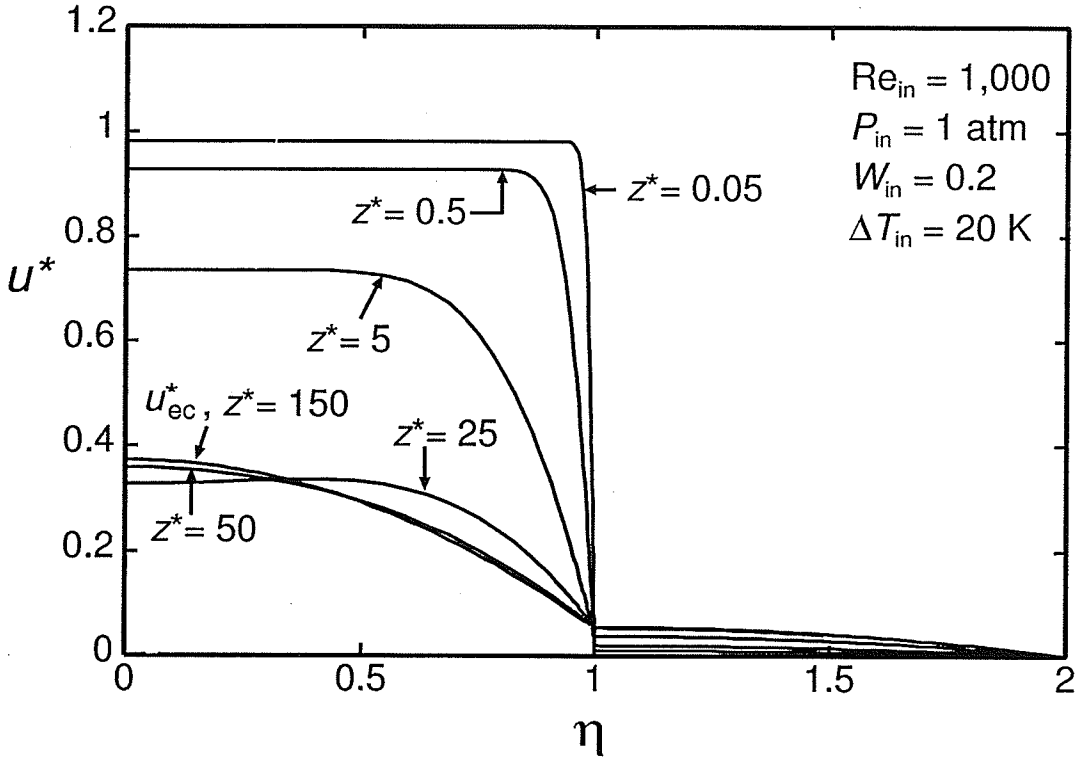

Figure 6.1 Dimensionless velocity profiles

As the mixture loses mass, it loses speed; the liquid film is gaining mass and accelerating. As z^* increases from 25 to 150, the velocity near the centerline increases while the mixture velocity near the interface continues to decrease. The increase in centerline velocity will be discussed later. A boundary layer can be seen to form in the mixture region at the liquid-mixture interface. As z^* increases, the boundary layer thickness increases. Far from the inlet ($z^* = 150$), the condensation process shuts off and the velocity profile converges to the exact solution for u_{ec}^*.

The dimensionless temperature profiles in Figure 6.2 indicate that the temperature profiles in the liquid region are nearly linear, and that the interface temperature decreases along the length of the tube, resulting in lower heat transfer across the film. The

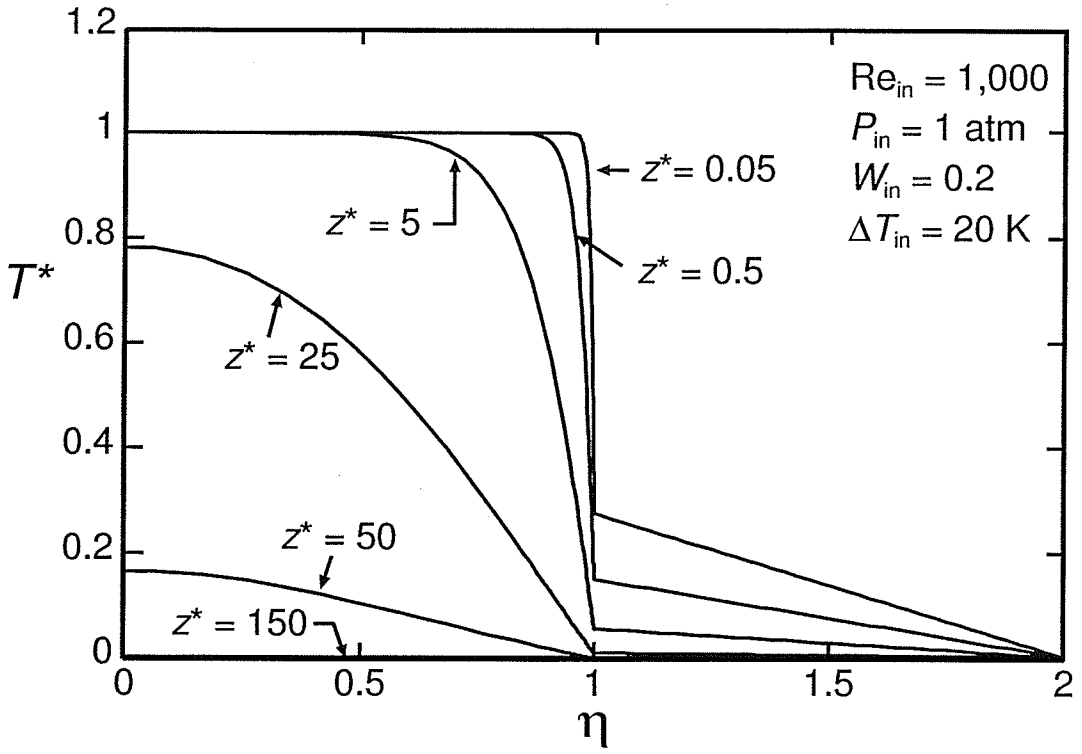

Figure 6.2 Dimensionless temperature profiles

temperature in the mixture region also decreases continuously along the tube. The mixture temperature T_M starts at T_{in} (T^* =1) at z^* = 0 and approaches T_{wall} (T^* = 0) at z^* = 150. The slope at the interface also decreases with increasing z^*. At z^* = 150, $T^* \approx$ 0 everywhere and the condensation process is shut off.

Figure 6.3 shows the profiles of the gas mass fraction, W. Near the inlet (up to z^* = 0.5), $W = W_{in}$ for the majority of the cross section but increases rapidly near the interface due to the interface impermeability condition. Along the length of the tube, the gas mass fraction increases at the centerline and the slope near the interface decreases. Far from the inlet, at z^* = 150, the gas mass fraction profile is fairly flat and is equal to the end of condensation value of 0.71.

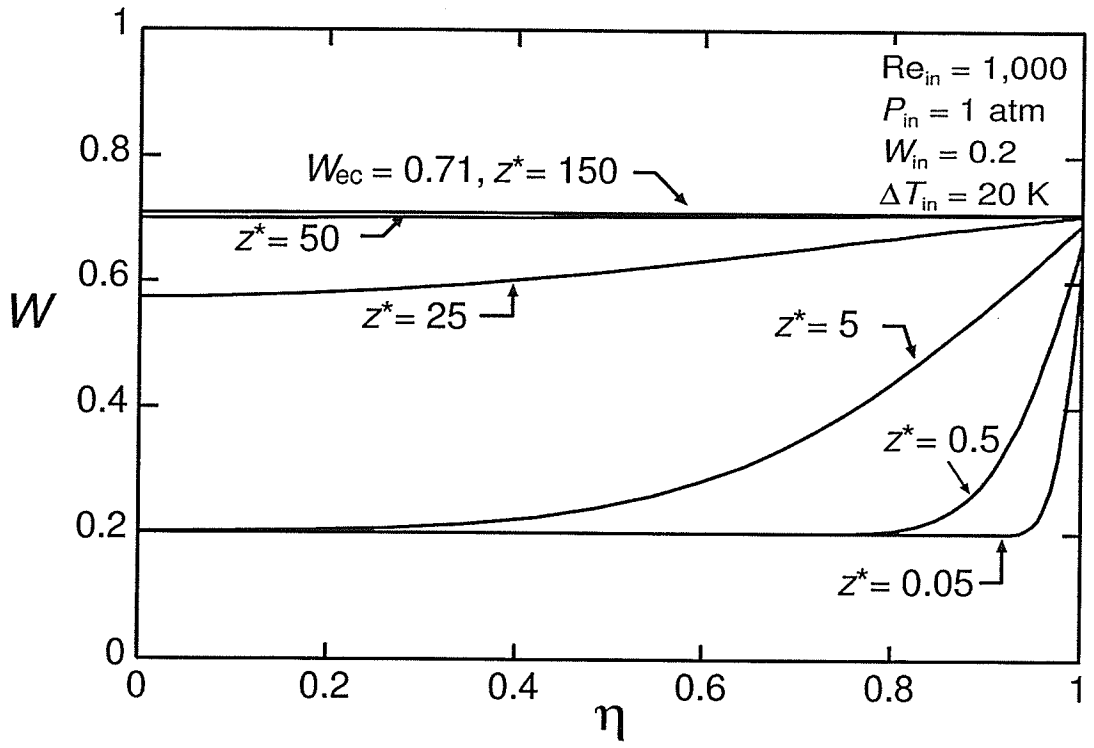

Figure 6.3 Gas mass fraction profiles

Figure 6.4 shows dimensionless velocity profiles at different z^* locations for the case of $W_{in} = 0.6$, $P_{in} = 1$ atm, $Re_{in} = 1000$ and $\Delta T_{in} = 20$ K. In this case, the much higher amount of gas significantly reduces the condensation rate. Comparing the velocity profiles in Figure 6.4 to the profiles in Figure 6.1 (for an inlet gas mass fraction of 0.2), several differences can be observed. First, the mixture velocity does not decrease as rapidly in Figure 6.4 as it did in Figure 6.1. This trend is due to the much lower rate of mass removal from the mixture for $W_{in} = 0.6$. Second, because the mixture is not losing mass rapidly, a boundary layer development similar to that for a single phase pipe flow is seen. This development is seen in the increase in centerline velocity up to approximately $z^* = 25$, compared to the decrease in centerline velocity up to $z^* = 25$ seen in Figure 6.1. Finally, in the case of $W_{in} = 0.6$, the centerline velocity decreases from $z^* = 25$ to

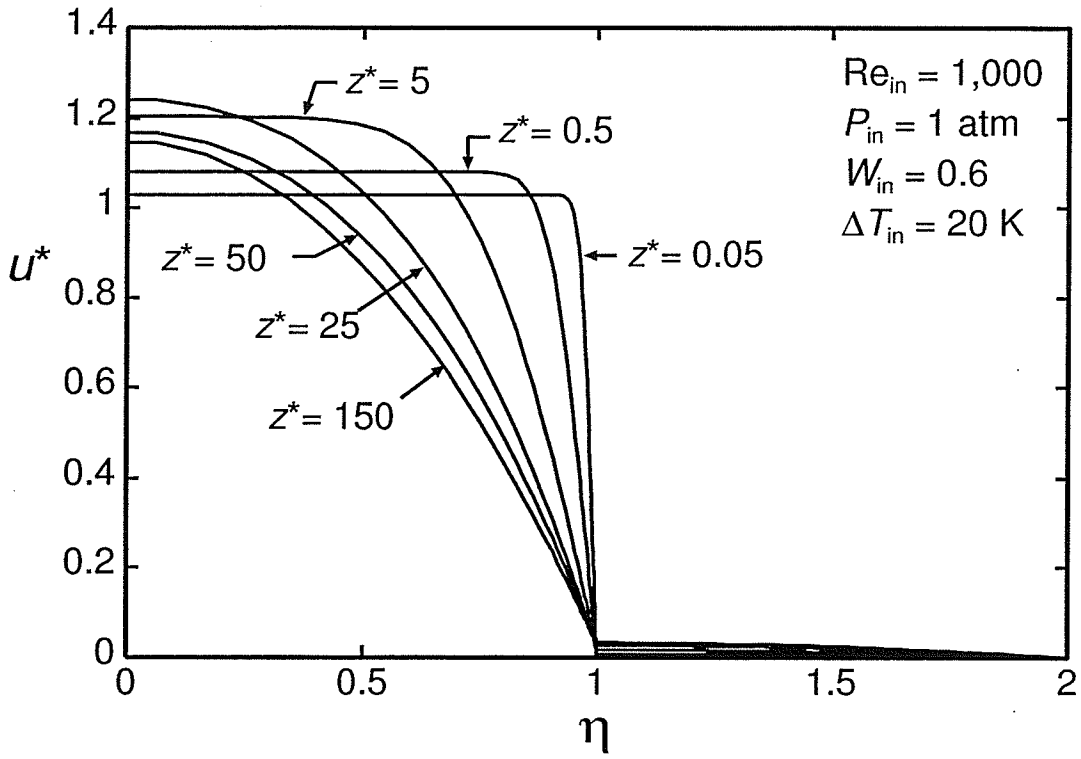

Figure 6.4 Dimensionless velocity profiles for $W_{in} = 0.6$

z^* =150, while the centerline velocity increased after $z^* = 25$ in the case of $W_{in} = 0.2$. These opposing trends will be discussed in the following section with reference to Figure 6.5.

Figure 6.5 shows the axial variation of the dimensionless centerline velocity for different inlet gas mass fractions. For the case of pure steam ($W_{in} = 0$), the centerline velocity decreases to zero once all the steam has condensed. Under these conditions, flow reversal occurs for $W_{in} < 0.08$. For all the other cases ($W_{in} \geq 0.08$), u_c^* reaches the analytically predicted end of condensation value at large z^* and remains constant. As noted in the discussion of Figure 6.1, when $W_{in} = 0.2$, u_c^* decreases due to the high

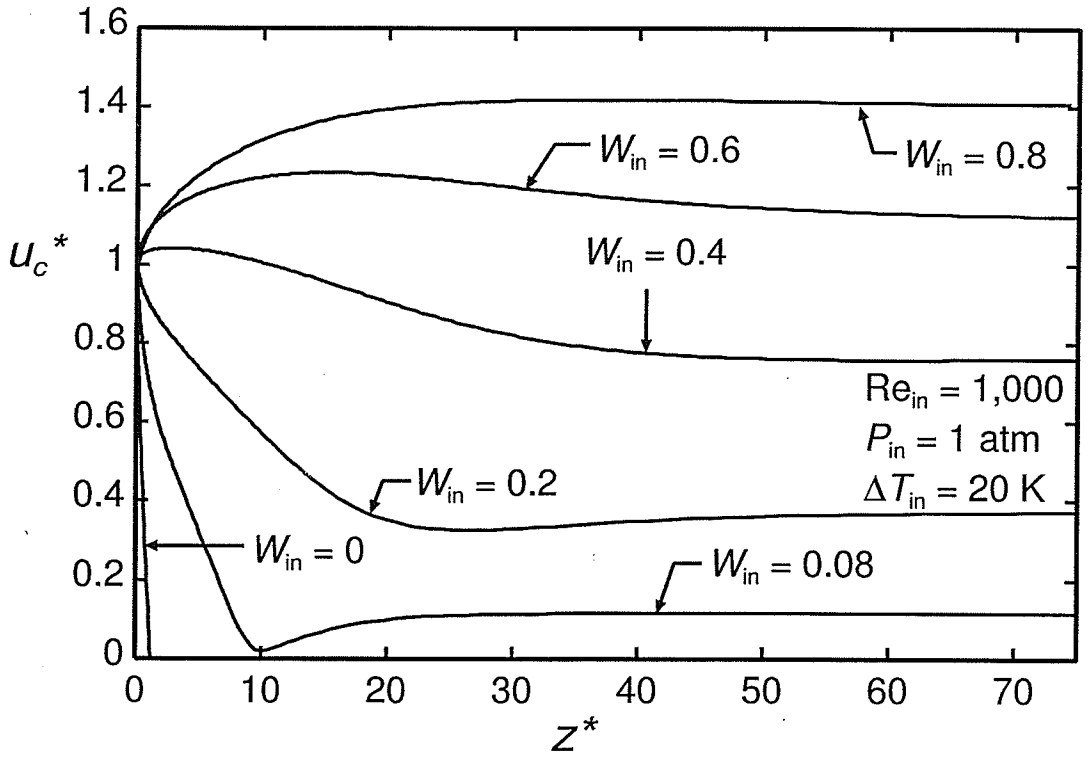

Figure 6.5 Centerline velocity distribution

condensation rate until $z^* \approx 25$, where it starts increasing. After $z^* = 25$, the condensation rate is very small and the increase in u_c^* is due to the increase in the amount of heavier gas at the centerline from $z^* = 25$ to $z^* = 50$; the W increase at the centerline is seen in Figure 6.3. Since the total mixture mass is not changing rapidly, the increase in gas mass fraction near the center line results in a higher centerline velocity. For the case of $W_{in} = 0.6$, the velocity at the centerline increases until $z^* \approx 20$. As mentioned earlier, this trend is due to hydrodynamic development dominating over the effects of mass removal. At $z^* \approx 20$ the centerline velocity starts to decrease. This decrease in the centerline velocity results from condensation beginning to have an effect in removing mass from the mixture. This reduction of mixture mass is consistent with the velocity profiles seen in Figure 6.4. When $W_{in} = 0.8$, the condensation rate is so low that the hydrodynamic

development dominates for the entire length of the tube; therefore, the centerline velocity continues to increase until it reaches the 'end of condensation' where it levels off.

6.3 Film Thickness and Nusselt Number Distributions

Figures 6.6 and 6.7 show the dimensionless film thickness and the Nusselt number distributions for an inlet pressure of 1 atm, an inlet Reynolds number of 1,000, a temperature difference of 20 K, and an inlet gas mass fraction of 0.2. Figure 6.6 shows how the rate of change in film thickness, $d\delta^*/dz^*$, is highest near the inlet and decreases until the film thickness reaches $\delta^*_{ec} = 0.00655$. At this point, the condensation process shuts off and the film thickness remains constant with z^*. The rate of change in film thickness is largest near the inlet because the heat transfer rate, and thus the condensation rate, is largest near the inlet. This trend in the heat transfer rate is confirmed in Figure 6.7. The Nusselt number is largest at the inlet, and then decreases to zero at the end of condensation.

6.4 The Effect of Re_{in}, ΔT_{in}, P_{in} and W_{in}

Figures 6.8 and 6.9 examine the effects of changing the inlet-to-wall temperature difference, ΔT_{in}, and the inlet gas mass fraction, W_{in}, on the film thickness and the Nusselt number. The Reynolds number is 1,000, and the inlet pressure is 1 atm. For fixed P_{in} and W_{in}, increasing ΔT_{in} corresponds to decreasing T_{wall}.

In Figure 6.8 it can be seen that as ΔT_{in} increases, $d\delta^*/dz^*$ increases near the tube inlet for both values of W_{in}. In addition, $d\delta^*/dz^*$ also increases with decreasing W_{in} at the

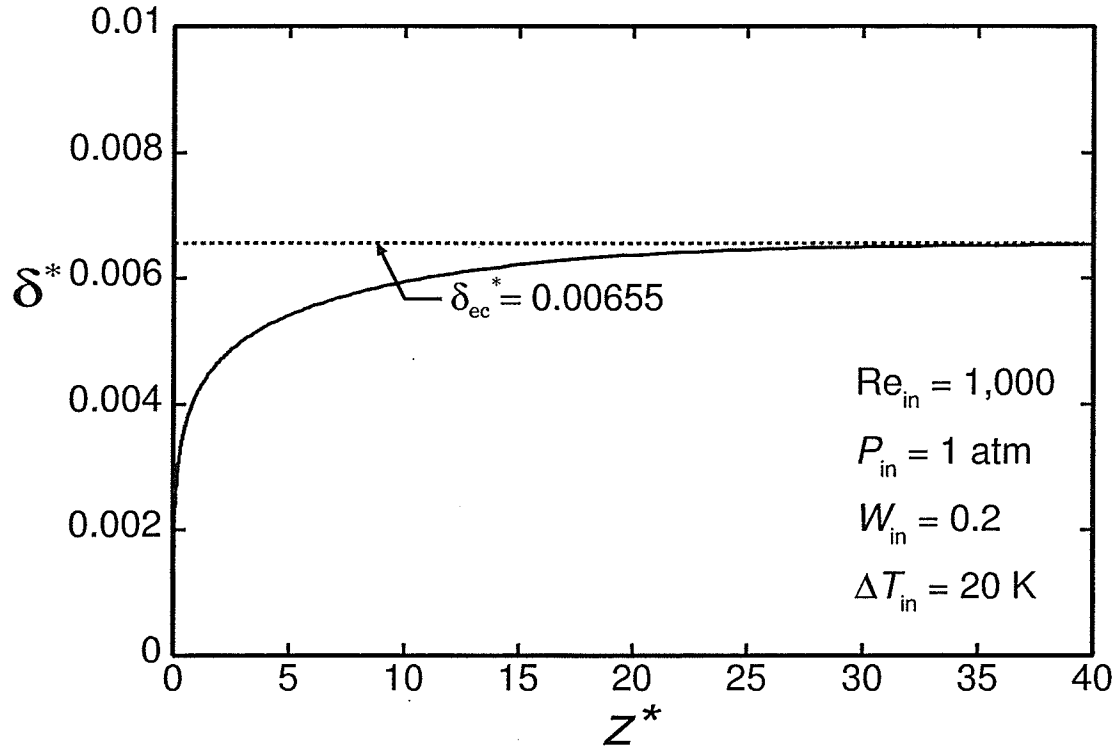

Figure 6.6 Dimensionless film thickness distribution

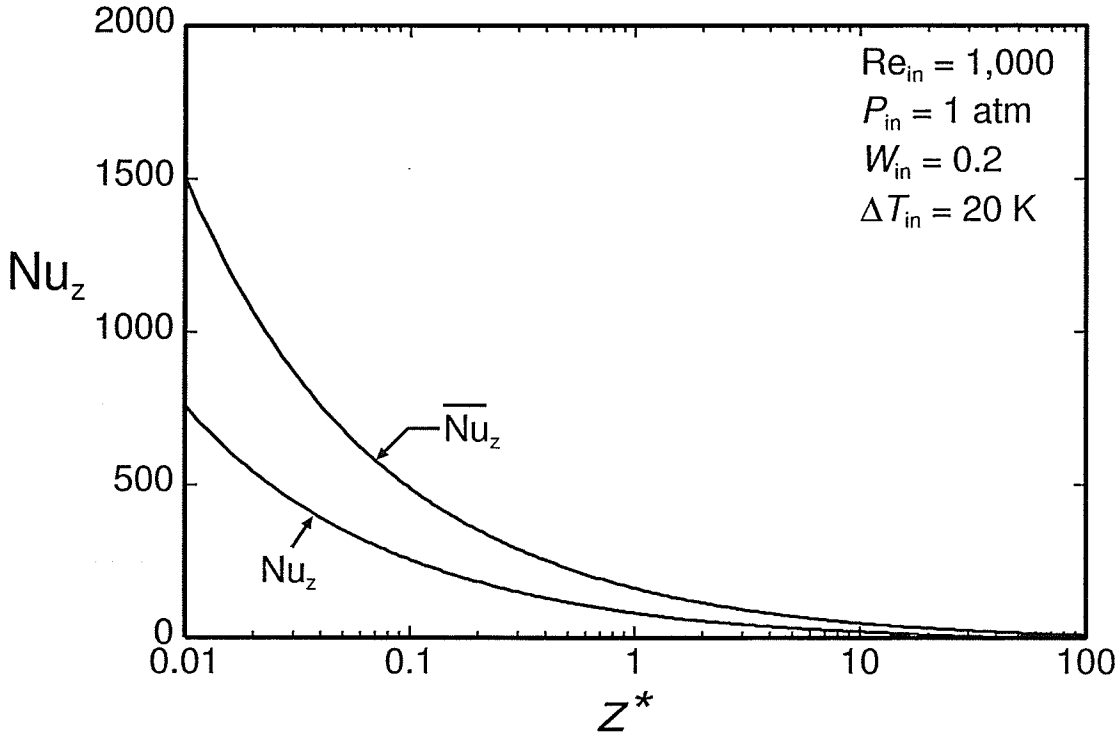

Figure 6.7 Nusselt number distribution

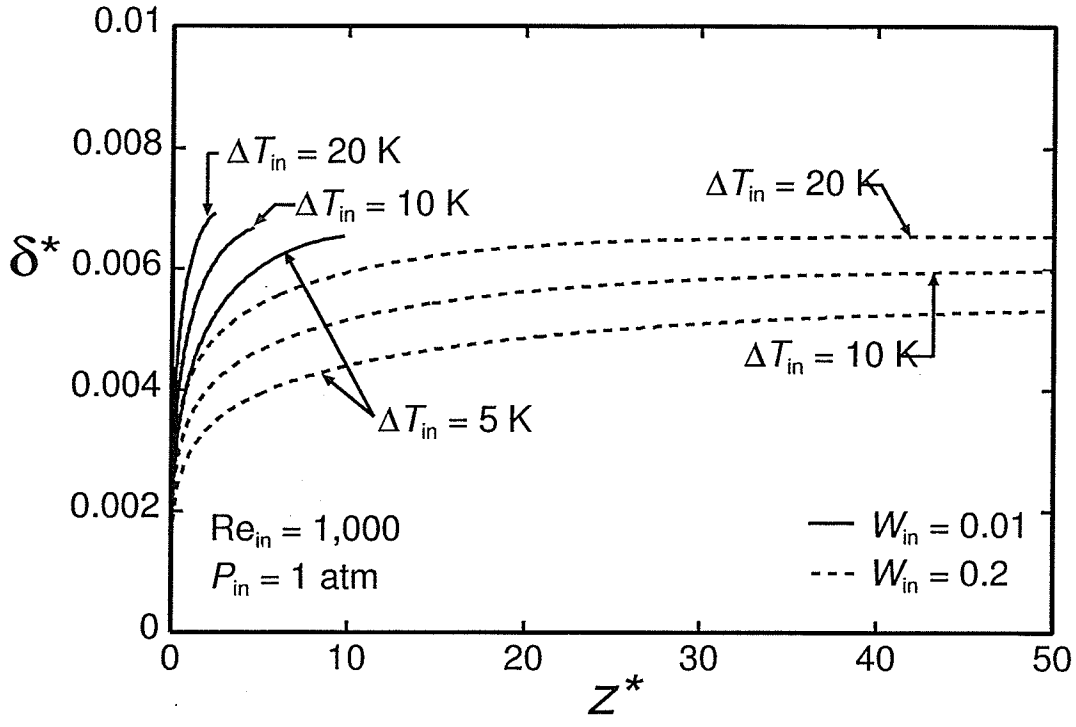

Figure 6.8 Effect of ΔT_{in} and W_{in} on the dimensionless film thickness

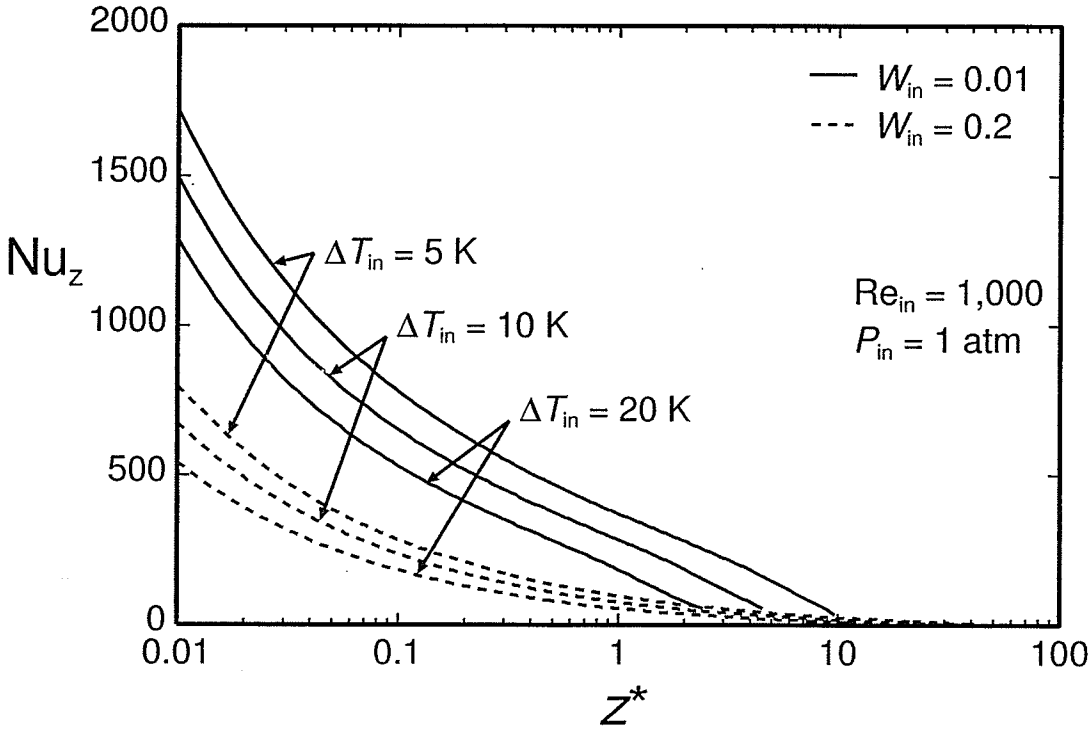

Figure 6.9 Effect of ΔT_{in} and W_{in} on the local Nusselt number

same ΔT_{in}. It is expected that a higher ΔT_{in} and lower inlet gas mass fraction will each result in a greater heat transfer rate. For $W_{in} = 0.01$, the condensation rate is high and flow reversal occurs, so the end of condensation is never reached. When $W_{in} = 0.01$, there is also a significant decrease in the tube length at which flow reversal occurs as ΔT_{in} increases. It is also observed from Figure 6.8 that the film thickness at the end of condensation increases with increasing ΔT_{in} for both inlet gas mass fraction values. When W_{in}, Re_{in}, and P_{in} are fixed, there is a fixed amount of vapor mass flow at the inlet. Therefore, the difference in film thickness is due to a difference in the amount of vapor condensed. At higher ΔT_{in}, the lower wall temperature results in a lower mixture temperature at the end of condensation. A lower mixture temperature corresponds to a decreased amount of vapor in the mixture, and thus more mass in the liquid and a thicker film for higher ΔT_{in}.

The effect of ΔT_{in} and W_{in} on Nusselt number can be seen in Figure 6.9. These results show that Nu_z decreases with increasing ΔT_{in}; which is consistent with the thicker film and thus more resistance to heat transfer. A comparison of the curves for $W_{in} = 0.01$ with the curves for $W_{in} = 0.2$ in Figure 6.9 shows how the presence of air greatly reduces the heat transfer rate.

Figures 6.10 and 6.11 demonstrate how a change in Re_{in} affects the film thickness and the Nusselt number for steam-air at $P_{in} = 1$ atm, $W_{in} = 0.2$, and $\Delta T_{in} = 5$ K and 20 K. From Figure 6.10 it can be seen that as the Reynolds number increases, $d\delta^*/dz^*$ increases near the tube inlet and the film thickness at the end of condensation also increases;

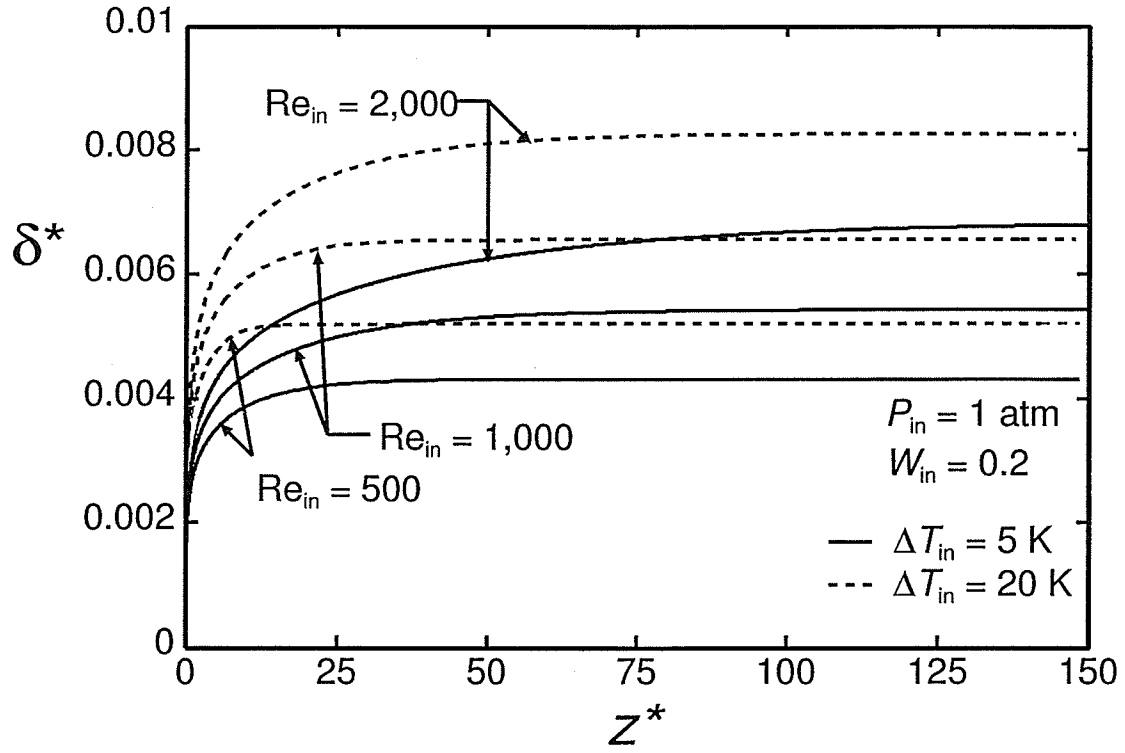

Figure 6.10 Effect of Re_{in} and ΔT_{in} on the dimensionless film thickness

therefore, a larger Reynolds number results in higher condensation rates. In addition, the length of the pipe required for complete condensation increases with increasing Reynolds number.

The effect of changing Re_{in} on the heat transfer rate is shown in Figure 6.11 in terms of $(Nu_z/Re_{in}^{0.43})$ versus z^*. The results for the three values of Re_{in} (Re_{in} = 500, 1,000, and 2,000) for both values of ΔT_{in} (ΔT_{in} = 5 and 20 K) are shown in this figure. For each ΔT_{in}, the results for all three Re_{in} values collapse fairly well onto the same curve. Although this was not an attempt at a correlation, several different exponents for Re_{in} were tested and 0.43 was selected for the purpose of this graph.

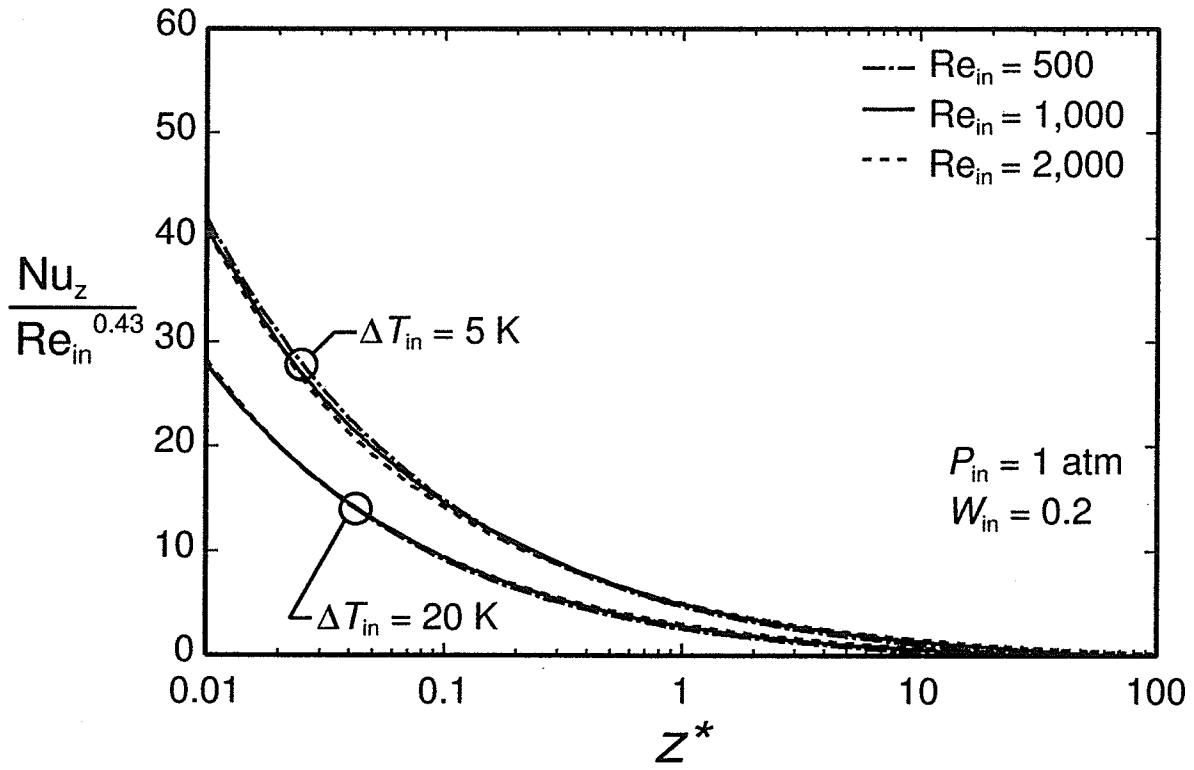

Figure 6.11 Effect of Re_{in} and ΔT_{in} on the local Nusselt number

Finally, the effect of changing P_{in} is shown in Figures 6.12 and 6.13 for Re_{in} = 1,000 and ΔT_{in} = 5 K. Results are shown for three different inlet pressures (P_{in} = 0.5, 1 and 2 atm) and two different inlet gas mass fractions (W_{in} = 0.01 and 0.2). In Figures 6.12 and 6.13, increasing P_{in} at the same W_{in} causes an increase in the inlet temperature. Because the temperature difference is constant, T_{wall} will increase. In Figure 6.12, it is seen that for W_{in} = 0.01, increasing the inlet pressure decreases the rate of increase in film thickness, $d\delta^*/dz^*$, and shortens the length at which reversal occurs. For W_{in} = 0.2, δ^*_{ec} decreases with increasing inlet pressure. These trends are expected to be primarily related to changes in the properties. Figure 6.13 shows that Nusselt number decreases near the inlet for increasing inlet pressures. However, for $z^* \geq 0.1$, a change in the inlet pressure does not have much effect on Nusselt number.

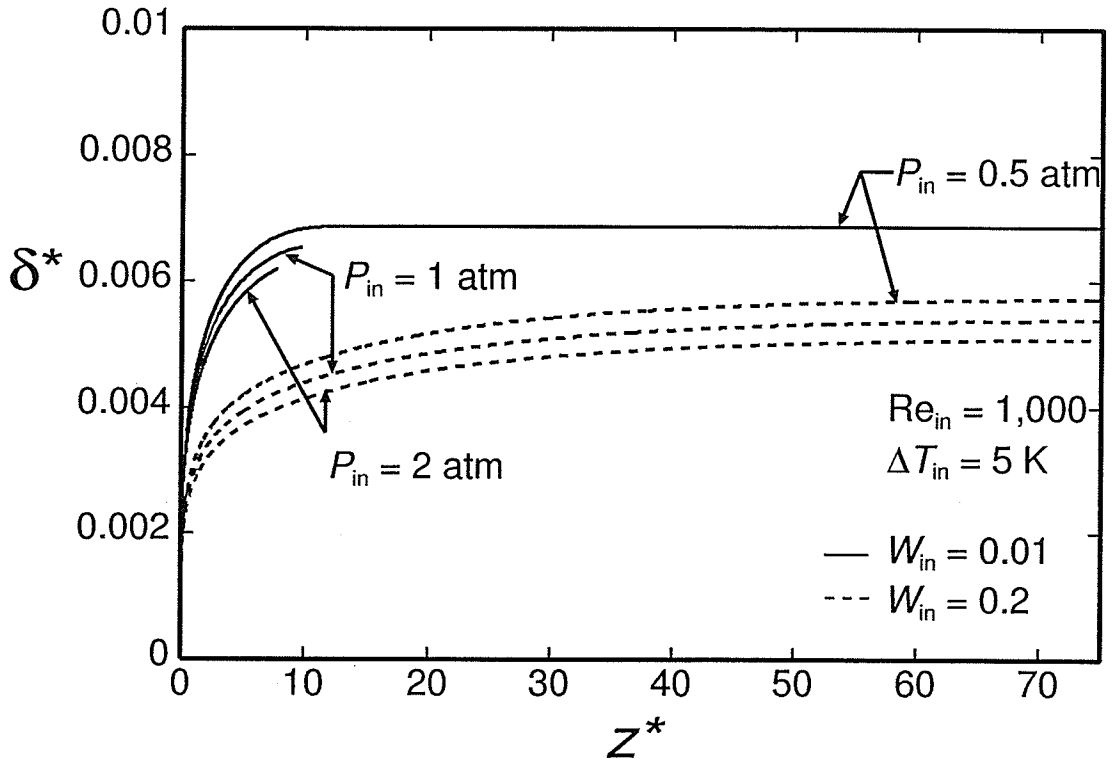

Figure 6.12 Effect of P_{in} and W_{in} on the dimensionless film thickness

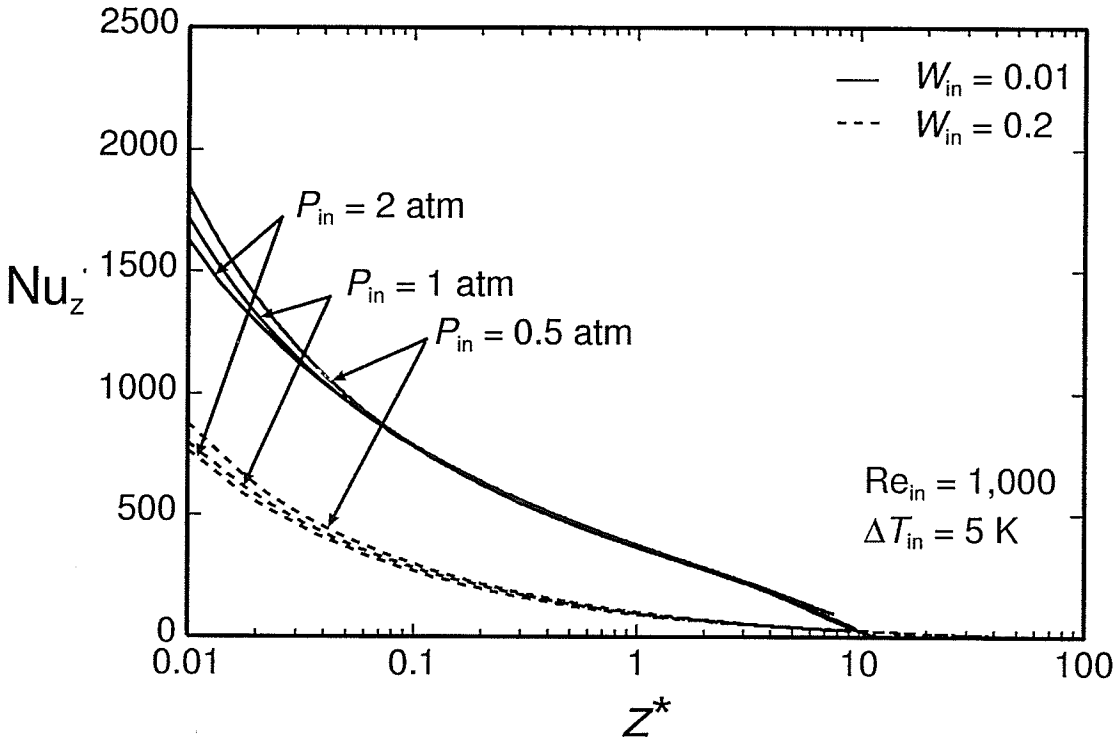

Figure 6.13 Effect of P_{in} and W_{in} on the local Nusselt number

6.5 Summary

Several conclusions can be drawn from the laminar results presented in this chapter. The presence of gas in the mixture was found to greatly inhibit the heat transfer process. The film thickness increased when either ΔT_{in} or Re_{in} was increased or when W_{in} or P_{in} was decreased. The Nusselt number increased with increasing Re_{in} or decreasing ΔT_{in} or W_{in}. Beyond $z^* \approx 0.1$, changing P_{in} had negligible effect on Nusselt number for the conditions studied.

CHAPTER 7

COMPARISONS WITH EXPERIMENTS

7.1 Introduction

To further validate the numerical model and compare the predictions of different turbulence models, three experiments were chosen: Goodykoontz and Dorsch (1966), Siddique (1992), and Kuhn (1995). Several test cases were chosen from each of these experiments and for each case the program was run using three different turbulence models. The turbulence models are shown in Table 1 below.

Table 7.1 Turbulence models

Model	Mixture Region	Liquid Film
1	Pletcher's (1974) Mixing Length Model	Pletcher's (1974) Mixing Length Model
2	Jones and Launder (1972) Low Reynolds Number k-ε Model	Jones and Launder (1972) Low Reynolds Number k-ε Model
3	Jones and Launder (1972) Low Reynolds Number k-ε Model	Pletcher's (1974) Mixing Length Model

From this point on, the models will be referred to by their numbers shown in the left column of Table 7.1. For each test case chosen from the experiments, heat transfer coefficient results were obtained for each of the three turbulence models. The results from all three models were compared with those found in the experiments. In order to make accurate comparisons, the boundary conditions in the model were set to emulate those found in the experiments.

7.2 Comparisons with Goodykoontz and Dorsch (1966)

Goodykoontz and Dorsch (1966) performed experiments for pure steam condensation in a 15.9-mm diameter vertical tube. They presented 14 test cases with the following range of conditions:

Re_{in}: 27,000 to 85,000

P_{in}: 100 kPa to 400 kPa

ΔT_{in}: 5 to 18 K

From these 14 test cases, the following six were chosen for comparisons:

Table 7.2 Runs Chosen from Goodykoontz and Dorsch (1966)

Run #	Re_{in}	P_{in} (kPa)	ΔT_{in} (K)	x_{in}
3	82,900	243	11.8	0.99
4	90,500	252	12.6	0.99
5	37,600	269	14.8	0.96
6	45,100	307	13.2	0.96
7	64,500	265	16.8	0.97
9	27,800	138	12.5	0.94

In Table 7.2 above, the parameter x_{in} refers to the inlet quality at z = 0. These six cases captured the maximum and minimum inlet Reynolds numbers as well as four different Reynolds numbers within these limits. Test runs with inlet superheat were avoided.

The inlet of the test section used in Goodykoontz and Dorsch's experiments consisted of a 14.4-cm adiabatic section which allowed the velocity profile to reach a fully developed profile at $z = 0$ (beginning of cooling). To model these inlet conditions, a fully developed inlet velocity profile and a fully developed turbulent viscosity profile were used in the model. These profiles were obtained by running the program for single-phase pipe flow with the same inlet Reynolds number until a fully developed flow was reached. The resulting fully developed velocity and turbulent viscosity profiles were then used as the inlet profiles for the condensation model run.

The wall temperature was set to match the experiments by fitting a polynomial to the measured wall temperatures and using this polynomial to calculate T_{wall} at each station. From Table 7.2 above it can be seen that the six test cases chosen from Goodykoontz and Dorsch's experiments each had a quality, $x_{in} < 1$, at the inlet of the test section. In the present model however, the steam was saturated with a quality $x = 1$ at the inlet. In order to make an accurate comparison, the location $z = 0$ in the model was taken as the point at which the quality matched that from the inlet conditions of the experiments. The wall temperature was maintained at the inlet T_{wall} until this quality was reached at which point the polynomial was then used to calculate $T_{wall}(z)$.

Figures 7.1 to 7.3 show how the heat transfer coefficients calculated from the model compare with the values found from the experiments for all three turbulence models.

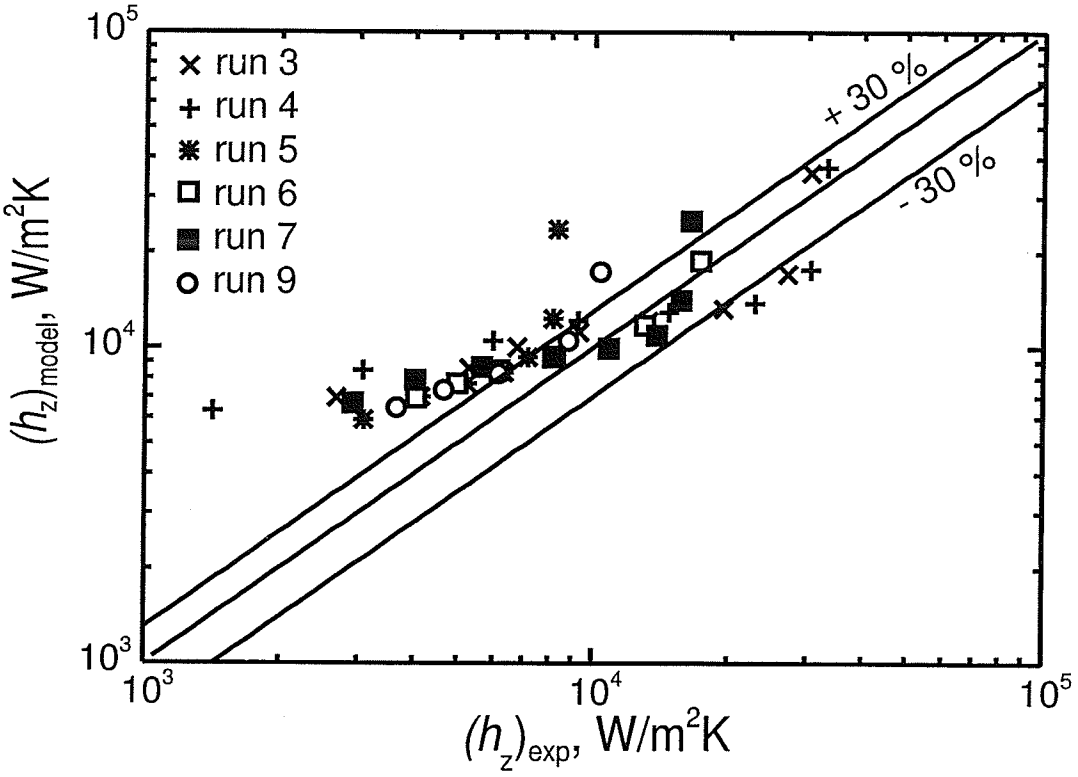

Figure 7.1 Comparison with Goodykoontz and Dorsch (1966) using model 1

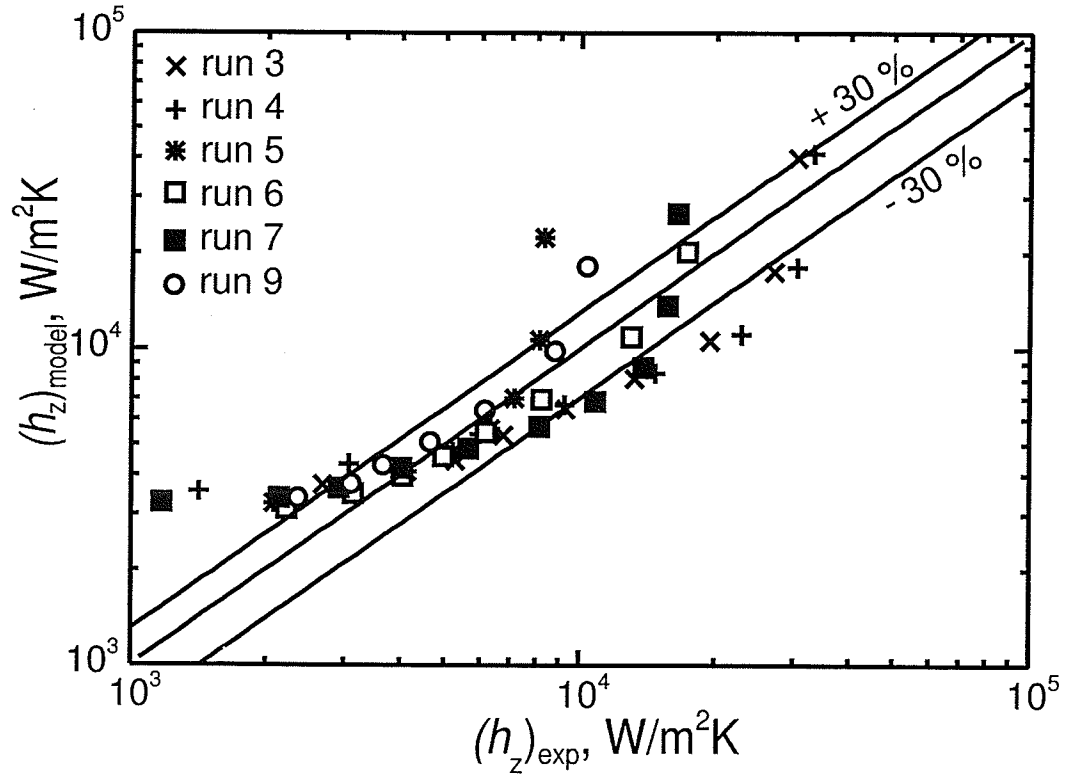

Figure 7.2 Comparison with Goodykoontz and Dorsch (1966) using model 2

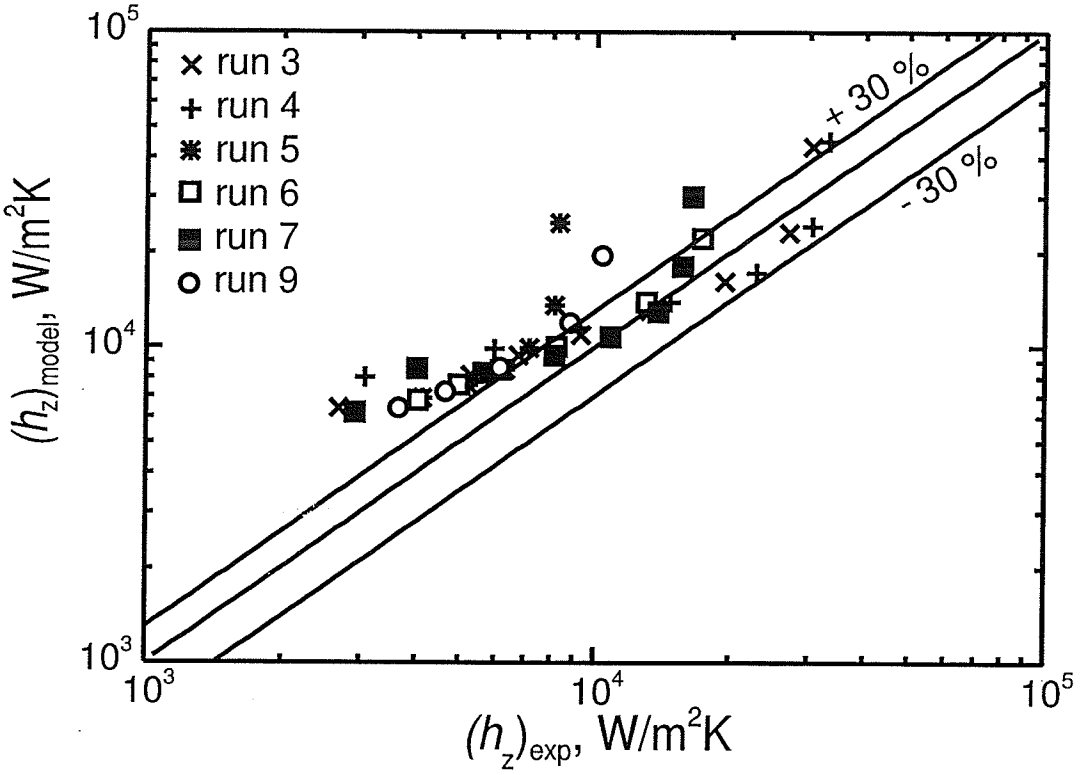

Figure 7.3 Comparison with Goodykoontz and Dorsch (1966) using model 3

From these plots it can be seen that the turbulence model that best predicts Goodykoontz and Dorsch's results is model 2. It was found that with model 2, 61% of the numerical results were within ± 40% of Goodykoontz and Dorsch's data and 73% were within ± 50% of their data. This agreement can also be observed in Figures 7.4 to 7.9. These plots show each run individually with results from all three turbulence models.

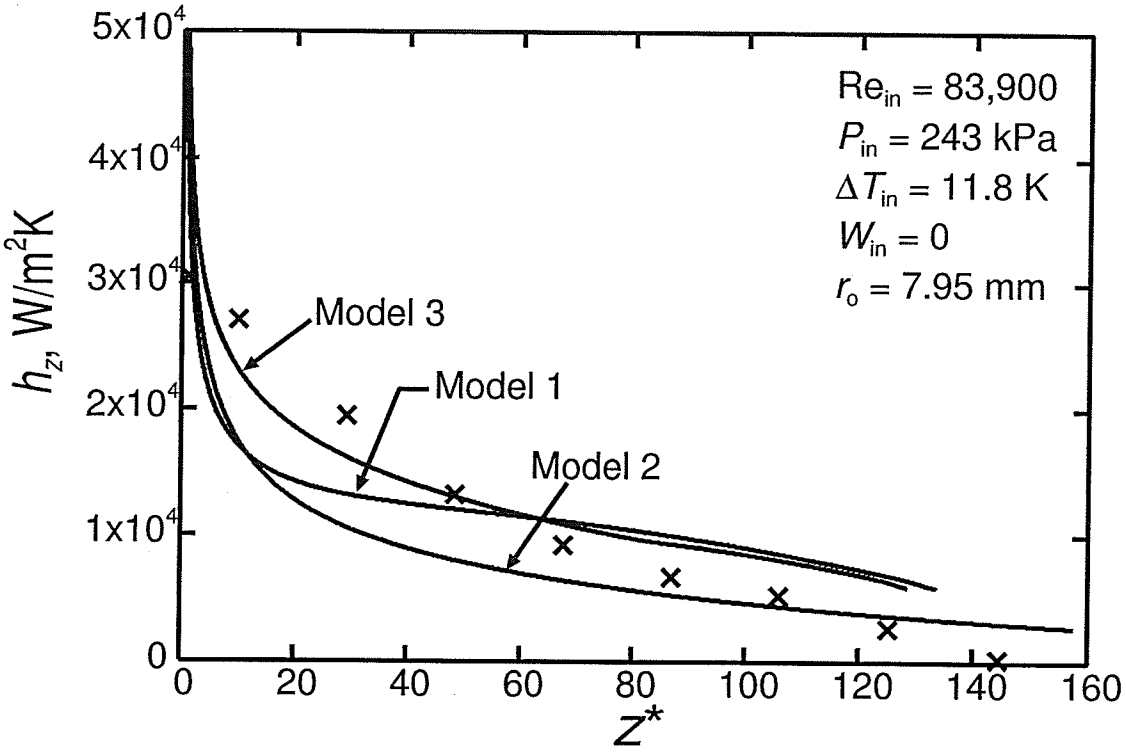

Figure 7.4 Local heat transfer coefficient distribution for run 3 of Goodykoontz and Dorsch (1966)

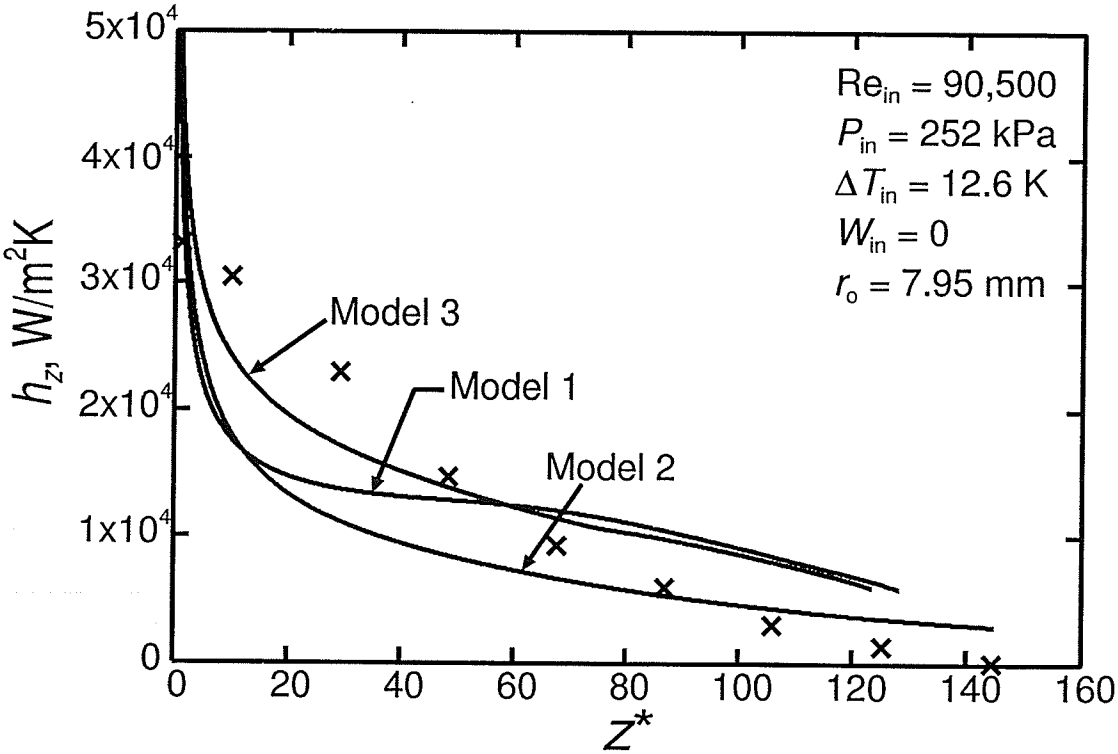

Figure 7.5 Local heat transfer coefficient distribution for run 4 of Goodykoontz and Dorsch (1966)

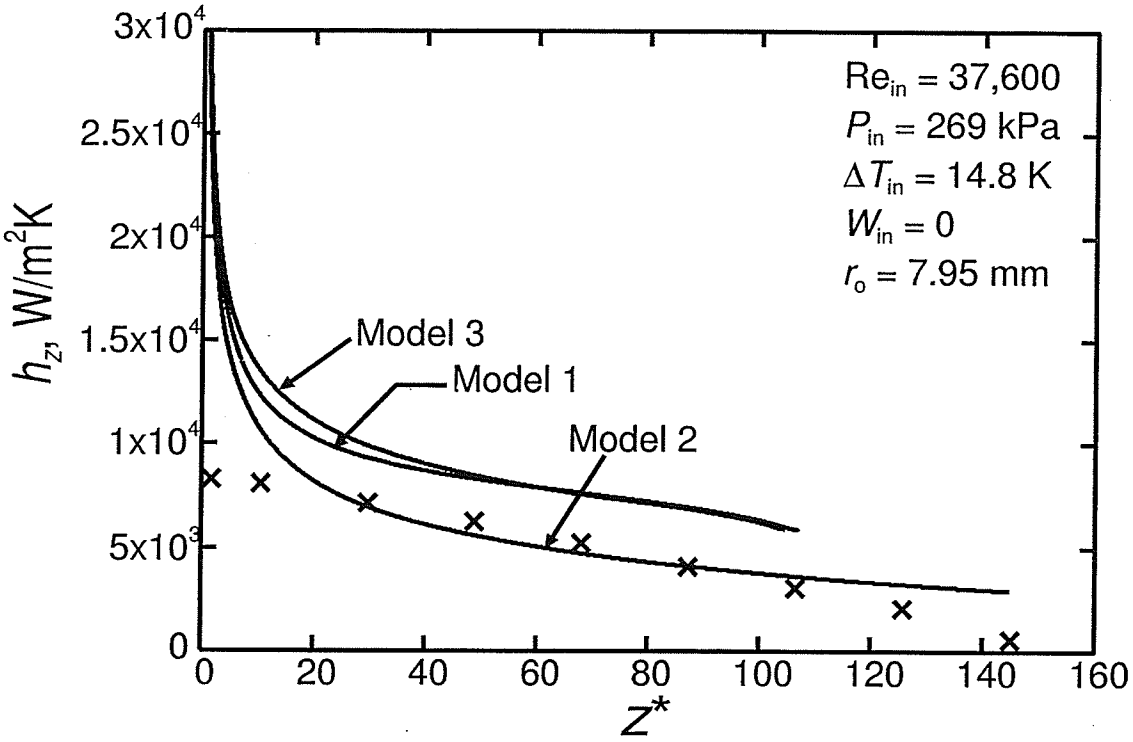

Figure 7.6 Local heat transfer coefficient distribution for run 5 of Goodykoontz and Dorsch (1966)

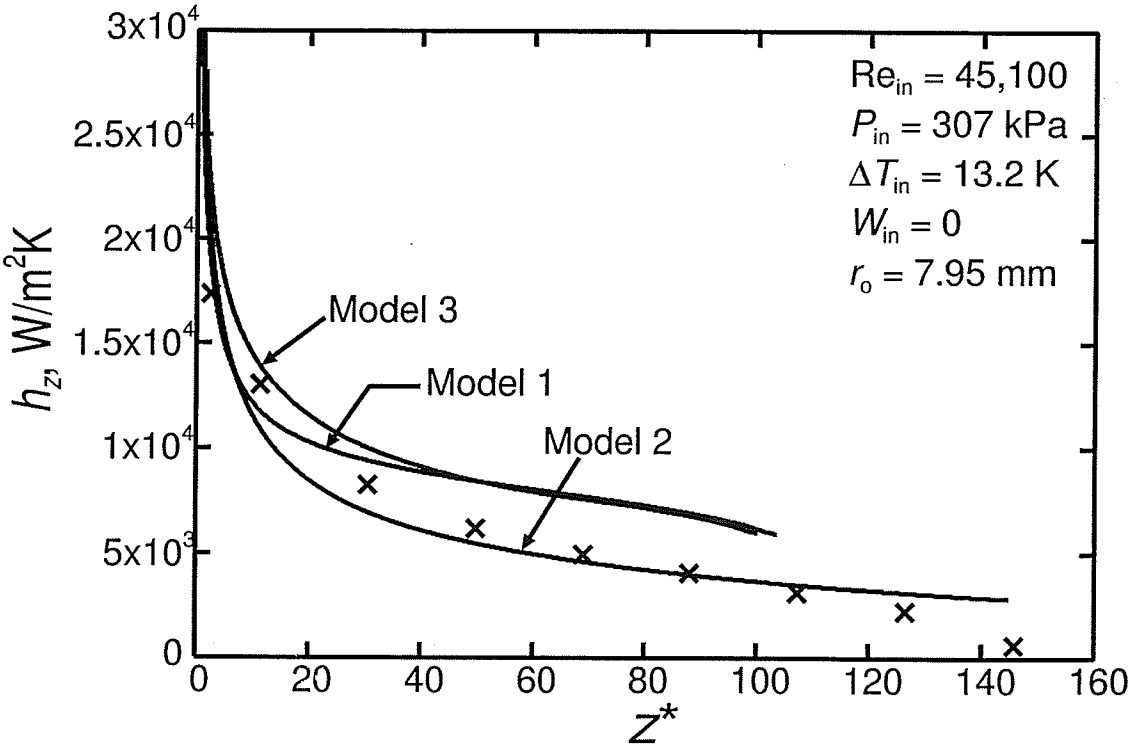

Figure 7.7 Local heat transfer coefficient distribution for run 6 of Goodykoontz and Dorsch (1966)

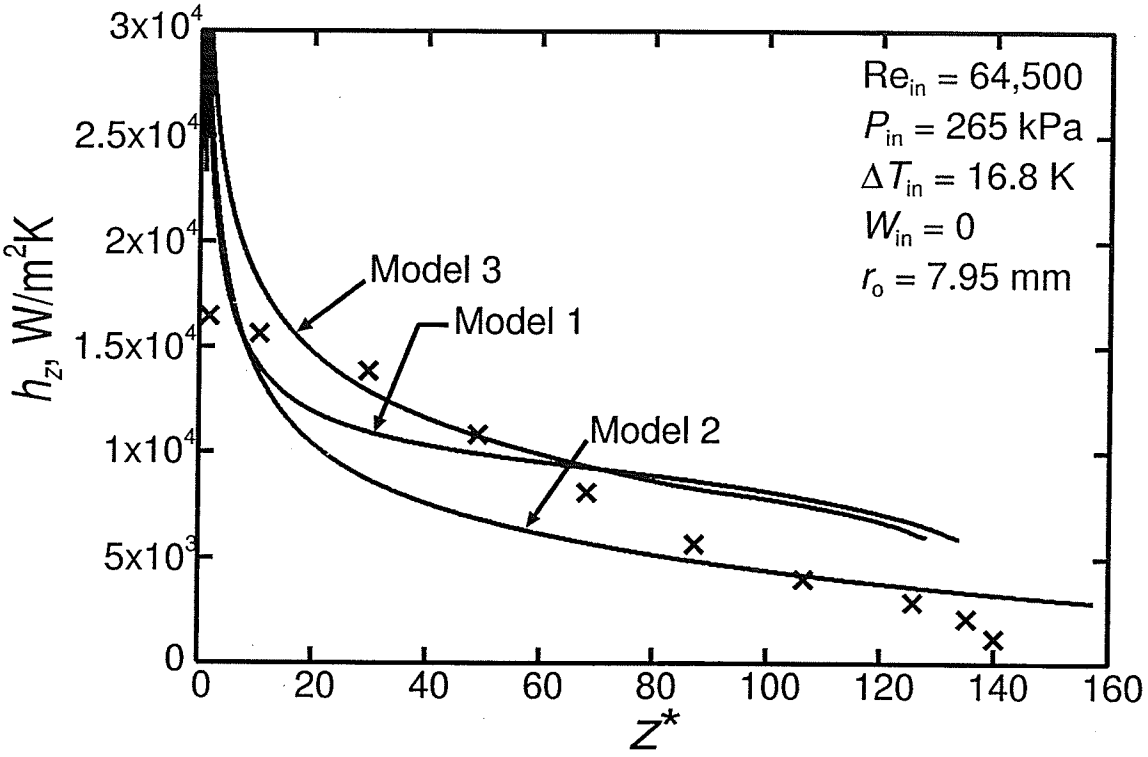

Figure 7.8 Local heat transfer coefficient distribution for run 7 of Goodykoontz and Dorsch (1966)

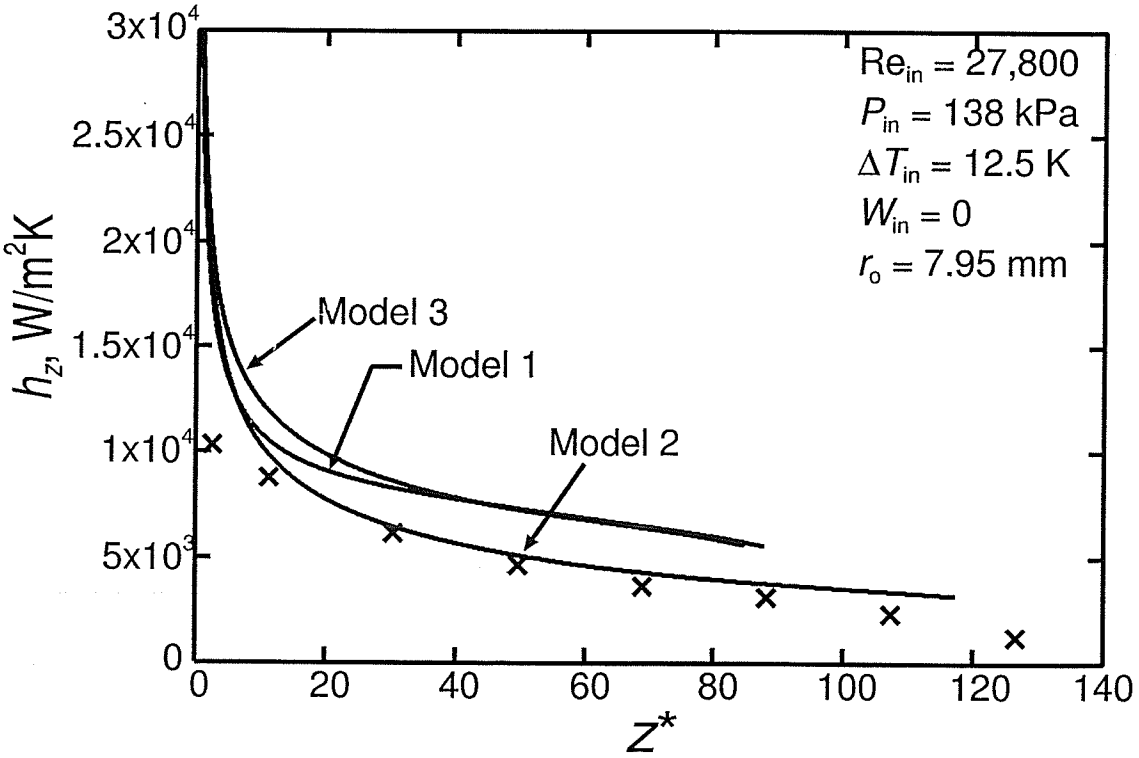

Figure 7.9 Local heat transfer coefficient distribution for run 9 of Goodykoontz and Dorsch (1966)

7.2 Comparisons with Siddique (1992)

Siddique (1992) performed experiments for steam condensation with either air or helium as the non-condensable gas. The inlet conditions corresponded to lower Reynolds numbers than those used by Goodykoontz and Dorsch (1966), but included cases with inlet gas mass fractions of up to 35%. A total of 52 runs were done with air as the non-condensable gas. The ranges of inlet parameters were as follows:

r_o: 2.3 cm

Re_{in}: 4,800 to 24,000

P_{in}: 100 kPa to 500 kPa

W_{in}: 9% to 35%;

ΔT_{in}: 1 to 60 K

The present model was compared with eight different runs from Siddique's experiments. These eight runs were chosen such that they covered the entire range of parameters. Four runs were selected at the minimum flow rate and four at the maximum flow rate. At each flow rate, two runs were selected at the lowest pressure and two at the highest pressure. In addition, at each pressure level, one run was selected at the lowest gas mass fraction and one at the highest. The following table summarizes the eight cases chosen for comparison.

Table 7.3 Runs chosen from Siddique (1992)

Run #	Re_{in}	P_{in} (kPa)	ΔT_{in} (K)	W_{in}
1	6,000	107	7.4	0.09
6	7,330	133	28.8	0.33
13	4,840	389	26.2	0.11
17	5,790	475	60.3	0.34
35	17,300	109	0.7	0.11
40	23,700	137	1.8	0.35
47	19,200	386	6.5	0.10
52	23,100	485	15.3	0.35

Siddique's test section included an adiabatic inlet length which resulted in a fully developed velocity profile at the inlet to the condenser. The wall temperature was not constant but decreased along the length of the tube. In order to model these conditions, a fully developed inlet velocity and turbulent viscosity profile were used and a polynomial was fit to the measured wall temperatures and was used to calculate the wall temperatures in the model.

Figures 7.10 to 7.12 show how the heat transfer coefficients predicted by models 1, 2 and 3 compare with the experimental results from all eight runs. The turbulence models that showed the best agreement with the data were models 2 and 3. It was found that model 3

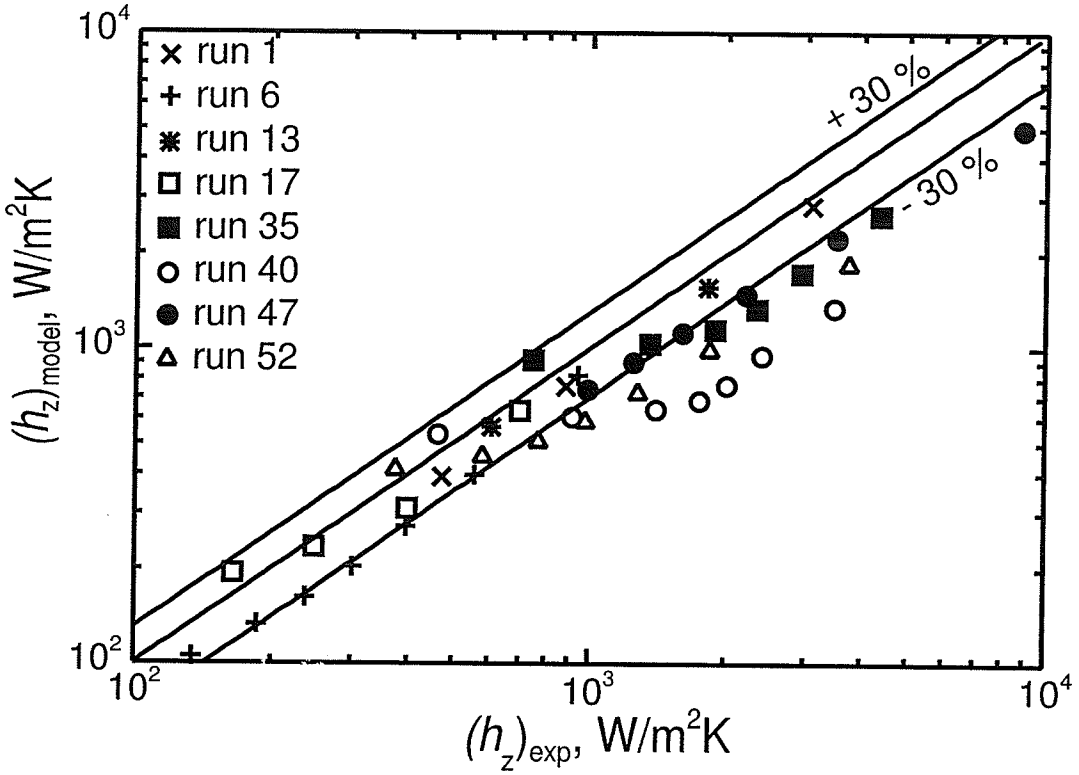

Figure 7.10 Comparison with Siddique (1992) using model 1

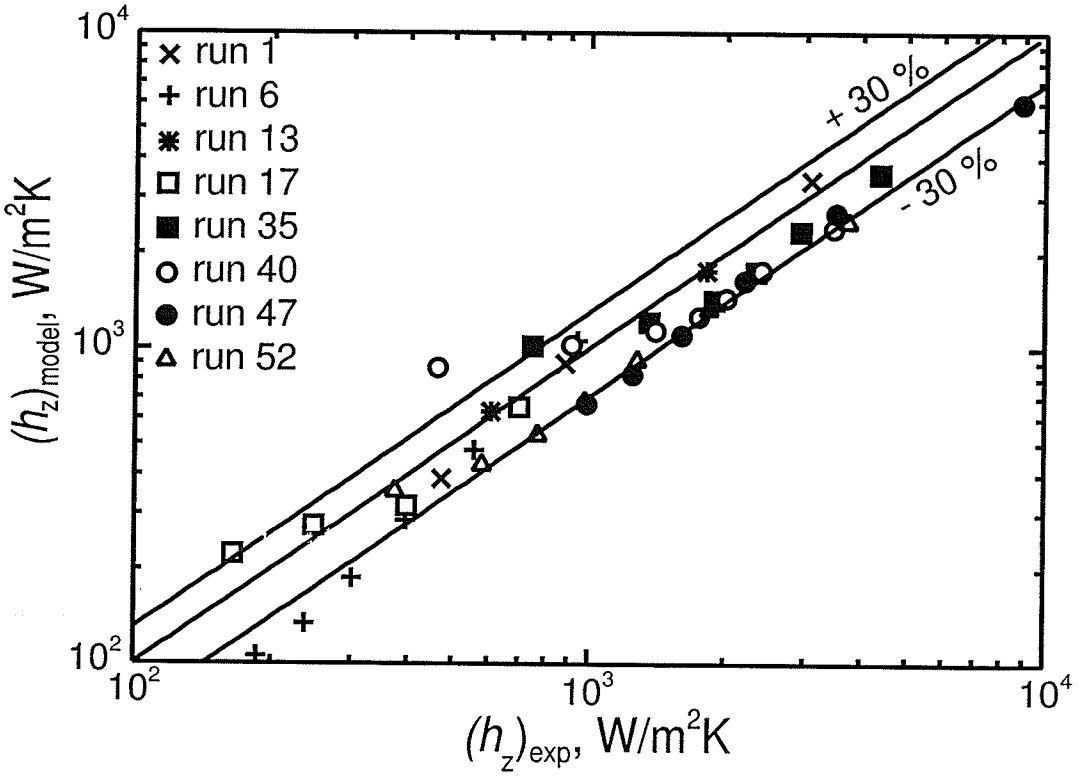

Figure 7.11 Comparison with Siddique (1992) using model 2

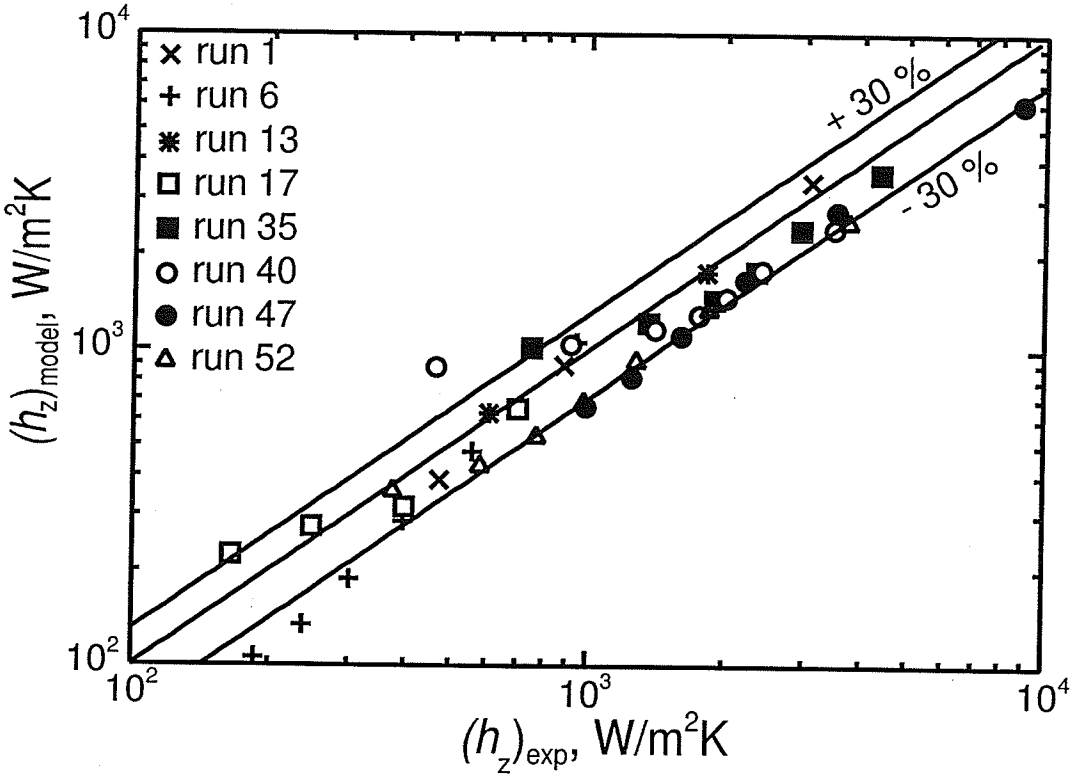

Figure 7.12 Comparison with Siddique (1992) using model 3

was slightly better than model 2 with 64% of the numerical results falling within ± 30% of Siddique's results and 89% were within ± 40% of Siddique's data. Siddique reported that the experimental uncertainty was ± 17.3%. In general, the numerical model predicted Siddique's results better than the results from Goodykoontz and Dorsch's (1966) experiments. Figures 7.13 to 7.20 show individual plots for each of the eight runs. Again, it can be observed that both model 2 and model 3 show the best agreement with the experimental results.

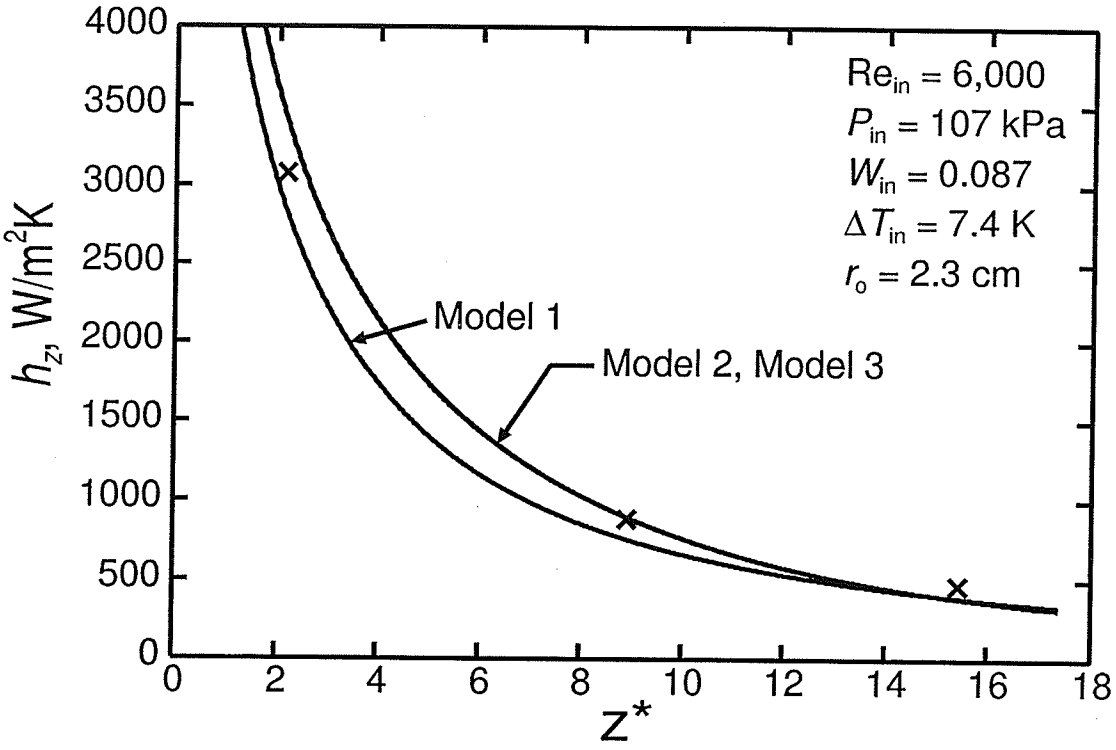

Figure 7.13 Local heat transfer coefficient distribution for run 1 of Siddique (1992)

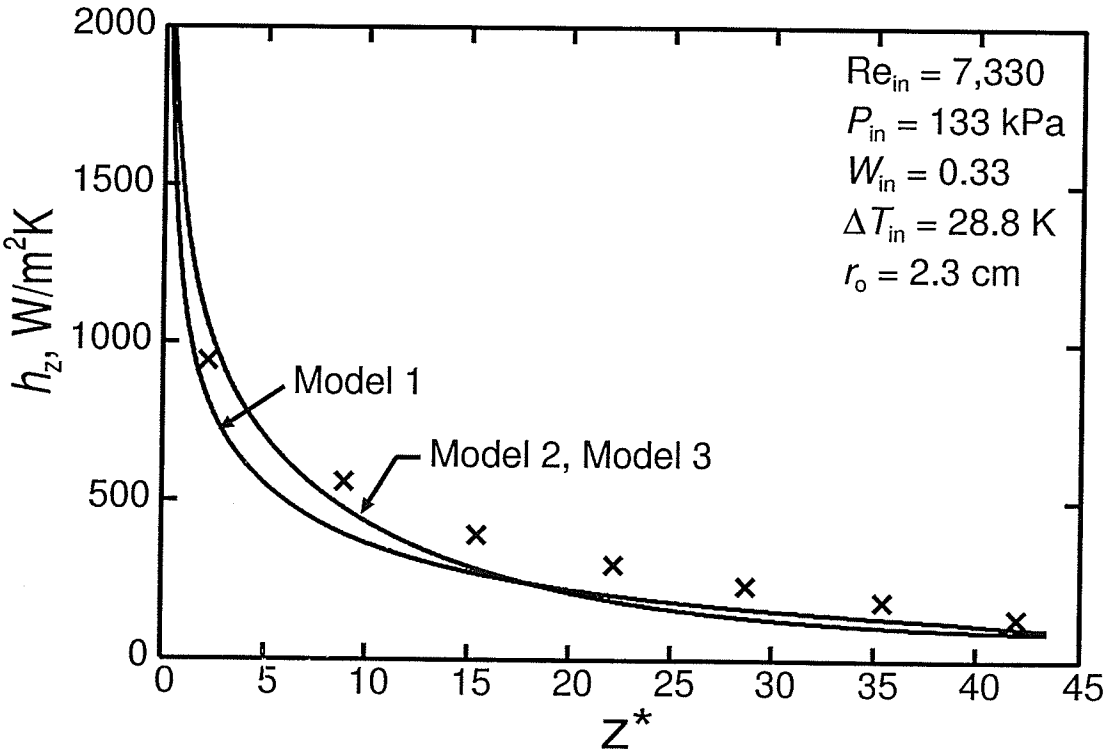

Figure 7.14 Local heat transfer coefficient distribution for run 6 of Siddique (1992)

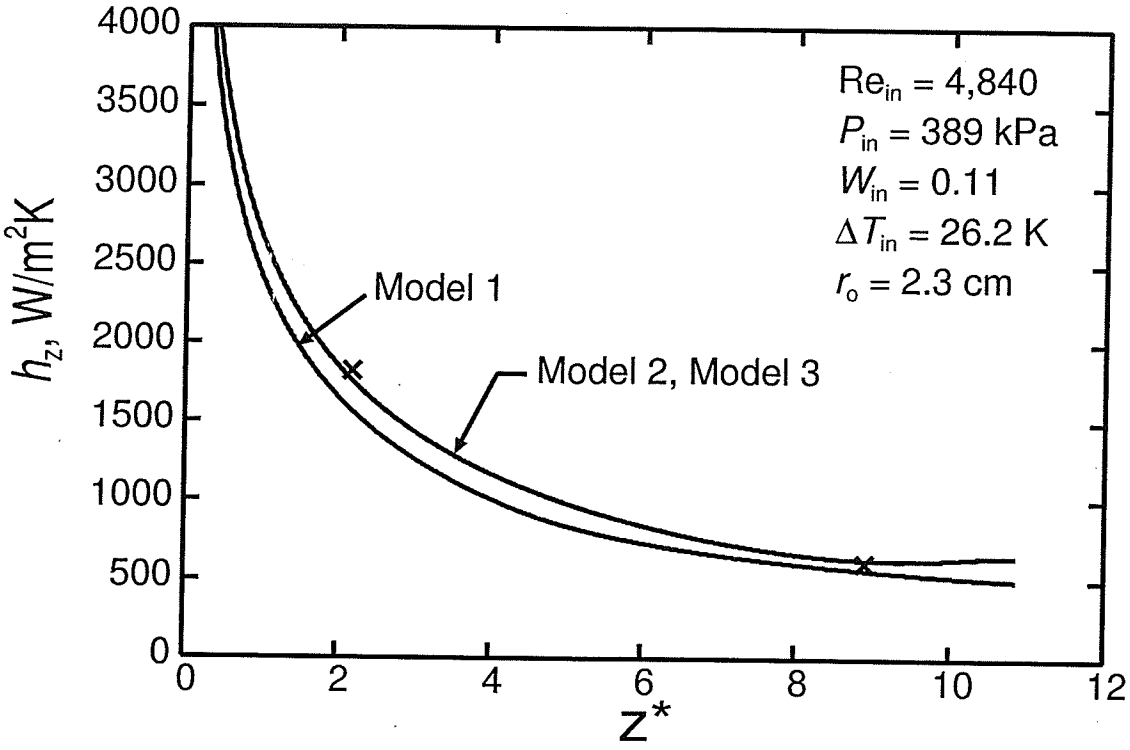

Figure 7.15 Local heat transfer coefficient distribution for run 13 of Siddique (1992)

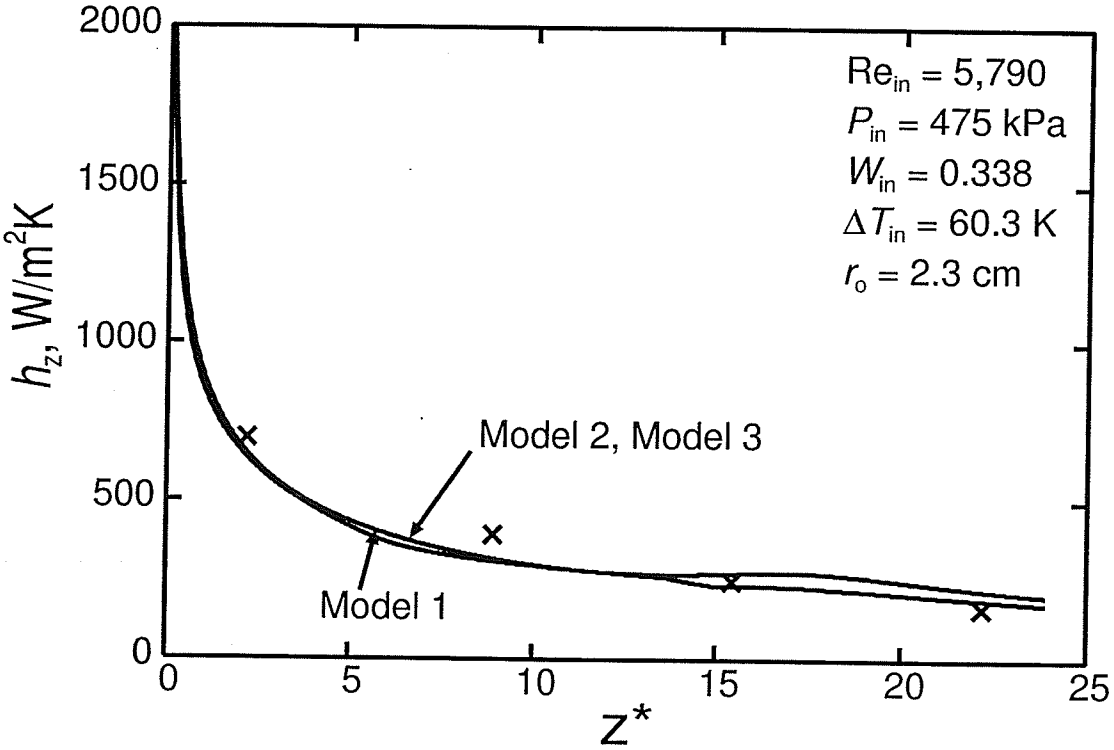

Figure 7.16 Local heat transfer coefficient distribution for run 17 of Siddique (1992)

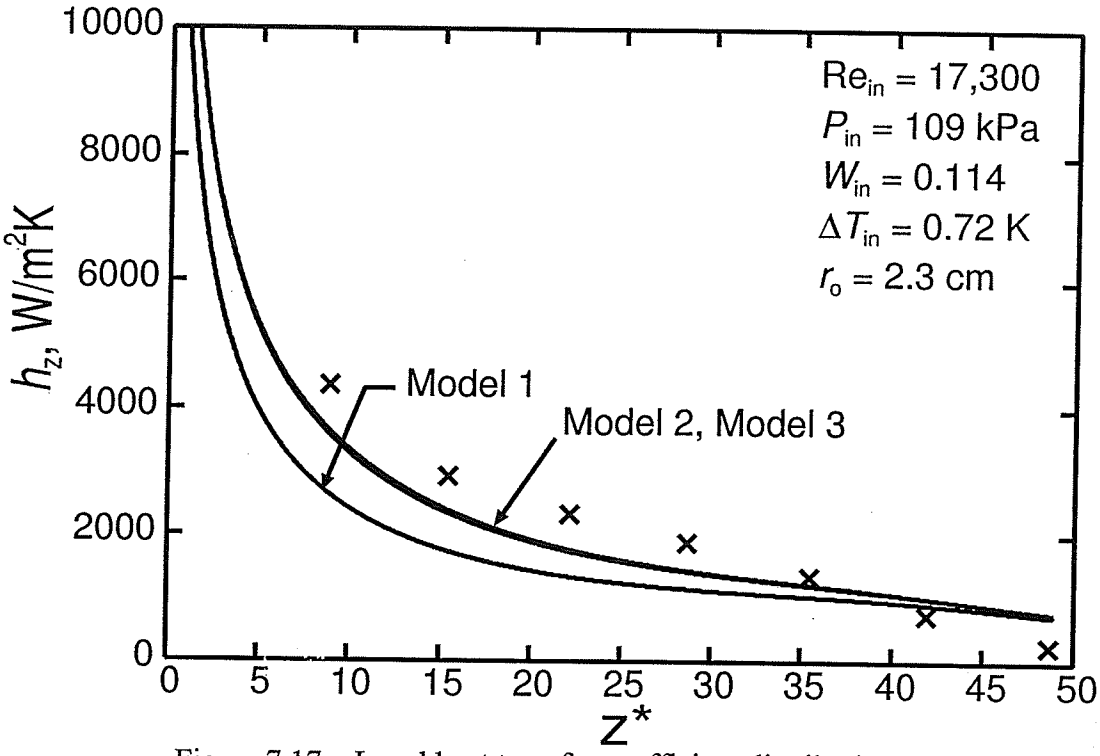

Figure 7.17 Local heat transfer coefficient distribution for run 35 of Siddique (1992)

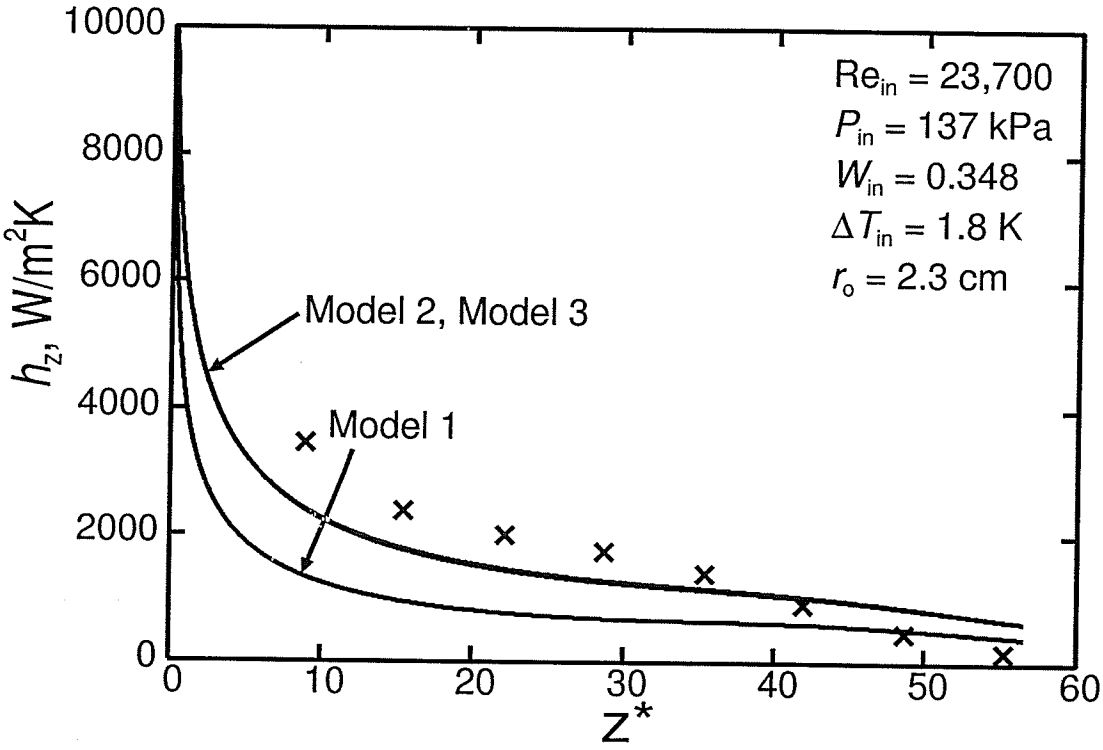

Figure 7.18 Local heat transfer coefficient distribution for run 40 of Siddique (1992)

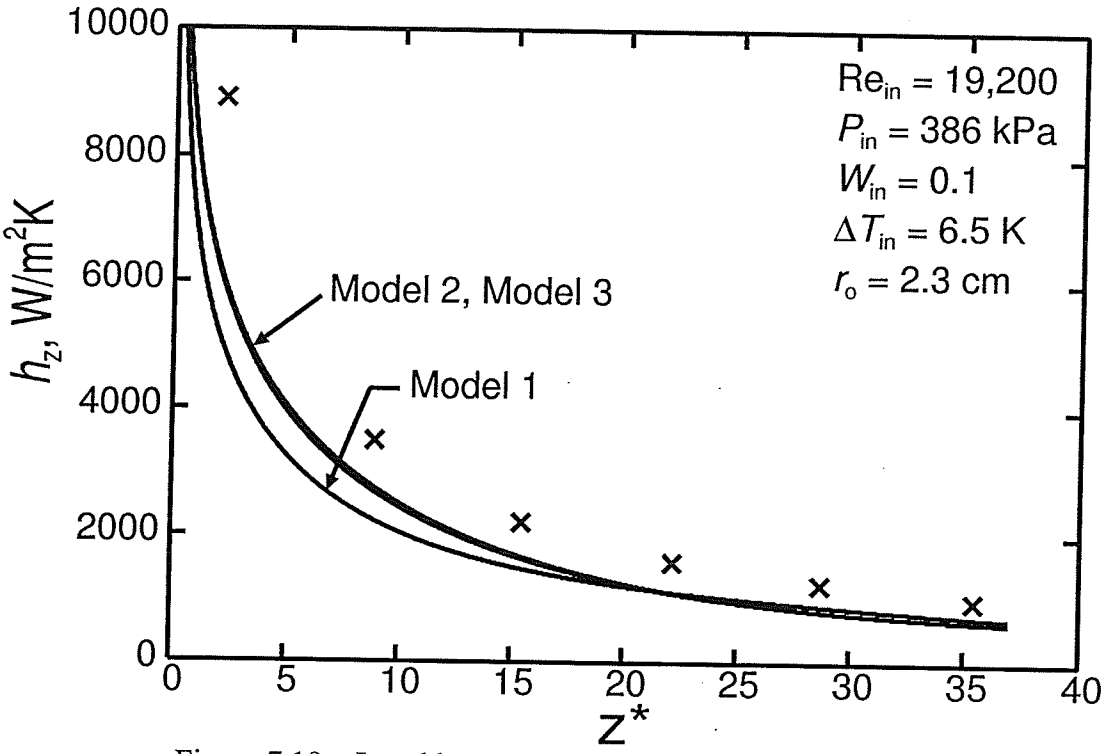

Figure 7.19 Local heat transfer coefficient distribution for run 47 of Siddique (1992)

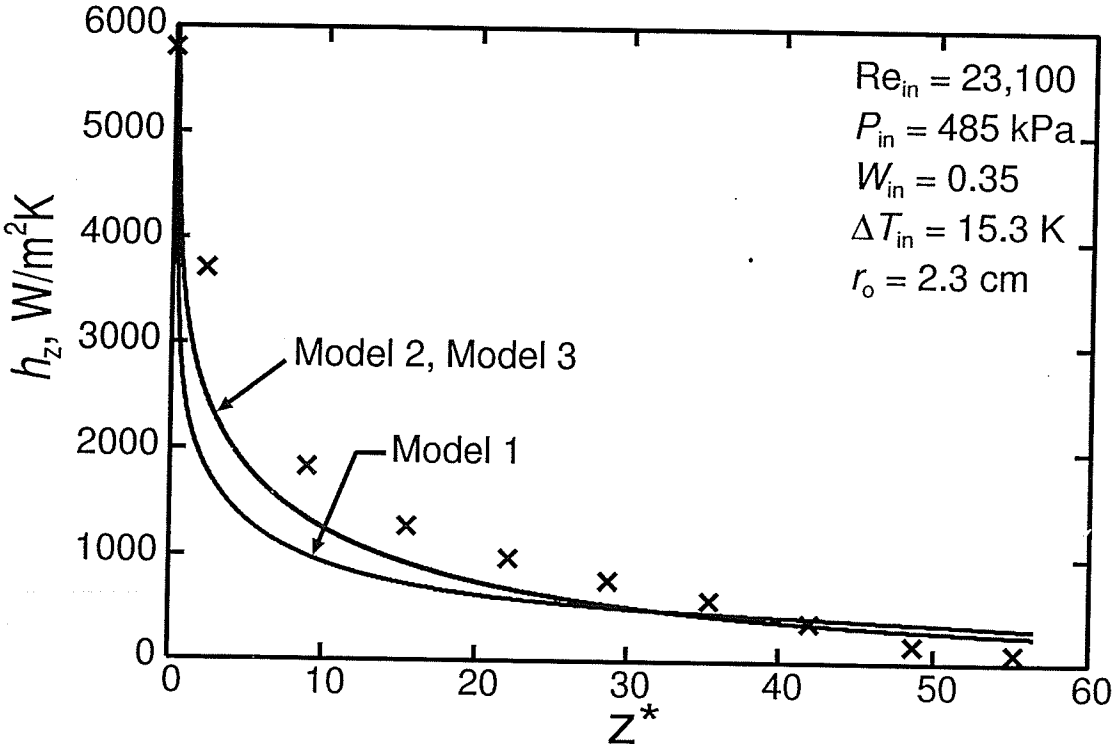

Figure 7.20 Local heat transfer coefficient distribution for run 52 of Siddique (1992)

7.3 Comparisons with Kuhn (1995)

Kuhn (1995) performed experiments for steam condensation in a vertical tube in the presence of either air or hydrogen. The inlet Reynolds numbers in these experiments fell between the large values found in Goodykoontz and Dorsch's (1966) experiments and the smaller values found in Siddique's (1992) experiments. The ranges of parameters used in Kuhn's experiments were:

r_o: 2.375 cm

Re_{in}: 15,000 to 50,000

P_{in}: 100 kPa to 500 kPa

W_{in}: 0 to 40%

ΔT_{in}: 4 to 40 K

A total of eight runs were selected from the 81 runs performed with steam-air. These runs were selected to cover the entire range of parameters mentioned above. Four of the eight runs selected were with pure steam and four were with the largest amount of gas (W_{in} = 40%). For each of these levels of gas, two runs were chosen at the lowest flow rate (one at the highest P_{in} and one at the lowest P_{in}) and two at the highest flow rate (one at the highest P_{in} and one at the lowest P_{in}). The following table summarizes the eight runs selected.

Table 7.4 Runs chosen from Kuhn (1995)

Run #	Re_{in}	P_{in} (kPa)	ΔT_{in} (K)	W_{in}
1.1-1	36,500	116	4.3	0
1.1-5	32,200	502	17.8	0
1.4-2	18,500	108	5.9	0
1.4-5	15,700	499	12.9	0
3.5-2	48,900	205	13.9	0.38
3.5-5	43,700	493	28.8	0.37
4.5-2	24,500	202	20.7	0.40
4.5-5	23,400	503	36.2	0.38

The test section from Kuhn's apparatus included a 50-cm adiabatic entrance region which allowed the flow to reach a fully developed velocity profile at $z = 0$. For this reason, a fully developed inlet velocity and turbulent viscosity profile were used in the model for these comparisons. Similar to Goodykoontz and Dorsch and Siddique's experiments, the wall temperature was set by fitting a polynomial to Kuhn's wall temperature measurements and using this polynomial to calculate the wall temperature at each station.

From Figures 7.21 to 7.23 it can be seen that both model 2 and model 3 show excellent agreements with Kuhn's results. It was found that with model 2, 86% of the numerical results were within 15% of Kuhn's data and 98% were within 30% of Kuhn's results.

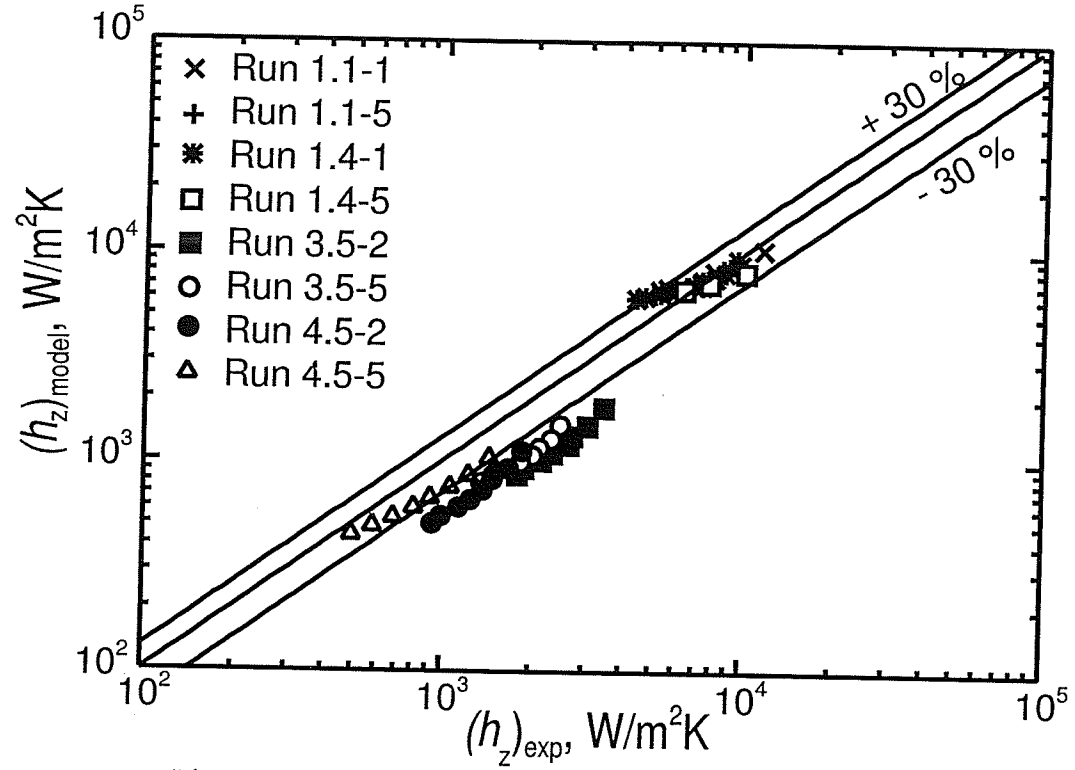

Figure 7.21 Comparison with Kuhn (1995) using model 1

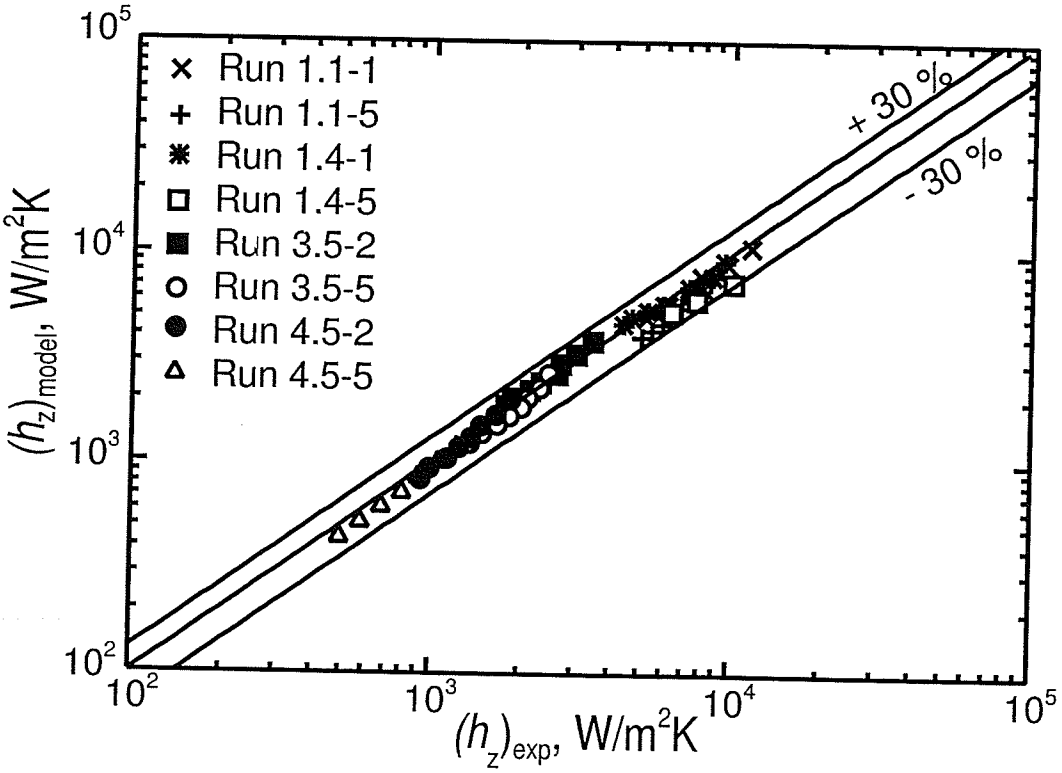

Figure 7.22 Comparison with Kuhn (1995) using model 2

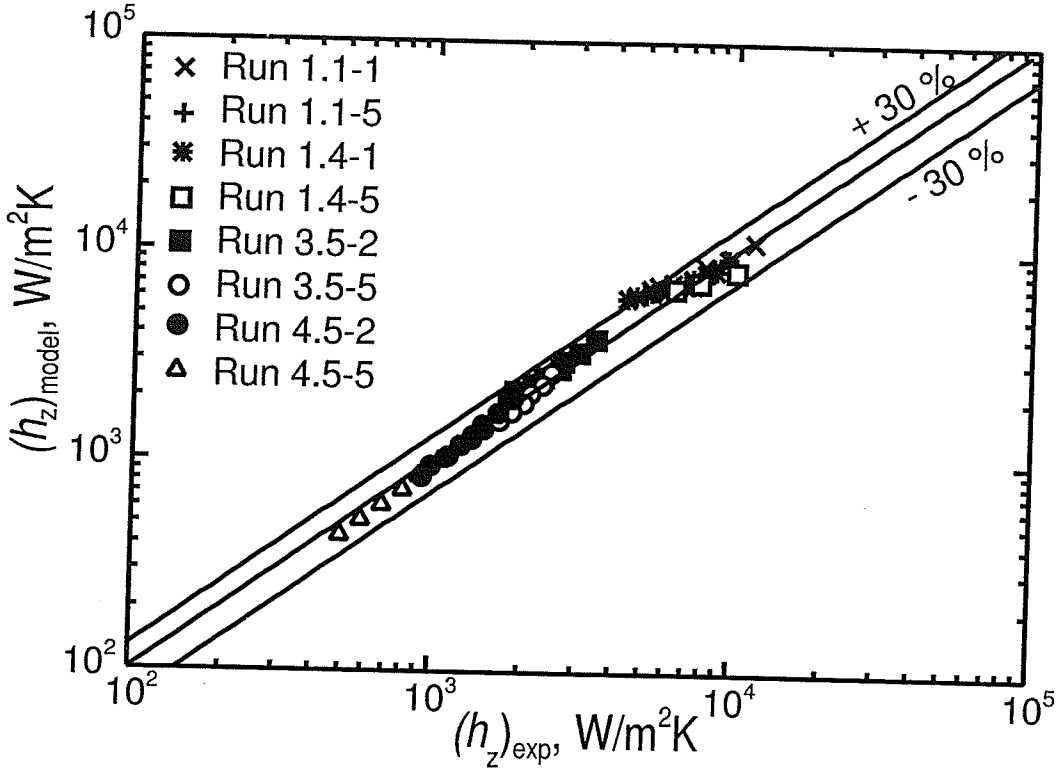

Figure 7.23 Comparison with Kuhn (1995) using model 3

Model 3 also showed excellent agreement with 84% of the numerical results falling within 15% of Kuhn's data and 97% falling within 30% of Kuhn's data. The experimental error associated with Kuhn's results was 18.7%; therefore, the numerical solution shows agreement that is for the most part, well within the experimental error. This agreement can also be observed in Figures 7.24 to 7.31. These plots show all eight runs individually with all three models. From these plots it can be seen that for the runs with pure steam, models 1 and 3 produce very similar results. These models both use the mixing length model in the liquid film but different models in the core. The similar results suggest that for the case of pure steam, the model used in the liquid has more of an affect on the results than the model used in the core. In contrast, for the runs that have

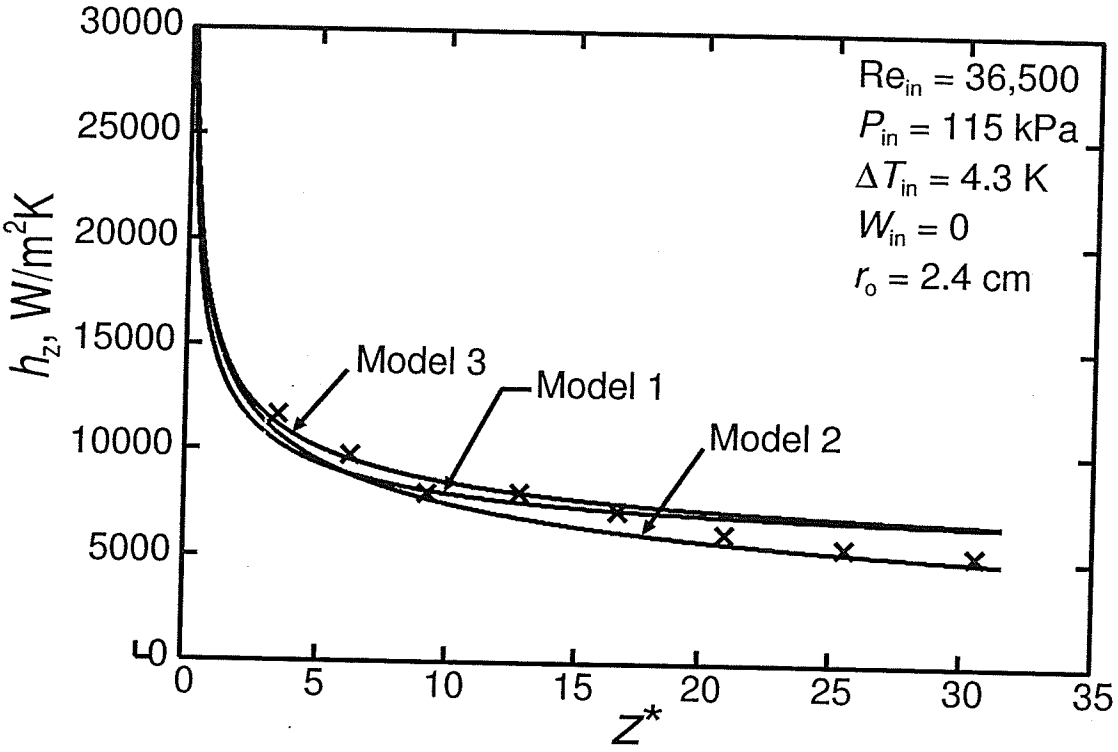

Figure 7.24 Local heat transfer coefficient distribution for run 1.1-1 of Kuhn (1995)

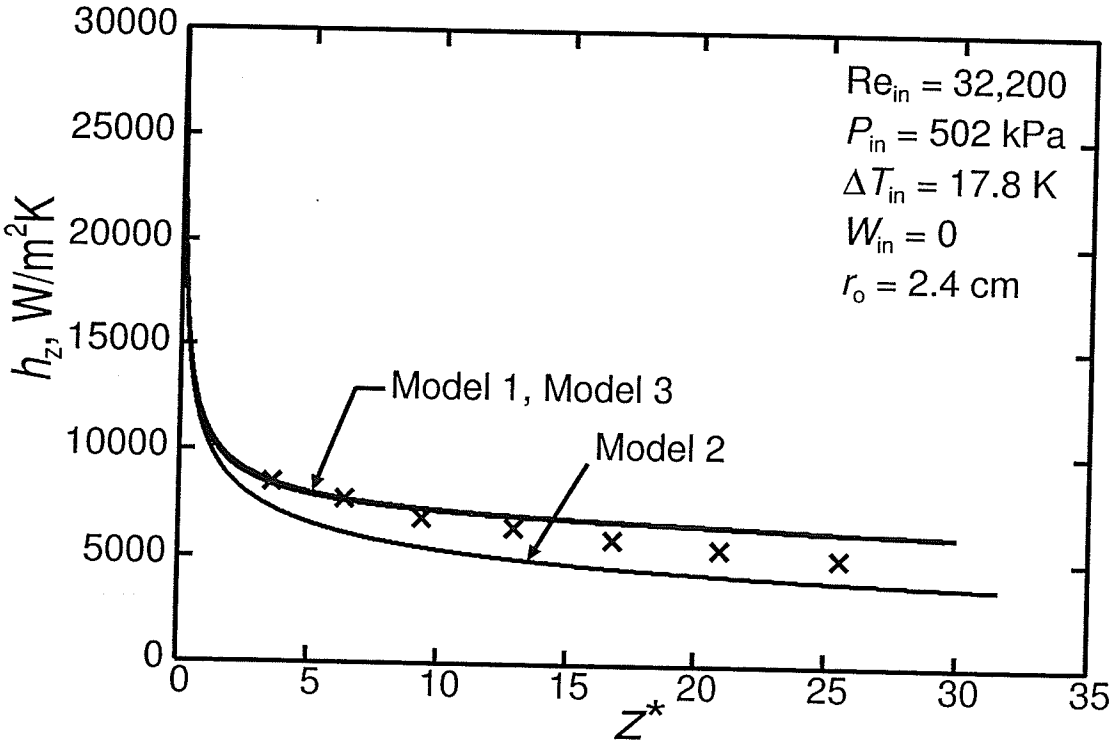

Figure 7.25 Local heat transfer coefficient distribution for run 1.1-5 of Kuhn (1995)

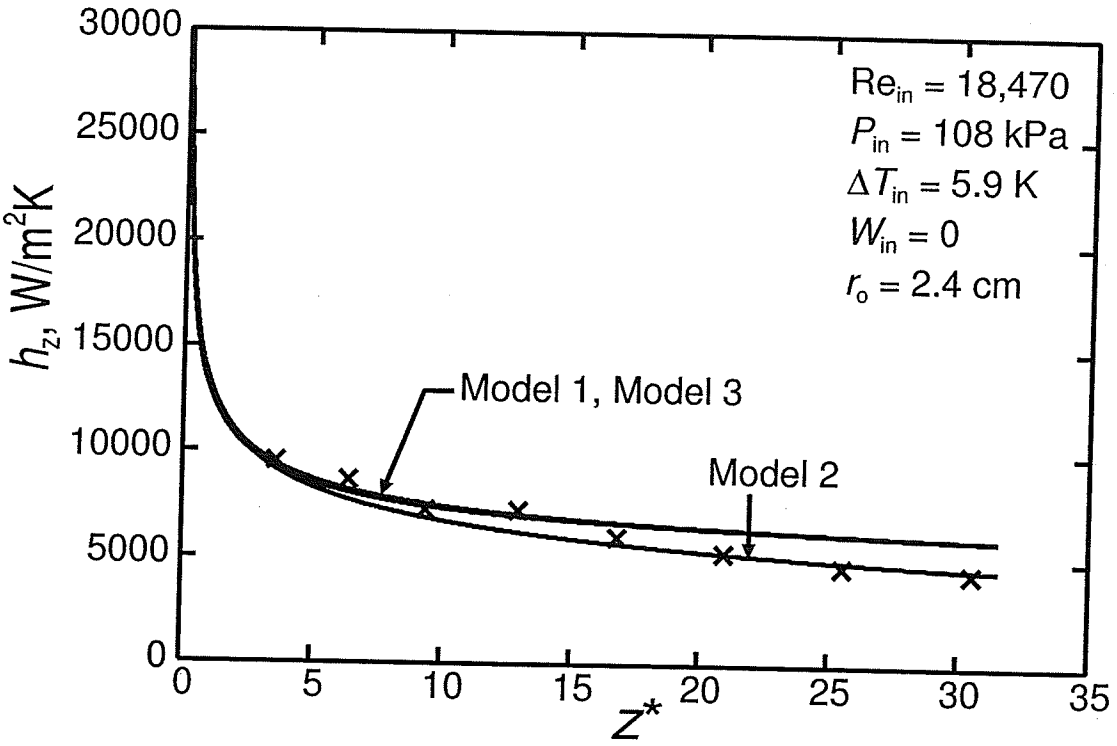

Figure 7.26 Local heat transfer coefficient distribution for run 1.4-1 of Kuhn (1995)

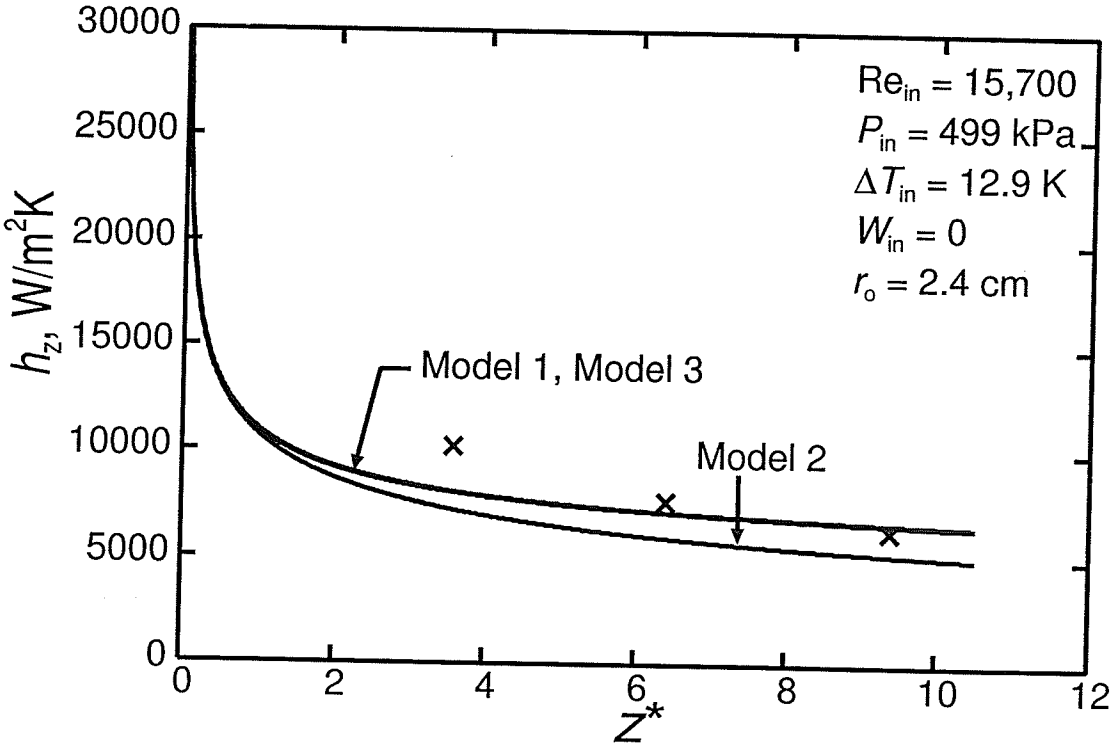

Figure 7.27 Local heat transfer coefficient distribution for run 1.4-5 of Kuhn (1995)

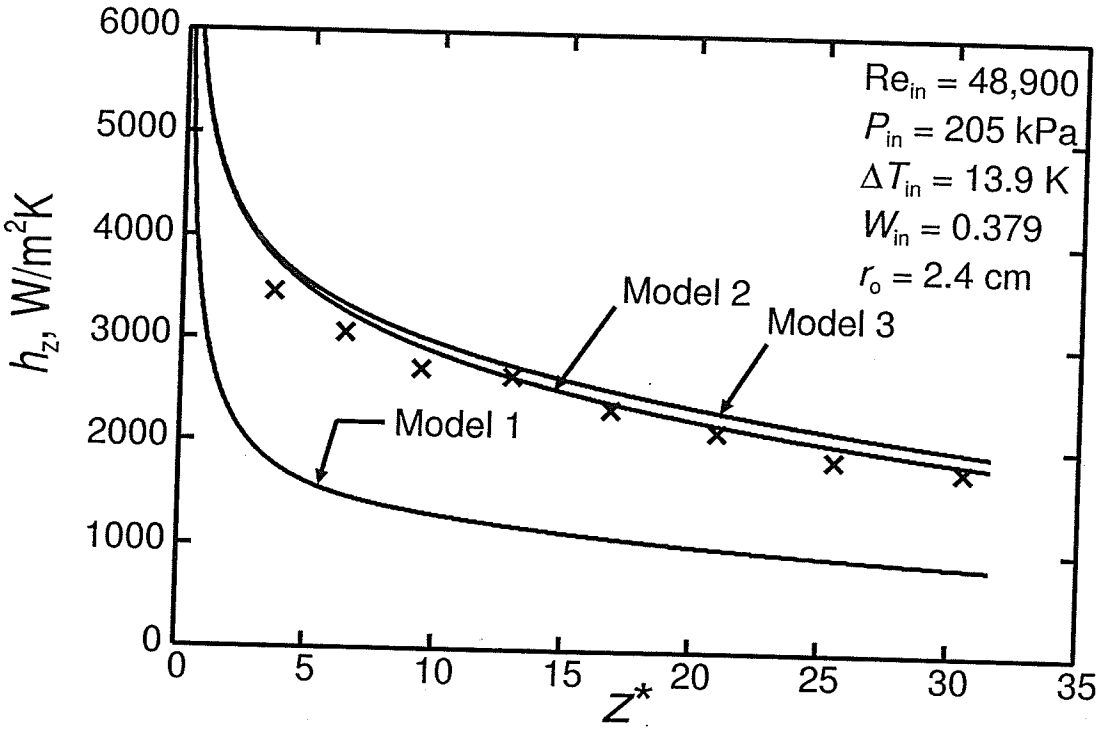

Figure 7.28 Local heat transfer coefficient distribution for run 3.5-2 of Kuhn (1995)

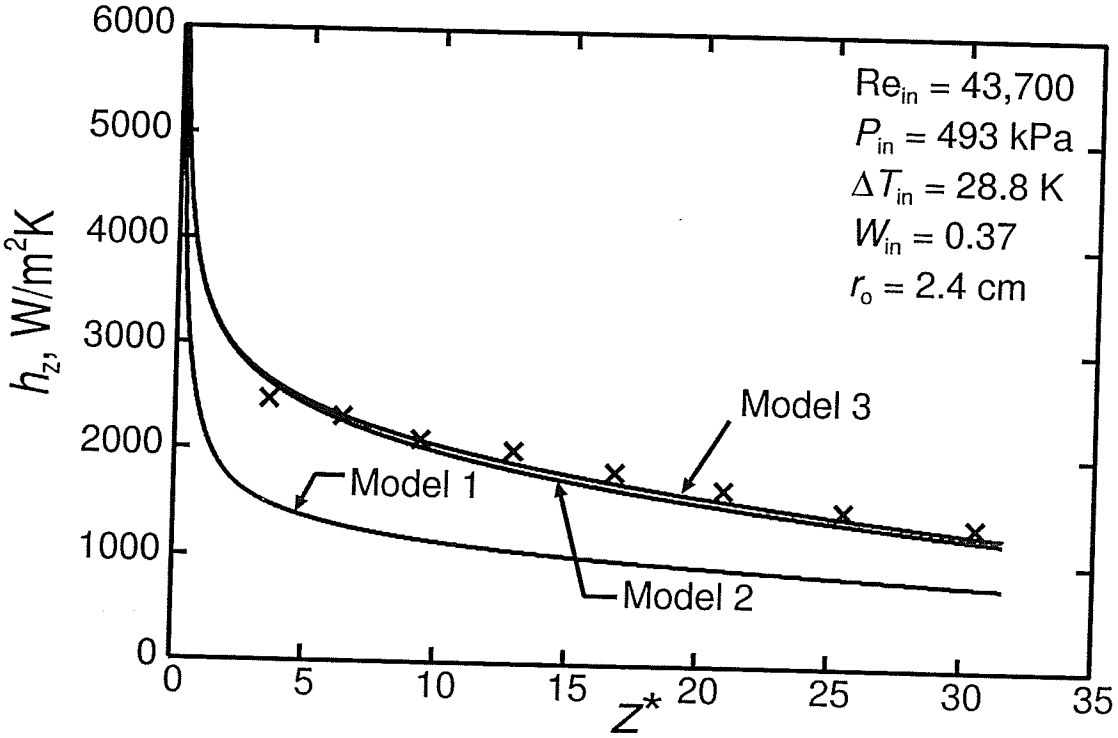

Figure 7.29 Local heat transfer coefficient distribution for run 3.5-5 of Kuhn (1995)

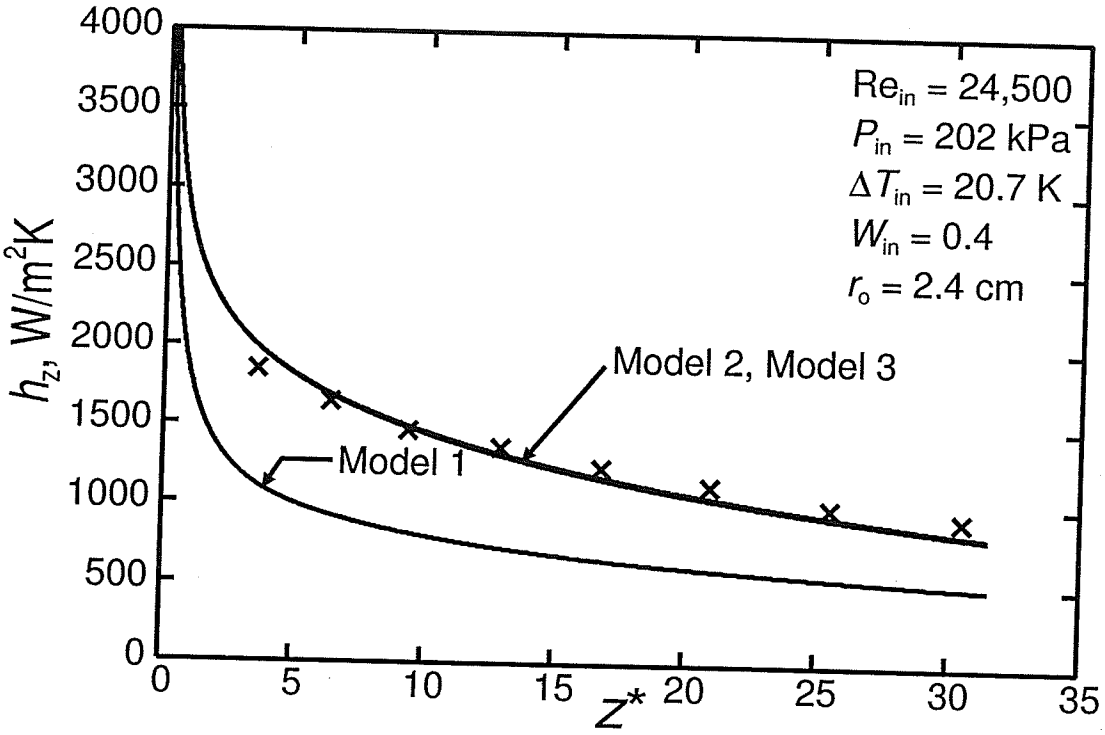

Figure 7.30 Local heat transfer coefficient distribution for run 4.5-2 of Kuhn (1995)

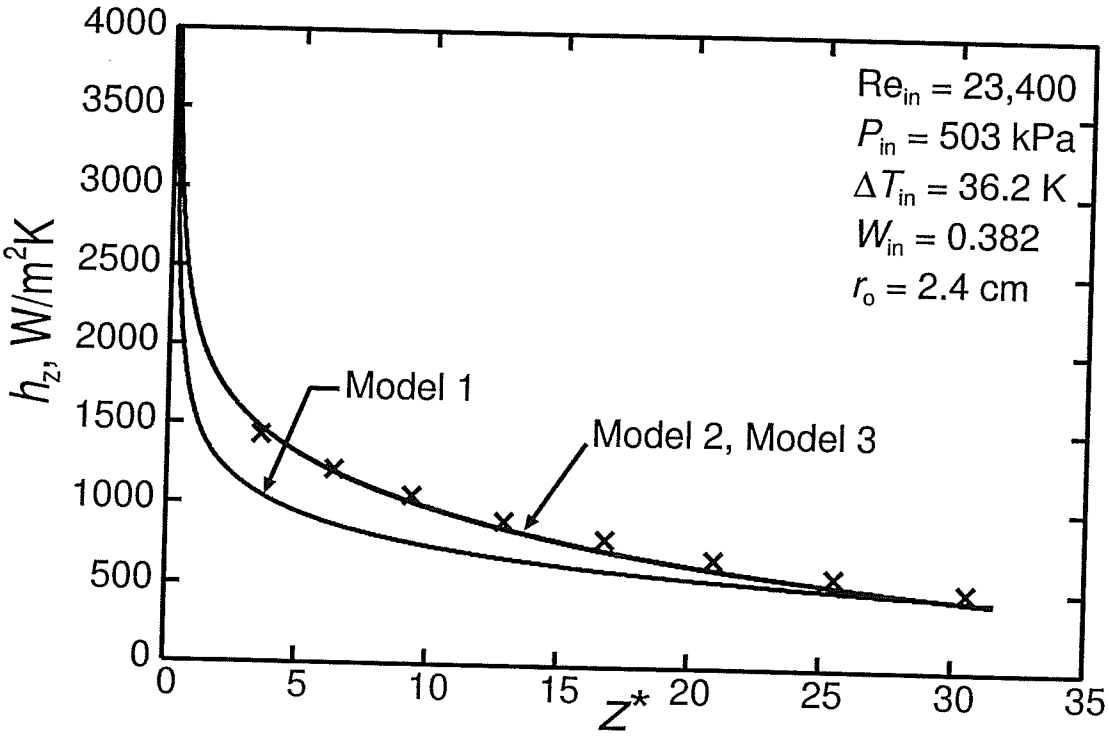

Figure 7.31 Local heat transfer coefficient distribution for run 4.5-5 of Kuhn (1995)

large amounts of air, models 2 and 3 show similar results. These models both use the k-ε two-equation model in the core but different models in the film. This suggests that for cases with large amounts of air, the turbulence model in the core has more of an effect than that used in the film. From these plots it can also be seen that the agreement is much better with Kuhn than it was with both Siddique and Goodykoontz and Dorsch.

7.4 Errors Associated with Experiments

From the above comparisons it was found that the present numerical results compare much better with Kuhn's (1995) results than with Siddique (1992) and Goodykoontz and Dorsch (1966). There are several possible reasons for the deviation between the present model and the experiments including surface waves and the possibility of liquid entrainment in the core, which were not included in the model. In addition, the method that was used in determining the heat flux and the heat transfer coefficient in the experiments could have a large influence on the experimental results.

In all three experiments discussed in the above sections, the local heat transfer coefficient was calculated as follows:

$$h_z = \frac{q''_{wall}}{T_{sb} - T_{wall}} \tag{7.1}$$

Where q''_{wall} is the local heat flux at the wall, h_z is the local heat transfer coefficient and T_{sb} is the saturation temperature corresponding to the partial pressure of steam which is

evaluated using the average gas mass fraction across the tube. In this equation, the heat flux was calculated from an energy balance on the coolant in the annulus with the following equation:

$$q''_{\text{wall}} = \frac{-\dot{m}_{\text{cw}} C_{p,\text{cw}}}{\pi r_{\text{o}}} \frac{dT_{\text{b,cw}}(z)}{dz} \tag{7.2}$$

Where $\dot{m}_{\text{cw}}$ is the mass flow rate of the coolant, $C_{p,\text{cw}}$ is the specific heat of the coolant, and $T_{\text{b,cw}}$ is the local bulk temperature of the coolant.

Goodykoontz and Dorsch (1966), Siddique (1992), and Kuhn (1995) all used different methods to measure the coolant bulk temperature. The various methods used to determine the coolant bulk temperature can greatly affect the local heat transfer coefficient.

Goodykoontz and Dorsch (1966) tried to measure the coolant bulk temperature directly by inserting thermocouples into the annulus(one thermocouple per axial station) and using the local temperatures as the coolant bulk temperatures. With this method, large errors could result for cases of low coolant Reynolds numbers where large temperature differences exist across the annulus.

Siddique (1992) used a different approach to measure the coolant bulk temperature. Air bubbles were inserted into the coolant to promote mixing and the coolant bulk

temperature was then measured by inserting thermocouples into the annulus (one thermocouple at each axial location). This method introduced uncertainties in the bulk temperature measurements due to local fluctuations.

Kuhn (1995) studied the existing techniques used in determining the coolant bulk temperature and developed a new method. In this method, a numerical approach was used to determine a relationship between the local coolant bulk temperature, the coolant flow rate, and the inner and outer wall temperatures of the annulus. The numerical solution was developed by first solving the velocity profile in the annulus assuming a hydro-dynamically fully developed flow. Next, the temperature profile in the annulus was solved by assuming a thermally fully developed turbulent flow with a uniform heat flux at the inner wall. This temperature profile was dependent on both the inner wall temperature (T_{wi}) and the outer wall temperature (T_{wo}). The bulk temperature ($T_{b,cw}$) was then calculated using the standard definition for their specific annulus geometry and the specific coolant used (water). This bulk temperature was found to be a function of T_{wi}, T_{wo} and the mass flow rate of the coolant. The relationship between $T_{b,cw}$ and the independent variables T_{wi}, T_{wo} and $\dot{m}_{cw}$ was tabulated based on their numerical calculations. During their experiments they installed a thermocouple at both the inner and outer walls of the annulus at each axial station. From these measurements and the measured mass flow rate of the cooling water they were able to determine the local bulk temperature from the tabulated values.

Among the three different methods of measuring the coolant bulk temperature, Kuhn's

method appears to be the most accurate. It is interesting to note that the present numerical results agree best with Kuhn's experimental results.

7.5 Summary

Table 7.5 below shows a summary of how the numerical predictions compare with the experimental results for all three turbulence models.

Table 7.5 Summary of comparisons with Kuhn (1995), Siddique (1992), and Goodykoontz and Dorsch (1966)

Model	Kuhn (1995)		Siddique (1992)		Goodykoontz and Dorsch (1966)	
	Within ± 15%	Within ± 30%	Within ± 30%	Within ± 40%	Within ± 40%	Within ± 50%
1	33%	55%	45%	70%	48%	57%
2	86%	98%	61%	89%	61%	73%
3	84%	97%	64%	89%	52%	60%

From this table along the with Figures 7.1 to 7.31, it can be seen that the turbulence model that shows the best agreement with all three experiments is the k-ε model applied to both the liquid and the mixture regions of the flow (model 2). In addition, the numerical model showed the best agreement with Kuhn's experimental results with 98% of the present results falling within ± 30% of Kuhn's data. The larger errors associated with comparisons made with Siddique and Goodykoontz and Dorsch's data are likely due to either surface waves, liquid entrainment in the core, or the method which they used to determine the coolant bulk temperature and thus the local heat flux.

CHAPTER 8

TURBULENT FLOW COMPUTATION RESULTS AND DISCUSSION

8.1 Introduction

In this chapter, results are presented for turbulent steam condensation in vertical tubes both with and without the presence of air. The turbulence model selected for the purpose of this study was the k-ε model applied to both the mixture core and the liquid film. The input variables are the inlet Reynolds number, the inlet gas mass fraction, the inlet pressure, and the inlet temperature difference between the mixture and the tube wall. At the inlet, the pressure, gas mass fraction, and velocity are all uniform across the tube and the temperature of the tube wall is maintained constant along its entire length.

Throughout this chapter, the process of turbulent flow condensation will be discussed for the case of pure steam followed by the study of steam condensation in the presence of air. Detailed results for film thickness, Nusselt number, velocity, mass fraction, pressure, temperature, and turbulent kinetic energy will be used to discuss these results. Following this, the effect of each of the input parameters mentioned above will be studied by examining the distributions of the dimensionless film thickness and local Nusselt number.

8.2 Pure Steam

For the case of turbulent pure steam condensation in a vertical tube, the numerical model was solved using a 2-cm diameter tube with the following inlet conditions: $Re_{in} = 40{,}000$, $P_{in} = 1$ atm and $\Delta T_{in} = 5$ K. Figure 8.1 shows the dimensionless velocity profiles at seven

different axial locations. The vapor region is from $\eta = 0$ (centerline) to $\eta = 1$ (interface) and the liquid region is from $\eta = 1$ to $\eta = 2$ (tube wall). At the inlet of the tube, the velocity profile in the core is uniform while the velocity in the film is zero. As condensation proceeds along the tube, the core loses mass resulting in a decreased velocity profile in the core. As the steam condenses, the liquid film gains mass, resulting in both a thicker and a faster moving film. At $z^* = 569$, flow reversal occurs; however, a very high percentage of the inlet vapor has already condensed at this location.

The turbulent kinetic energy profiles for the core region are shown in Figure 8.2. The turbulent kinetic energy is represented by k/u_τ^2 on the vertical axis and the horizontal

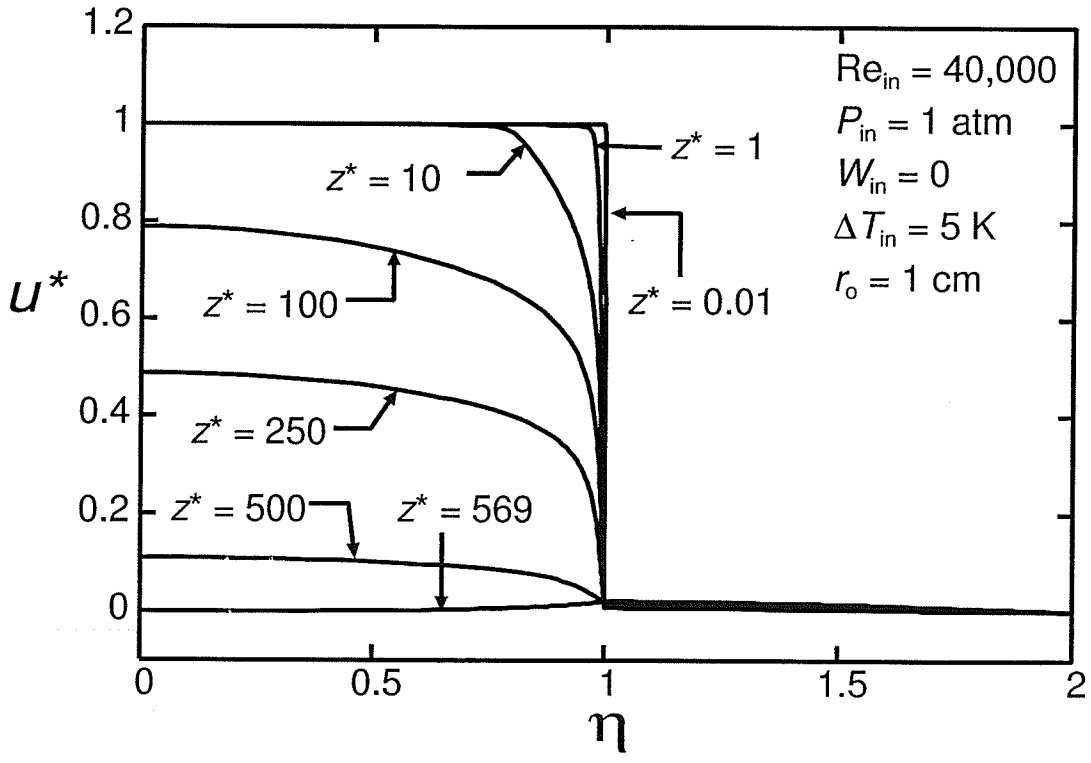

Figure 8.1 Velocity profiles for pure steam

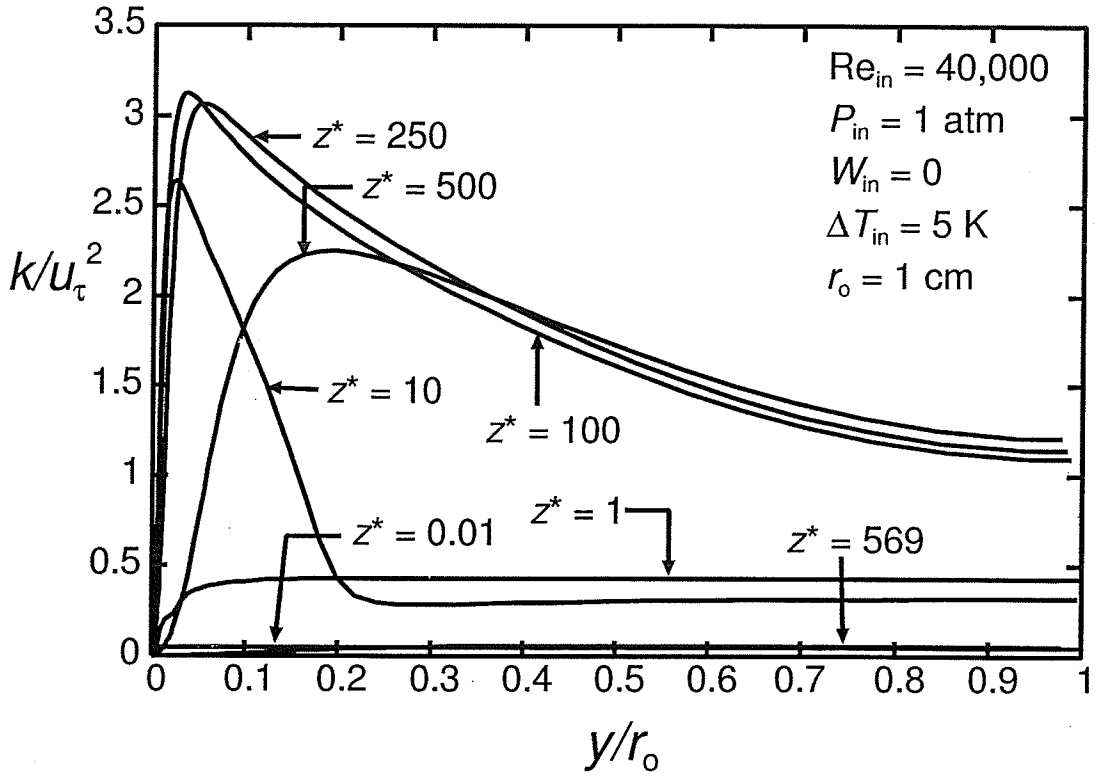

Figure 8.2 Turbulent kinetic energy profiles for pure steam

axis is the distance y/r_o measured from the interface towards the centerline. The production term $\mu_L\left(\frac{\partial u}{\partial r}\right)^2$ in the kinetic energy equation depends on the u-velocity profile; when the u-velocity gradient in the radial direction increases, the production term increases resulting in an increase in the turbulent kinetic energy. Near the inlet, the kinetic energy is small across the tube; this is due to the near uniform velocity profile at this axial location and thus a small production term. As z^* increases to 100, the kinetic energy increases with a maximum occurring near the interface. This increase is due to the velocity profile changing from uniform to a more fully developed shape thus increasing the production term. The peak in the turbulent kinetic energy profile occurring

near the interface can be attributed to the increasing mean velocity gradient as y/r_o approaches zero. After $z^* = 100$, the kinetic energy profile decreases due to the decreasing velocity in the core. At $z^* = 569$ when the velocity reverses, the kinetic energy drops to zero, due to very small velocities at this location.

Figures 8.3 and 8.4 show the dimensionless film thickness and Nusselt number distributions. In Figure 8.3, the slope of the curve, $\frac{d\delta^*}{dz^*}$, is largest near the inlet due to the high condensation rate and decreases along the tube. This high condensation rate near the inlet can also be observed in Figure 8.4; the Nusselt number is largest near the inlet and decreases as z* increases.

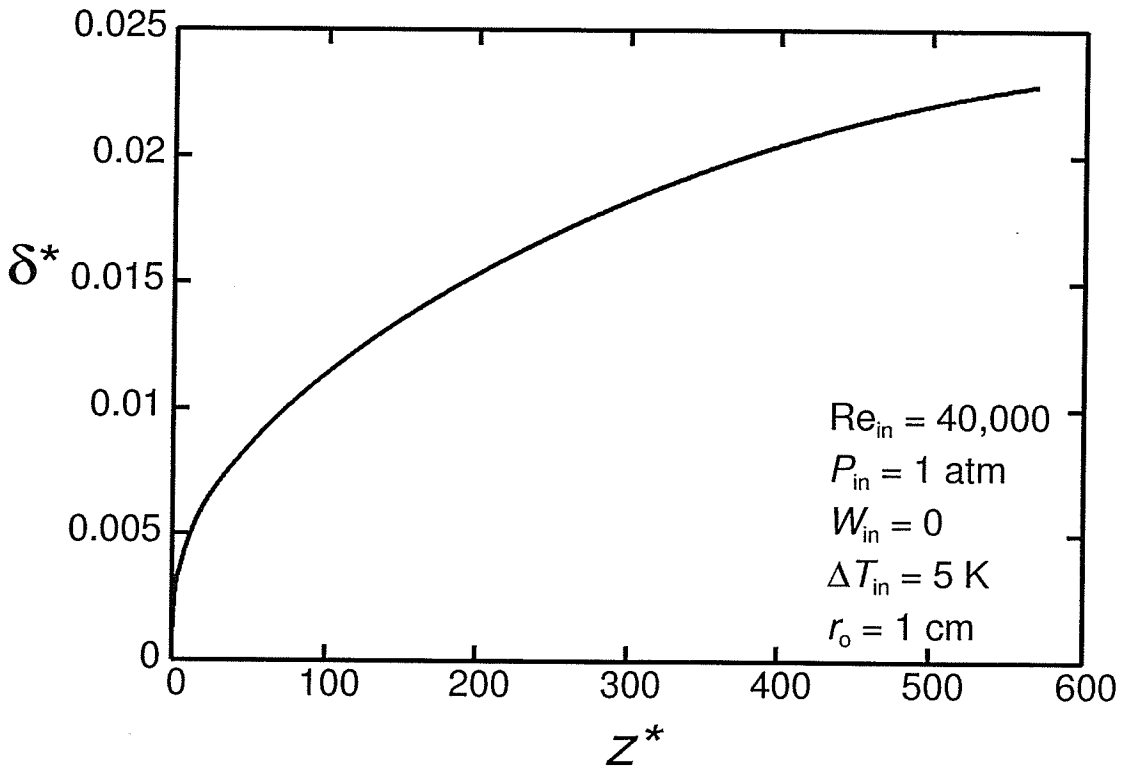

Figure 8.3 Dimensionless film thickness distribution for pure steam

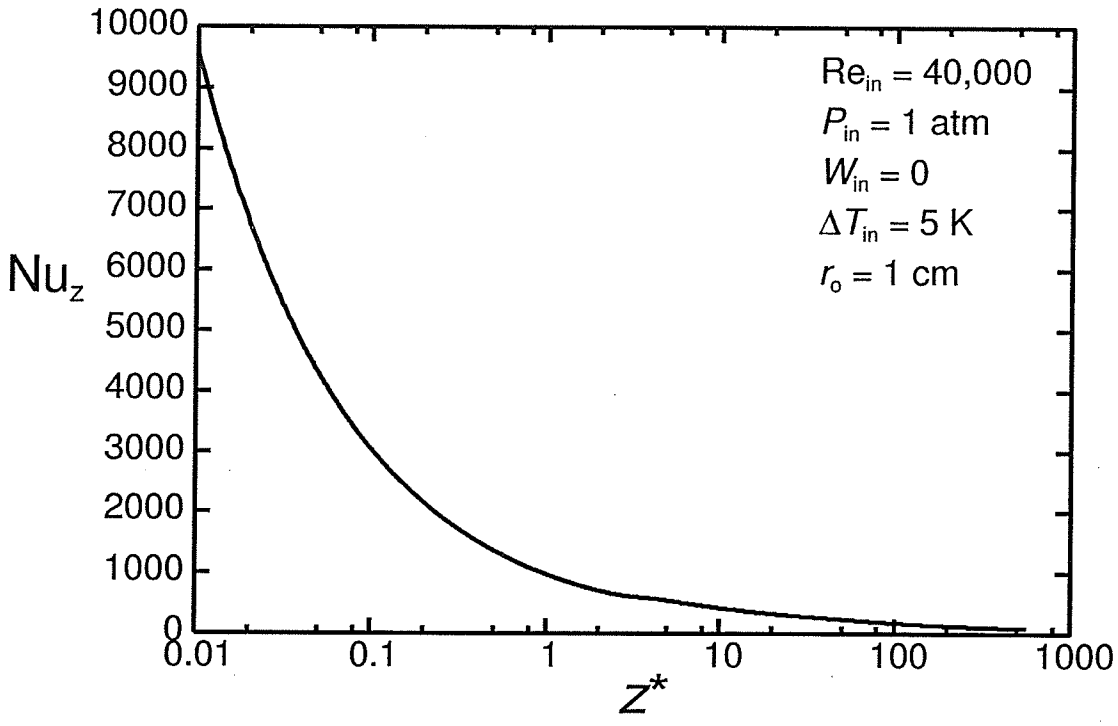

Figure 8.4 Local Nusselt number distribution for pure steam

8.3 Steam-Air Mixtures

The results of the steam-air run, shown in Figures 8.5 to 8.11, are for a 2-cm diameter tube with Re_{in} = 40,000, P_{in} = 1 atm, ΔT_{in} = 5 K, and W_{in} = 0.1. Figure 8.5 shows the dimensionless velocity profiles for various axial locations. At the inlet, the profile is uniform in the mixture region and zero in the liquid. As z^* increases to 10, the velocity profile in the mixture tends to a fully developed profile while the velocity in the liquid increases due to condensation. Comparing the velocity profiles in Figure 8.5 to those found in Figure 8.1 for the case of pure steam it can be seen that the centerline velocity in Figure 8.5 increases from z^* = 0 to z^* = 10 whereas the centerline velocity in Figure 8.1 decreased. The reason for this is that as z^* increases, a boundary layer develops in the mixture at the interface with the liquid. As a result, the centerline velocity increases as

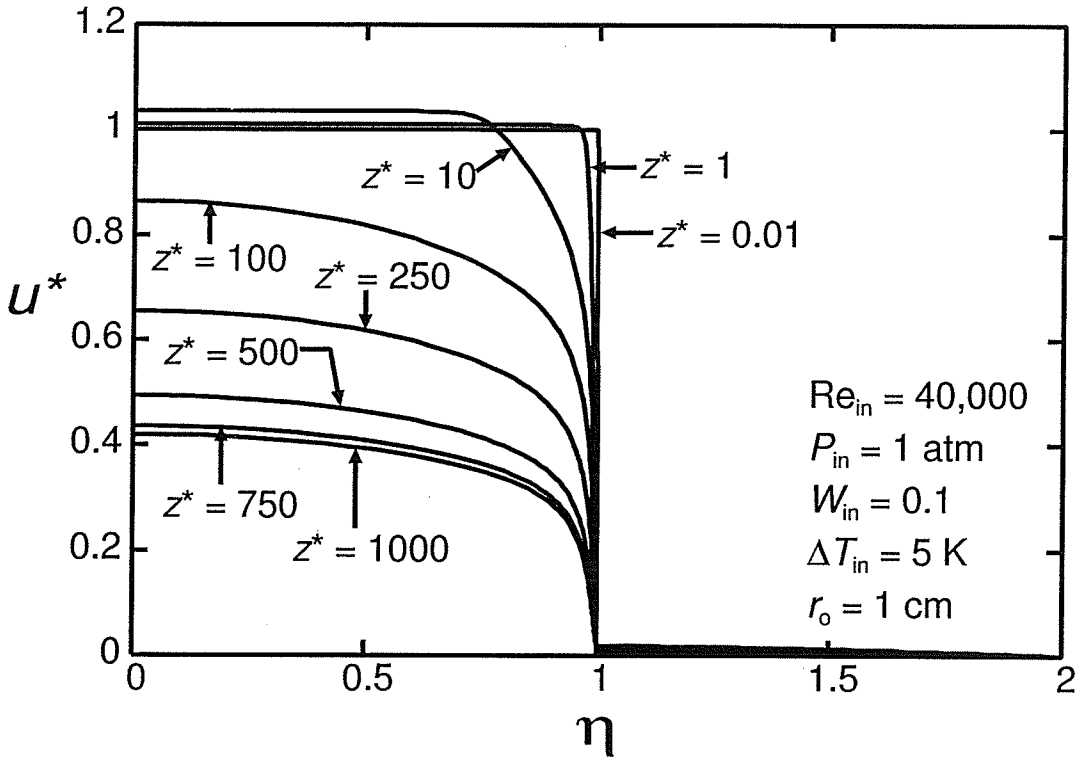

Figure 8.5 Dimensionless velocity profiles for a steam-air mixture

can be seen from Figure 8.5. However, for the case of pure steam, the condensation rate is large and thus the velocity in the core decreases due to the loss of steam and offsets the increasing centerline velocity. As z^* increases from 10 to 1000 in Figure 8.5, the velocity in the mixture continues to decrease while the velocity in the liquid increases.

Figure 8.6 shows the gas mass fraction profiles at various z^* locations. Near the inlet, the gas mass fraction is equal to W_{in} across the majority of the core but increases at the interface due to the impermeability boundary condition. As z^* increases and more steam condenses, W increases across the core and at $z^* = 1000$, the gas mass fraction is uniform and is approximately equal to 0.285.

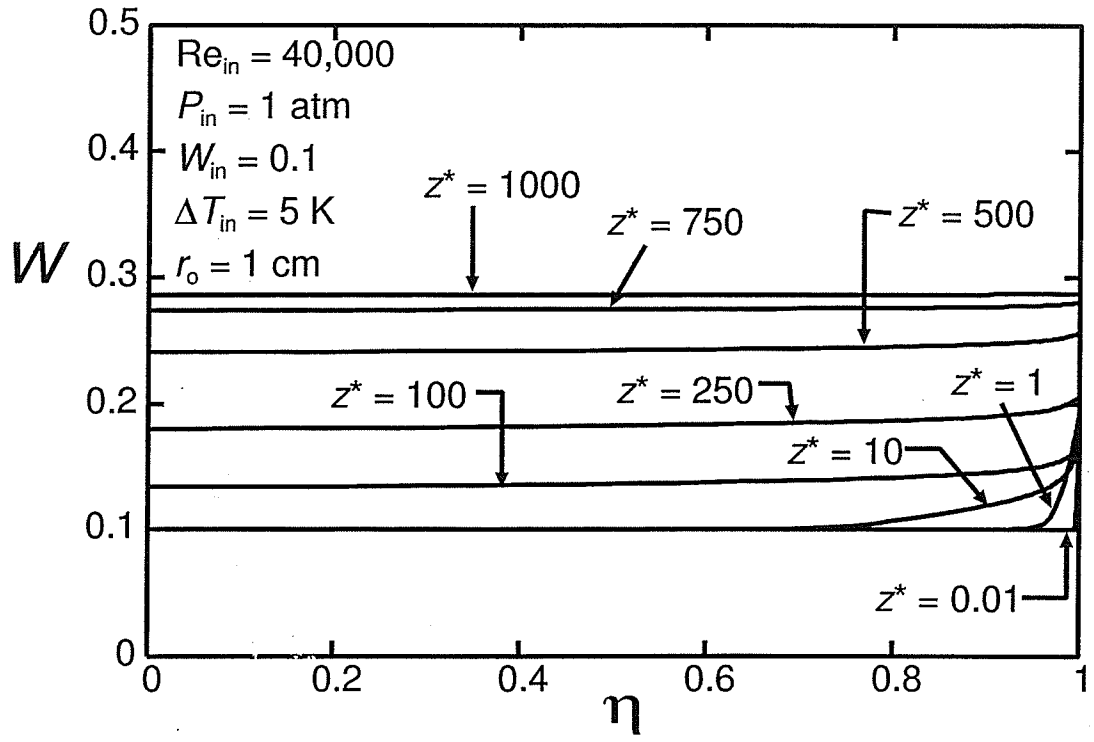

Figure 8.6 Gas mass fraction profiles for a steam-air mixture

Figure 8.7 shows how the dimensionless pressure P^* varies along the length of the tube, where $P^* = \frac{P - P_{in}}{0.5\rho_{in}u_{in}^2}$. In the present model, there are three components that influence P^*: one is the change in momentum which for this problem causes P^* to rise, the second is the wall friction which causes P^* to drop, and the third is the force of gravity which is small relative to the other two components but causes P^* to rise. From the definition of P^*, it is known that at the inlet ($z^* = 0$) P^* will equal zero. It can be seen in Figure 8.7 that shortly after the inlet, at $z^* = 0.001$, $P^* \approx -0.5$; this drop in P^* from $z^* = 0$ to 0.001 is due to the large frictional force near the inlet. As z^* increases further, the change in momentum becomes more significant relative to the wall friction causing P^* to increase. Near $z^* = 0.1$, the slope of the curve decreases, but remains positive right up to $z^* = 1000$.

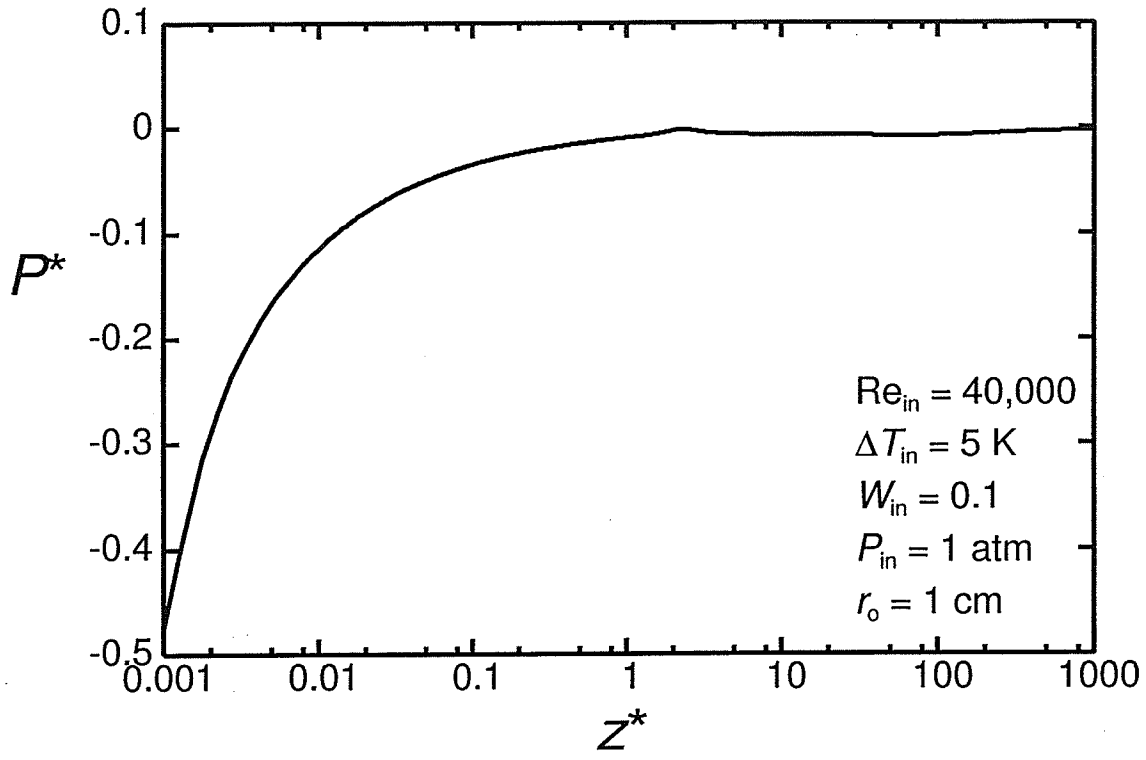

Figure 8.7 Dimensionless pressure distribution for a steam-air mixture

Figure 8.8 shows the temperature profiles along the length of the tube. Near the inlet ($z^* = 0.01$), the mixture temperature is uniform and equal to the inlet temperature and drops sharply at the interface, while in the liquid region, the profile is nearly linear. Between $z^* = 0.01$ and 10, the temperature in the mixture remains equal to the inlet temperature across most of the core region, while the interfacial temperature rises. The interfacial temperature (T_{int}) is a function of both the pressure (P) and the interfacial gas mass fraction (W_{int}); T_{int} decreases with W_{int} and increases with P and thus P^*. From Figure 8.7 it can be seen that from $z^* = 0.01$ to 10, P^* increases significantly resulting in an increase in the interfacial temperature. Beyond $z^* = 10$, T_{int} decreases continuously. Figure 8.7 shows that the change in P^* is not significant beyond $z^* = 10$ and therefore, P^* does not

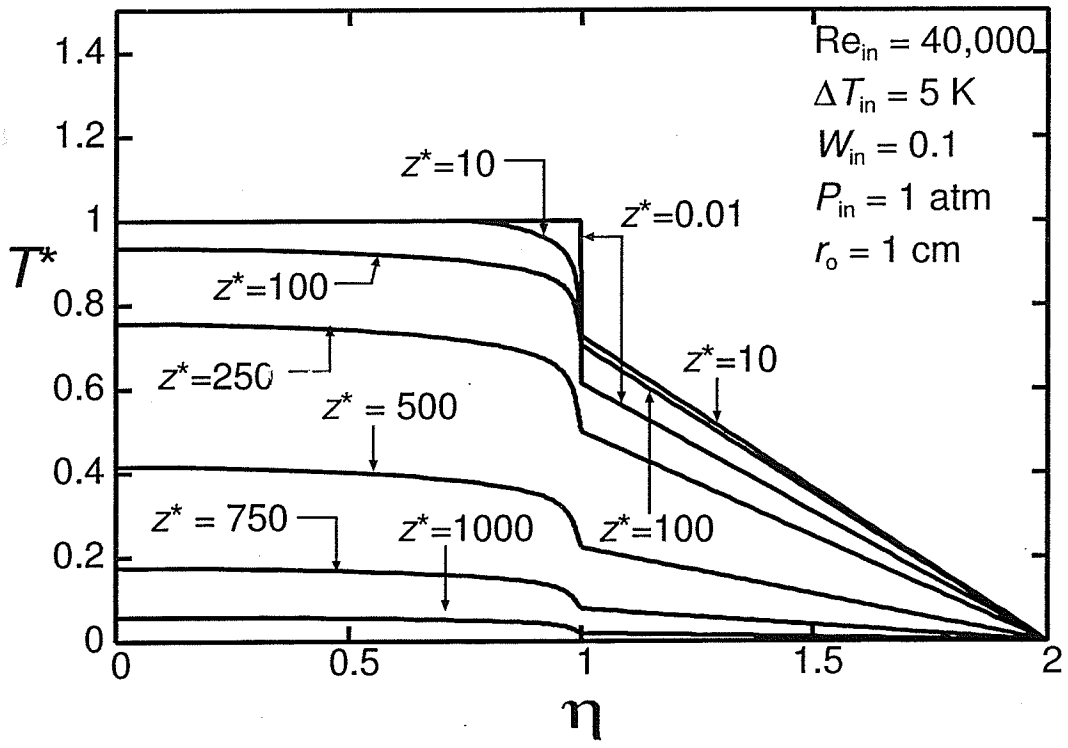

Figure 8.8 Dimensionless temperature profiles for a steam-air mixture

have much of an effect on the temperature profile; the decrease in T_{int} is therefore due to the increase in W_{int}. From $z^* = 10$ to $z^* = 1000$, the temperature across the entire tube drops and T^* approaches zero as we approach the end of condensation.

The turbulent kinetic energy profiles in the mixture region are shown in Figure 8.9. Near the inlet, the kinetic energy is close to zero due to the flat velocity profile across the core. As z^* increases and the velocity profile takes on the shape of a fully developed profile, the kinetic energy profile increases with its peak value occurring near the interface and dropping to zero at the interface. With the presence of air, the kinetic energy profile does not drop back to zero as it did for the case of pure steam. The reason for this is that the

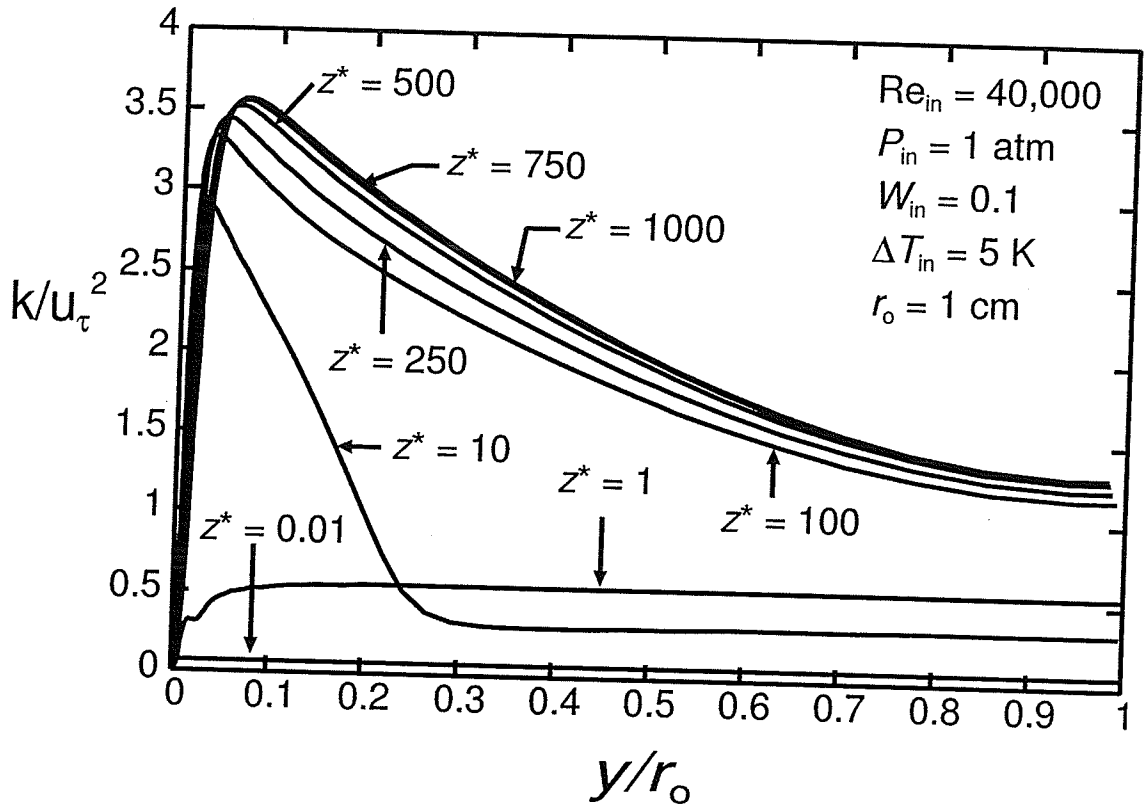

Figure 8.9 Turbulent kinetic energy profiles for a steam-air mixture

velocity profile maintains the shape of a fully developed profile due to the presence of gas and therefore the kinetic energy will also maintain its shape.

The dimensionless film thickness and Nusselt number distributions are shown in Figures 8.10 and 8.11. From Figure 8.10 it can be seen that the film thickness increases rapidly near the inlet due to the large condensation rate and levels off near the end. This trend can also be observed in Figure 8.11; the Nusselt number is large near the inlet and drops to small values near the end.

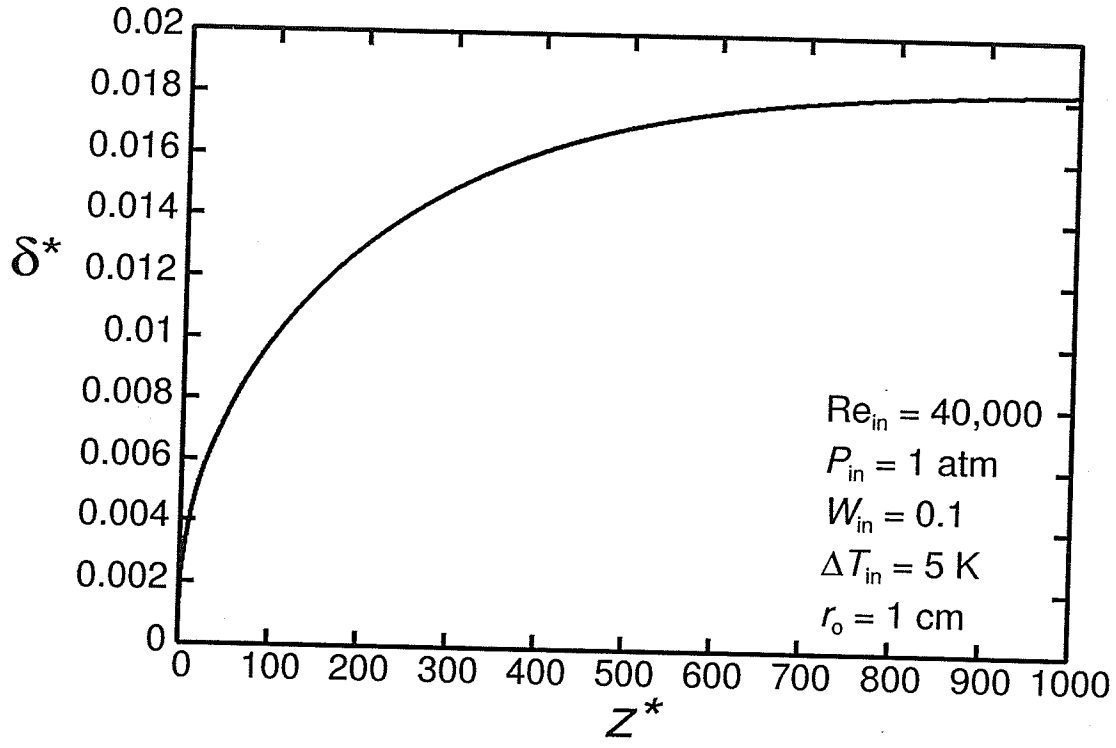

Figure 8.10 Dimensionless film thickness distribution for a steam-air mixture

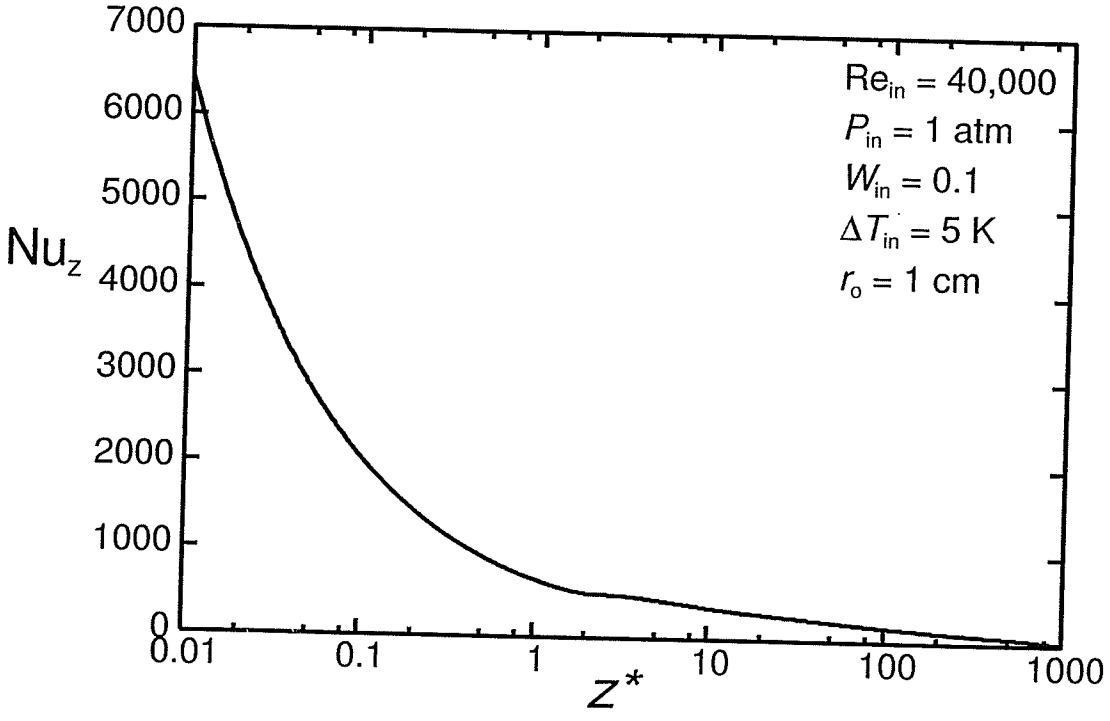

Figure 8.11 Local Nusselt number distribution for a steam-air mixture

8.4 Effect of Re_{in}

Figure 8.12 compares the dimensionless film thickness for three different inlet-Reynolds numbers. For all three cases shown in this figure, P_{in} = 1 atm, W_{in} = 0.1, ΔT_{in} = 8 K, and r_o = 1 cm. The three curves represent inlet Reynolds numbers of 20,000, 40,000, and 60,000. From these curves it can be seen that near the inlet, the film thickness decreases with increasing Reynolds number. Further along the length of the tube, the film thickness curves cross and the film thickness decreases with decreasing Re_{in}. The final film thickness at the "end of condensation" does therefore increase with an increase in Re_{in}, which is the expected behavior.

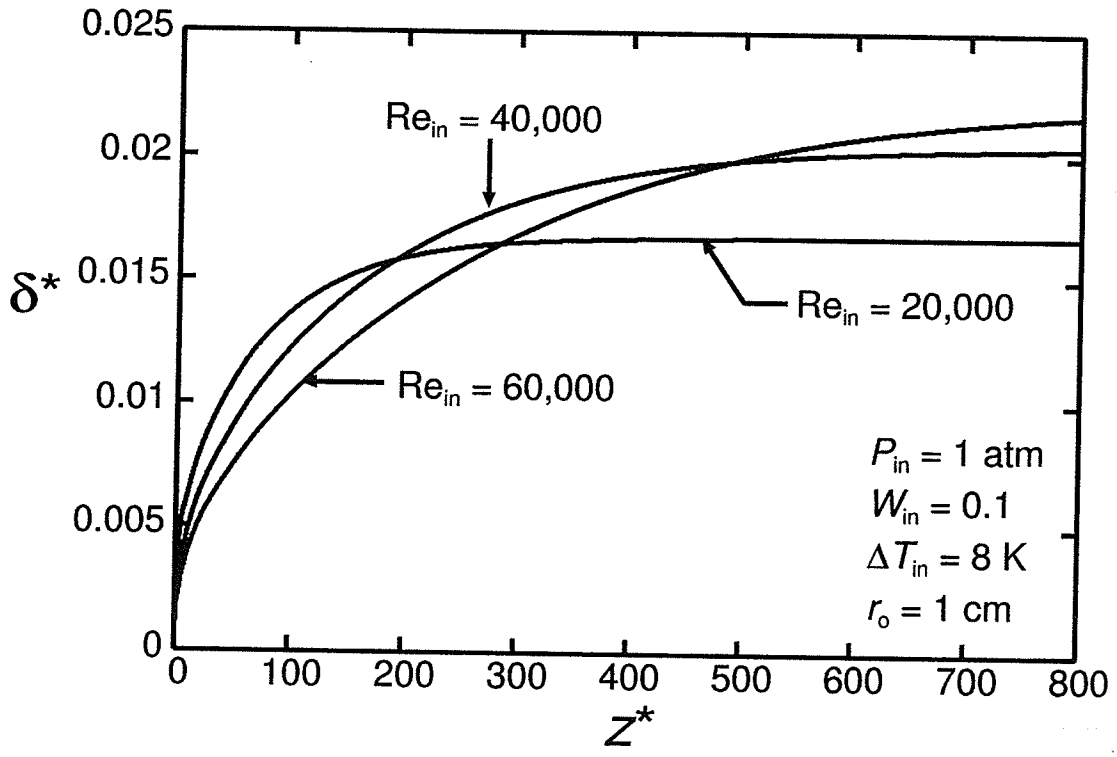

Figure 8.12 Effect of Re_{in} on the dimensionless film thickness

Although the film is thinner near the inlet for the higher Re_{in}, the total mass flow rate across the film is larger. For this to occur, the velocity of the film must be significantly higher for the larger inlet Reynolds numbers. This is shown in Figure 8.13, where the velocity profile in the liquid film is plotted at $z^* = 100$ for all three cases of Re_{in}. From this figure it can be seen that as Re_{in} increases, the liquid velocity increases and the film thickness decreases (as can be determined from the distance on the horizontal axis, y/r_o, where the velocity is the highest).

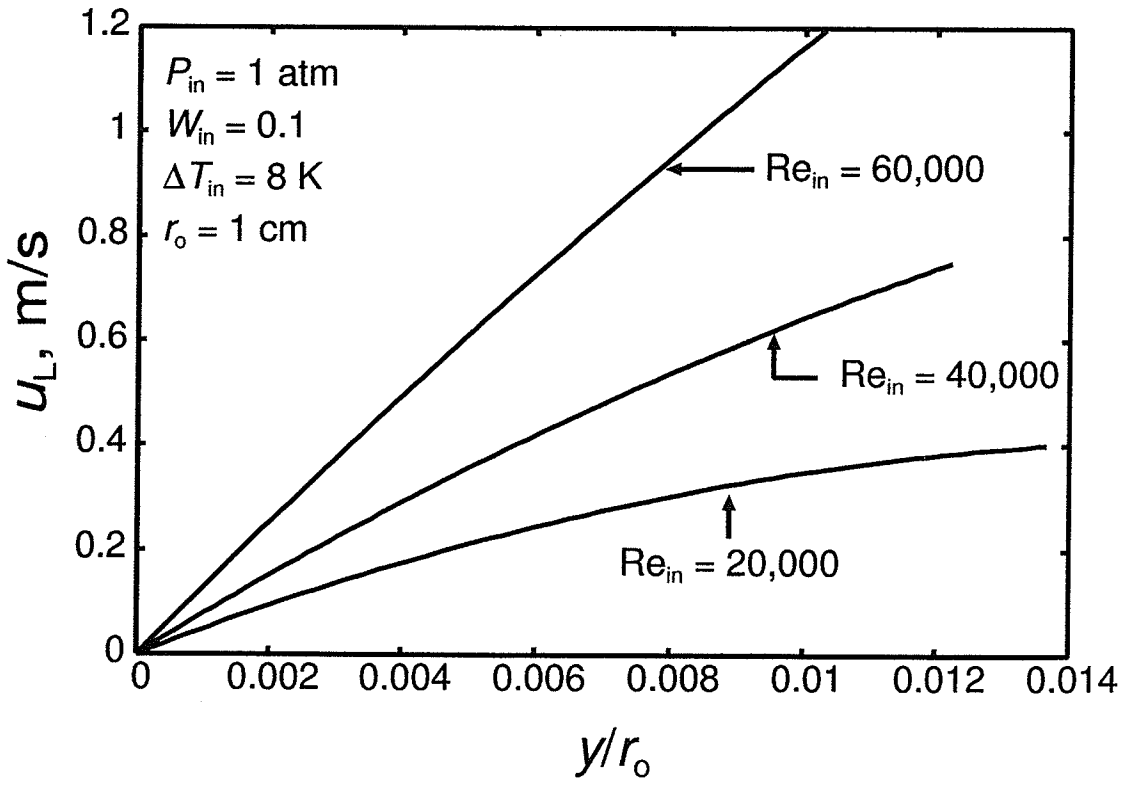

Figure 8.13 Effect of Re_{in} on the velocity profile in the liquid film at $z^* = 100$

The thinner, faster moving film resulting from the higher inlet Reynolds numbers is likely due to the interfacial shear stress acting on the film. The expected trend is that as the interfacial shear increases, the velocity in the film increases and the film thickness decreases. Figure 8.14 shows the axial distribution of the interfacial shear stress for the three cases of Re_{in} with the same conditions used in Figures 8.12 and 8.13. The results in Figure 8.14 confirm the significant increase in interfacial shear with Re_{in}.

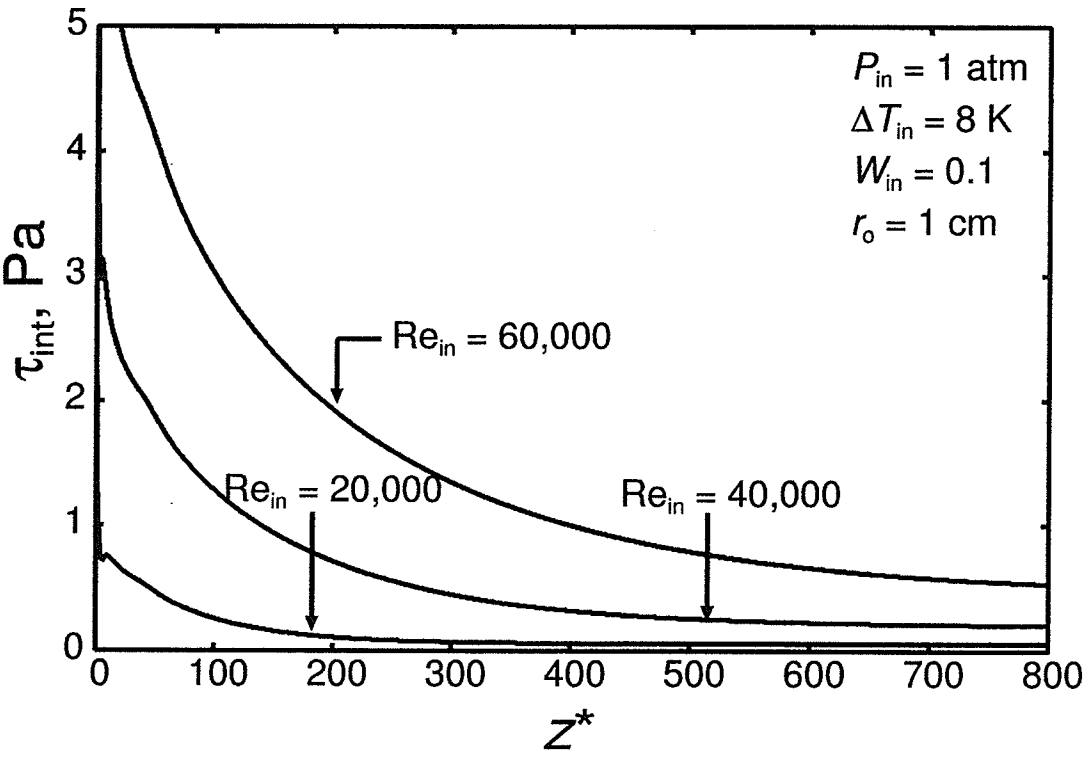

Figure 8.14 Effect of Re_{in} on the interfacial shear stress distribution

Figure 8.15 shows the local Nusselt number for the same three inlet-Reynolds numbers used in Figures 8.12 to 8.14. These results show that the Nusselt number increases with increasing Re_{in}. The form of Nu_z dependence on Re_{in} is examined in Figure 8.16 by plotting ($Nu_z/Re_{in}^{0.5}$) versus z^*. The results for the three values of Re_{in} (Re_{in} = 20,000, 40,000, and 60,000) with P_{in} = 1 atm, W_{in} = 0.1, ΔT_{in} = 8 K, and r_o = 1 cm are shown in this figure. The results for all three Re_{in}-values collapse fairly well into one curve. This result gives a starting point for developing an algebraic correlation; however, much more work is needed to achieve this goal.

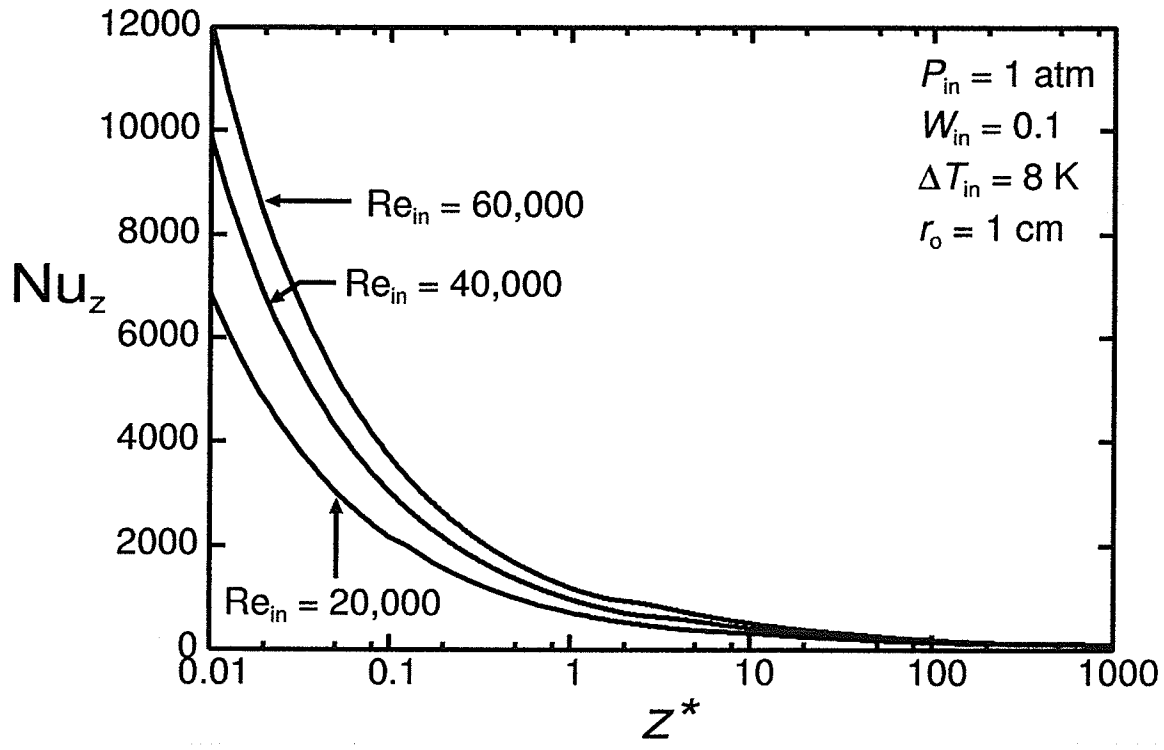

Figure 8.15 Effect of Re_{in} on the local Nusselt number

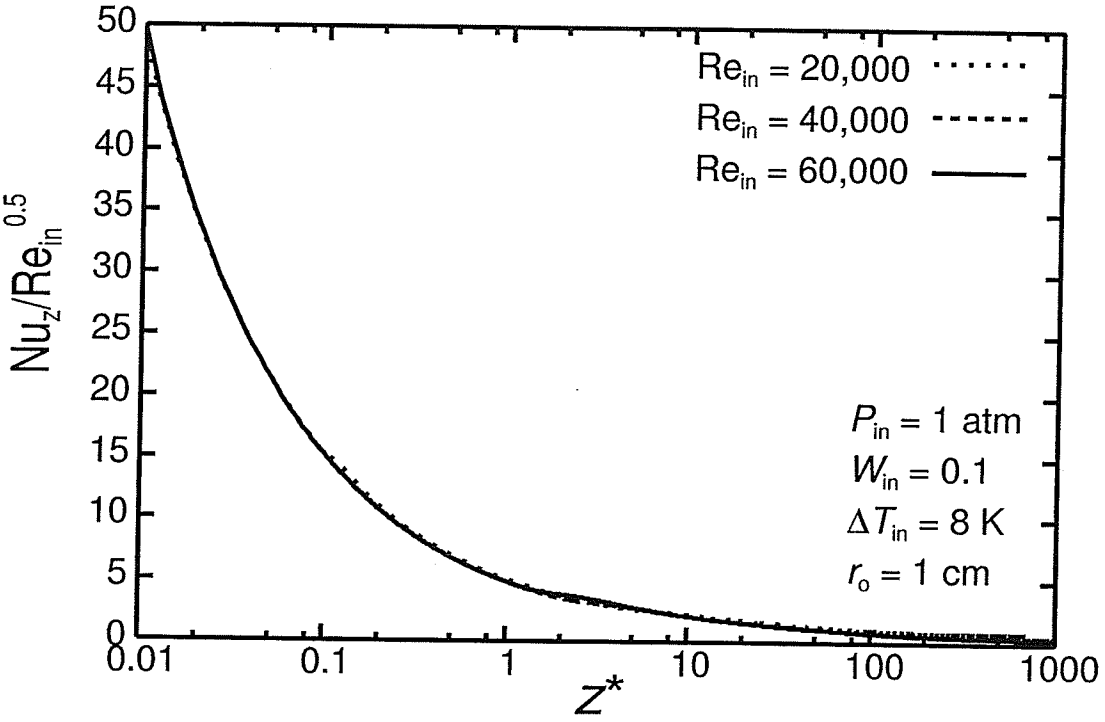

Figure 8.16 $Nu_z/Re_{in}^{0.5}$ vs. z^* for various Re_{in}

8.5 Effect of ΔT_{in}

Figures 8.17 and 8.18 show the effects of both inlet Reynolds number and temperature difference between the inlet and the wall on film thickness and local Nusselt number. The independent parameters for the runs shown in these figures are: P_{in} = 1 atm, W_{in} = 0.1, r_o = 1 cm, ΔT_{in} = 5 and 10 K, and Re_{in} = 20,000 and 40,000. From Figure 8.17 it can be seen that the film thickness increases with increasing ΔT_{in}. In addition, the temperature difference has a greater effect on the film thickness for higher Reynolds numbers. When comparing the curves for ΔT_{in} = 5 and 10 K it can be seen that the curve for Re_{in} = 20,000 crosses the curve for Re_{in} = 40,000 at a lower z* value for ΔT_{in} = 10 K. The reason for this is that for ΔT_{in} = 10 K, the condensation rate is higher near the inlet and therefore, less distance is required for the steam to fully condense and for the film thickness curve to level off.

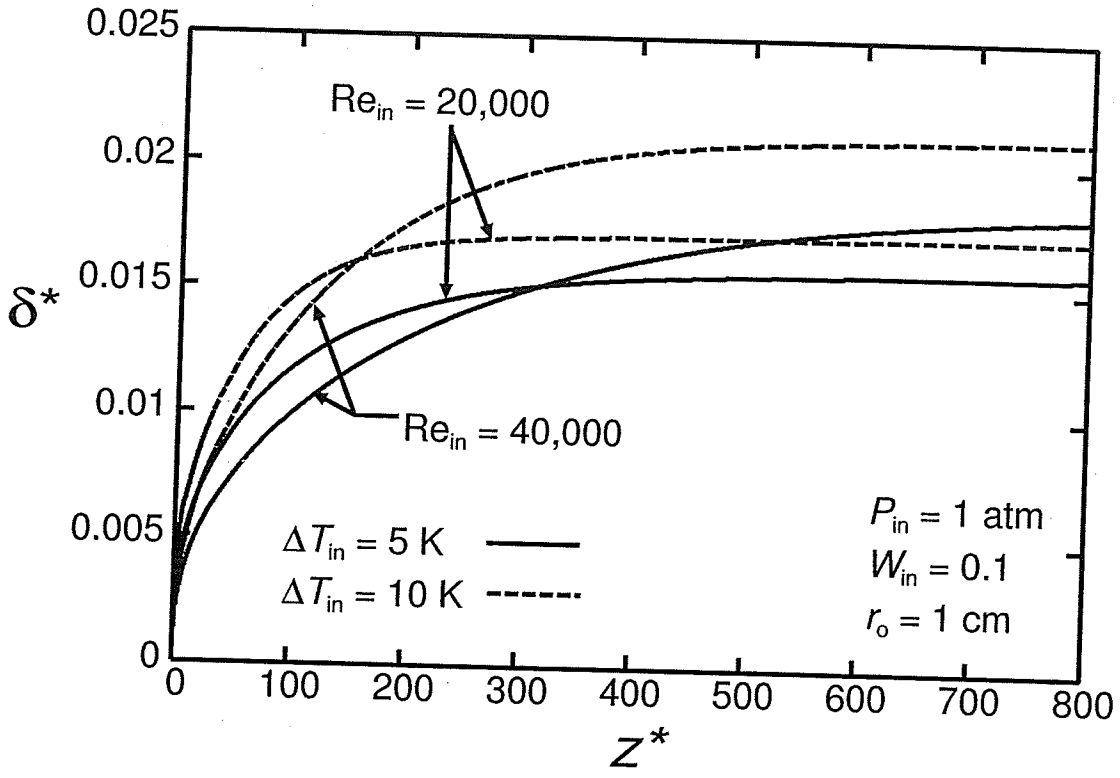

Figure 8.17 Effect of ΔT_{in} and Re_{in} on the dimensionless film thickness

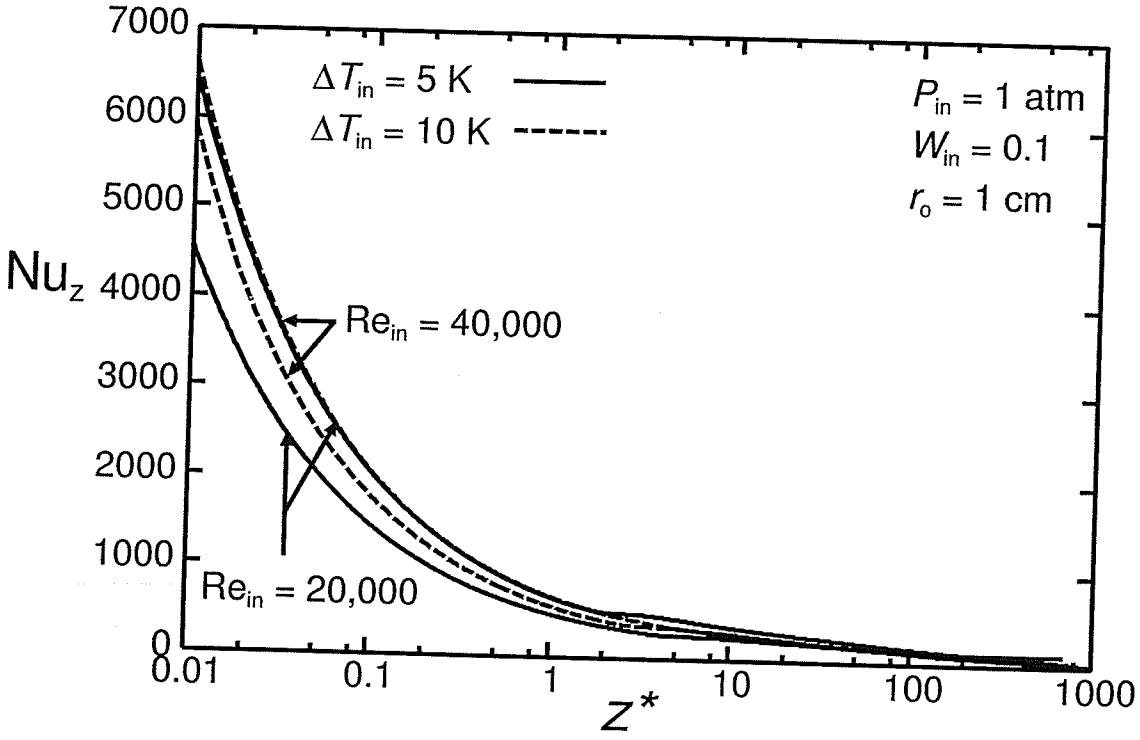

Figure 8.18 Effect of ΔT_{in} and Re_{in} on the local Nusselt number

Figure 8.18 shows the local Nusselt number distribution for these same runs. From this figure it can be seen that increasing ΔT_{in} results in a decrease in the local Nusselt number. The reason for this is that for the higher ΔT_{in}, the film is much thicker resulting in a lower heat transfer coefficient and thus a lower Nusselt number. It must be pointed out that a decrease in the heat transfer coefficient does not necessarily mean a decrease in the heat flux since the heat flux depends on the product of the heat transfer coefficient and the temperature difference.

8.6 Effect of W_{in}

Figures 8.19 and 8.20 show the effect of inlet gas mass fraction on film thickness and Nusselt number. The input parameters for these figures are Re_{in} = 40,000, P_{in} = 1 atm, ΔT = 5 K, r_o = 1 cm and W_{in} = 0, 0.05, 0.1 and 0.2. Although the results shown in these figures are for a maximum gas mass fraction of 20%, the numerical model is capable of producing results for gas mass fractions up to 60%. The dimensionless film thickness distributions are shown in Figure 8.19. As W_{in} increases, the film thickness decreases and levels off at lower z^* values. For the case of pure steam (W_{in} = 0), flow reversal occurs at $z^* \approx 580$. Figure 8.20 shows the effect of W_{in} on the local Nusselt number. From this figure it can be seen that as W_{in} increases, the local Nusselt number decreases. Comparing the case of W_{in} = 0 to W_{in} = 0.2 it can be noted that the Nusselt number and thus the heat flux at the wall doubles when the air is removed.

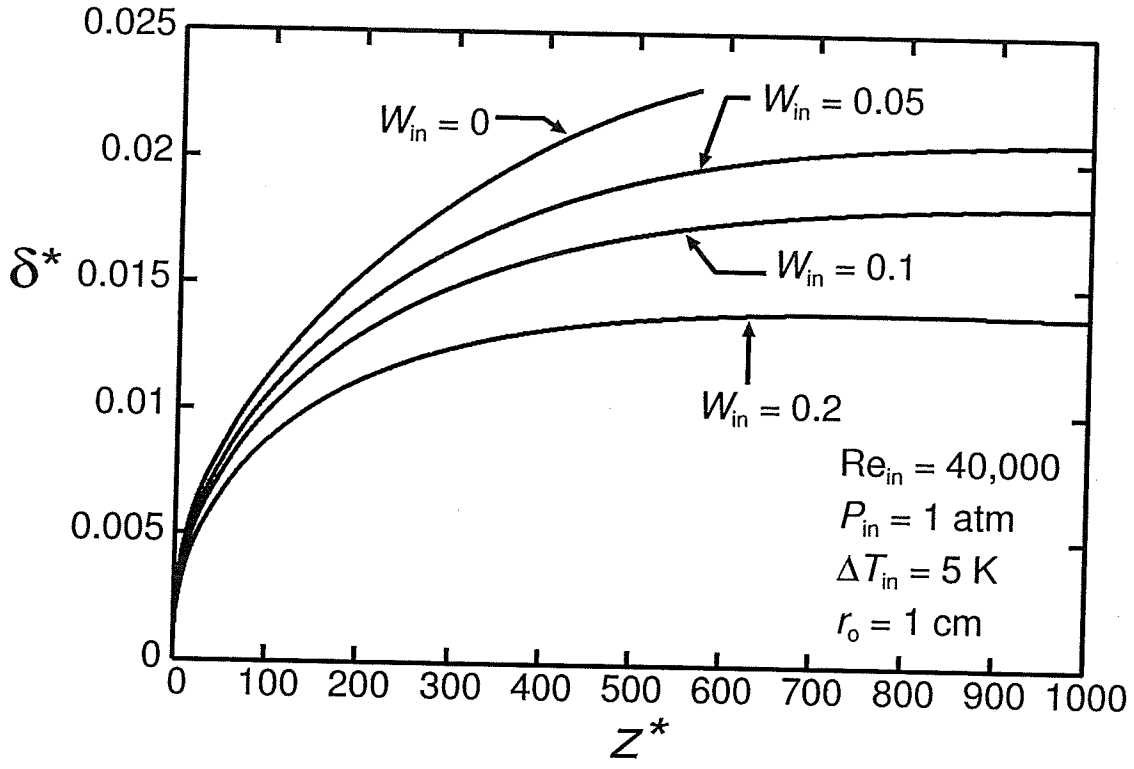

Figure 8.19 Effect of W_{in} on the dimensionless film thickness

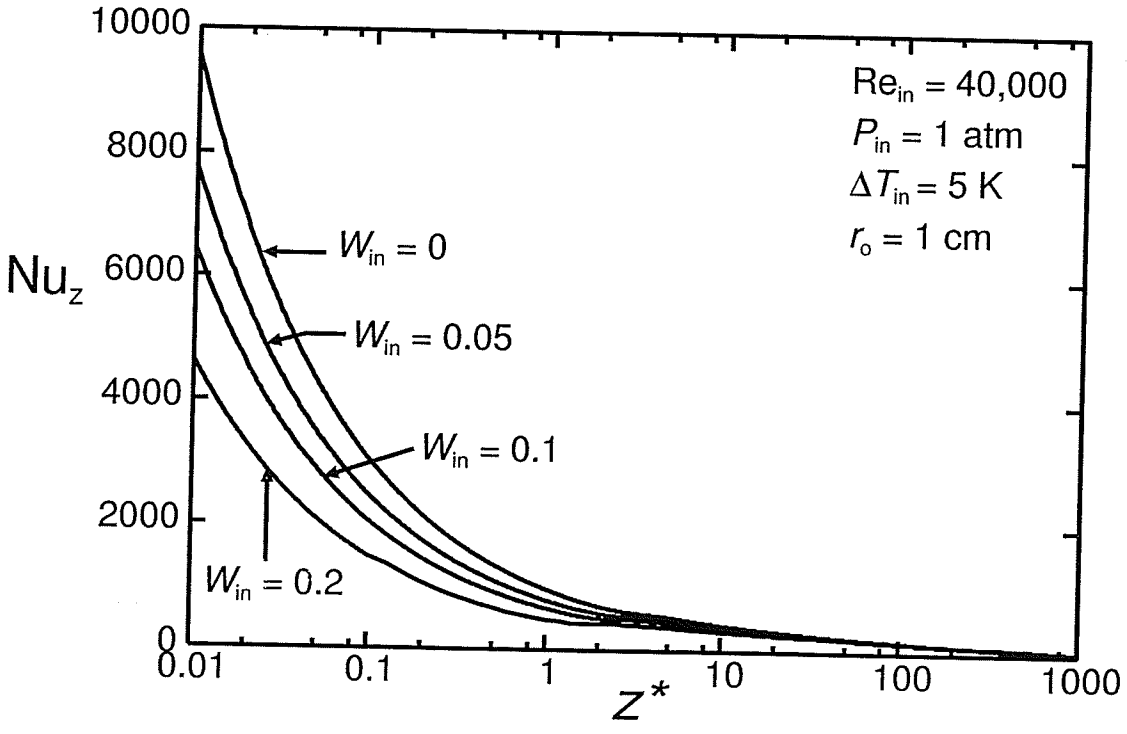

Figure 8.20 Effect of W_{in} on the local Nusselt number

Figure 8.21 and 8.22 show the effects of both ΔT_{in} and W_{in} on film thickness and Nusselt number. The inlet parameters are: Re_{in} = 40,000, P_{in} = 1 atm, r_o = 1 cm, W_{in} = 0 and 0.1 and ΔT_{in} = 5, 10 and 20 K. From Figure 8.21 it can be seen that for the case of W_{in} = 0, flow reversal occurs at lower z^* as ΔT_{in} increases; this is due to the larger condensation rate for higher ΔT_{in}. Similar trends as those found in previous figures can be observed here including an increase in δ^* with increasing ΔT_{in} and decreasing W_{in}. Figure 8.22 shows the local Nusselt number distribution for these same runs. The Nusselt number was again found to decrease with the addition of air and with increasing ΔT_{in}. When comparing the effects of W_{in} and ΔT_{in} it can be seen that increasing W_{in} from 0 to 0.1 has a greater effect on the Nusselt number than increasing ΔT_{in} from 5 to 20 K.

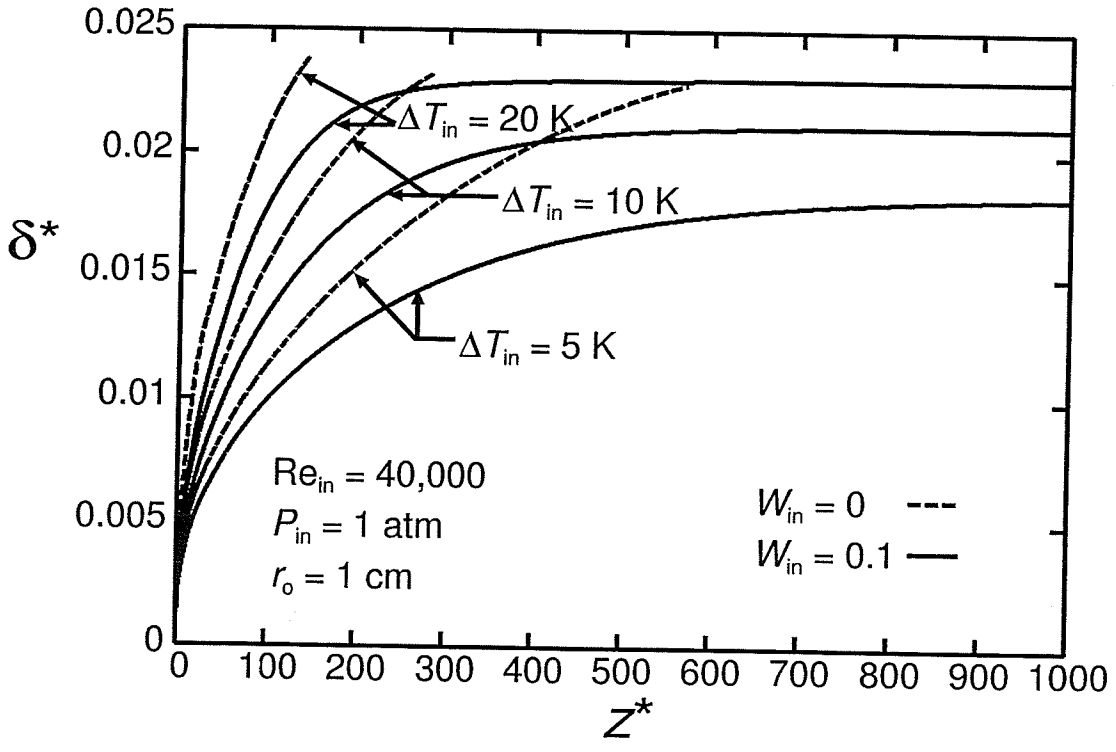

Figure 8.21 Effect of ΔT_{in} and W_{in} on the dimensionless film thickness

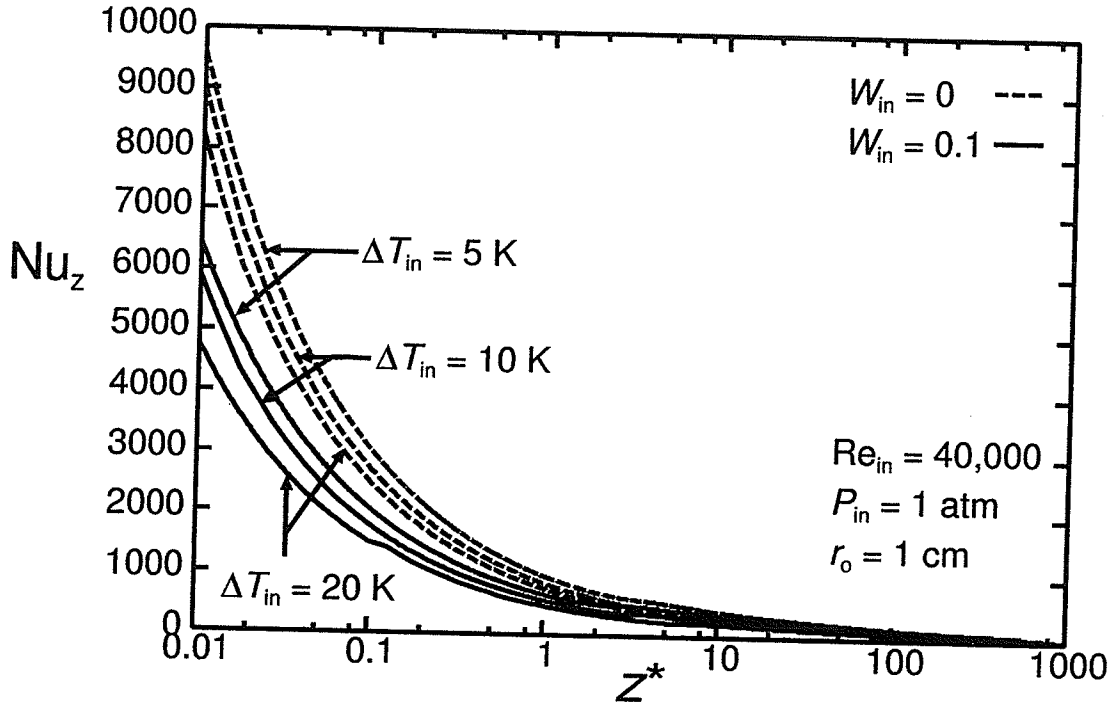

Figure 8.22 Effect of ΔT_{in} and W_{in} on the local Nusselt number

8.7 Effect of P_{in}

The effect of inlet pressure is shown in Figures 8.23 and 8.24. The inlet Reynolds number for these figures is 40,000, the radius is 1 cm, and the inlet temperature difference is 5 K. Two values were used for the inlet gas mass fraction (W_{in} = 0 and W_{in} = 0.1) and three values for the inlet pressure (P_{in} = 1, 2, and 4 atm). Figure 8.23 shows the dimensionless film thickness distributions. Near the inlet, the film thickness increases with the inlet pressure whereas near the end of the condenser or near flow reversal, the film thickness decreases with increasing inlet pressure. Varying the inlet pressure also appears to have a greater affect for the case of pure steam. The local Nusselt number distribution is shown in Figure 8.24. Near the inlet, the Nusselt number decreases with P_{in}, while at larger z^* values, the Nusselt number increases with P_{in}.

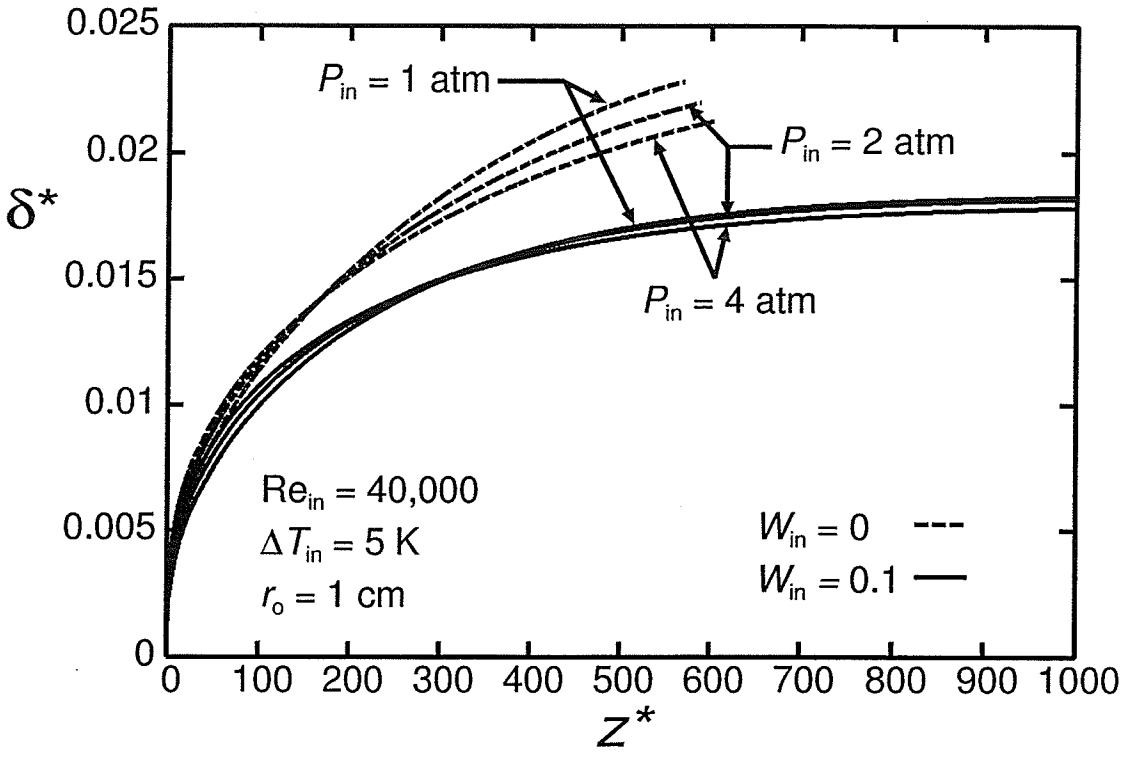

Figure 8.23 Effect of P_{in} and W_{in} on the dimensionless film thickness

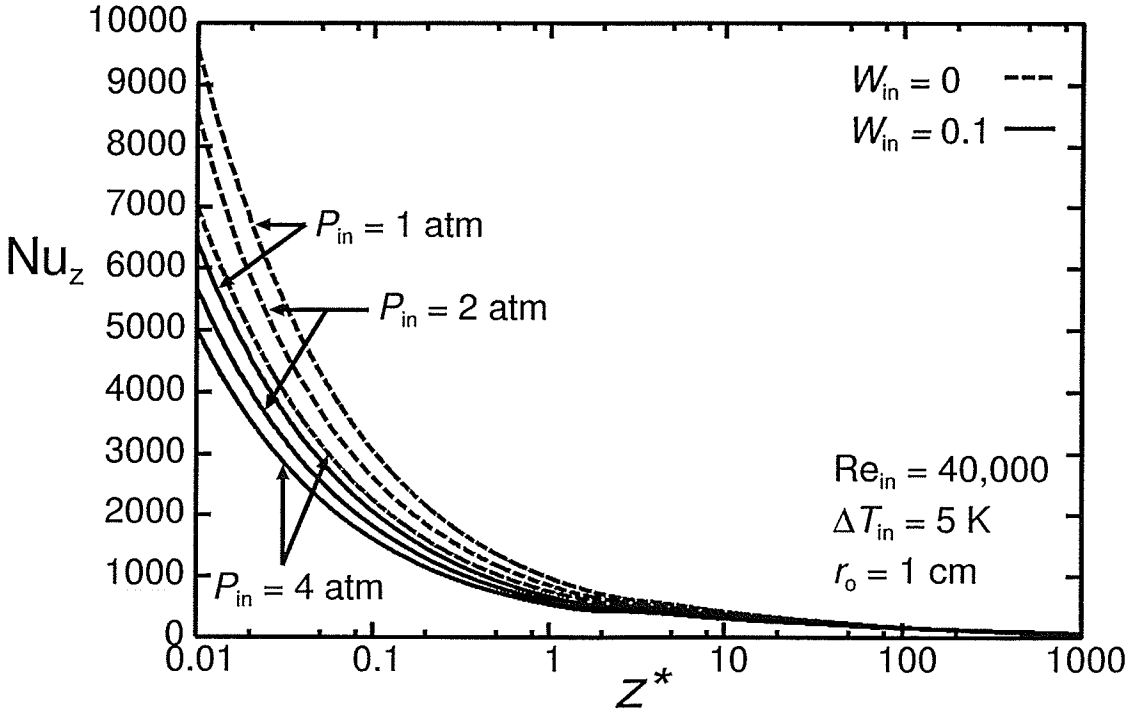

Figure 8.24 Effect of P_{in} and W_{in} on the local Nusselt number

The effect of inlet pressure on both film thickness and local Nusselt number is mainly due to the property changes that occur when varying the pressure. This was proven by keeping the properties constant and varying the inlet pressure for both the case of pure steam (Figures 8.25 and 8.26), and a steam-air mixture (Figures 8.27 and 8.28). Figures 8.25 to 8.28 show the effect of inlet pressure on the dimensionless film thickness and the local Nusselt number for fixed properties. From these plots it can be seen that when the properties are held constant, the effect of varying the inlet pressure is negligible on both the film thickness and the local Nusselt number.

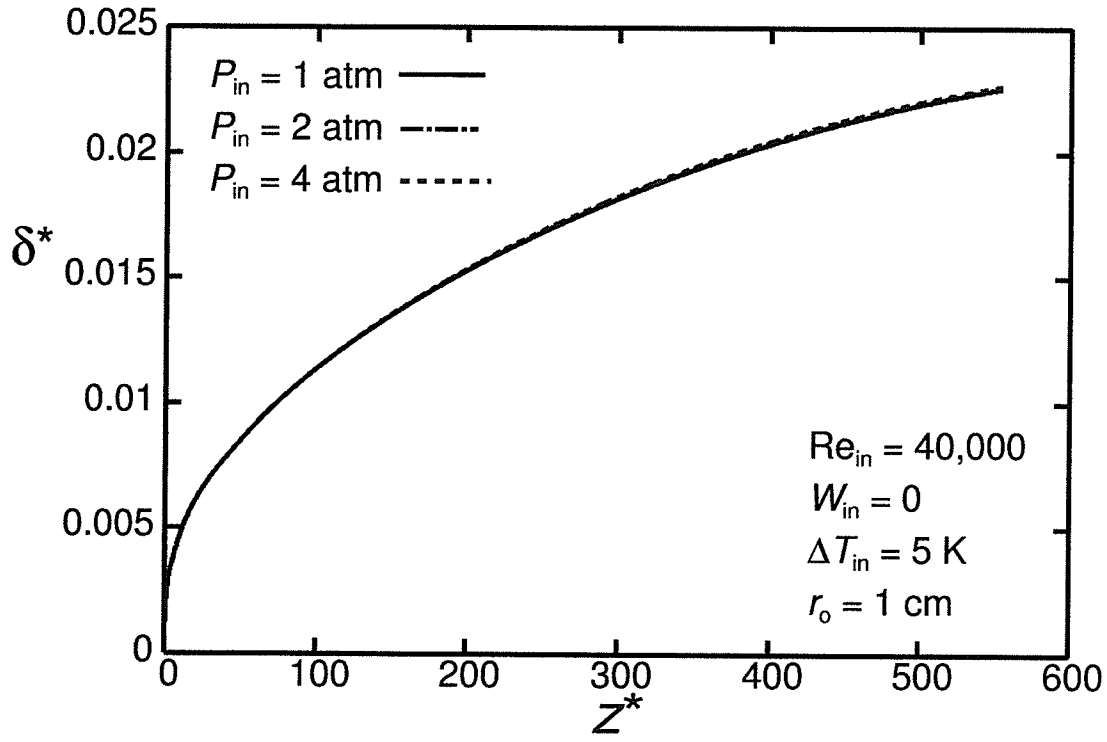

Figure 8.25 Effect of P_{in} on the dimensionless film thickness for pure steam with fixed properties

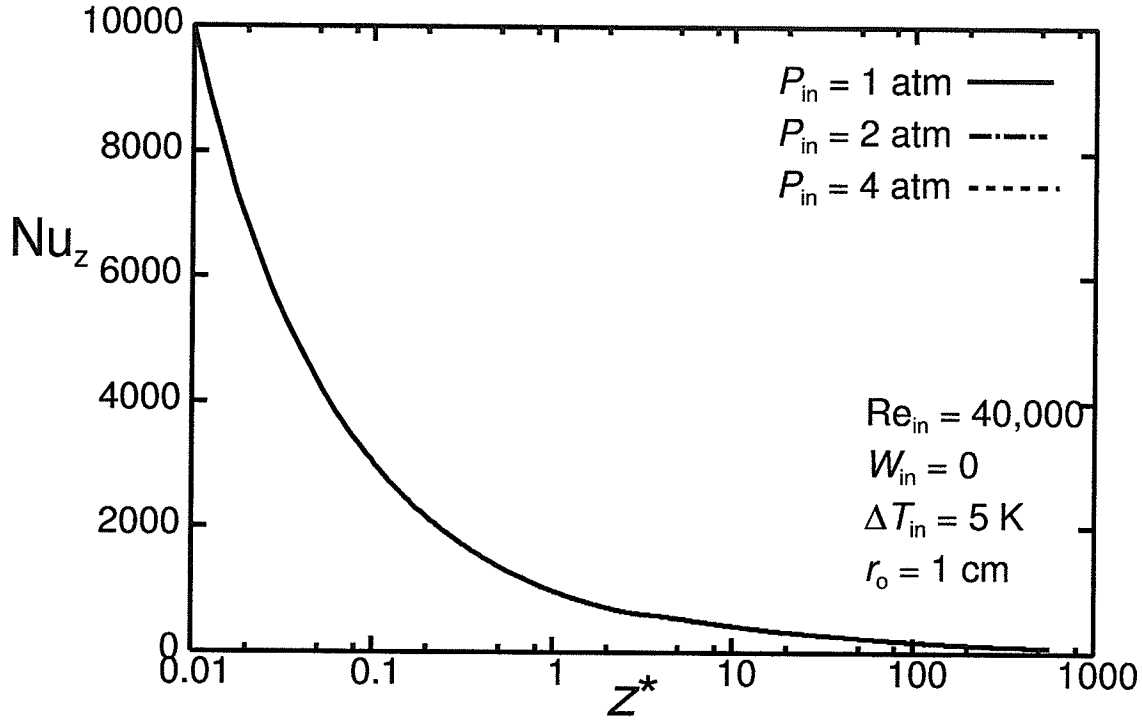

Figure 8.26 Effect of P_{in} on the local Nusselt number for pure steam with fixed properties

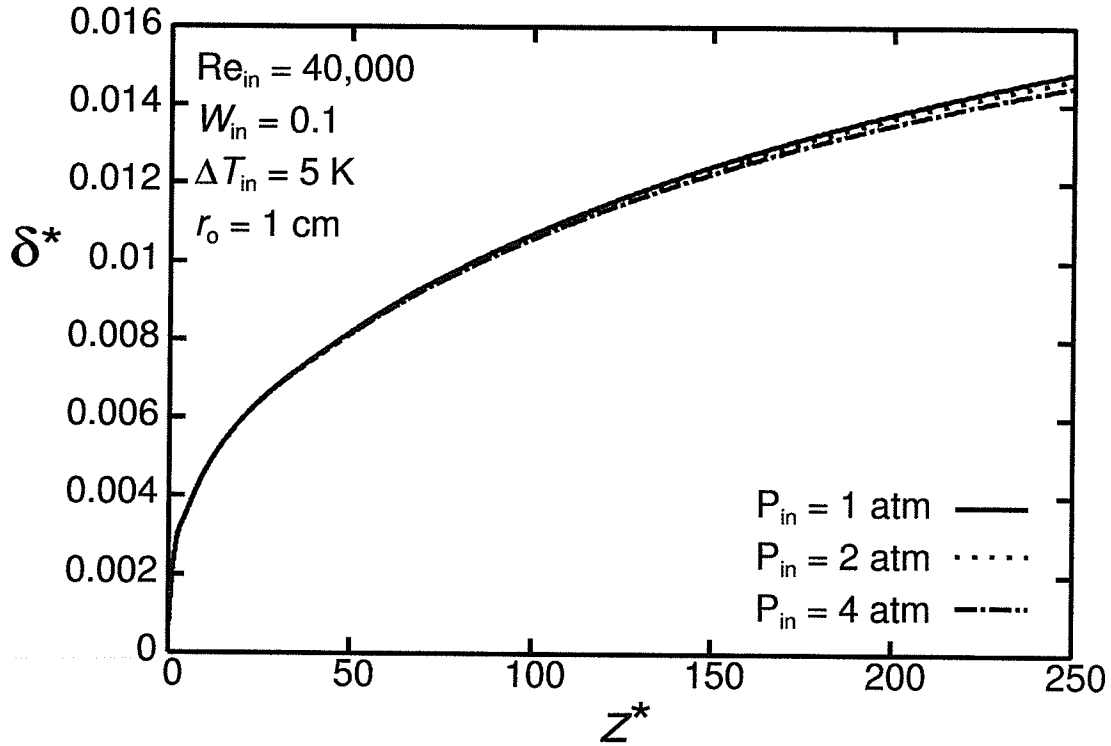

Figure 8.27 Effect of P_{in} on the dimensionless film thickness for a steam-air mixture with fixed properties

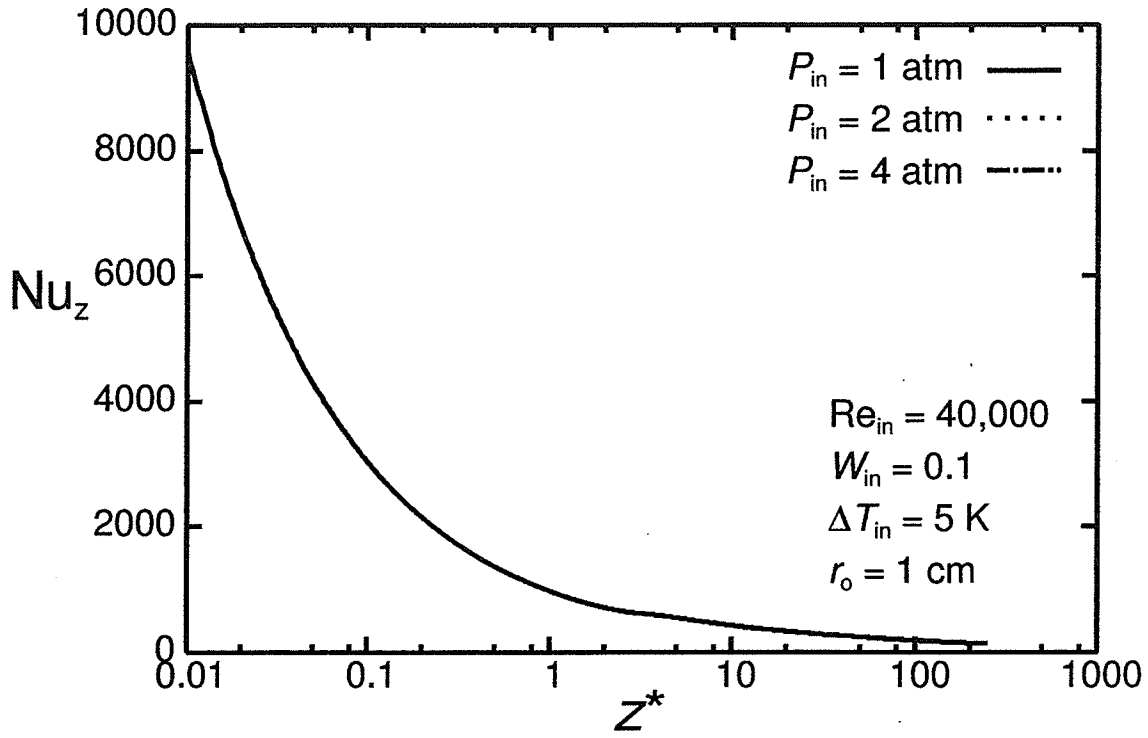

Figure 8.28 Effect of P_{in} on the local Nusselt number for a steam-air mixture with fixed properties

8.8 Summary

The results presented in Sections 8.2 and 8.3 for the cases of turbulent pure steam and steam-air mixtures showed similar trends as those found in the laminar flow results with the exception of one difference. The velocity profiles in the core resembled a fully developed turbulent profile and were therefore flatter than the profiles for laminar flow.

From the parametric studies several trends were observed. The dimensionless film thickness was found to increase with increasing inlet temperature difference, and/or with decreasing inlet gas mass fraction. Near the inlet, the film thickness increased with decreasing Reynolds number while further along the tube the curves crossed and beyond that, the film thickness was found to increase with increasing Reynolds number. When

varying the inlet pressure, the film thickness curves cross. Near the inlet, the film thickness increases with increasing pressure while further away from the inlet the opposite trend is found; the film thickness increases with decreasing pressure. The local Nusselt number was found to increase with decreasing inlet gas mass fraction, with decreasing inlet temperature difference and with increasing inlet Reynolds number. When varying the inlet pressure, different trends were observed near the inlet of the tube and the end of the tube. Near the inlet, the Nusselt number increased with decreasing pressure while further along the tube, the Nusselt number increased with increasing pressure.

CHAPTER 9

CONLUSIONS AND RECOMMENDATIONS

9.1 Conclusions

A numerical model was developed based on the full set of governing equations for turbulent condensation of a vapor in a vertical tube in the presence of gas. This model produces results for both laminar and turbulent flow conditions. For the case of laminar flow, a fully-coupled approach is used to solve the governing equations; while for the case of turbulent flow, the turbulent parameters are calculated separately from the governing equations. A parametric study was completed for the case of laminar flow and the following trends were observed: The film thickness increased when either ΔT_{in} or Re_{in} was increased or when W_{in} or P_{in} was decreased and the Nusselt number increased with increasing Re_{in} or decreasing ΔT_{in} or W_{in}.

For the case of turbulent flow, the following three turbulence models were employed to model turbulence in both the core and the film:

- Pletcher's (1974) mixing length model applied to both the core and the film
- Jones and Launder's (1972) low Reynolds number k-ε model applied to both the core and the film
- Jones and Launder's (1972) low Reynolds number k-ε model applied to the core and Pletcher's mixing length model applied to the film

When using the Jones and Launder low Reynolds number k-ε model across the liquid film along with boundary conditions of zero for both k and ε at the wall and the interface, the turbulent viscosity was dampened across the entire film. These findings are consistent with previous numerical models (e.g., Yuann, 1993).

The local heat transfer coefficient results from each of the three turbulence models above were compared with experimental results of Goodykoontz and Dorsch (1996), Siddique (1992), and Kuhn (1995). From these comparisons it was concluded that the model that showed the best agreement with all three experiments was the Jones and Launder low Reynolds number k-ε model applied to both the core and the film. With this model 73% of the results were within ± 50% of Goodykoontz and Dorsch's data, 89% of the results were within ± 40% of Siddique's data, and 98% of the results were within ± 30% of Kuhn's data.

A parametric study was performed for the case of turbulent flow using the k-ε model in both the core and the film. The dimensionless film thickness was found to increase with increasing ΔT_{in} and/or with decreasing W_{in}. When varying Re_{in}, two different trends were observed; near the inlet, the film thickness increased with decreasing Re_{in} and near the end, the film thickness increased with increasing Re_{in}. When varying the inlet pressure, the film thickness curves crossed. Near the inlet, the film thickness increases with increasing pressure while further away from the inlet the opposite trend is found; the film thickness increases with decreasing pressure. The local Nusselt number was found to increase with decreasing W_{in}, with decreasing ΔT_{in}, and with increasing Re_{in}. Near the

inlet, the Nusselt number increased with decreasing P_{in} while further along the tube, the Nusselt number increased with P_{in}.

9.2 Recommendations

The following recommendations are made for future work:

1. More research should be done in selecting an appropriate turbulence model for the film. A k-ω model as well as other k-ε models should be employed and compared with the three turbulence models used in this thesis.
2. Empirical correlations should be added to account for a wavy interface. This would also require new interfacial boundary conditions.
3. The present model could be extended to model both horizontal and inclined tubes.

REFERENCES

Akai, M., Inoue, A., and Aoki, S., 1981, "The Prediction of Stratified Two-Phase Flow with a Two-Equation Model of Turbulence", *International Journal of Multiphase Flow*, Vol. 7, pp. 21-39.

Behie, A., Collins, D., Forsyth Jr., P.A., and Sammon, P.H., 1985, "Fully Coupled Multiblock Wells in Oil Simulation", *Society of Petroleum Engineers Journal*, pp. 535-542.

Bellinghausen, R., and Renz, U., 1992, "Heat Transfer and Film Thickness during Condensation of Steam Flowing at High Velocity in a Vertical Pipe", *International Journal of Heat and Mass Transfer*, Vol. 35, No. 3, pp. 683-689.

Boussinesq, 1877, "Theorie de l'Ecoulement Tourbillant", *Mem. Pres. Acad. SciXXIII*, pp. 46.

Chen, S.L., Gerner, F.M., and Tien, C.L., 1987, "General Film Condensation Correlations", *Experimental Heat Transfer*, Vol. 1, pp. 93-107.

Chen, S.L., and Ke, M.T., 1993, "Forced Convective Film Condensation Inside Vertical Tubes", *International Journal of Multiphase Flow*, Vol. 19, No. 6, pp. 1045-1060.

Chin, Y.S., 1995, *Numerical Solution of the Complete Two-Phase Model for Laminar Film Condensation with a Noncondensable Gas*, M.Sc. thesis, University of Manitoba.

Chin, Y.S., Ormiston, S.J., and Soliman, H.M., 1998, "A Two-Phase Boundary-Layer Model for Laminar Mixed-Convection Condensation with a Noncondensable Gas on Inclined Plates", *Heat and Mass Transfer*, Vol. 34, pp. 271-277.

Dehbi, A., and Guentay, S., 1997, "A Model for the Performance of a Vertical Tube Condenser in the Presence of Noncondensable Gases", Nuclear *Engineering and Design*, Vol. 177, pp. 41-52.

Dobran, F., and Thorsen, R.S., 1980, "Forced Flow Laminar Filmwise Condensation of a Pure Saturated Vapor in a Vertical Tube", *International Journal of Heat and Mass Transfer*, Vol. 23, pp. 161-177.

Ghiaasiaan, S.M., Kamboj, B.K., and Abdel-Khalik, S.I., 1995, "Two-Fluid Modeling of Condensation in the Presence of Noncondensables in Two-Phase Channel Flows", *Nuclear Science and Engineering*, Vol. 119, pp. 1-17.

Goodykoontz, J.H., and Dorsch, R.G., 1996, "Local Heat-Transfer Coefficients for Condensation of Steam in Vertical Downflow within a 5/8-Inch-Diameter Tube", NASA Technical Note D-3326.

Groff, M.K., Ormiston, S.J., and Soliman, H.M., 2002, "An Algebraically-Explicit Correlation for Forced-Convection Condensation of Steam-Air and Steam-Hydrogen on Horizontal Plates", *International Communications in Heat and Mass Transfer*, Vol. 29, No. 8, pp. 1047-1056.

Groff, M.K., Ormiston, S.J., and Soliman, H.M., 2004, "Analysis of Laminar Film Condensation from Vapor-Gas Mixtures in Vertical Tubes", *Proceedings of the Third International Symposium on Two-Phase Flow Modelling and Experimentation*, Pisa, Italy, Paper No. MK01.

Hasanein, H.A., Kazimi, M.S., Golay M.W., 1996, "Forced Convection In-Tube Steam Condensation in the Presence of Noncondensable Gases", *International Journal of Heat and Mass Transfer*, Vol. 39, No. 13, pp. 2625-2639.

Hrenya, C.M., Bolio, E.J., Chakrabarti, D.B., and Sinclair, J.L., 1995, "Comparison of Low Reynolds Number k-ε Turbulence Models in Predicting Fully Developed Pipe Flow", *Chemical Engineering Science*, Vol. 50, No. 12, pp. 1923-1941.

Incropera, F.P., and DeWitt, D.P., 1996, *Fundamentals of Heat and Mass Transfer*, Fourth Ed., John Wiley & Sons.

Irvine Jr., T.F., and Liley, P.E., 1984, *Steam and Gas Tables with Computer Equations*, Academic Press.

Issa, R.I., 1988, "Prediction of Turbulent, Stratified, Two-Phase Flow in Inclined Pipes and Channels", *International Journal of Multiphase Flow*, Vol. 14, pp. 401-413.

Jones, W.P., and Launder, B.E., 1972, "The Prediction of Laminarization with a Two-Equation Model of Turbulence", *International Journal of Heat and Mass Transfer*, Vol. 15, pp. 301-314.

Kim, S.J., and No, H.C., 2000, "Turbulent Film Condensation of High Pressure Steam in a Vertical Tube", *International Journal of Heat and Mass Transfer*, Vol. 43, pp. 4031-4042.

Kuhn, S.Z., 1995, *Investigation of Heat Transfer from Condensing Steam-Gas Mixtures and Turbulent Film Flowing Downward Inside a Vertical Tube*, PhD Thesis, University of California at Berkeley.

Kuhn, S.Z., Schrock, V.E., and Peterson, P.F., 1997, "An Investigation of Condensation from Steam-Gas Mixtures Flowing Downward Inside a Vertical Tube", *Nuclear Engineering and Design*, Vol. 177, pp. 53-69.

Newton, C.H., and Behnia, M., 2000, "Numerical Calculation of Turbulent Stratified Gas-Liquid Pipe Flows", *International Journal of Multiphase Flow*, Vol. 26, pp. 327-337.

Nikuradse, J., 1932, Gesetzmassigkeit der Turbulenten Stromung in Glatten Rohren", *VDI, Forschungsheft*, No. 356.

No, H.C., and Park, S.H., 2002, "Non-Iterative Condensation Modeling for Steam Condensation with Non-Condensable Gas in a Vertical Tube", *International Journal of Heat and Mass Transfer*, Vol. 45, pp. 845-854.

Oh, S., and Revankar, S.T., 2005, "Analysis of the Complete Condensation in a Vertical Tube Passive Condenser", *International Communications in Heat and Mass Transfer*, Vol. 32, pp. 716-727.

Oh, S., and Revankar, S.T., 2005, "Complete Condensation in a Vertical Tube Passive Condenser", *International Communications in Heat and Mass Transfer*, Vol. 32, pp. 593-602.

Oh, S., and Revankar, S.T., 2005, "Effect of Noncondensable Gas in a Vertical Tube Condenser", *Nuclear Engineering and Design*, Vol. 235, No. 16, pp. 1699-1712.

Panday, P.K., 2003, "Two-Dimensional Turbulent Film Condensation of Vapours Flowing Inside a Vertical Tube and Between Parallel Plates: A Numerical Approach", *International Journal of Refrigeration*, Vol. 26, pp. 492-503.

Patel, V.C., Rodi, W., and Sheuerer, G., 1984, "Turbulence Models for Near-Wall and Low Reynolds Number Flows: A Review", *American Institute of Aeronautics and Astronautics Journal*, Vol. 23, No. 9, pp. 1308-1319.

Pletcher, R.H., 1974, "Prediction of Transpired Turbulent Boundary Layers", *Transactions of ASME Heat Transfer*, 96C, pp. 89-94.

Pohner, J.A., and Desai, P.V., 1989, "A Two-Fluid Analysis of Filmwise Condensation in Tubes", *International Journal of Engineering Science*, Vol. 27, No. 5, pp. 549-564.

Prandtl, 1926, "Uber Die Ausgebildete Turbulenz", *2nd Proceedings International Congress in Applied Mechanics*, pp. 62-75.

Reid, R.C., Prausnitz, J.M., and Sherwood, T.K., 1977, *The Properties of Gases and Liquids*, Third Ed., McGraw-Hill.

Revankar, S.T., and Pollock, D., 2005, "Laminar Film Condensation in a Vertical Tube in the Presence of Noncondensable Gas", *Applied Mathematical Modelling*, Vol. 29, Issue 4, pp. 341-359.

Rodi, W., 1993, *Turbulence Models and Their Application in Hydraulics – A State of the Art Review*, 3rd Ed, IAHR Monograph Series.

Rose, J.W., 1988, "Fundamentals of Condensation Heat Transfer: A Laminar Film Condensation", *JSME International Journal*, Series II, Vol. 31, No. 3, pp. 357-375.

Schlichting, H., 1968, *Boundary Layer Theory*, 6th Ed., Mcgraw Hill Book Company.

Shaw, M.M., 1979, "A General Correlation for Heat Transfer during Film Condensation Inside Pipes", *International Journal of Heat and Mass Transfer*, Vol. 22, pp. 547-556.

Siddique, M., 1992, *The Effects of Noncondensable Gases on Steam Condensation Under Forced Convection Conditions*, PhD Thesis, Massachusetts Institute of Technology.

Siddique, M., Golay, M.W., and Kazimi, M.S., 1993, "Local Heat Transfer Coefficients for Forced-Convection Condensation of Steam in a Vertical Tube in the Presence of a Noncondensable Gas", *Nuclear Technology*, Vol. 102, pp. 386-402.

Siddique, M., Golay, M.W., and Kazimi, M.S., 1994, "Theoretical Modelling of Forced Convection Condensation of Steam in a Vertical Tube in the Presence of a Non-Condensable Gas", *Nuclear Technology*, Vol. 106, pp. 202-215.

Siow, E.C., 2001, *Numerical Solution of Two-Phase Model for Laminar Film Condensation of Vapour-Gas Mixtures in Channels*, M.Sc. Thesis, University of Manitoba.

Siow, E.C., Ormiston, S.J., and Soliman, H.M., 2002, "Fully Coupled Solution of a Two-Phase Model for Laminar Film Condensation of Vapor-Gas Mixtures in Horizontal Channels", *International Journal of Heat and Mass Transfer*, Vol. 45, pp. 3689-3702.

Srzic, V., 1997, *Modeling of Mixed-Convection Laminar Film Condensation from Mixtures of a Vapor and a Lighter Non-Condensable Gas*, M.Sc. Thesis, University of Manitoba.

Srzic, V., Soliman, H.M., and Ormiston, S.J., 1999, "Analysis of Laminar Mixed-Convection Condensation on Isothermal Plates using the Full Boundary-Layer Equations: Mixtures of a Vapor and a Lighter Gas", *International Journal of Heat and Mass Transfer*, Vol. 31, pp. 685-695.

Thakre, S.S., and Joshi, J.B., 2000, "CFD Modeling of Heat Transfer in Turbulent Pipe Flows", *AIChE Journal*, Vol. 46, No. 9, pp. 1798-1812.

Vierow, K.M., 1990, *Behaviour of Steam-Air Systems Condensing in Concurrent Vertical Downflow*, M.Sc. Thesis, University of California at Berkeley.

Wang, C.Y., and Tu, C.J., 1988, "Effects of Non-Condensable Gas on Laminar Film Condensation in a Vertical Tube", *International Journal of Heat and Mass Transfer*, Vol. 31, No. 11, pp. 2339-2345.

Wilcox, D.C., 2002, *Turbulence Modeling for CFD*, 2nd Ed., DCW Industries.

Yuann, R.Y., 1993, *Condensation from Vapor-Gas Mixtures for Forced Downflow Inside a Tube*, PhD Thesis, University of California at Berkeley.

Yuann, Schrock, and Chen, 1995, "Numerical Modeling of Condensation from Vapor-Gas Mixtures for Forced Down Flow inside a Tube", *NURETH*, Vol. 7, pp. 377-401.

APPENDIX A

Transformation of Governing Equations, k-ε Model and Boundary Conditions

A.1 Coordinate Transformation

Given the transformation equations:

$$z = \chi \qquad \text{for } z \geq 0 \tag{A.1}$$

$$r = \delta(\eta - 2) + r_o \qquad \text{for } (r_o - \delta) \leq r \leq r_o \tag{A.2}$$

$$r = \eta(r_o - \delta) \qquad \text{for } 0 \leq r \leq (r_o - \delta) \tag{A.3}$$

In derivative form:

$$\partial\chi = \partial z \qquad \text{for } z \geq 0 \tag{A.4}$$

$$\partial r = \delta\partial\eta \qquad \text{for } (r_o - \delta) \leq r \leq r_o \tag{A.5}$$

$$\partial r = (r_o - \delta)\partial\eta \qquad \text{for } 0 \leq r \leq (r_o - \delta) \tag{A.6}$$

If $\phi = \{u_L, v_L, T_L, u_M, v_M, T_M, W\}$ it's partial derivatives are transformed as:

$$\frac{\partial\phi}{\partial z} = \frac{\partial\phi}{\partial\chi}\frac{\partial\chi}{\partial z} + \frac{\partial\phi}{\partial\eta}\frac{\partial\eta}{\partial\delta}\frac{\partial\delta}{\partial z}$$

$$= \frac{\partial\phi}{\partial\chi} + \frac{\partial\phi}{\partial\eta}\frac{\partial}{\partial\delta}\left(2 - \frac{(r_o - r)}{\delta}\right)\frac{\partial\delta}{\partial\chi}$$

$$= \frac{\partial\phi}{\partial\chi} + \frac{(r_o - r)}{\delta^2}\frac{\partial\phi}{\partial\eta}\frac{\partial\delta}{\partial\chi}$$

$$= \frac{\partial\phi}{\partial\chi} - \frac{(\eta - 2)}{\delta}\frac{\partial\phi}{\partial\eta}\frac{\partial\delta}{\partial\chi}, \qquad \text{for } z \geq 0 \text{ and } (r_o - \delta) \leq r \leq r_o \tag{A.7}$$

$$\frac{\partial \phi}{\partial r} = \frac{\partial \phi}{\partial \eta}\frac{\partial \eta}{\partial r}$$

$$= \frac{\partial \phi}{\partial \eta}\frac{\partial}{\partial r}\left(2 - \frac{(r_o - r)}{\delta}\right)$$

$$= \frac{1}{\delta}\frac{\partial \phi}{\partial \eta}, \qquad \text{for } z \geq 0 \text{ and } (r_o - \delta) \leq r \leq r_o \qquad \text{(A.8)}$$

$$\frac{\partial \phi}{\partial z} = \frac{\partial \phi}{\partial \chi}\frac{\partial \chi}{\partial z} + \frac{\partial \phi}{\partial \eta}\frac{\partial \eta}{\partial \delta}\frac{\partial \delta}{\partial z}$$

$$= \frac{\partial \phi}{\partial \chi} + \frac{\partial \phi}{\partial \eta}\frac{\partial}{\partial \delta}\left(\frac{r}{r_o - \delta}\right)\frac{\partial \delta}{\partial \chi}$$

$$= \frac{\partial \phi}{\partial \chi} + \frac{r}{(r_o - \delta)^2}\frac{\partial \phi}{\partial \eta}\frac{\partial \delta}{\partial \chi}$$

$$= \frac{\partial \phi}{\partial \chi} + \frac{\eta}{(r_o - \delta)}\frac{\partial \phi}{\partial \eta}\frac{d\delta}{d\chi}, \qquad \text{for } z \geq 0 \text{ and } 0 \leq r \leq (r_o - \delta) \qquad \text{(A.9)}$$

$$\frac{\partial \phi}{\partial r} = \frac{\partial \phi}{\partial \eta}\frac{\partial \eta}{\partial r}$$

$$= \frac{\partial \phi}{\partial \eta}\frac{\partial}{\partial r}\left(\frac{r}{r_o - \delta}\right)$$

$$= \frac{1}{r_o - \delta}\frac{\partial \phi}{\partial \eta}, \qquad \text{for } z \geq 0 \text{ and } 0 \leq r \leq (r_o - \delta) \qquad \text{(A.10)}$$

A.2 Normal Mass Flux

Referring to Figure B.1:

$$z_w = \chi_w$$
$$z_e = \chi_e \qquad \text{(A.11)}$$

$$\left.\begin{aligned} r_{w,n} &= \delta_w(\eta_n - 2) + r_o \\ r_{e,n} &= \delta_e(\eta_n - 2) + r_o \end{aligned}\right\} \qquad \text{for } (r_o - \delta) \le r \le r_o \qquad \text{(A.12)}$$

$$\left.\begin{aligned} r_{w,n} &= \eta_n(r_o - \delta_w) \\ r_{e,n} &= \eta_n(r_o - \delta_e) \end{aligned}\right\} \qquad \text{for } 0 \le r \le (r_o - \delta) \qquad \text{(A.13)}$$

In the liquid region, the mass flow rate normal to the north face is:

$$\dot{m}_{L,n} = \left[\rho_{L,n} v_{L,n}(z_e - z_w) + \rho_{L,n} u_{L,n}(r_{w,n} - r_{e,n})\right] 2\pi r_n$$

$$\frac{\dot{m}_{L,n}}{(2\pi r_n \Delta\chi)} = \rho_{L,n} v_{L,n} - \rho_{L,n} u_{L,n}(\eta_n - 2)\frac{(\delta_e - \delta_w)}{\Delta\chi} \qquad \text{for } (r_o - \delta) \le r \le r_o \qquad \text{(A.14)}$$

Similarly, in the mixture region:

$$\dot{m}_{M,n} = \left[\rho_{M,n} v_{M,n}(z_e - z_w) + \rho_{M,n} u_{M,n}(r_{w,n} - r_{e,n})\right] 2\pi r_n$$

$$\frac{\dot{m}_{M,n}}{(2\pi r_n \Delta\chi)} = \rho_{M,n} v_{M,n} + \rho_{M,n} u_{M,n} \eta_n \frac{(\delta_e - \delta_w)}{\Delta\chi} \qquad \text{for } 0 \le r \le (r_o - \delta) \qquad \text{(A.15)}$$

Define the variable, J'', normal mass flux:

$$J''_L = \rho_L v_L - \rho_L u_L(\eta - 2)\frac{d\delta}{d\chi} \qquad \text{for } (r_o - \delta) \le r \le r_o \qquad \text{(A.16)}$$

$$J''_M = \rho_M v_M + \rho_M u_M \eta_M \frac{d\delta}{d\chi} \qquad \text{for } 0 \le r \le (r_o - \delta) \qquad \text{(A.17)}$$

A.3 Governing Equation Transformation

Liquid Continuity Equation

$$\frac{\partial}{\partial z}(\rho_L u_L) + \frac{1}{r}\frac{\partial}{\partial r}(r\rho_L v_L) = 0 \qquad \text{(A.18)}$$

$$\frac{1}{r}\frac{\partial}{\partial z}(r\rho_L u_L)+\frac{1}{r}\frac{\partial}{\partial r}(r\rho_L v_L)=0 \tag{A.19}$$

$$\frac{1}{r}\frac{\partial}{\partial \chi}(r\rho_L u_L)-\frac{(\eta-2)}{r\delta}\frac{\partial}{\partial \eta}(r\rho_L u_L)\frac{d\delta}{d\chi}+\frac{1}{r\delta}\frac{\partial}{\partial \eta}(r\rho_L v_L)=0 \tag{A.20}$$

The second term of (A.20) can be written as:

$$-\frac{(\eta-2)}{r\delta}\frac{\partial}{\partial \eta}(r\rho_L u_L)\frac{d\delta}{d\chi}=-\frac{1}{r\delta}\frac{\partial}{\partial \eta}\left(r\rho_L u_L(\eta-2)\frac{d\delta}{d\chi}\right)+\frac{\rho_L u_L}{\delta}\frac{d\delta}{d\chi} \tag{A.21}$$

Substituting (A.21) into (A.20) and rearranging gives the following:

$$\frac{1}{r}\frac{\partial}{\partial \chi}(r\rho_L u_L)-\frac{1}{r\delta}\frac{\partial}{\partial \eta}\left(r\rho_L u_L(\eta-2)\frac{d\delta}{d\chi}\right)+\frac{\rho_L u_L}{\delta}\frac{d\delta}{d\chi}+\frac{1}{r\delta}\frac{\partial}{\partial \eta}(r\rho_L v_L)=0 \tag{A.22}$$

Term 1 of equation (A.22) can be re-written as:

$$\frac{1}{r\delta}\frac{\partial}{\partial \chi}(r\delta\rho_L u_L)=\frac{1}{r}\frac{\partial}{\partial \chi}(r\rho_L u_L)+\frac{\rho_L u_L}{\delta}\frac{d\delta}{d\chi} \tag{A.23}$$

Substitute the above equation into (A.22) to get:

$$\frac{1}{r\delta}\frac{\partial}{\partial \chi}(r\delta\rho_L u_L)+\frac{1}{r\delta}\frac{\partial}{\partial \eta}(r\rho_L v_L)-\frac{1}{r\delta}\frac{\partial}{\partial \eta}((\eta-2)r\rho_L u_L)\frac{d\delta}{d\chi}=0 \tag{A.24}$$

Note that:

$$\frac{1}{r\delta}\frac{\partial}{\partial \eta}(rJ_L'')=\frac{1}{r\delta}\frac{\partial}{\partial \eta}(r\rho_L v_L)-\frac{1}{r\delta}\frac{\partial}{\partial \eta}((\eta-2)r\rho_L u_L)\frac{d\delta}{d\chi} \tag{A.25}$$

Substituting the above into equation (A.24) results in:

$$\frac{1}{r\delta}\frac{\partial}{\partial\chi}\left(r\delta\rho_L u_L\right)+\frac{1}{r\delta}\frac{\partial}{\partial\eta}\left(rJ_L''\right)=0 \tag{A.26}$$

Liquid Momentum Equation

$$\frac{\partial}{\partial z}\left(\rho_L u_L u_L\right)+\frac{1}{r}\frac{\partial}{\partial r}\left(r\rho_L u_L v_L\right)=\frac{1}{r}\frac{\partial}{\partial r}\left(r\mu_{L,\text{eff}}\frac{\partial u_L}{\partial r}\right)+\rho_L g-\frac{dP}{dz} \tag{A.27}$$

$$\frac{1}{r}\frac{\partial}{\partial z}\left(r\rho_L u_L u_L\right)+\frac{1}{r}\frac{\partial}{\partial r}\left(r\rho_L u_L v_L\right)=\frac{1}{r}\frac{\partial}{\partial r}\left(r\mu_{L,\text{eff}}\frac{\partial u_L}{\partial r}\right)+\rho_L g-\frac{dP}{dz} \tag{A.28}$$

$$\begin{aligned}\frac{1}{r}\frac{\partial}{\partial\chi}\left(r\rho_L u_L u_L\right)-\frac{(\eta-2)}{r\delta}\frac{d\delta}{d\chi}\frac{\partial}{\partial\eta}\left(r\rho_L u_L u_L\right)+\frac{1}{r\delta}\frac{\partial}{\partial\eta}\left(r\rho_L u_L v_L\right)\\ =\frac{1}{r\delta}\frac{\partial}{\partial\eta}\left(\frac{r\mu_{L,\text{eff}}}{\delta}\frac{\partial u_L}{\partial\eta}\right)+\rho_L g-\frac{dP}{d\chi}\end{aligned} \tag{A.29}$$

The second term of (A.29) can be written as:

$$-\frac{(\eta-2)}{r\delta}\frac{d\delta}{d\chi}\frac{\partial}{\partial\eta}\left(r\rho_L u_L u_L\right)=-\frac{1}{r\delta}\frac{\partial}{\partial\eta}\left(r\rho_L u_L u_L(\eta-2)\frac{d\delta}{d\chi}\right)+\frac{\rho_L u_L u_L}{\delta}\frac{d\delta}{d\chi} \tag{A.30}$$

Substituting the above equation into (A.29) gives:

$$\begin{aligned}\frac{1}{r}\frac{\partial}{\partial\chi}\left(r\rho_L u_L u_L\right)-\frac{1}{r\delta}\frac{\partial}{\partial\eta}\left(r\rho_L u_L u_L(\eta-2)\frac{d\delta}{d\chi}\right)+\frac{\rho_L u_L u_L}{\delta}\frac{d\delta}{d\chi}+\frac{1}{r\delta}\frac{\partial}{\partial\eta}\left(r\rho_L u_L v_L\right)\\ =\frac{1}{r\delta}\frac{\partial}{\partial\eta}\left(\frac{r\mu_{L,\text{eff}}}{\delta}\frac{\partial u_L}{\partial\eta}\right)+\rho_L g-\frac{dP}{d\chi}\end{aligned} \tag{A.31}$$

Term 1 in the above equation can be re-written as:

$$\frac{1}{r\delta}\frac{\partial}{\partial\chi}\left(r\delta\rho_L u_L u_L\right)=\frac{1}{r}\frac{\partial}{\partial\chi}\left(r\rho_L u_L u_L\right)+\frac{\rho_L u_L u_L}{\delta}\frac{d\delta}{d\chi} \tag{A.32}$$

Substituting into equation (A.31) gives:

$$\frac{1}{r\delta}\frac{\partial}{\partial\chi}\left(r\delta\rho_{\mathrm{L}}u_{\mathrm{L}}u_{\mathrm{L}}\right)-\frac{1}{r\delta}\frac{\partial}{\partial\eta}\left(r\rho_{\mathrm{L}}u_{\mathrm{L}}u_{\mathrm{L}}(\eta-2)\frac{d\delta}{d\chi}\right)+\frac{1}{r\delta}\frac{\partial}{\partial\eta}\left(r\rho_{\mathrm{L}}u_{\mathrm{L}}v_{\mathrm{L}}\right)$$
$$=\frac{1}{r\delta}\frac{\partial}{\partial\eta}\left(\frac{r\mu_{\mathrm{L,eff}}}{\delta}\frac{\partial u_{\mathrm{L}}}{\partial\eta}\right)+\rho_{\mathrm{L}}g-\frac{dP}{d\chi} \tag{A.33}$$

Note that:

$$\frac{1}{r\delta}\frac{\partial}{\partial\eta}\left(rJ_{\mathrm{L}}''u_{L}\right)=\frac{1}{r\delta}\frac{\partial}{\partial\eta}\left(r\rho_{\mathrm{L}}u_{\mathrm{L}}v_{\mathrm{L}}\right)-\frac{1}{r\delta}\frac{\partial}{\partial\eta}\left((\eta-2)r\rho_{\mathrm{L}}u_{\mathrm{L}}u_{\mathrm{L}}\right)\frac{d\delta}{d\chi} \tag{A.34}$$

Substituting into equation (A.33) results in:

$$\frac{1}{r\delta}\frac{\partial}{\partial\chi}\left(r\delta\rho_{\mathrm{L}}u_{\mathrm{L}}u_{\mathrm{L}}\right)+\frac{1}{r\delta}\frac{\partial}{\partial\eta}\left(rJ_{\mathrm{L}}''u_{\mathrm{L}}\right)=\frac{1}{r\delta}\frac{\partial}{\partial\eta}\left(\frac{r\mu_{\mathrm{L,eff}}}{\delta}\frac{\partial u_{\mathrm{L}}}{\partial\eta}\right)+\rho_{\mathrm{L}}g-\frac{dP}{d\chi} \tag{A.35}$$

Liquid Energy Equation

$$\frac{\partial}{\partial z}\left(\rho_{\mathrm{L}}u_{\mathrm{L}}C_{P,\mathrm{L}}T_{\mathrm{L}}\right)+\frac{1}{r}\frac{\partial}{\partial r}\left(r\rho_{\mathrm{L}}v_{\mathrm{L}}C_{P,\mathrm{L}}T_{\mathrm{L}}\right)=\frac{1}{r}\frac{\partial}{\partial r}\left(r\lambda_{\mathrm{L,eff}}\frac{\partial T_{\mathrm{L}}}{\partial r}\right) \tag{B.36}$$

$$\frac{1}{r}\frac{\partial}{\partial z}\left(r\rho_{\mathrm{L}}u_{\mathrm{L}}C_{P,\mathrm{L}}T_{\mathrm{L}}\right)+\frac{1}{r}\frac{\partial}{\partial r}\left(r\rho_{\mathrm{L}}v_{\mathrm{L}}C_{P,\mathrm{L}}T_{\mathrm{L}}\right)=\frac{1}{r}\frac{\partial}{\partial r}\left(r\lambda_{\mathrm{L,eff}}\frac{\partial T_{\mathrm{L}}}{\partial r}\right) \tag{A.37}$$

$$\frac{1}{r}\frac{\partial}{\partial\chi}\left(r\rho_{\mathrm{L}}u_{\mathrm{L}}C_{P,\mathrm{L}}T_{\mathrm{L}}\right)-\frac{(\eta-2)}{r\delta}\frac{d\delta}{d\chi}\frac{\partial}{\partial\eta}\left(r\rho_{\mathrm{L}}u_{\mathrm{L}}C_{P,\mathrm{L}}T_{\mathrm{L}}\right)$$
$$+\frac{1}{r\delta}\frac{\partial}{\partial\eta}\left(r\rho_{\mathrm{L}}v_{\mathrm{L}}C_{P,\mathrm{L}}T_{\mathrm{L}}\right)=\frac{1}{r\delta}\frac{\partial}{\partial\eta}\left(\frac{r\lambda_{\mathrm{L,eff}}}{\delta}\frac{\partial T_{\mathrm{L}}}{\partial\eta}\right) \tag{A.38}$$

The second term of (A.38) can be written as:

$$-\frac{(\eta-2)}{r\delta}\frac{d\delta}{d\chi}\frac{\partial}{\partial\eta}\left(r\rho_{\mathrm{L}}u_{\mathrm{L}}C_{P,\mathrm{L}}T_{\mathrm{L}}\right)=-\frac{1}{r\delta}\frac{\partial}{\partial\eta}\left(r\rho_{\mathrm{L}}u_{\mathrm{L}}C_{P,\mathrm{L}}T_{\mathrm{L}}(\eta-2)\frac{d\delta}{d\chi}\right)+\frac{\rho_{\mathrm{L}}u_{\mathrm{L}}C_{P,\mathrm{L}}T_{\mathrm{L}}}{\delta}\frac{d\delta}{d\chi} \tag{A.39}$$

Substituting the above equation into (A.38) gives:

$$\frac{1}{r}\frac{\partial}{\partial\chi}\left(r\rho_{\mathrm{L}}u_{\mathrm{L}}C_{P,\mathrm{L}}T_{\mathrm{L}}\right)-\frac{1}{r\delta}\frac{\partial}{\partial\eta}\left(r\rho_{L}u_{\mathrm{L}}C_{P,\mathrm{L}}T_{\mathrm{L}}(\eta-2)\frac{d\delta}{d\chi}\right)+\frac{\rho_{\mathrm{L}}u_{\mathrm{L}}C_{P,\mathrm{L}}T_{\mathrm{L}}}{\delta}\frac{d\delta}{d\chi}+\frac{1}{r\delta}\frac{\partial}{\partial\eta}\left(r\rho_{\mathrm{L}}v_{\mathrm{L}}C_{P,\mathrm{L}}T_{\mathrm{L}}\right)=\frac{1}{r\delta}\frac{\partial}{\partial\eta}\left(\frac{r\lambda_{\mathrm{L,eff}}}{\delta}\frac{\partial T_{\mathrm{L}}}{\partial\eta}\right) \tag{A.40}$$

Term 1 in the above equation can be re-written as:

$$\frac{1}{r\delta}\frac{\partial}{\partial\chi}\left(r\delta\rho_{\mathrm{L}}u_{\mathrm{L}}C_{P,\mathrm{L}}T_{\mathrm{L}}\right)=\frac{1}{r}\frac{\partial}{\partial\chi}\left(r\rho_{\mathrm{L}}u_{\mathrm{L}}C_{P,\mathrm{L}}T_{\mathrm{L}}\right)+\frac{\rho_{\mathrm{L}}u_{\mathrm{L}}C_{P,\mathrm{L}}T_{\mathrm{L}}}{\delta}\frac{d\delta}{d\chi} \tag{A.41}$$

Substituting into equation (A.40) gives:

$$\frac{1}{r\delta}\frac{\partial}{\partial\chi}\left(r\delta\rho_{\mathrm{L}}u_{\mathrm{L}}C_{P,\mathrm{L}}T_{\mathrm{L}}\right)-\frac{1}{r\delta}\frac{\partial}{\partial\eta}\left(r\rho_{\mathrm{L}}u_{\mathrm{L}}C_{P,\mathrm{L}}T_{\mathrm{L}}(\eta-2)\frac{d\delta}{d\chi}\right)+\frac{1}{r\delta}\frac{\partial}{\partial\eta}\left(r\rho_{\mathrm{L}}v_{\mathrm{L}}C_{P,\mathrm{L}}T_{\mathrm{L}}\right)=\frac{1}{r\delta}\frac{\partial}{\partial\eta}\left(\frac{r\lambda_{\mathrm{L,eff}}}{\delta}\frac{\partial T_{\mathrm{L}}}{\partial\eta}\right) \tag{A.42}$$

Note that:

$$\frac{1}{r\delta}\frac{\partial}{\partial\eta}\left(rJ''_{\mathrm{L}}C_{P,\mathrm{L}}T_{\mathrm{L}}\right)=\frac{1}{r\delta}\frac{\partial}{\partial\eta}\left(r\rho_{\mathrm{L}}v_{\mathrm{L}}C_{P,\mathrm{L}}T_{\mathrm{L}}\right)-\frac{1}{r\delta}\frac{\partial}{\partial\eta}\left((\eta-2)r\rho_{\mathrm{L}}u_{\mathrm{L}}C_{P,\mathrm{L}}T_{\mathrm{L}}\right)\frac{d\delta}{d\chi} \tag{A.43}$$

Substituting into equation (A.42) results in:

$$\frac{1}{r\delta}\frac{\partial}{\partial\chi}\left(r\delta\rho_{\mathrm{L}}u_{\mathrm{L}}C_{P,\mathrm{L}}T_{\mathrm{L}}\right)+\frac{1}{r\delta}\frac{\partial}{\partial\eta}\left(rJ''_{\mathrm{L}}C_{P,\mathrm{L}}T_{\mathrm{L}}\right)=\frac{1}{r\delta}\frac{\partial}{\partial\eta}\left(\frac{r\lambda_{\mathrm{L,eff}}}{\delta}\frac{\partial T_{\mathrm{L}}}{\partial\eta}\right) \tag{A.44}$$

Mixture Continuity Equation

$$\frac{\partial}{\partial z}\left(\rho_{\mathrm{M}}u_{\mathrm{M}}\right)+\frac{1}{r}\frac{\partial}{\partial r}\left(r\rho_{\mathrm{M}}v_{\mathrm{M}}\right)=0 \tag{A.45}$$

$$\frac{1}{r}\frac{\partial}{\partial z}\left(r\rho_{\mathrm{M}}u_{\mathrm{M}}\right)+\frac{1}{r}\frac{\partial}{\partial r}\left(r\rho_{\mathrm{M}}v_{\mathrm{M}}\right)=0 \tag{A.46}$$

$$\frac{1}{r}\frac{\partial}{\partial\chi}\left(r\rho_{\mathrm{M}}u_{\mathrm{M}}\right)+\frac{\eta}{r\left(r_{\mathrm{o}}-\delta\right)}\frac{\partial}{\partial\eta}\left(r\rho_{\mathrm{M}}u_{\mathrm{M}}\right)\frac{d\delta}{d\chi}+\frac{1}{r\left(r_{\mathrm{o}}-\delta\right)}\frac{\partial}{\partial\eta}\left(r\rho_{\mathrm{M}}v_{\mathrm{M}}\right)=0 \tag{A.47}$$

The second term of (A.47) can be written as:

$$\frac{\eta}{r\left(r_{\mathrm{o}}-\delta\right)}\frac{\partial}{\partial\eta}\left(r\rho_{\mathrm{M}}u_{\mathrm{M}}\right)\frac{d\delta}{d\chi}=\frac{1}{r\left(r_{\mathrm{o}}-\delta\right)}\frac{\partial}{\partial\eta}\left(r\rho_{\mathrm{M}}u_{\mathrm{M}}\eta\frac{d\delta}{d\chi}\right)-\frac{\rho_{\mathrm{M}}u_{\mathrm{M}}}{\left(r_{\mathrm{o}}-\delta\right)}\frac{d\delta}{d\chi} \tag{A.48}$$

Substituting (A.48) into (A.47) and rearranging gives the following:

$$\frac{1}{r}\frac{\partial}{\partial\chi}\left(r\rho_{\mathrm{M}}u_{\mathrm{M}}\right)+\frac{1}{r\left(r_{\mathrm{o}}-\delta\right)}\frac{\partial}{\partial\eta}\left(r\rho_{\mathrm{M}}u_{\mathrm{M}}\eta\frac{d\delta}{d\chi}\right)-\frac{\rho_{\mathrm{M}}u_{\mathrm{M}}}{\left(r_{\mathrm{o}}-\delta\right)}\frac{d\delta}{d\chi}+\frac{1}{r\left(r_{\mathrm{o}}-\delta\right)}\frac{\partial}{\partial\eta}\left(r\rho_{\mathrm{M}}v_{\mathrm{M}}\right)=0 \tag{A.49}$$

Term 1 of equation (A.49) can be re-written as:

$$\frac{1}{r\left(r_{\mathrm{o}}-\delta\right)}\frac{\partial}{\partial\chi}\left(r\left(r_{\mathrm{o}}-\delta\right)\rho_{\mathrm{M}}u_{\mathrm{M}}\right)=\frac{1}{r}\frac{\partial}{\partial\chi}\left(r\rho_{\mathrm{M}}u_{\mathrm{M}}\right)-\frac{\rho_{\mathrm{M}}u_{\mathrm{M}}}{\left(r_{\mathrm{o}}-\delta\right)}\frac{d\delta}{d\chi} \tag{A.50}$$

Substitute the above equation into (A.49) to get:

$$\frac{1}{r(r_o-\delta)}\frac{\partial}{\partial\chi}\left(r(r_o-\delta)\rho_M u_M\right)+\frac{1}{r(r_o-\delta)}\frac{\partial}{\partial\eta}\left(r\rho_M v_M\right)+\frac{1}{r(r_o-\delta)}\frac{\partial}{\partial\eta}\left(r\rho_M u_M\eta\right)\frac{d\delta}{d\chi}=0 \tag{A.51}$$

Note that:

$$\frac{1}{r(r_o-\delta)}\frac{\partial}{\partial\eta}\left(rJ''_M\right)=\frac{1}{r(r_o-\delta)}\frac{\partial}{\partial\eta}\left(r\rho_M v_M\right)+\frac{1}{r(r_o-\delta)}\frac{\partial}{\partial\eta}\left(r\rho_M u_M\eta\right)\frac{d\delta}{d\chi} \tag{A.52}$$

Substituting the above into equation (A.51) results in:

$$\frac{1}{r(r_o-\delta)}\frac{\partial}{\partial\chi}\left(r(r_o-\delta)\rho_M u_M\right)+\frac{1}{r(r_o-\delta)}\frac{\partial}{\partial\eta}\left(rJ''_M\right)=0 \tag{A.53}$$

Mixture Momentum Equation

$$\frac{\partial}{\partial z}\left(\rho_M u_M u_M\right)+\frac{1}{r}\frac{\partial}{\partial r}\left(r\rho_M u_M v_M\right)=\frac{1}{r}\frac{\partial}{\partial r}\left(r\mu_{M,\text{eff}}\frac{\partial u_M}{\partial r}\right)+\rho_M g-\frac{dP}{dz} \tag{A.54}$$

$$\frac{1}{r}\frac{\partial}{\partial z}\left(r\rho_M u_M u_M\right)+\frac{1}{r}\frac{\partial}{\partial r}\left(r\rho_M u_M v_M\right)=\frac{1}{r}\frac{\partial}{\partial r}\left(r\mu_{M,\text{eff}}\frac{\partial u_M}{\partial r}\right)+\rho_M g-\frac{dP}{dz} \tag{A.55}$$

$$\frac{1}{r}\frac{\partial}{\partial\chi}\left(r\rho_M u_M u_M\right)+\frac{\eta}{r(r_o-\delta)}\frac{d\delta}{d\chi}\frac{\partial}{\partial\eta}\left(r\rho_M u_M u_M\right)+\frac{1}{r(r_o-\delta)}\frac{\partial}{\partial\eta}\left(r\rho_M u_M v_M\right)=\frac{1}{r(r_o-\delta)}\frac{\partial}{\partial\eta}\left(\frac{r\mu_{M,\text{eff}}}{(r_o-\delta)}\frac{\partial u_M}{\partial\eta}\right)+\rho_M g-\frac{dP}{d\chi} \tag{A.56}$$

The second term of (A.56) can be written as:

$$\frac{\eta}{r(r_o-\delta)}\frac{d\delta}{d\chi}\frac{\partial}{\partial\eta}(r\rho_M u_M u_M)=\frac{1}{r(r_o-\delta)}\frac{\partial}{\partial\eta}\left(r\rho_M u_M u_M\eta\frac{d\delta}{d\chi}\right) - \frac{\rho_M u_M u_M}{(r_o-\delta)}\frac{d\delta}{d\chi} \tag{A.57}$$

Substituting the above equation into (A.56) gives:

$$\frac{1}{r}\frac{\partial}{\partial\chi}(r\rho_M u_M u_M)+\frac{1}{r(r_o-\delta)}\frac{\partial}{\partial\eta}\left(r\rho_M u_M u_M\eta\frac{d\delta}{d\chi}\right)-\frac{\rho_M u_M u_M}{(r_o-\delta)}\frac{d\delta}{d\chi}+ \frac{1}{r(r_o-\delta)}\frac{\partial}{\partial\eta}(r\rho_M u_M v_M)=\frac{1}{r(r_o-\delta)}\frac{\partial}{\partial\eta}\left(\frac{r\mu_{M,eff}}{(r_o-\delta)}\frac{\partial u_M}{\partial\eta}\right)+\rho_M g-\frac{dP}{d\chi} \tag{A.58}$$

Term 1 in the above equation can be re-written as:

$$\frac{1}{r(r_o-\delta)}\frac{\partial}{\partial\chi}(r(r_o-\delta)\rho_M u_M u_M)=\frac{1}{r}\frac{\partial}{\partial\chi}(r\rho_M u_M u_M)-\frac{\rho_M u_M u_M}{(r_o-\delta)}\frac{d\delta}{d\chi} \tag{A.59}$$

Substituting into equation (A.58) gives:

$$\frac{1}{r(r_o-\delta)}\frac{\partial}{\partial\chi}(r(r_o-\delta)\rho_M u_M u_M)+\frac{1}{r(r_o-\delta)}\frac{\partial}{\partial\eta}\left(r\rho_M u_M u_M\eta\frac{d\delta}{d\chi}\right)+ \frac{1}{r(r_o-\delta)}\frac{\partial}{\partial\eta}(r\rho_M u_M v_M)=\frac{1}{r(r_o-\delta)}\frac{\partial}{\partial\eta}\left(\frac{r\mu_{M,eff}}{(r_o-\delta)}\frac{\partial u_M}{\partial\eta}\right)+\rho_M g-\frac{dP}{d\chi} \tag{A.60}$$

Note that:

$$\frac{1}{r(r_o-\delta)}\frac{\partial}{\partial\eta}(rJ''_M u_M)=\frac{1}{r(r_o-\delta)}\frac{\partial}{\partial\eta}(r\rho_M u_M v_M)+ \frac{1}{r(r_o-\delta)}\frac{\partial}{\partial\eta}(r\rho_M u_M u_M\eta)\frac{d\delta}{d\chi} \tag{A.61}$$

Substituting into equation (A.60) results in:

$$\frac{1}{r(r_o-\delta)}\frac{\partial}{\partial\chi}\left(r(r_o-\delta)\rho_M u_M u_M\right)+\frac{1}{r(r_o-\delta)}\frac{\partial}{\partial\eta}\left(rJ''_M u_M\right)$$
$$=\frac{1}{r(r_o-\delta)}\frac{\partial}{\partial\eta}\left(\frac{r\mu_{M,eff}}{(r_o-\delta)}\frac{\partial u_M}{\partial\eta}\right)+\rho_M g-\frac{dP}{d\chi} \qquad (A.62)$$

Mixture Energy Equation

$$\frac{\partial}{\partial z}\left(\rho_M u_M C_{P,M} T_M\right)+\frac{1}{r}\frac{\partial}{\partial r}\left(r\rho_M v_M C_{P,M} T_M\right)=\frac{1}{r}\frac{\partial}{\partial r}\left(r\lambda_{M,eff}\frac{\partial T_M}{\partial r}\right)$$
$$+\frac{1}{r}\frac{\partial}{\partial r}\left(\rho_M r D_{eff}\left(C_{P,g}-C_{P,v}\right)\frac{\partial W}{\partial r}T_M\right) \qquad (A.63)$$

$$\frac{1}{r}\frac{\partial}{\partial z}\left(r\rho_M u_M C_{P,M} T_M\right)+\frac{1}{r}\frac{\partial}{\partial r}\left(r\rho_M v_M C_{P,M} T_M\right)=\frac{1}{r}\frac{\partial}{\partial r}\left(r\lambda_{M,eff}\frac{\partial T_M}{\partial r}\right)$$
$$+\frac{1}{r}\frac{\partial}{\partial r}\left(\rho_M r D_{eff}\left(C_{P,g}-C_{P,v}\right)\frac{\partial W}{\partial r}T_M\right) \qquad (A.64)$$

$$\frac{1}{r}\frac{\partial}{\partial\chi}\left(r\rho_M u_M C_{P,M} T_M\right)+\frac{\eta}{r(r_o-\delta)}\frac{d\delta}{d\chi}\frac{\partial}{\partial\eta}\left(r\rho_M u_M C_{P,M} T_M\right)+$$
$$\frac{1}{r(r_o-\delta)}\frac{\partial}{\partial\eta}\left(r\rho_M v_M C_{P,M} T_M\right)=\frac{1}{r(r_o-\delta)}\frac{\partial}{\partial\eta}\left(\frac{r\lambda_{M,eff}}{(r_o-\delta)}\frac{\partial T_M}{\partial\eta}\right) \qquad (A.65)$$
$$+\frac{1}{r(r_o-\delta)}\frac{\partial}{\partial\eta}\left(\frac{\rho_M r D_{eff}\left(C_{P,g}-C_{P,v}\right)}{(r_o-\delta)}\frac{\partial W}{\partial\eta}T_M\right)$$

The second term of (A.65) can be written as:

$$\frac{\eta}{r(r_o-\delta)}\frac{d\delta}{d\chi}\frac{\partial}{\partial\eta}\left(r\rho_M u_M C_{P,M} T_M\right)=$$
$$\frac{1}{r(r_o-\delta)}\frac{\partial}{\partial\eta}\left(r\rho_M u_M C_{P,M} T_M\eta\frac{d\delta}{d\chi}\right)-\frac{\rho_M u_M C_{P,M} T_M}{(r_o-\delta)}\frac{d\delta}{d\chi} \qquad (A.66)$$

Substituting the above equation into (A.65) gives:

$$\frac{1}{r}\frac{\partial}{\partial\chi}\left(r\rho_{\mathrm{M}}u_{\mathrm{M}}C_{P,\mathrm{M}}T_{\mathrm{M}}\right)+\frac{1}{r(r_{\mathrm{o}}-\delta)}\frac{\partial}{\partial\eta}\left(r\rho_{\mathrm{M}}u_{\mathrm{M}}C_{P,\mathrm{M}}T_{\mathrm{M}}\eta\frac{d\delta}{d\chi}\right)-\frac{\rho_{\mathrm{M}}u_{\mathrm{M}}C_{P,\mathrm{M}}T_{\mathrm{M}}}{(r_{\mathrm{o}}-\delta)}\frac{d\delta}{d\chi}$$
$$\frac{1}{r(r_{\mathrm{o}}-\delta)}\frac{\partial}{\partial\eta}\left(r\rho_{\mathrm{M}}v_{\mathrm{M}}C_{P,\mathrm{M}}T_{\mathrm{M}}\right)=\frac{1}{r(r_{\mathrm{o}}-\delta)}\frac{\partial}{\partial\eta}\left(\frac{r\lambda_{\mathrm{M,eff}}}{(r_{\mathrm{o}}-\delta)}\frac{\partial T_{\mathrm{M}}}{\partial\eta}\right) \quad \text{(A.67)}$$
$$\frac{1}{r(r_{\mathrm{o}}-\delta)}\frac{\partial}{\partial\eta}\left(\frac{\rho_{\mathrm{M}}rD_{\mathrm{eff}}\left(C_{P,\mathrm{g}}-C_{P,\mathrm{v}}\right)}{(r_{\mathrm{o}}-\delta)}\frac{\partial W}{\partial\eta}T_{\mathrm{M}}\right)$$

Term 1 in the above equation can be re-written as:

$$\frac{1}{r(r_{\mathrm{o}}-\delta)}\frac{\partial}{\partial\chi}\left(r(r_{\mathrm{o}}-\delta)\rho_{\mathrm{M}}u_{\mathrm{M}}C_{P,\mathrm{M}}T_{\mathrm{M}}\right)=$$
$$\frac{1}{r}\frac{\partial}{\partial\chi}\left(r\rho_{\mathrm{M}}u_{\mathrm{M}}C_{P,\mathrm{M}}T_{\mathrm{M}}\right)-\frac{\rho_{\mathrm{M}}u_{\mathrm{M}}C_{P,\mathrm{M}}T_{\mathrm{M}}}{(r_{\mathrm{o}}-\delta)}\frac{d\delta}{d\chi} \quad \text{(A.68)}$$

Substituting into equation (A.67) gives:

$$\frac{1}{r(r_{\mathrm{o}}-\delta)}\frac{\partial}{\partial\chi}\left(r(r_{\mathrm{o}}-\delta)\rho_{\mathrm{M}}u_{\mathrm{M}}C_{P,\mathrm{M}}T_{\mathrm{M}}\right)+\frac{1}{r(r_{\mathrm{o}}-\delta)}\frac{\partial}{\partial\eta}\left(r\rho_{\mathrm{M}}u_{\mathrm{M}}C_{P,\mathrm{M}}T_{\mathrm{M}}\eta\frac{d\delta}{d\chi}\right)+$$
$$\frac{1}{r(r_{\mathrm{o}}-\delta)}\frac{\partial}{\partial\eta}\left(r\rho_{\mathrm{M}}v_{\mathrm{M}}C_{P,\mathrm{M}}T_{\mathrm{M}}\right)=\frac{1}{r(r_{\mathrm{o}}-\delta)}\frac{\partial}{\partial\eta}\left(\frac{r\lambda_{\mathrm{M,eff}}}{(r_{\mathrm{o}}-\delta)}\frac{\partial T_{\mathrm{M}}}{\partial\eta}\right) \quad \text{(A.69)}$$
$$+\frac{1}{r(r_{\mathrm{o}}-\delta)}\frac{\partial}{\partial\eta}\left(\frac{\rho_{\mathrm{M}}rD_{\mathrm{eff}}\left(C_{P,\mathrm{g}}-C_{P,\mathrm{v}}\right)}{(r_{\mathrm{o}}-\delta)}\frac{\partial W}{\partial\eta}T_{\mathrm{M}}\right)$$

Note that:

$$\frac{1}{r(r_{\mathrm{o}}-\delta)}\frac{\partial}{\partial\eta}\left(rJ''_{\mathrm{M}}C_{P,\mathrm{M}}T_{\mathrm{M}}\right)=\frac{1}{r(r_{\mathrm{o}}-\delta)}\frac{\partial}{\partial\eta}\left(r\rho_{\mathrm{M}}v_{\mathrm{M}}C_{P,\mathrm{M}}T_{\mathrm{M}}\right)+$$
$$\frac{1}{r(r_{\mathrm{o}}-\delta)}\frac{\partial}{\partial\eta}\left(r\rho_{\mathrm{M}}u_{\mathrm{M}}C_{P,\mathrm{M}}T_{\mathrm{M}}\eta\right)\frac{d\delta}{d\chi} \quad \text{(A.70)}$$

Substituting into equation (A.69) results in:

$$\frac{1}{r(r_o-\delta)}\frac{\partial}{\partial\chi}\left(r(r_o-\delta)\rho_M u_M C_{P,M} T_M\right)+\frac{1}{r(r_o-\delta)}\frac{\partial}{\partial\eta}\left(rJ''_M C_{P,M} T_M\right)$$
$$=\frac{1}{r(r_o-\delta)}\frac{\partial}{\partial\eta}\left(\frac{r\lambda_{M,eff}}{(r_o-\delta)}\frac{\partial T_M}{\partial\eta}\right)+\frac{1}{r(r_o-\delta)}\frac{\partial}{\partial\eta}\left(\frac{\rho_M r D_{eff}\left(C_{P,g}-C_{P,v}\right)}{(r_o-\delta)}\frac{\partial W}{\partial\eta}T_M\right) \quad (A.71)$$

Mixture Mass Diffusion

$$\frac{\partial}{\partial z}(\rho_M u_M W)+\frac{1}{r}\frac{\partial}{\partial r}(r\rho_M v_M W)=\frac{1}{r}\frac{\partial}{\partial r}\left(r\rho_M D_{eff}\frac{\partial W}{\partial r}\right) \quad (A.72)$$

$$\frac{1}{r}\frac{\partial}{\partial z}(r\rho_M u_M W)+\frac{1}{r}\frac{\partial}{\partial r}(r\rho_M v_M W)=\frac{1}{r}\frac{\partial}{\partial r}\left(r\rho_M D_{eff}\frac{\partial W}{\partial r}\right) \quad (A.73)$$

$$\frac{1}{r}\frac{\partial}{\partial\chi}(r\rho_M u_M W)+\frac{\eta}{r(r_o-\delta)}\frac{d\delta}{d\chi}\frac{\partial}{\partial\eta}(r\rho_M u_M W)+\frac{1}{r(r_o-\delta)}\frac{\partial}{\partial\eta}(r\rho_M v_M W)$$
$$=\frac{1}{r(r_o-\delta)}\frac{\partial}{\partial\eta}\left(\frac{r\rho_M D_{eff}}{(r_o-\delta)}\frac{\partial W}{\partial\eta}\right) \quad (A.74)$$

The second term of (A.74) can be written as:

$$\frac{\eta}{r(r_o-\delta)}\frac{d\delta}{d\chi}\frac{\partial}{\partial\eta}(r\rho_M u_M W)=$$
$$\frac{1}{r(r_o-\delta)}\frac{\partial}{\partial\eta}\left(r\rho_M u_M W\eta\frac{d\delta}{d\chi}\right)-\frac{\rho_M u_M W}{(r_o-\delta)}\frac{d\delta}{d\chi} \quad (A.75)$$

Substituting the above equation into (A.65) gives:

$$\frac{1}{r}\frac{\partial}{\partial\chi}(r\rho_M u_M W)+\frac{1}{r(r_o-\delta)}\frac{\partial}{\partial\eta}\left(r\rho_M u_M W\eta\frac{d\delta}{d\chi}\right)-\frac{\rho_M u_M W}{(r_o-\delta)}\frac{d\delta}{d\chi}$$
$$\frac{1}{r(r_o-\delta)}\frac{\partial}{\partial\eta}(r\rho_M v_M W)=\frac{1}{r(r_o-\delta)}\frac{\partial}{\partial\eta}\left(\frac{r\rho_M D_{eff}}{(r_o-\delta)}\frac{\partial W}{\partial\eta}\right) \quad (A.76)$$

Term 1 in the above equation can be re-written as:

$$\frac{1}{r(r_o-\delta)}\frac{\partial}{\partial\chi}\left(r(r_o-\delta)\rho_M u_M W\right)=\frac{1}{r}\frac{\partial}{\partial\chi}\left(r\rho_M u_M W\right)-\frac{\rho_M u_M W}{(r_o-\delta)}\frac{d\delta}{d\chi} \tag{A.77}$$

Substituting into equation (A.76) gives:

$$\begin{aligned}&\frac{1}{r(r_o-\delta)}\frac{\partial}{\partial\chi}\left(r(r_o-\delta)\rho_M u_M W\right)+\frac{1}{r(r_o-\delta)}\frac{\partial}{\partial\eta}\left(r\rho_M u_M W\eta\frac{d\delta}{d\chi}\right)+\\&\frac{1}{r(r_o-\delta)}\frac{\partial}{\partial\eta}\left(r\rho_M v_M W\right)=\frac{1}{r(r_o-\delta)}\frac{\partial}{\partial\eta}\left(\frac{r\rho_M D_{eff}}{(r_o-\delta)}\frac{\partial W}{\partial\eta}\right)\end{aligned} \tag{A.78}$$

Note that:

$$\begin{aligned}&\frac{1}{r(r_o-\delta)}\frac{\partial}{\partial\eta}\left(rJ''_M W\right)=\frac{1}{r(r_o-\delta)}\frac{\partial}{\partial\eta}\left(r\rho_M v_M W\right)+\\&\frac{1}{r(r_o-\delta)}\frac{\partial}{\partial\eta}\left(r\rho_M u_M W\eta\right)\frac{d\delta}{d\chi}\end{aligned} \tag{A.79}$$

Substituting into equation (A.78) results in:

$$\begin{aligned}&\frac{1}{r(r_o-\delta)}\frac{\partial}{\partial\chi}\left(r(r_o-\delta)\rho_M u_M W\right)+\frac{1}{r(r_o-\delta)}\frac{\partial}{\partial\eta}\left(rJ''_M W\right)\\&=\frac{1}{r(r_o-\delta)}\frac{\partial}{\partial\eta}\left(\frac{r\rho_M D_{eff}}{(r_o-\delta)}\frac{\partial W}{\partial\eta}\right)\end{aligned} \tag{A.80}$$

A.4 $k-\varepsilon$ Equation Transformation

Liquid Kinetic Energy Equation

$$\frac{1}{r}\frac{\partial}{\partial z}\left(r\rho_L u_L k_L\right)+\frac{1}{r}\frac{\partial}{\partial r}\left(r\rho_L v_L k_L\right)=\frac{1}{r}\frac{\partial}{\partial r}\left[r\left(\mu_L+\frac{\mu_L^t}{\sigma_k}\right)\frac{\partial k_L}{\partial r}\right]+G_L-\rho_L\varepsilon_L-D_L \tag{A.81}$$

Where, $G_L = \mu_L^t \left(\frac{\partial u_L}{\partial r} \right)^2$ (A.82)

And, $D_L = 2\mu_L \left(\frac{\partial \sqrt{k_L}}{\partial r} \right)^2$ (A.83)

$$\frac{\partial}{\partial \chi}(\rho_L u_L k_L) - \frac{(\eta-2)}{r\delta}\frac{d\delta}{d\chi}\frac{\partial}{\partial \eta}(r\rho_L u_L k_L) + \frac{1}{r\delta}\frac{\partial}{\partial \eta}(r\rho_L v_L k_L) = \frac{1}{r\delta}\frac{\partial}{\partial \eta}\left[\frac{r}{\delta}\left(\mu_L + \frac{\mu_L^t}{\sigma_k}\right)\frac{\partial k_L}{\partial \eta}\right] + G_L - \rho_L \varepsilon_L - D_L \quad \text{(A.84)}$$

Where $G_L = \mu_L^t \left[\frac{1}{\delta}\frac{\partial u_L}{\partial \eta_L} \right]^2$ (A.85)

And $D_L = 2\mu_L \left(\frac{1}{\delta}\frac{\partial \sqrt{k_L}}{\partial \eta} \right)^2$ (A.86)

Term 2 of Equation (A.84) can be re-written as:

$$\frac{(\eta-2)}{r\delta}\frac{d\delta}{d\chi}\frac{\partial}{\partial \eta}(r\rho_L u_L k_L) = \frac{1}{r\delta}\frac{\partial}{\partial \eta}\left(r(\eta-2)\rho_L u_L k_L \frac{d\delta}{d\chi}\right) - \frac{\rho_L u_L k_L}{\delta}\frac{d\delta}{d\chi} \quad \text{(A.87)}$$

Substitute Equation (A.87) into Equation (A.84):

$$\frac{\partial}{\partial \chi}(\rho_L u_L k_L) - \frac{1}{r\delta}\frac{\partial}{\partial \eta}\left(r(\eta-2)\rho_L u_L k_L \frac{d\delta}{d\chi}\right) + \frac{\rho_L u_L k_L}{\delta}\frac{d\delta}{d\chi} + \frac{1}{r\delta}\frac{\partial}{\partial \eta}(r\rho_L v_L k_L) = \frac{1}{r\delta}\frac{\partial}{\partial \eta}\left[\frac{r}{\delta}\left(\mu_L + \frac{\mu_L^t}{\sigma_k}\right)\frac{\partial k_L}{\partial \eta}\right] + G_L - \rho_L \varepsilon_L - D_L \quad \text{(A.88)}$$

In order to define the velocity, v in terms of the mass flux, use the following:

$$\frac{1}{r\delta}\frac{\partial}{\partial\eta}\left(rJ_{\mathrm{L}}''k_{\mathrm{L}}\right)=\frac{1}{r\delta}\frac{\partial}{\partial\eta}\left(r\rho_{\mathrm{L}}v_{\mathrm{L}}k_{\mathrm{L}}\right)-\frac{1}{r\delta}\frac{\partial}{\partial\eta}\left(r\rho_{\mathrm{L}}u_{\mathrm{L}}(\eta-2)\frac{d\delta}{d\chi}k_{\mathrm{L}}\right) \tag{A.89}$$

Substitute Equation (A.89) into Equation (A.88)

$$\frac{\partial}{\partial\chi}\left(\rho_{\mathrm{L}}u_{\mathrm{L}}k_{\mathrm{L}}\right)+\frac{\rho_{\mathrm{L}}u_{\mathrm{L}}k_{\mathrm{L}}}{\delta}\frac{d\delta}{d\chi}+\frac{1}{r\delta}\frac{\partial}{\partial\eta}\left(rJ_{\mathrm{L}}''k_{\mathrm{L}}\right)= \frac{1}{r\delta}\frac{\partial}{\partial\eta}\left[\frac{r}{\delta}\left(\mu_{\mathrm{L}}+\frac{\mu_{\mathrm{L}}^{\mathrm{t}}}{\sigma_k}\right)\frac{\partial k_{\mathrm{L}}}{\partial\eta}\right]+G_{\mathrm{L}}-\rho_{\mathrm{L}}\varepsilon_{\mathrm{L}}-D_{\mathrm{L}} \tag{A.90}$$

Term 2 of Equation (A.90) can be re-written as:

$$\frac{\rho_{\mathrm{L}}u_{\mathrm{L}}k_{\mathrm{L}}}{\delta}\frac{d\delta}{d\chi}=\frac{1}{r\delta}\frac{\partial}{\partial\chi}\left(r\delta\rho_{\mathrm{L}}u_{\mathrm{L}}k_{\mathrm{L}}\right)-\frac{\partial}{\partial\chi}\left(\rho_{\mathrm{L}}u_{\mathrm{L}}k_{\mathrm{L}}\right) \tag{A.91}$$

Substituting Equation (A.91) into Equation (A.90) results in the following:

$$\frac{1}{r\delta}\frac{\partial}{\partial\chi}\left(r\delta\rho_{\mathrm{L}}u_{\mathrm{L}}k_{\mathrm{L}}\right)+\frac{1}{r\delta}\frac{\partial}{\partial\eta}\left(rJ_{\mathrm{L}}"k_{\mathrm{L}}\right)= \frac{1}{r\delta}\frac{\partial}{\partial\eta}\left[\frac{r}{\delta}\left(\mu_{\mathrm{L}}+\frac{\mu_{L}^{t}}{\sigma_k}\right)\frac{\partial k_{L}}{\partial\eta}\right]+G_{\mathrm{L}}-\rho_{\mathrm{L}}\varepsilon_{\mathrm{L}}-D_{\mathrm{L}} \tag{A.92}$$

Mixture Kinetic Energy Equation

$$\frac{1}{r}\frac{\partial}{\partial z}\left(r\rho_{\mathrm{M}}u_{\mathrm{M}}k_{\mathrm{M}}\right)+\frac{1}{r}\frac{\partial}{\partial r}\left(r\rho_{\mathrm{M}}v_{\mathrm{M}}k_{\mathrm{M}}\right)=\frac{1}{r}\frac{\partial}{\partial r}\left[r\left(\mu_{\mathrm{M}}+\frac{\mu_{\mathrm{M}}^{\mathrm{t}}}{\sigma_k}\right)\frac{\partial k_{\mathrm{M}}}{\partial r}\right] \tag{A.93}$$
$$+G_{\mathrm{M}}-\rho_{\mathrm{M}}\varepsilon_{\mathrm{M}}-D_{\mathrm{M}}$$

$$\text{Where, } G_{\mathrm{M}}=\mu_{\mathrm{M}}^{\mathrm{t}}\left(\frac{\partial u_{\mathrm{M}}}{\partial r}\right)^2 \tag{A.94}$$

$$\text{And, } D_M = 2\mu_M\left(\frac{\partial\sqrt{k_M}}{\partial r}\right)^2 \tag{A.95}$$

$$\frac{\partial}{\partial\chi}(\rho_M u_M k_M)+\frac{\eta}{(r_o-\delta)r}\frac{d\delta}{d\chi}\frac{\partial}{\partial\eta}(r\rho_M u_M k_M)+\frac{1}{r(r_o-\delta)}\frac{\partial}{\partial\eta}(r\rho_M v_M k_M)= \frac{1}{r(r_o-\delta)}\frac{\partial}{\partial\eta}\left[\frac{r}{(r_o-\delta)}\left(\mu_M+\frac{\mu_M^t}{\sigma_k}\right)\frac{\partial k_M}{\partial\eta}\right]+G_M-\rho_M\varepsilon_M-D_M \tag{A.96}$$

$$\text{Where } G_M = \mu_M^t\left[\frac{1}{(r_o-\delta)}\frac{\partial u_M}{\partial\eta}\right]^2 \tag{A.97}$$

$$\text{And } D_M = 2\mu_M\left(\frac{1}{(r_o-\delta)}\frac{\partial\sqrt{k_M}}{\partial\eta}\right)^2 \tag{A.98}$$

Term 2 of Eqn (A.96) can be re-written as:

$$\frac{1}{r}\frac{\eta}{(r_o-\delta)}\frac{d\delta}{d\chi}\frac{\partial}{\partial\eta}(r\rho_M u_M k_M)=\frac{1}{r(r_o-\delta)}\frac{\partial}{\partial\eta}\left(r\eta\rho_M u_M k_M\frac{d\delta}{d\chi}\right)- \frac{\rho_M u_M k_M}{(r_o-\delta)}\frac{d\delta}{d\chi} \tag{A.99}$$

Substitute Equation (A.99) into Equation (A.96):

$$\frac{\partial}{\partial\chi}(\rho_M u_M k_M)+\frac{1}{r(r_o-\delta)}\frac{\partial}{\partial\eta}\left(r\eta\rho_M u_M k_M\frac{d\delta}{d\chi}\right)- \frac{\rho_M u_M k_M}{(r_o-\delta)}\frac{d\delta}{d\chi}+\frac{1}{r(r_o-\delta)}\frac{\partial}{\partial\eta}(r\rho_M v_M k_M)= \frac{1}{r(r_o-\delta)}\frac{\partial}{\partial\eta}\left[\frac{r}{(r_o-\delta)}\left(\mu_M+\frac{\mu_M^t}{\sigma_k}\right)\frac{\partial k_M}{\partial\eta}\right]+G_M-\rho_M\varepsilon_M-D_M \tag{A.100}$$

In order to define the velocity, v in terms of the mass flux, use the following:

$$\frac{1}{r(r_o-\delta)}\frac{\partial}{\partial\eta}\left(rJ''_M k_M\right)=\frac{1}{r(r_o-\delta)}\frac{\partial}{\partial\eta}\left(r\rho_M v_M k_M\right)+ \frac{1}{r(r_o-\delta)}\frac{\partial}{\partial\eta}\left(r\rho_M u_M \eta\frac{d\delta}{d\chi}k_M\right) \tag{A.101}$$

Substitute Equation (A.101) into Equation (A.100)

$$\frac{\partial}{\partial\chi}\left(\rho_M u_M k_M\right)-\frac{\rho_M u_M k_M}{(r_o-\delta)}\frac{d\delta}{d\chi}+\frac{1}{r(r_o-\delta)}\frac{\partial}{\partial\eta}\left(rJ''_M k_M\right)= \frac{1}{r(r_o-\delta)}\frac{\partial}{\partial\eta}\left[\frac{r}{(r_o-\delta)}\left(\mu_M+\frac{\mu_M^t}{\sigma_k}\right)\frac{\partial k_M}{\partial\eta}\right]+G_M-\rho_M\varepsilon_M-D_M \tag{A.102}$$

Term 2 of Equation (A.102) can be re-written as:

$$\frac{\rho_M u_M k_M}{(r_o-\delta)}\frac{d\delta}{d\chi}=-\frac{1}{(r_o-\delta)}\frac{\partial}{\partial\chi}\left((r_o-\delta)\rho_M u_M k_M\right)+ \frac{\partial}{\partial\chi}\left(\rho_M u_M k_M\right) \tag{A.103}$$

Substituting Equation (A.103) into Equation (A.102) results in the following:

$$\frac{1}{r(r_o-\delta)}\frac{\partial}{\partial\chi}\left(r(r_o-\delta)\rho_M u_M k_M\right)+\frac{1}{r(r_o-\delta)}\frac{\partial}{\partial\eta}\left(rJ''_M k_M\right)= \frac{1}{r(r_o-\delta)}\frac{\partial}{\partial\eta}\left[\frac{r}{(r_o-\delta)}\left(\mu_M+\frac{\mu_M^t}{\sigma_k}\right)\frac{\partial k_M}{\partial\eta}\right]+G_M-\rho_M\varepsilon_M-D_M \tag{A.104}$$

Liquid Dissipation Rate Equation

$$\frac{1}{r}\frac{\partial}{\partial z}\left(r\rho_L u_L\varepsilon_L\right)+\frac{1}{r}\frac{\partial}{\partial r}\left(r\rho_L v_L\varepsilon_L\right)=\frac{1}{r}\frac{\partial}{\partial r}\left[r\left(\mu_L+\frac{\mu_L^t}{\sigma_\varepsilon}\right)\frac{\partial\varepsilon_L}{\partial r}\right] + C_{\varepsilon 1}f_1\frac{\varepsilon_L}{k_L}G_L-C_{\varepsilon 2}f_2\rho_L\frac{\varepsilon_L^{\,2}}{k_L}+E_L \tag{A.105}$$

Where, $G_L = \mu_L^t \left(\frac{\partial u_L}{\partial r} \right)^2$ (A.106)

$$E_L = 2\frac{\mu_L \mu_L^t}{\rho_L}\left(\frac{\partial^2 u_L}{\partial r^2}\right)^2$$
$$f_1 = 1, \quad f_2 = 1 - 0.3e^{-\mathrm{Re}_T^2}$$
$$\mathrm{R}_{L,\tau}{}^2 = \frac{k_L{}^4}{\varepsilon_L{}^2 \nu_L{}^2},$$
$$C_{\varepsilon 1} = 1.55, \quad C_{\varepsilon 2} = 2.0 \qquad \text{(A.107)}$$

$$\frac{1}{r}\frac{\partial}{\partial \chi}(r\rho_L u_L \varepsilon_L) - \frac{(\eta_L - 2)}{r\delta}\frac{d\delta}{d\chi}\frac{\partial}{\partial \eta}(r\rho_L u_L \varepsilon_L) + \frac{1}{r\delta}\frac{\partial}{\partial \eta}(r\rho_L v_L \varepsilon_L) =$$
$$\frac{1}{r\delta}\frac{\partial}{\partial \eta}\left[\frac{r}{\delta}\left(\mu_L + \frac{\mu_L^t}{\sigma_\varepsilon}\right)\frac{\partial \varepsilon_L}{\partial \eta}\right] + C_{\varepsilon 1} f_1 \frac{\varepsilon_L}{k_L} G_L - C_{\varepsilon 2} f_2 \rho_L \frac{\varepsilon_L{}^2}{k_L} + E_L \qquad \text{(A.108)}$$

Where $G_L = \mu_L^t \left[\frac{1}{\delta}\frac{\partial u_L}{\partial \eta} \right]^2$ (A.109)

And $E_L = \frac{2\mu_L \mu_L^t}{\rho_L \delta^2}\left(\frac{\partial^2 u_L}{\partial \eta^2}\right)^2$ (A.110)

Term 2 of Equation (A.110) can be re-written as:

$$\frac{(\eta - 2)}{r\delta}\frac{d\delta}{d\chi}\frac{\partial}{\partial \eta}(r\rho_L u_L \varepsilon_L) = \frac{1}{r\delta}\frac{\partial}{\partial \eta}\left(r(\eta - 2)\rho_L u_L \varepsilon_L \frac{d\delta}{d\chi}\right) - \frac{\rho_L u_L \varepsilon_L}{\delta}\frac{d\delta}{d\chi} \qquad \text{(A.111)}$$

Substitute Equation (A.111) into Equation (A.108):

$$\frac{1}{r}\frac{\partial}{\partial\chi}(r\rho_L u_L \varepsilon_L) - \frac{1}{r\delta}\frac{\partial}{\partial\eta}\left(r(\eta-2)\rho_L u_L \varepsilon_L \frac{d\delta}{d\chi}\right) + \frac{\rho_L u_L \varepsilon_L}{\delta}\frac{d\delta}{d\chi} +$$

$$\frac{1}{r\delta}\frac{\partial}{\partial\eta}(r\rho_L v_L \varepsilon_L) = \frac{1}{r\delta}\frac{\partial}{\partial\eta}\left[\frac{r}{\delta}\left(\mu_L + \frac{\mu_L^t}{\sigma_\varepsilon}\right)\frac{\partial\varepsilon_L}{\partial\eta}\right] + C_{\varepsilon 1} f_1 \frac{\varepsilon_L}{k_L} G_L - \qquad \text{(A.112)}$$

$$\rho_L f_2 C_{\varepsilon 2} \frac{{\varepsilon_L}^2}{k_L} + E_L$$

In order to define the velocity, v in terms of the mass flux, use the following:

$$\frac{1}{r\delta}\frac{\partial}{\partial\eta}(rJ_L''\varepsilon_L) = \frac{1}{r\delta}\frac{\partial}{\partial\eta}(r\rho_L v_L \varepsilon_L) - \frac{1}{r\delta}\frac{\partial}{\partial\eta}\left(r(\eta-2)\rho_L u_L \varepsilon_L \frac{d\delta}{d\chi}\right) \qquad \text{(A.113)}$$

Substitute Equation (A.113) into Equation (A.112)

$$\frac{1}{r}\frac{\partial}{\partial\chi}(r\rho_L u_L \varepsilon_L) + \frac{\rho_L u_L \varepsilon_L}{\delta}\frac{d\delta}{d\chi} + \frac{1}{r\delta}\frac{\partial}{\partial\eta}(rJ_L''\varepsilon_L) =$$
$$\frac{1}{r\delta}\frac{\partial}{\partial\eta}\left[\frac{r}{\delta}\left(\mu_L + \frac{\mu_L^t}{\sigma_\varepsilon}\right)\frac{\partial\varepsilon_L}{\partial\eta}\right] + C_{\varepsilon 1} f_1 \frac{\varepsilon_L}{k_L} G_L - \rho_L C_{\varepsilon 2} f_2 \frac{{\varepsilon_L}^2}{k_L} + E_L \qquad \text{(A.114)}$$

Term 2 of Equation (A.114) can be re-written as:

$$\frac{\rho_L u_L \varepsilon_L}{\delta}\frac{d\delta}{d\chi} = \frac{1}{r\delta}\frac{\partial}{\partial\chi}(r\delta\rho_L u_L \varepsilon_L) - \frac{1}{r}\frac{\partial}{\partial\chi}(r\rho_L u_L \varepsilon_L) \qquad \text{(A.115)}$$

Substituting Equation (A.115) into Equation (A.114) results in the following:

$$\frac{1}{r\delta}\frac{\partial}{\partial\chi}(r\delta\rho_L u_L \varepsilon_L) + \frac{1}{r\delta}\frac{\partial}{\partial\eta_L}(rJ_L''\varepsilon_L) =$$
$$\frac{1}{r\delta}\frac{\partial}{\partial\eta_L}\left[\frac{r}{\delta}\left(\mu_L + \frac{\mu_L^t}{\sigma_\varepsilon}\right)\frac{\partial\varepsilon_L}{\partial\eta_L}\right] + C_{\varepsilon 1} f_1 \frac{\varepsilon_L}{k_L} G_L - \rho_L C_{\varepsilon 2} f_2 \frac{{\varepsilon_L}^2}{k_L} + E_L \qquad \text{(A.116)}$$

Mixture Dissipation Rate Equation

$$\frac{1}{r}\frac{\partial}{\partial z}\left(r\rho_{\mathrm{M}}u_{\mathrm{M}}\varepsilon_{\mathrm{M}}\right)+\frac{1}{r}\frac{\partial}{\partial r}\left(r\rho_{\mathrm{M}}v_{\mathrm{M}}\varepsilon_{\mathrm{M}}\right)=\frac{1}{r}\frac{\partial}{\partial r}\left[r\left(\mu_{\mathrm{M}}+\frac{\mu_{\mathrm{M}}^{\mathrm{t}}}{\sigma_{\varepsilon}}\right)\frac{\partial\varepsilon_{\mathrm{M}}}{\partial r}\right]$$
$$+C_{\varepsilon 1}f_1\frac{\varepsilon_{\mathrm{M}}}{k_{\mathrm{M}}}G_{\mathrm{M}}-C_{\varepsilon 2}f_2\rho_{\mathrm{M}}\frac{{\varepsilon_{\mathrm{M}}}^2}{k_{\mathrm{M}}}+E_{\mathrm{M}} \qquad \text{(A.117)}$$

$$\text{Where, } G_{\mathrm{M}}=\mu_{\mathrm{M}}^{\mathrm{t}}\left(\frac{\partial u_{\mathrm{M}}}{\partial r}\right)^2 \qquad \text{(A.118)}$$

$$E=2\frac{\mu_{\mathrm{M}}\mu_{\mathrm{M}}^{\mathrm{t}}}{\rho_L}\left(\frac{\partial^2 u_{\mathrm{M}}}{\partial r^2}\right)^2$$
$$f_1=1,\quad f_2=1-0.3e^{-\mathrm{Re}_T{}^2} \qquad \text{(A.119)}$$
$$\mathrm{R}_{\mathrm{M},\tau}{}^2=\frac{{k_{\mathrm{M}}}^4}{{\varepsilon_{\mathrm{M}}}^2{\nu_{\mathrm{M}}}^2},$$
$$C_{\varepsilon 1}=1.55,\quad C_{\varepsilon 2}=2.0$$

$$\frac{1}{r}\frac{\partial}{\partial\chi}\left(r\rho_{\mathrm{M}}u_{\mathrm{M}}\varepsilon_{\mathrm{M}}\right)-\frac{\eta}{r(r_{\mathrm{o}}-\delta)}\frac{d\delta}{d\chi}\frac{\partial}{\partial\eta}\left(r\rho_{\mathrm{M}}u_{\mathrm{M}}\varepsilon_{\mathrm{M}}\right)+$$
$$\frac{1}{r(r_{\mathrm{o}}-\delta)}\frac{\partial}{\partial\eta}\left(r\rho_{\mathrm{M}}v_{\mathrm{M}}\varepsilon_{\mathrm{M}}\right)=\frac{1}{r(r_{\mathrm{o}}-\delta)}\frac{\partial}{\partial\eta}\left[\frac{r}{(r_{\mathrm{o}}-\delta)}\left(\mu_{\mathrm{M}}+\frac{\mu_{\mathrm{M}}^{\mathrm{t}}}{\sigma_{\varepsilon}}\right)\frac{\partial\varepsilon_{\mathrm{M}}}{\partial\eta}\right] \qquad \text{(A.120)}$$
$$+C_{\varepsilon 1}f_1\frac{\varepsilon_{\mathrm{M}}}{k_{\mathrm{M}}}G_{\mathrm{M}}-\rho_{\mathrm{M}}C_{\varepsilon 2}f_2\frac{{\varepsilon_{\mathrm{M}}}^2}{k_{\mathrm{M}}}+E_{\mathrm{M}}$$

$$\text{Where } G_{\mathrm{M}}=\mu_{\mathrm{M}}^{\mathrm{t}}\left[\frac{1}{(r_{\mathrm{o}}-\delta)}\frac{\partial u_{\mathrm{M}}}{\partial\eta}\right]^2 \qquad \text{(A.121)}$$

$$\text{And } E_{\mathrm{M}}=\frac{2\mu_{\mathrm{M}}\mu_{\mathrm{M}}^{\mathrm{t}}}{\rho_{\mathrm{M}}(r_{\mathrm{o}}-\delta)^2}\left(\frac{\partial^2 u_{\mathrm{M}}}{\partial\eta^2}\right)^2 \qquad \text{(A.122)}$$

Term 2 of Equation (A.122) can be re-written as:

$$\frac{\eta}{r(r_o-\delta)}\frac{d\delta}{d\chi}\frac{\partial}{\partial\eta}(r\rho_M u_M \varepsilon_M)=\frac{1}{r(r_o-\delta)}\frac{\partial}{\partial\eta}\left(r\eta\rho_M u_M \varepsilon_M \frac{d\delta}{d\chi}\right)-\frac{\rho_M u_M \varepsilon_M}{(r_o-\delta)}\frac{d\delta}{d\chi} \tag{A.123}$$

Substitute Equation (A.123) into Equation (A.120):

$$\frac{1}{r}\frac{\partial}{\partial\chi}(r\rho_M u_M \varepsilon_M)-\frac{1}{r(r_o-\delta)}\frac{\partial}{\partial\eta}\left(r\eta\rho_M u_M \varepsilon_M \frac{d\delta}{d\chi}\right)-\frac{\rho_M u_M \varepsilon_M}{(r_o-\delta)}\frac{d\delta}{d\chi}+\frac{1}{r(r_o-\delta)}\frac{\partial}{\partial\eta}(r\rho_M v_M \varepsilon_M)=\frac{1}{r(r_o-\delta)}\frac{\partial}{\partial\eta}\left[\frac{r}{(r_o-\delta)}\left(\mu_M+\frac{\mu_M^t}{\sigma_\varepsilon}\right)\frac{\partial\varepsilon_M}{\partial\eta}\right]+C_{\varepsilon 1}f_1\frac{\varepsilon_M}{k_M}G_M-C_{\varepsilon 2}f_2\rho_M\frac{\varepsilon_M^{\,2}}{k_M}+E_M \tag{A.124}$$

In order to define the velocity, v in terms of the mass flux, use the following:

$$\frac{1}{r(r_o-\delta)}\frac{\partial}{\partial\eta}(rJ_M''\varepsilon_M)=\frac{1}{r(r_o-\delta)}\frac{\partial}{\partial\eta}(r\rho_M v_M \varepsilon_M)+\frac{1}{r(r_o-\delta)}\frac{\partial}{\partial\eta}\left(r\rho_M u_M \eta\frac{d\delta}{d\chi}\varepsilon_M\right) \tag{A.125}$$

Substitute Equation (A.125) into Equation (A.124)

$$\frac{1}{r}\frac{\partial}{\partial\chi}(r\rho_M u_M \varepsilon_M)-\frac{\rho_M u_M \varepsilon_M}{(r_o-\delta)}\frac{d\delta}{d\chi}+\frac{1}{r(r_o-\delta)}\frac{\partial}{\partial\eta}(rJ_M''\varepsilon_M)=\frac{1}{r(r_o-\delta)}\frac{\partial}{\partial\eta}\left[\frac{r}{(r_o-\delta)}\left(\mu_M+\frac{\mu_M^t}{\sigma_\varepsilon}\right)\frac{\partial\varepsilon_M}{\partial\eta}\right]+C_{\varepsilon 1}f_1\frac{\varepsilon_M}{k_M}G_M-C_{\varepsilon 2}f_2\rho_M\frac{\varepsilon_M^{\,2}}{k_M}+E_M \tag{A.126}$$

Term 2 of Equation (A.126) can be re-written as:

$$\frac{\rho_M u_M \varepsilon_M}{(r_o-\delta)}\frac{d\delta}{d\chi} = -\frac{1}{r(r_o-\delta)}\frac{\partial}{\partial\chi}\left(r(r_o-\delta)\rho_M u_M \varepsilon_M\right) + \frac{1}{r}\frac{\partial}{\partial\chi}\left(r\rho_M u_M \varepsilon_M\right) \quad \text{(A.127)}$$

Substituting Equation (A.127) into Equation (A.126) results in the following:

$$\frac{1}{r(r_o-\delta)}\frac{\partial}{\partial\chi}\left(r(r_o-\delta)\rho_M u_M \varepsilon_M\right) + \frac{1}{r(r_o-\delta)}\frac{\partial}{\partial\eta}\left(rJ''_M \varepsilon_M\right) = \frac{1}{r(r_o-\delta)}\frac{\partial}{\partial\eta}\left[\frac{r}{(r_o-\delta)}\left(\mu_M + \frac{\mu_M^t}{\sigma_\varepsilon}\right)\frac{\partial\varepsilon_M}{\partial\eta}\right] + C_{\varepsilon 1}\frac{\varepsilon_M}{k_M}G_M - C_{\varepsilon 2}\rho_M\frac{{\varepsilon_M}^2}{k_M} \quad \text{(A.128)}$$

A.5 Boundary Condition Transformation

Tube Wall ($\eta = 2$)

- $u_L = 0$ (A.129)
- $J''_L = 0$ (A.130)
- $T_L = T_{wall}$ (A.131)

Center Line ($\eta = 0$)

- $\frac{\partial u_M}{\partial r} = 0$

$$\frac{1}{(r_o-\delta)}\frac{\partial u_M}{\partial\eta} = 0$$

$$\frac{\partial u_M}{\partial\eta} = 0 \quad \text{(A.132)}$$

- $J''_{M} = 0$ (A.133)

- $\dfrac{\partial T_{M}}{\partial r} = 0$

$$\frac{1}{r_o - \delta}\frac{\partial T_{M}}{\partial \eta} = 0$$

$$\frac{\partial T_{M}}{\partial \eta} = 0 \quad \text{(A.134)}$$

- $\dfrac{\partial W}{\partial r} = 0$

$$\frac{1}{(r_o - \delta)}\frac{\partial W}{\partial \eta} = 0$$

$$\frac{\partial W}{\partial \eta} = 0 \quad \text{(A.135)}$$

Liquid-Mixture Interface ($\eta = 1$)

- $u_{L} = u_{M}$ (A.136)

- $\mu_{L,eff}\dfrac{\partial u_{L}}{\partial r} = \mu_{M,eff}\dfrac{\partial u_{M}}{\partial r}$

$$\frac{\mu_{L,eff}}{\delta}\frac{\partial u_{L}}{\partial \eta} = \frac{\mu_{M,eff}}{(r_o - \delta)}\frac{\partial u_{M}}{\partial \eta} \quad \text{(A.137)}$$

- $J''_{L} = J''_{M}$ (A.138)

- $T_{L} = T_{M} = T_{sat@P_v}$ (A.139)

- $J''_{i}W - \rho_{M}D_{eff}\dfrac{\partial W}{\partial r} = 0$

$$J''_{M}W - \frac{\rho_{M}D_{eff}}{(r_o - \delta)}\frac{\partial W}{\partial \eta} = 0 \quad \text{(A.140)}$$

- $$\lambda_{\mathrm{L,eff}} \frac{\partial T_{\mathrm{L}}}{\partial r} = \lambda_{\mathrm{M,eff}} \frac{\partial T_{\mathrm{M}}}{\partial r} - J_i'' h_{\mathrm{fg}}$$

$$\frac{\lambda_{\mathrm{L,eff}}}{\delta} \frac{\partial T_{\mathrm{L}}}{\partial \eta} = \frac{\lambda_{\mathrm{M,eff}}}{(r_{\mathrm{o}} - \delta)} \frac{\partial T_{\mathrm{M}}}{\partial \eta} - J_{\mathrm{M}}'' h_{\mathrm{fg}} \qquad \text{(A.141)}$$

Overall Conservation of Mass

- $$\int_0^{r_{\mathrm{o}}-\delta} \rho_{\mathrm{M}} u_{\mathrm{M}} r dr + \int_{r_{\mathrm{o}}-\delta}^{r_{\mathrm{o}}} \rho_{\mathrm{L}} u_{\mathrm{L}} r dr = \frac{\dot{m}_{\mathrm{in}}}{2\pi}$$

$$\int_0^1 \rho_{\mathrm{M}} u_{\mathrm{M}} \eta_{\mathrm{M}} (r_{\mathrm{o}} - \delta)^2 d\eta + \int_1^2 \rho_{\mathrm{L}} u_{\mathrm{L}} \delta(\delta(\eta - 2) + r_{\mathrm{o}}) d\eta = \frac{\dot{m}_{\mathrm{in}}}{2\pi} \qquad \text{(A.142)}$$

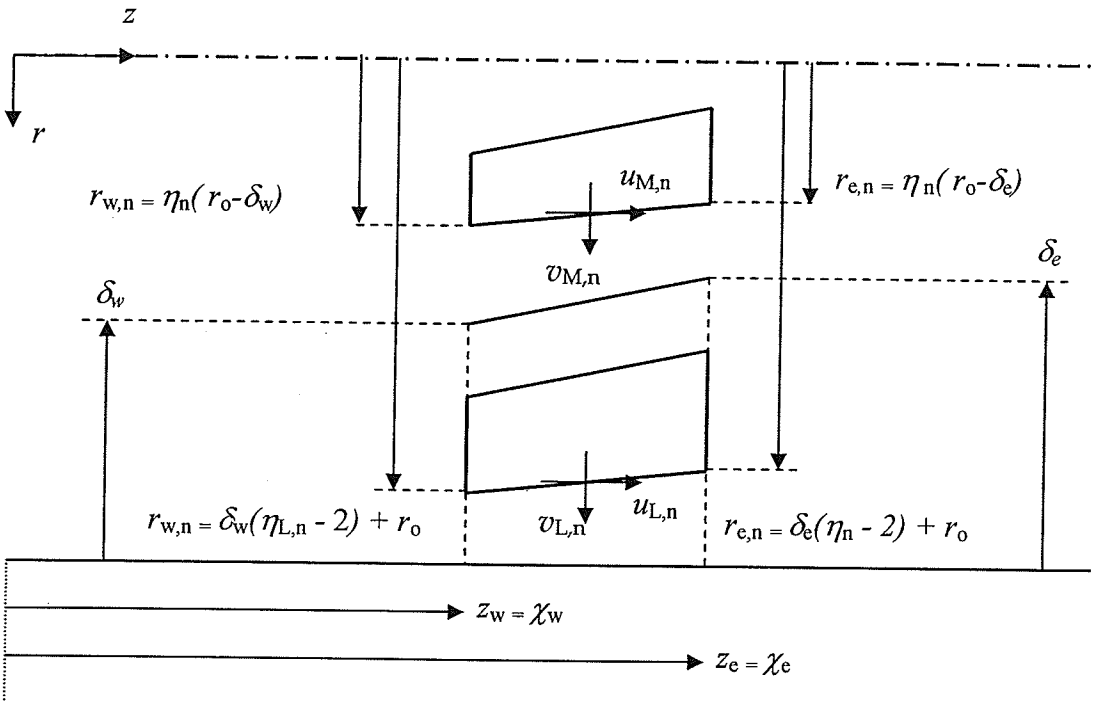

Figure A.1 Flows at the north face

APPENDIX B

Discretization of Governing Equations

B.1 Discretized Equations in the Liquid Region

Liquid Continuity Equation

$$a_{\mathrm{L,S}}^{JJ} J_{\mathrm{L,S}} + a_{\mathrm{L,P}}^{Ju} u_{\mathrm{L,P}} + a_{\mathrm{L,P}}^{JJ} J_{\mathrm{L,P}} + a_{\mathrm{L,P}}^{J\delta} \delta_{\mathrm{P}} = b_{\mathrm{L,P}}^{J} \tag{B.1}$$

where,

$$a_{\mathrm{L,S}}^{JJ} = -1 \tag{B.2}$$

$$a_{\mathrm{L,P}}^{Ju} = 2\pi\left(r_{\mathrm{o}} + \delta_{\mathrm{e}}^{o}\left(\eta_{\mathrm{P}} - 2\right)\right)\Delta\eta_{\mathrm{P}}\rho_{\mathrm{L,e}}\delta_{\mathrm{e}}^{o} \tag{B.3}$$

$$a_{\mathrm{L,P}}^{JJ} = +1 \tag{B.4}$$

$$a_{\mathrm{L,P}}^{J\delta} = 4\pi\left(r_{\mathrm{o}} + 2\delta_{\mathrm{e}}^{\mathrm{o}}\left(\eta_{\mathrm{P}} - 2\right)\right)\Delta\eta_{\mathrm{P}}\rho_{\mathrm{L,e}}u_{\mathrm{L,P}}^{\mathrm{o}} \tag{B.5}$$

$$\begin{aligned} b_{\mathrm{L,P}}^{J} = {} & 4\pi\left(r_{\mathrm{o}} + 2\delta_{\mathrm{e}}^{\mathrm{o}}\left(\eta_{\mathrm{P}} - 2\right)\right)\delta_{\mathrm{P}}^{\mathrm{o}}\Delta\eta_{\mathrm{P}}\rho_{\mathrm{L,e}}u_{\mathrm{L,P}}^{\mathrm{o}} \\ & + 2\pi\left(\delta_{\mathrm{w}}\left(\eta_{\mathrm{P}} - 2\right) + r_{\mathrm{o}}\right)\delta_{\mathrm{w}}\Delta\eta_{\mathrm{P}}\rho_{\mathrm{L,w}}u_{\mathrm{L,w}} \end{aligned} \tag{B.6}$$

Liquid Momentum Equation

$$a_{\mathrm{L,S}}^{uu} u_{\mathrm{L,S}} + a_{\mathrm{L,S}}^{uJ} J_{\mathrm{L,S}} + a_{\mathrm{L,P}}^{uu} u_{\mathrm{L,P}} + a_{\mathrm{L,P}}^{uJ} J_{\mathrm{L,P}} + a_{\mathrm{L,N}}^{uu} u_{\mathrm{L,N}} + a_{\mathrm{L,P}}^{u\delta} \delta_{\mathrm{P}} + a_{\mathrm{L,P}}^{uP} P_{\mathrm{P}}^{'} = b_{\mathrm{L,P}}^{u} \tag{B.7}$$

where:

$$a_{\mathrm{L,S}}^{uu} = -\left(RSS + \alpha_{\mathrm{s}}^{u}\right)J_{\mathrm{L,S}}^{\mathrm{o}} - 2\pi\left(\delta_{\mathrm{P}}^{\mathrm{o}}\left(\eta_{\mathrm{s}} - 2\right) + r_{\mathrm{o}}\right)\frac{\beta_{\mathrm{s}}^{u}\mu_{\mathrm{L,s,eff}}\Delta\chi}{\delta_{\mathrm{P}}^{\mathrm{o}}\left(\eta_{\mathrm{P}} - \eta_{\mathrm{S}}\right)} \tag{B.8}$$

$$a_{L,S}^{uJ} = -u_{\mathrm{L,s}}^{\mathrm{o}} \tag{B.9}$$

$$\begin{aligned} a_{\mathrm{L,P}}^{uu} = {} & 4\pi\left(\delta_{\mathrm{e}}^{\mathrm{o}}\left(\eta_{\mathrm{P}} - 2\right) + r_{\mathrm{o}}\right)\delta_{\mathrm{e}}^{\mathrm{o}}\rho_{\mathrm{L,e}}u_{\mathrm{L,P}}^{\mathrm{o}}\Delta\eta_{\mathrm{P}} + \left(RNP + \alpha_{\mathrm{n}}^{u}\right)J_{\mathrm{L,P}}^{\mathrm{o}} - \left(RSP - \alpha_{\mathrm{s}}^{u}\right)J_{\mathrm{L,S}}^{\mathrm{o}} \\ & + 2\pi\left(\delta_{\mathrm{P}}^{\mathrm{o}}\left(\eta_{\mathrm{n}} - 2\right) + r_{\mathrm{o}}\right)\frac{\beta_{\mathrm{n}}^{u}\mu_{\mathrm{L,n,eff}}\Delta\chi}{\delta_{P}^{o}\left(\eta_{\mathrm{N}} - \eta_{\mathrm{P}}\right)} + 2\pi\left(\delta_{\mathrm{P}}^{\mathrm{o}}\left(\eta_{\mathrm{s}} - 2\right) + r_{\mathrm{o}}\right)\frac{\beta_{\mathrm{s}}^{u}\mu_{\mathrm{L,s,eff}}\Delta\chi}{\delta_{\mathrm{P}}^{\mathrm{o}}\left(\eta_{\mathrm{P}} - \eta_{\mathrm{S}}\right)} \end{aligned} \tag{B.10}$$

$$a_{\mathrm{L,P}}^{uJ} = u_{\mathrm{L,n}}^{\mathrm{o}} \tag{B.11}$$

$$a_{\mathrm{L,N}}^{uu} = \left(RNN - \alpha_{\mathrm{n}}^{u}\right) J_{\mathrm{L,P}}^{\mathrm{o}} - 2\pi\left(\delta_{\mathrm{P}}^{\mathrm{o}}\left(\eta_{\mathrm{L,n}} - 2\right) + r_{\mathrm{o}}\right)\frac{\beta_{\mathrm{n}}^{u}\mu_{\mathrm{L,n,eff}}\Delta\chi}{\delta_{\mathrm{P}}^{\mathrm{o}}\left(\eta_{\mathrm{L,N}} - \eta_{\mathrm{L,P}}\right)} \tag{B.12}$$

$$\begin{aligned} a_{\mathrm{L,P}}^{u\delta} &= 4\pi\left(2\delta_{\mathrm{e}}^{\mathrm{o}}\left(\eta_{\mathrm{P}} - 2\right) + r_{\mathrm{o}}\right)\rho_{\mathrm{L,e}}{u_{\mathrm{L,P}}^{\mathrm{o}}}^{2}\Delta\eta_{\mathrm{P}} \\ &\quad - 2\pi\left(2\delta_{\mathrm{P}}^{\mathrm{o}}\left(\eta_{\mathrm{P}} - 2\right) + r_{\mathrm{o}}\right)\rho_{\mathrm{L,P}} g\Delta\eta_{\mathrm{P}}\Delta\chi \\ &\quad + 2\pi\left(2\delta_{\mathrm{P}}^{\mathrm{o}}\left(\eta_{\mathrm{P}} - 2\right) + r_{\mathrm{o}}\right)P_{\mathrm{P}}'^{\mathrm{o}}\Delta\eta_{\mathrm{P}}\Delta\chi \\ &\quad + \frac{2\pi r_{\mathrm{o}}\mu_{\mathrm{L,n,eff}}\Delta\chi}{{\delta_{\mathrm{P}}^{\mathrm{o}}}^{2}}\frac{\partial u_{\mathrm{L}}}{\partial\eta}\bigg|_{n}^{o} - \frac{2\pi r_{\mathrm{o}}\mu_{\mathrm{L,s,eff}}\Delta\chi}{{\delta_{\mathrm{P}}^{\mathrm{o}}}^{2}}\frac{\partial u_{\mathrm{L}}}{\partial\eta}\bigg|_{s}^{o} \end{aligned} \tag{B.13}$$

$$a_{\mathrm{L,P}}^{up} = 2\pi\left(\delta_{\mathrm{P}}^{\mathrm{o}}\left(\eta_{\mathrm{P}} - 2\right) + r_{\mathrm{o}}\right)\delta_{\mathrm{P}}^{\mathrm{o}}\Delta\eta_{\mathrm{P}}\Delta\chi \tag{B.14}$$

$$\begin{aligned} b_{\mathrm{L,P}}^{u} &= 4\pi\left(2\delta_{\mathrm{e}}^{\mathrm{o}}\left(\eta_{\mathrm{P}} - 2\right) + r_{\mathrm{o}}\right)\delta_{\mathrm{P}}^{\mathrm{o}}\rho_{\mathrm{L,e}}{u_{\mathrm{L,P}}^{\mathrm{o}}}^{2}\Delta\eta_{\mathrm{P}} \\ &\quad + 2\pi\left(\delta_{\mathrm{e}}^{\mathrm{o}}\left(\eta_{\mathrm{P}} - 2\right) + r_{\mathrm{o}}\right)\delta_{\mathrm{e}}^{\mathrm{o}}\rho_{\mathrm{L,e}}{u_{\mathrm{L,P}}^{\mathrm{o}}}^{2}\Delta\eta_{\mathrm{P}} \\ &\quad + 2\pi\left(\delta_{\mathrm{w}}\left(\eta_{\mathrm{P}} - 2\right) + r_{\mathrm{o}}\right)\delta_{\mathrm{w}}\rho_{\mathrm{L,w}}{u_{\mathrm{L,W}}}^{2}\Delta\eta_{\mathrm{P}} \\ &\quad + J_{\mathrm{L,P}}^{\mathrm{o}}u_{\mathrm{L,n}}^{\mathrm{o}} - J_{\mathrm{L,S}}^{\mathrm{o}}u_{\mathrm{L,s}}^{\mathrm{o}} + \frac{2\pi r_{\mathrm{o}}\mu_{\mathrm{L,n,eff}}\Delta\chi}{\delta_{\mathrm{P}}^{\mathrm{o}}}\frac{\partial u_{\mathrm{L}}}{\partial\eta}\bigg|_{\mathrm{n}}^{\mathrm{o}} \\ &\quad - \frac{2\pi r_{\mathrm{o}}\mu_{\mathrm{L,s,eff}}\Delta\chi}{\delta_{\mathrm{P}}^{\mathrm{o}}}\frac{\partial u_{\mathrm{L}}}{\partial\eta}\bigg|_{\mathrm{s}}^{\mathrm{o}} - 2\pi\left(\eta_{\mathrm{P}} - 2\right){\delta_{\mathrm{P}}^{\mathrm{o}}}^{2}\rho_{\mathrm{L,P}} g\Delta\eta_{\mathrm{P}}\Delta\chi \\ &\quad + 2\pi\left(2\delta_{\mathrm{P}}^{\mathrm{o}}\left(\eta_{\mathrm{P}} - 2\right) + r_{\mathrm{o}}\right)\delta_{\mathrm{P}}^{\mathrm{o}}P_{\mathrm{P}}'^{\mathrm{o}}\Delta\eta_{\mathrm{P}}\Delta\chi \end{aligned} \tag{B.15}$$

Liquid Energy Equation

$$\begin{aligned} &a_{\mathrm{L,S}}^{TJ}J_{\mathrm{L,S}} + a_{\mathrm{L,S}}^{TT}T_{\mathrm{L,S}} + a_{\mathrm{L,P}}^{Tu}u_{\mathrm{L,P}} + a_{\mathrm{L,P}}^{TJ}J_{\mathrm{L,P}} + \\ &\qquad a_{\mathrm{L,P}}^{TT}T_{\mathrm{L,P}} + a_{\mathrm{L,N}}^{TT}T_{\mathrm{L,N}} + a_{\mathrm{L,P}}^{T\delta}\delta_{\mathrm{P}} = b_{\mathrm{L,P}}^{T} \end{aligned} \tag{B.16}$$

where,

$$a_{\mathrm{L,S}}^{TJ} = -C_{P,\mathrm{L,s}}T_{\mathrm{L,s}}^{\mathrm{o}} \tag{B.17}$$

$$a_{\mathrm{L,S}}^{TT} = -C_{P,\mathrm{L,s}}\left(RSS + \alpha_{\mathrm{s}}^{T}\right)J_{\mathrm{L,S}}^{\mathrm{o}} - 2\pi\left(\delta_{\mathrm{P}}^{\mathrm{o}}\left(\eta_{\mathrm{s}} - 2\right) + r_{\mathrm{o}}\right)\frac{\beta_{\mathrm{s}}^{T}\lambda_{\mathrm{L,s,eff}}\Delta\chi}{\delta_{\mathrm{P}}^{\mathrm{o}}\left(\eta_{\mathrm{P}} - \eta_{\mathrm{S}}\right)} \tag{B.18}$$

$$a_{\mathrm{L,P}}^{\mathrm{Tu}} = 2\pi\left(\delta_{\mathrm{e}}^{\mathrm{o}}\left(\eta_{\mathrm{P}} - 2\right) + r_{\mathrm{o}}\right)\delta_{\mathrm{e}}^{\mathrm{o}}\rho_{\mathrm{L,e}}C_{P,\mathrm{L,e}}T_{\mathrm{L,P}}^{\mathrm{o}}\Delta\eta_{\mathrm{P}} \tag{B.19}$$

$$a_{\mathrm{L,P}}^{Tu} = 2\pi\left(\delta_{\mathrm{e}}^{\mathrm{o}}\left(\eta_{\mathrm{P}}-2\right)+r_{\mathrm{o}}\right)\delta_{\mathrm{e}}^{\mathrm{o}}\rho_{\mathrm{L,e}}C_{P,\mathrm{L,e}}T_{\mathrm{L,P}}^{\mathrm{o}}\Delta\eta_{\mathrm{P}} \tag{B.20}$$

$$a_{\mathrm{L,P}}^{TJ} = C_{P,\mathrm{L,n}}T_{\mathrm{L,n}}^{\mathrm{o}} \tag{B.21}$$

$$\begin{aligned} a_{\mathrm{L,P}}^{TT} &= 2\pi\left(\delta_{\mathrm{e}}^{\mathrm{o}}\left(\eta_{\mathrm{P}}-2\right)+r_{\mathrm{o}}\right)\delta_{\mathrm{e}}^{\mathrm{o}}\rho_{\mathrm{L,e}}C_{P,\mathrm{L,e}}u_{\mathrm{L,P}}^{\mathrm{o}}\Delta\eta_{\mathrm{P}} + C_{P,\mathrm{L,n}}\left(RNP+\alpha_{\mathrm{n}}^{T}\right)J_{\mathrm{L,P}}^{\mathrm{o}} \\ &\quad - C_{P,\mathrm{L,s}}\left(RSP-\alpha_{\mathrm{s}}^{T}\right)J_{\mathrm{L,S}}^{\mathrm{o}} + 2\pi\left(\delta_{\mathrm{P}}^{\mathrm{o}}\left(\eta_{\mathrm{n}}-2\right)+r_{\mathrm{o}}\right)\frac{\beta_{\mathrm{n}}^{T}\lambda_{\mathrm{L,n,eff}}\Delta\chi}{\delta_{\mathrm{P}}^{\mathrm{o}}\left(\eta_{\mathrm{N}}-\eta_{\mathrm{P}}\right)} \\ &\quad + 2\pi\left(\delta_{\mathrm{P}}^{\mathrm{o}}\left(\eta_{\mathrm{s}}-2\right)+r_{\mathrm{o}}\right)\frac{\beta_{\mathrm{s}}^{T}\lambda_{\mathrm{L,s,eff}}\Delta\chi}{\delta_{\mathrm{P}}^{\mathrm{o}}\left(\eta_{\mathrm{P}}-\eta_{\mathrm{S}}\right)} \end{aligned} \tag{B.22}$$

$$a_{\mathrm{L,N}}^{\mathrm{TT}} = C_{P,\mathrm{L,n}}\left(RNN-\alpha_{\mathrm{n}}^{\mathrm{T}}\right)J_{\mathrm{L,P}}^{\mathrm{o}} - 2\pi\left(\delta_{\mathrm{P}}^{\mathrm{o}}\left(\eta_{\mathrm{n}}-2\right)+r_{\mathrm{o}}\right)\frac{\beta_{\mathrm{n}}^{T}\lambda_{\mathrm{L,n,eff}}\Delta\chi}{\delta_{\mathrm{P}}^{\mathrm{o}}\left(\eta_{\mathrm{N}}-\eta_{\mathrm{P}}\right)} \tag{B.23}$$

$$\begin{aligned} a_{\mathrm{L,P}}^{T\delta} &= 4\pi\left(2\delta_{\mathrm{e}}^{\mathrm{o}}\left(\eta_{\mathrm{P}}-2\right)+r_{\mathrm{o}}\right)\rho_{\mathrm{L,e}}C_{P,\mathrm{L,e}}T_{\mathrm{L,P}}^{\mathrm{o}}u_{\mathrm{L,P}}^{\mathrm{o}}\Delta\eta_{\mathrm{P}} + \frac{2\pi r_{\mathrm{o}}\lambda_{\mathrm{L,n,eff}}\Delta\chi}{\delta_{\mathrm{P}}^{\mathrm{o}2}}\frac{\partial T_{\mathrm{L}}}{\partial\eta}\bigg|_{\mathrm{n}}^{\mathrm{o}} \\ &\quad - \frac{2\pi r_{\mathrm{o}}\lambda_{\mathrm{L,s,eff}}\Delta\chi}{\delta_{\mathrm{P}}^{\mathrm{o}2}}\frac{\partial T_{\mathrm{L}}}{\partial\eta}\bigg|_{\mathrm{s}}^{\mathrm{o}} \end{aligned} \tag{B.24}$$

$$\begin{aligned} b_{\mathrm{L,P}}^{T} &= 4\pi\left(2\delta_{\mathrm{e}}^{\mathrm{o}}\left(\eta_{\mathrm{P}}-2\right)+r_{\mathrm{o}}\right)\delta_{\mathrm{P}}^{\mathrm{o}}\rho_{\mathrm{L,e}}C_{P,\mathrm{L,e}}T_{\mathrm{L,P}}^{\mathrm{o}}u_{\mathrm{L,P}}^{\mathrm{o}}\Delta\eta_{\mathrm{P}} \\ &\quad + 2\pi\left(\delta_{\mathrm{e}}^{\mathrm{o}}\left(\eta_{\mathrm{P}}-2\right)+r_{\mathrm{o}}\right)\delta_{\mathrm{P}}^{\mathrm{o}}\rho_{\mathrm{L,e}}C_{P,\mathrm{L,e}}T_{\mathrm{L,P}}^{\mathrm{o}}u_{\mathrm{L,P}}^{\mathrm{o}}\Delta\eta_{\mathrm{P}} \\ &\quad + 2\pi\left(\delta_{\mathrm{w}}^{\mathrm{o}}\left(\eta_{\mathrm{P}}-2\right)+r_{\mathrm{o}}\right)\delta_{\mathrm{w}}^{\mathrm{o}}\rho_{\mathrm{L,w}}C_{P,\mathrm{L,w}}T_{\mathrm{L,W}}^{\mathrm{o}}u_{\mathrm{L,W}}^{\mathrm{o}}\Delta\eta_{\mathrm{P}} \\ &\quad + C_{P,\mathrm{L,n}}J_{\mathrm{L,P}}^{\mathrm{o}}T_{\mathrm{L,n}}^{\mathrm{o}} - C_{P,\mathrm{L,s}}J_{\mathrm{L,S}}^{\mathrm{o}}T_{\mathrm{L,s}}^{\mathrm{o}} \\ &\quad + \frac{2\pi r_{\mathrm{o}}\lambda_{\mathrm{L,n,eff}}\Delta\chi}{\delta_{\mathrm{P}}^{\mathrm{o}}}\frac{\partial T_{\mathrm{L}}}{\partial\eta}\bigg|_{\mathrm{n}}^{\mathrm{o}} - \frac{2\pi r_{\mathrm{o}}\lambda_{\mathrm{L,s,eff}}\Delta\chi}{\delta_{\mathrm{P}}^{\mathrm{o}}}\frac{\partial T_{\mathrm{L}}}{\partial\eta}\bigg|_{\mathrm{s}}^{\mathrm{o}} \end{aligned} \tag{B.25}$$

B.2 Discretized Equations in the Mixture Region

Mixture Continuity Equation

$$a_{\mathrm{M,S}}^{JJ}J_{\mathrm{M,S}} + a_{\mathrm{M,P}}^{Ju}u_{\mathrm{M,P}} + a_{\mathrm{M,P}}^{JJ}J_{\mathrm{M,P}} + a_{\mathrm{M,P}}^{J\delta}\delta_{\mathrm{P}} = b_{\mathrm{M,P}}^{J} \tag{B.26}$$

where,

$$a_{\mathrm{M,S}}^{JJ} = -1 \tag{B.27}$$

$$a_{\mathrm{M,P}}^{Ju} = 2\pi\left(r_{\mathrm{o}} - \delta_{\mathrm{e}}^{\mathrm{o}}\right)^2 \rho_{\mathrm{M,e}} \eta_{\mathrm{P}} \Delta\eta_{\mathrm{P}} \tag{B.28}$$

$$a_{\mathrm{M,P}}^{JJ} = +1 \tag{B.29}$$

$$a_{\mathrm{M,P}}^{J\delta} = -8\pi\left(r_{\mathrm{o}} - \delta_{\mathrm{e}}^{\mathrm{o}}\right)\rho_{\mathrm{M,e}} u_{\mathrm{M,P}}^{\mathrm{o}} \eta_{\mathrm{P}} \Delta\eta_{\mathrm{P}} \tag{B.30}$$

$$b_{\mathrm{M,P}}^{J} - 8\pi\left(r_{\mathrm{o}} - \delta_{\mathrm{e}}^{\mathrm{o}}\right)\delta_{\mathrm{P}}^{\mathrm{o}} \rho_{\mathrm{M,e}} u_{\mathrm{M,P}}^{\mathrm{o}} \eta_{\mathrm{P}} \Delta\eta_{\mathrm{P}} + 2\pi\left(r_{\mathrm{o}} - \delta_{\mathrm{w}}\right)^2 \rho_{\mathrm{M,w}} u_{\mathrm{M,w}} \eta_{\mathrm{P}} \Delta\eta_{\mathrm{P}} \tag{B.31}$$

Mixture Momentum Equation

$$a_{\mathrm{M,S}}^{uu} u_{\mathrm{M,S}} + a_{\mathrm{M,S}}^{uJ} J_{\mathrm{M,S}} + a_{\mathrm{M,P}}^{uu} u_{\mathrm{M,P}} + a_{\mathrm{M,P}}^{uJ} J_{\mathrm{M,P}} + a_{\mathrm{M,N}}^{uu} u_{\mathrm{M,N}} + a_{\mathrm{M,P}}^{u\delta} \delta_{\mathrm{P}} + a_{\mathrm{M,P}}^{uP} P_{\mathrm{P}}^{'} = b_{\mathrm{M,P}}^{u} \tag{B.32}$$

where,

$$a_{\mathrm{M,S}}^{uu} = -\left(RSS + \alpha_{\mathrm{s}}^{u}\right) J_{\mathrm{M,S}}^{\mathrm{o}} - 2\pi\eta_{\mathrm{s}} \frac{\beta_{\mathrm{s}}^{u} \mu_{\mathrm{M,s,eff}} \Delta\chi}{\left(\eta_{\mathrm{P}} - \eta_{\mathrm{S}}\right)} \tag{B.33}$$

$$a_{\mathrm{M,S}}^{uJ} = -u_{\mathrm{M,s}}^{\mathrm{o}} \tag{B.34}$$

$$a_{\mathrm{M,P}}^{uu} = 4\pi\left(r_{\mathrm{o}} - \delta_{\mathrm{e}}^{\mathrm{o}}\right)^2 \rho_{\mathrm{M,e}} u_{\mathrm{M,P}}^{\mathrm{o}} \eta_{\mathrm{P}} \Delta\eta_{\mathrm{P}} + \left(RNP + \alpha_{\mathrm{n}}^{u}\right) J_{\mathrm{M,P}}^{\mathrm{o}} - \left(RSP - \alpha_{\mathrm{s}}^{u}\right) J_{\mathrm{M,S}}^{\mathrm{o}} + 2\pi\eta_{\mathrm{n}} \mu_{\mathrm{M,n,eff}} \left(\frac{\beta_{\mathrm{n}}^{u}}{\eta_{\mathrm{N}} - \eta_{\mathrm{P}}}\right)\Delta\chi + 2\pi\eta_{\mathrm{s}} \mu_{\mathrm{M,s,eff}} \left(\frac{\beta_{\mathrm{s}}^{u}}{\eta_{\mathrm{P}} - \eta_{\mathrm{S}}}\right)\Delta\chi \tag{B.35}$$

$$a_{\mathrm{M,P}}^{uJ} = u_{\mathrm{M,n}}^{\mathrm{o}} \tag{B.36}$$

$$a_{\mathrm{M,N}}^{uu} = \left(RNN - \alpha_{\mathrm{n}}^{u}\right) J_{\mathrm{M,P}}^{\mathrm{o}} - 2\pi\eta_{\mathrm{n}} \frac{\beta_{\mathrm{n}}^{u} \mu_{\mathrm{M,n,eff}} \Delta\chi}{\left(\eta_{\mathrm{N}} - \eta_{\mathrm{P}}\right)} \tag{B.37}$$

$$a_{\mathrm{M,P}}^{u\delta} = -8\pi\eta_{\mathrm{P}} \Delta\eta_{\mathrm{P}} \left(r_{\mathrm{o}} - \delta_{\mathrm{e}}^{\mathrm{o}}\right)\rho_{\mathrm{M,e}} {u_{\mathrm{M,P}}^{\mathrm{o}}}^{2} + 4\pi\eta_{\mathrm{P}} \rho_{\mathrm{M,e}} g \Delta\eta_{\mathrm{P}} \Delta\chi (r_{\mathrm{o}} - \delta_{\mathrm{P}}^{\mathrm{o}}) - 4\pi\eta_{\mathrm{P}} \left.\frac{dP}{d\chi}\right|_{\mathrm{P}}^{\mathrm{o}} \Delta\eta_{\mathrm{P}} \Delta\chi (r_{\mathrm{o}} - \delta_{\mathrm{P}}^{\mathrm{o}}) \tag{B.38}$$

$$a_{\mathrm{M,P}}^{up} = 2\pi\left(r_{\mathrm{o}} - \delta_{\mathrm{P}}^{\mathrm{o}}\right)^2 \eta_{\mathrm{P}} \Delta\eta_{\mathrm{P}} \Delta\chi \tag{B.39}$$

$$
\begin{aligned}
b^{u}_{\mathrm{M,P}} &= 2\pi\eta_{\mathrm{P}}\Delta\eta_{\mathrm{P}}\left(r_{\mathrm{o}}-\delta_{e}^{o}\right)^{2}\rho_{\mathrm{M,e}}u^{\mathrm{o}}_{\mathrm{M,P}}u^{\mathrm{o}}_{\mathrm{M,P}} \\
&\quad -8\pi\eta_{\mathrm{P}}\Delta\eta_{\mathrm{P}}\rho_{\mathrm{M,e}}{u_{\mathrm{M,P}}}^{\mathrm{o}2}\left(r_{\mathrm{o}}-\delta_{e}^{o}\right)\delta^{\mathrm{o}}_{\mathrm{P}} \\
&\quad +2\pi\eta_{\mathrm{P}}\Delta\eta_{\mathrm{P}}\left(r_{\mathrm{o}}-\delta_{\mathrm{w}}\right)^{2}\rho_{\mathrm{M,w}}{u_{\mathrm{M,W}}}^{2} \\
&\quad +2\pi\eta_{\mathrm{P}}\rho_{\mathrm{M,e}}g\Delta\eta_{P}\Delta\chi({r_{\mathrm{o}}}^{2}-{\delta^{\mathrm{o}2}_{\mathrm{P}}}) \\
&\quad -4\pi\eta_{\mathrm{P}}\delta^{\mathrm{o}}_{\mathrm{P}}\left.\frac{dP}{d\chi}\right|^{\mathrm{o}}_{\mathrm{P}}\Delta\eta_{\mathrm{P}}\Delta\chi(r_{\mathrm{o}}-\delta^{\mathrm{o}}_{\mathrm{P}}) \\
&\quad +J^{\mathrm{o}}_{\mathrm{M,P}}{u_{\mathrm{M,n}}}^{\mathrm{o}}-J^{\mathrm{o}}_{\mathrm{M,S}}u^{\mathrm{o}}_{\mathrm{M,s}}
\end{aligned}
\tag{B.40}
$$

Mixture Energy Equation

$$
\begin{aligned}
&a^{TJ}_{\mathrm{M,S}}J_{\mathrm{M,S}}+a^{TT}_{\mathrm{M,S}}T_{\mathrm{M,S}}+a^{TW}_{\mathrm{M,S}}W_{\mathrm{S}}+a^{Tu}_{\mathrm{M,P}}u_{\mathrm{M,P}}+a^{TJ}_{\mathrm{M,P}}J_{\mathrm{M,P}}+ \\
&\qquad a^{TT}_{\mathrm{M,P}}T_{\mathrm{M,P}}+a^{TW}_{\mathrm{M,P}}W_{P}+a^{TT}_{M,N}T_{\mathrm{M,N}}+a^{TW}_{M,N}W_{N}+a^{T\delta}_{\mathrm{M,P}}\delta_{\mathrm{P}}=b^{T}_{\mathrm{M,P}}
\end{aligned}
\tag{B.41}
$$

where

$$
a^{TJ}_{\mathrm{M,S}}=-C_{P,\mathrm{M,s}}T^{\mathrm{o}}_{\mathrm{M,s}} \tag{B.42}
$$

$$
\begin{aligned}
a^{TT}_{\mathrm{M,S}} &= -C_{P,\mathrm{M,s}}\left(RSS+\alpha^{T}_{\mathrm{s}}\right)J^{\mathrm{o}}_{\mathrm{M,S}}-2\pi\eta_{\mathrm{s}}\frac{\beta^{T}_{\mathrm{s}}\lambda_{\mathrm{M,s,eff}}\Delta\chi}{\left(\eta_{\mathrm{P}}-\eta_{\mathrm{S}}\right)} \\
&\quad +2\pi\eta_{\mathrm{s}}\rho_{\mathrm{M,s}}D_{\mathrm{s,eff}}\left(C_{P,\mathrm{g}}-C_{P,\mathrm{v}}\right)\Delta\chi\left.\frac{\partial W}{\partial\eta}\right|^{\mathrm{o}}_{\mathrm{s}}\left(RSS+\alpha^{T}_{\mathrm{s}}\right)
\end{aligned}
\tag{B.43}
$$

$$
a^{TW}_{\mathrm{M,S}}=-2\pi\eta_{\mathrm{s}}\frac{\beta^{T}_{\mathrm{s}}\rho_{\mathrm{M,s}}D_{\mathrm{s,eff}}\left(C_{P,\mathrm{g}}-C_{P,\mathrm{v}}\right)_{\mathrm{s}}T^{\mathrm{o}}_{\mathrm{M,s}}\Delta\chi}{\left(\eta_{\mathrm{P}}-\eta_{\mathrm{S}}\right)} \tag{B.44}
$$

$$
a^{Tu}_{\mathrm{M,P}}=2\pi\left(r_{\mathrm{o}}-\delta^{\mathrm{o}}_{\mathrm{e}}\right)^{2}\rho_{\mathrm{M,e}}C_{P,\mathrm{M,e}}T^{\mathrm{o}}_{\mathrm{M,P}}\eta_{\mathrm{P}}\Delta\eta_{\mathrm{P}} \tag{B.45}
$$

$$
a^{TJ}_{\mathrm{M,P}}=C_{P,\mathrm{M,n}}T^{\mathrm{o}}_{\mathrm{M,n}} \tag{B.46}
$$

$$a_{\mathrm{M,P}}^{TT} = 2\pi\left(r_{\mathrm{o}} - \delta_{\mathrm{e}}^{\mathrm{o}}\right)^2 \rho_{\mathrm{M,e}} C_{P,\mathrm{M,e}} u_{\mathrm{M,P}}^{\mathrm{o}} \eta_{\mathrm{P}} \Delta\eta_{\mathrm{P}} + C_{P,\mathrm{M,n}}\left(RNP + \alpha_{\mathrm{n}}^{T}\right) J_{\mathrm{M,P}}^{\mathrm{o}}$$
$$- C_{P,\mathrm{M,s}}\left(RSP - \alpha_{\mathrm{s}}^{T}\right) J_{\mathrm{M,S}}^{\mathrm{o}} + 2\pi\eta_{\mathrm{n}} \frac{\beta_{\mathrm{n}}^{T} \lambda_{\mathrm{M,n,eff}} \Delta\chi}{\left(\eta_{\mathrm{N}} - \eta_{\mathrm{P}}\right)} + 2\pi\eta_{\mathrm{s}} \frac{\beta_{\mathrm{s}}^{T} \lambda_{\mathrm{M,s,eff}} \Delta\chi}{\left(\eta_{\mathrm{P}} - \eta_{\mathrm{S}}\right)}$$
$$- 2\pi\eta_{\mathrm{n}} \rho_{\mathrm{M,n}} D_{\mathrm{n,eff}} \left(C_{P,\mathrm{g}} - C_{P,\mathrm{v}}\right)_{\mathrm{n}} \Delta\chi \left.\frac{\partial W}{\partial \eta}\right|_{\mathrm{n}}^{\mathrm{o}} \left(RNP + \alpha_{\mathrm{n}}^{T}\right) \tag{B.47}$$
$$+ 2\pi\eta_{\mathrm{n}} \rho_{\mathrm{M,s}} D_{\mathrm{s,eff}} \left(C_{P,\mathrm{g}} - C_{P,\mathrm{v}}\right)_{s} \Delta\chi \left.\frac{\partial W}{\partial \eta}\right|_{\mathrm{s}}^{\mathrm{o}} \left(RSP - \alpha_{\mathrm{s}}^{T}\right)$$

$$a_{\mathrm{M,P}}^{TW} = 2\pi\eta_{\mathrm{n}} \frac{\beta_{\mathrm{M,n}}^{T} \rho_{\mathrm{M,n}} D_{\mathrm{n,eff}} \left(C_{P,\mathrm{g}} - C_{P,\mathrm{v}}\right)_{\mathrm{n}} T_{\mathrm{M,n}}^{\mathrm{o}} \Delta\chi}{\left(\eta_{\mathrm{N}} - \eta_{\mathrm{P}}\right)}$$
$$+ 2\pi\eta_{\mathrm{s}} \frac{\beta_{\mathrm{M,s}}^{T} \rho_{\mathrm{M,s}} D_{\mathrm{s,eff}} \left(C_{P,\mathrm{g}} - C_{P,\mathrm{v}}\right)_{\mathrm{s}} T_{\mathrm{M,s}}^{\mathrm{o}} \Delta\chi}{\left(\eta_{\mathrm{P}} - \eta_{\mathrm{S}}\right)} \tag{B.48}$$

$$a_{\mathrm{M,N}}^{TT} = C_{P,\mathrm{M,n}}\left(RNN - \alpha_{\mathrm{n}}\right) J_{\mathrm{M,P}}^{\mathrm{o}} - 2\pi\eta_{\mathrm{n}} \frac{\beta_{\mathrm{n}}^{T} \lambda_{\mathrm{M,n,eff}} \Delta\chi}{\left(\eta_{\mathrm{N}} - \eta_{\mathrm{P}}\right)}$$
$$- 2\pi\eta_{\mathrm{n}} \rho_{\mathrm{M,n}} D_{\mathrm{n,eff}} \left(C_{P,\mathrm{g}} - C_{P,\mathrm{v}}\right)_{\mathrm{n}} \Delta\chi \left.\frac{\partial W}{\partial \eta}\right|_{\mathrm{n}}^{\mathrm{o}} \left(RNN - \alpha_{\mathrm{n}}^{T}\right) \tag{B.49}$$

$$a_{\mathrm{M,N}}^{TW} = -2\pi\eta_{\mathrm{n}} \frac{\beta_{\mathrm{n}}^{T} \rho_{\mathrm{M,n}} D_{\mathrm{n,eff}} \left(C_{P,\mathrm{g}} - C_{P,\mathrm{v}}\right)_{\mathrm{n}} T_{\mathrm{M,n}}^{\mathrm{o}} \Delta\chi}{\left(\eta_{\mathrm{N}} - \eta_{\mathrm{P}}\right)} \tag{B.50}$$

$$a_{\mathrm{M,P}}^{T\delta} = -8\pi\left(r_{\mathrm{o}} - \delta_{\mathrm{e}}^{\mathrm{o}}\right) \rho_{\mathrm{M,e}} C_{P,\mathrm{M,e}} T_{\mathrm{M,P}}^{\mathrm{o}} u_{\mathrm{M,P}}^{\mathrm{o}} \eta_{\mathrm{P}} \Delta\eta_{\mathrm{P}} \tag{B.51}$$

$$
\begin{aligned}
b_{\mathrm{M,P}}^{T} = & -8\pi\left(r_{\mathrm{o}}-\delta_{e}^{o}\right)\delta_{\mathrm{P}}^{\mathrm{o}}\rho_{\mathrm{M,e}}C_{P,\mathrm{M,e}}T_{\mathrm{M,P}}^{\mathrm{o}}u_{\mathrm{M,P}}^{\mathrm{o}}\eta_{\mathrm{P}}\Delta\eta_{\mathrm{P}} \\
& +2\pi\left(r_{\mathrm{o}}-\delta_{e}^{o}\right)^{2}\rho_{\mathrm{M,e}}C_{P,\mathrm{M,e}}T_{\mathrm{M,P}}^{\mathrm{o}}u_{\mathrm{M,P}}^{\mathrm{o}}\eta_{\mathrm{P}}\Delta\eta_{\mathrm{P}} \\
& +2\pi\left(r_{\mathrm{o}}-\delta_{\mathrm{w}}^{\mathrm{o}}\right)^{2}\rho_{\mathrm{M,w}}C_{P,\mathrm{M,w}}T_{\mathrm{M,W}}^{\mathrm{o}}u_{\mathrm{M,W}}^{\mathrm{o}}\eta_{\mathrm{P}}\Delta\eta_{\mathrm{P}} \\
& +C_{P,\mathrm{M,n}}J_{\mathrm{M,P}}^{\mathrm{o}}T_{\mathrm{M,n}}^{\mathrm{o}}-C_{P,\mathrm{M,s}}J_{\mathrm{M,S}}^{\mathrm{o}}T_{\mathrm{M,s}}^{\mathrm{o}} \\
& -2\pi\eta_{\mathrm{n}}\rho_{\mathrm{M,n}}D_{\mathrm{n,eff}}\left(C_{P,\mathrm{g}}-C_{P,\mathrm{v}}\right)_{\mathrm{n}}\Delta\chi\left.\frac{\partial W}{\partial\eta}\right|_{\mathrm{n}}^{\mathrm{o}}T_{\mathrm{M,n}}^{\mathrm{o}} \\
& +2\pi\eta_{\mathrm{s}}\rho_{\mathrm{M,s}}D_{\mathrm{s,eff}}\left(C_{P,\mathrm{g}}-C_{P,\mathrm{v}}\right)_{\mathrm{s}}\Delta\chi\left.\frac{\partial W}{\partial\eta}\right|_{s}^{o}T_{\mathrm{M,s}}^{\mathrm{o}}
\end{aligned}
\tag{B.52}
$$

Mixture Mass Diffusion Equation

$$
a_{\mathrm{M,S}}^{WJ}J_{\mathrm{M,S}}+a_{\mathrm{M,S}}^{WW}W_{\mathrm{S}}+a_{\mathrm{M,P}}^{Wu}u_{\mathrm{M,P}}+a_{\mathrm{M,P}}^{WJ}J_{\mathrm{M,P}}+a_{\mathrm{M,N}}^{WW}W_{\mathrm{N}}+a_{\mathrm{M,P}}^{W\delta}\delta_{\mathrm{P}}=b_{\mathrm{M,P}}^{W} \tag{B.53}
$$

where

$$
a_{\mathrm{M,S}}^{WJ}=-W_{\mathrm{s}}^{\mathrm{o}} \tag{B.54}
$$

$$
a_{\mathrm{M,S}}^{WW}=-\left(RSS+\alpha_{\mathrm{s}}^{W}\right)J_{\mathrm{M,S}}^{\mathrm{o}}-2\pi\eta_{\mathrm{S}}\frac{\beta_{\mathrm{s}}^{W}\rho_{\mathrm{M,s}}D_{\mathrm{s,eff}}\Delta\chi}{\left(\eta_{\mathrm{P}}-\eta_{S}\right)} \tag{B.55}
$$

$$
a_{\mathrm{M,P}}^{Wu}=2\pi\left(r_{\mathrm{o}}-\delta_{\mathrm{e}}^{\mathrm{o}}\right)^{2}\rho_{\mathrm{M,e}}W_{\mathrm{P}}^{\mathrm{o}}\eta_{\mathrm{P}}\Delta\eta_{\mathrm{P}} \tag{B.56}
$$

$$
a_{\mathrm{M,P}}^{WJ}=W_{\mathrm{n}}^{\mathrm{o}} \tag{B.57}
$$

$$
\begin{aligned}
a_{\mathrm{M,P}}^{WW} = & 2\pi\left(r_{\mathrm{o}}-\delta_{\mathrm{e}}^{\mathrm{o}}\right)^{2}\rho_{\mathrm{M,e}}u_{\mathrm{M,P}}^{\mathrm{o}}\eta_{\mathrm{P}}\Delta\eta_{\mathrm{P}}+\left(RNP+\alpha_{\mathrm{n}}^{W}\right)J_{\mathrm{M,P}}^{\mathrm{o}}-\left(RSP-\alpha_{\mathrm{s}}^{W}\right)J_{\mathrm{M,S}}^{\mathrm{o}} \\
& +2\pi\eta_{\mathrm{n}}\frac{\beta_{\mathrm{n}}^{W}\rho_{\mathrm{M,n}}D_{\mathrm{n,eff}}\Delta\chi}{\left(\eta_{\mathrm{N}}-\eta_{\mathrm{P}}\right)}+2\pi\eta_{\mathrm{s}}\frac{\beta_{\mathrm{s}}^{W}\rho_{\mathrm{M,s}}D_{\mathrm{s,eff}}\Delta\chi}{\left(\eta_{\mathrm{P}}-\eta_{\mathrm{S}}\right)}
\end{aligned}
\tag{B.58}
$$

$$
a_{\mathrm{M,P}}^{W\delta}=-8\pi\left(r_{\mathrm{o}}-\delta_{\mathrm{e}}^{\mathrm{o}}\right)\rho_{\mathrm{M,e}}u_{\mathrm{M,P}}^{\mathrm{o}}\eta_{\mathrm{P}}\Delta\eta_{\mathrm{P}} \tag{B.59}
$$

$$
\begin{aligned}
b_{\mathrm{M,P}}^{W} = & -8\pi\left(r_{\mathrm{o}}-\delta_{\mathrm{e}}^{\mathrm{o}}\right)\delta_{\mathrm{P}}^{\mathrm{o}}\rho_{\mathrm{M,e}}u_{\mathrm{M,P}}^{\mathrm{o}}W_{\mathrm{P}}^{\mathrm{o}}\eta_{\mathrm{P}}\Delta\eta_{\mathrm{P}} \\
& +2\pi\left(r_{\mathrm{o}}-\delta_{\mathrm{e}}^{\mathrm{o}}\right)^{2}\rho_{\mathrm{M,e}}u_{\mathrm{M,P}}^{\mathrm{o}}W_{\mathrm{P}}^{\mathrm{o}}\eta_{\mathrm{P}}\Delta\eta_{\mathrm{P}} \\
& +2\pi\left(r_{\mathrm{o}}-\delta_{\mathrm{w}}\right)^{2}\rho_{\mathrm{M,w}}u_{\mathrm{M,W}}W_{\mathrm{W}}\eta_{\mathrm{P}}\Delta\eta_{\mathrm{P}}+J_{\mathrm{M,P}}^{\mathrm{o}}W_{\mathrm{n}}^{\mathrm{o}}-J_{\mathrm{M,S}}^{\mathrm{o}}W_{\mathrm{S}}^{\mathrm{o}}
\end{aligned}
\tag{B.60}
$$

APPENDIX C

Discretization of k-ε Model

C.1 Discretized Kinetic Energy Equation

Liquid kinetic energy equation

$$a_{\mathrm{L,S}}^{kk}k_{\mathrm{L,S}}+a_{\mathrm{L,N}}^{kk}k_{\mathrm{L,N}}+a_{\mathrm{L,P}}^{kk}k_{\mathrm{L,P}}=b_{\mathrm{L,P}}^{k} \tag{C.1}$$

$$a_{\mathrm{L,S}}^{kk}=-J_{\mathrm{L,s}}\left(RSS+\alpha_{\mathrm{s}}^{k}\right)-2\pi\Delta\chi\beta_{\mathrm{s}}^{k}\left(\delta_{\mathrm{P}}\left(\eta_{\mathrm{s}}-2\right)+r_{\mathrm{o}}\right)\frac{\left(\mu_{\mathrm{L,s}}+\dfrac{\mu_{\mathrm{L,s}}^{\mathrm{t}}}{\sigma_{k}}\right)}{\delta_{\mathrm{P}}\left(\eta_{\mathrm{P}}-\eta_{\mathrm{S}}\right)}+ \tag{C.2}$$
$$\frac{4\pi\Delta\chi\mu_{\mathrm{L,P}}\left(\delta_{\mathrm{P}}\left(\eta_{\mathrm{P}}-2\right)+r_{\mathrm{o}}\right)}{\delta_{\mathrm{P}}\Delta\eta_{\mathrm{P}}}\left(1-\sqrt{\frac{k_{\mathrm{L,n}}^{\mathrm{o}}}{k_{\mathrm{L,s}}^{\mathrm{o}}}}\right)\left(RSS+\alpha_{\mathrm{s}}^{k}\right)$$

$$a_{\mathrm{L,N}}^{kk}=J_{\mathrm{L,n}}\left(RNN-\alpha_{\mathrm{n}}^{k}\right)-2\pi\Delta\chi\beta_{\mathrm{s}}^{k}\left(\delta_{\mathrm{P}}\left(\eta_{\mathrm{n}}-2\right)+r_{\mathrm{o}}\right)\frac{\left(\mu_{\mathrm{L,n}}+\dfrac{\mu_{\mathrm{L,n}}^{\mathrm{t}}}{\sigma_{k}}\right)}{\delta_{P}\left(\eta_{\mathrm{N}}-\eta_{\mathrm{P}}\right)}+ \tag{C.3}$$
$$\frac{4\pi\Delta\chi\mu_{\mathrm{L,P}}\left(\delta_{\mathrm{P}}\left(\eta_{\mathrm{P}}-2\right)+r_{\mathrm{o}}\right)}{\delta_{\mathrm{P}}\Delta\eta_{\mathrm{P}}}\left(1-\sqrt{\frac{k_{\mathrm{L,s}}^{\mathrm{o}}}{k_{\mathrm{L,n}}^{\mathrm{o}}}}\right)\left(RNN-\alpha_{\mathrm{n}}^{k}\right)$$

$$a_{\mathrm{L,P}}^{kk}=2\pi\Delta\eta_{\mathrm{P}}\left(\delta_{\mathrm{e}}\left(\eta_{\mathrm{P}}-2\right)+r_{\mathrm{o}}\right)\delta_{\mathrm{e}}\rho_{\mathrm{L,e}}u_{\mathrm{L,e}}+J_{\mathrm{L,n}}\left(RNP+\alpha_{\mathrm{n}}^{k}\right)-J_{\mathrm{L,s}}\left(RSP-\alpha_{\mathrm{s}}^{k}\right)+$$
$$2\pi\Delta\chi\beta_{\mathrm{n}}^{k}\left(\delta_{\mathrm{P}}\left(\eta_{\mathrm{n}}-2\right)+r_{\mathrm{o}}\right)\frac{\left(\mu_{\mathrm{L,n}}+\dfrac{\mu_{\mathrm{L,n}}^{\mathrm{t}}}{\sigma_{K}}\right)}{\delta_{\mathrm{P}}\left(\eta_{\mathrm{N}}-\eta_{\mathrm{P}}\right)}+2\pi\Delta\chi\beta_{\mathrm{s}}^{k}\left(\delta_{\mathrm{P}}\left(\eta_{\mathrm{s}}-2\right)+r_{\mathrm{o}}\right)\frac{\left(\mu_{\mathrm{L,s}}+\dfrac{\mu_{\mathrm{L,s}}^{\mathrm{t}}}{\sigma_{k}}\right)}{\delta_{\mathrm{P}}\left(\eta_{\mathrm{P}}-\eta_{\mathrm{S}}\right)}$$
$$+\frac{4\pi\Delta\chi\mu_{\mathrm{L,P}}\left(\delta_{\mathrm{P}}\left(\eta_{\mathrm{P}}-2\right)+r_{\mathrm{o}}\right)}{\delta_{\mathrm{P}}\Delta\eta_{\mathrm{P}}}\left[\left(1-\sqrt{\frac{k_{\mathrm{L,s}}^{\mathrm{o}}}{k_{\mathrm{L,n}}^{\mathrm{o}}}}\right)\left(RNP+\alpha_{\mathrm{n}}^{k}\right)+\left(1-\sqrt{\frac{k_{\mathrm{L,n}}^{\mathrm{o}}}{k_{\mathrm{L,s}}^{\mathrm{o}}}}\right)\left(RSP-\alpha_{\mathrm{s}}^{k}\right)\right]+$$
$$\frac{0.18\pi\Delta\chi\Delta\eta_{\mathrm{P}}\left(\delta_{\mathrm{P}}\left(\eta_{\mathrm{P}}-2\right)+r_{\mathrm{o}}\right)\delta_{\mathrm{P}}{\rho_{\mathrm{L,P}}}^{2}}{\mu_{\mathrm{L,P}}^{\mathrm{t}}}\left[\begin{array}{l}\dfrac{\exp\left(\dfrac{-2.5}{1+\mathrm{Re}_{\mathrm{L}}^{\mathrm{t}}/50}\right){\rho_{\mathrm{L,P}}}^{2}{k_{\mathrm{L,P}}^{\mathrm{o}}}^{3}}{10\mu_{\mathrm{L,P}}\varepsilon_{\mathrm{L,P}}\left(1+\mathrm{Re}_{\mathrm{L}}^{\mathrm{t}}/50\right)^{2}}\\ +2k_{\mathrm{L,P}}^{\mathrm{o}}\exp\left(\dfrac{-2.5}{1+\mathrm{Re}_{\mathrm{L}}^{\mathrm{t}}/50}\right)\end{array}\right] \tag{C.4}$$
$$+\frac{0.18\pi\Delta\chi\Delta\eta_{\mathrm{P}}\left(\delta_{\mathrm{P}}\left(\eta_{\mathrm{P}}-2\right)+r_{\mathrm{o}}\right)\delta_{\mathrm{P}}{\rho_{\mathrm{L,P}}}^{2}k_{\mathrm{L,P}}^{\mathrm{o}}}{\mu_{\mathrm{L,P}}^{\mathrm{t}}}\exp\left(\frac{-2.5}{1+\mathrm{Re}_{\mathrm{L}}^{\mathrm{t}}/50}\right)$$

$$b_{\mathrm{L,P}}^{k} = 2\pi\Delta\eta\left(\delta_{\mathrm{w}}\left(\eta_{\mathrm{P}}-2\right)+r_{o}\right)\delta_{\mathrm{w}}\rho_{\mathrm{L,w}}u_{\mathrm{L,w}}k_{\mathrm{L,W}} + 2\pi\Delta\chi\Delta\eta\left(\delta_{\mathrm{P}}\left(\eta_{\mathrm{P}}-2\right)+r_{\mathrm{o}}\right)\delta_{\mathrm{P}}G_{\mathrm{P}} +$$

$$\frac{0.18\pi\Delta\chi\Delta\eta_{\mathrm{P}}\left(\delta_{\mathrm{P}}\left(\eta_{\mathrm{P}}-2\right)+r_{\mathrm{o}}\right)\delta_{\mathrm{P}}{\rho_{\mathrm{L,P}}}^{2}{k_{\mathrm{L,P}}^{\mathrm{o}}}}{\mu_{\mathrm{L,P}}^{\mathrm{t}}}\left[\begin{array}{l}\dfrac{\exp\left(\dfrac{-2.5}{1+\mathrm{Re}_{\mathrm{L}}^{\mathrm{t}}/50}\right){\rho_{\mathrm{L,P}}}^{2}{k_{\mathrm{L,P}}^{\mathrm{o}}}^{3}}{10\mu_{\mathrm{L,P}}\varepsilon_{\mathrm{L,P}}\left(1+\mathrm{Re}_{\mathrm{L}}^{\mathrm{t}}/50\right)^{2}} \\ +2k_{\mathrm{L,P}}^{\mathrm{o}}\exp\left(\dfrac{-2.5}{1+\mathrm{Re}_{\mathrm{L}}^{\mathrm{t}}/50}\right)\end{array}\right] \qquad \text{(C.5)}$$

Mixture kinetic energy equation

$$a_{\mathrm{M,S}}^{kk}k_{\mathrm{M,S}} + a_{\mathrm{M,N}}^{kk}k_{\mathrm{M,N}} + a_{\mathrm{M,P}}^{kk}k_{\mathrm{M,P}} = b_{\mathrm{M,P}}^{k} \qquad \text{(C.6)}$$

$$a_{\mathrm{M,S}}^{kk} = -J_{\mathrm{M,s}}\left(RSS+\alpha_{\mathrm{s}}^{k}\right) - 2\pi\Delta\chi\beta_{\mathrm{s}}^{k}\eta_{\mathrm{s}}\frac{\left(\mu_{\mathrm{M,s}}+\dfrac{\mu_{\mathrm{M,s}}^{\mathrm{t}}}{\sigma_{k}}\right)}{\left(\eta_{\mathrm{P}}-\eta_{\mathrm{S}}\right)}$$
$$+\frac{4\pi\Delta\chi\eta_{\mathrm{P}}\mu_{\mathrm{M,P}}}{\Delta\eta_{\mathrm{P}}}\left(1-\sqrt{\frac{k_{\mathrm{M,n}}^{\mathrm{o}}}{k_{\mathrm{M,s}}^{\mathrm{o}}}}\right)\left(RSS+\alpha_{\mathrm{s}}^{\mathrm{k}}\right) \qquad \text{(C.7)}$$

$$a_{\mathrm{M,N}}^{kk} = J_{\mathrm{M,n}}\left(RNN-\alpha_{\mathrm{n}}^{k}\right) - 2\pi\Delta\chi\beta_{\mathrm{n}}^{k}\eta_{\mathrm{n}}\frac{\left(\mu_{\mathrm{M,n}}+\dfrac{\mu_{\mathrm{M,n}}^{\mathrm{t}}}{\sigma_{k}}\right)}{\left(\eta_{\mathrm{N}}-\eta_{\mathrm{P}}\right)}$$
$$+\frac{4\pi\Delta\chi\eta_{\mathrm{P}}\mu_{\mathrm{M,P}}}{\Delta\eta_{\mathrm{P}}}\left(1-\sqrt{\frac{k_{\mathrm{M,s}}^{\mathrm{o}}}{k_{\mathrm{M,n}}^{\mathrm{o}}}}\right)\left(RNN-\alpha_{\mathrm{n}}^{k}\right) \qquad \text{(C.8)}$$

$$a_{\mathrm{M,P}}^{kk} = 2\pi\Delta\eta_{\mathrm{P}}\eta_{\mathrm{P}}(r_{\mathrm{o}}-\delta_{\mathrm{e}})^2\rho_{\mathrm{M,e}}u_{\mathrm{M,e}} + J_{\mathrm{M,n}}\left(RNP+\alpha_{\mathrm{n}}^{k}\right) - J_{\mathrm{M,s}}\left(RSP-\alpha_{\mathrm{s}}^{k}\right) +$$
$$2\pi\Delta\chi\beta_{\mathrm{n}}^{k}\eta_{\mathrm{n}}\frac{\left(\mu_{\mathrm{M,n}}+\dfrac{\mu_{\mathrm{M,n}}^{\mathrm{t}}}{\sigma_K}\right)}{(\eta_{\mathrm{N}}-\eta_{\mathrm{P}})} - 2\pi\Delta\chi\beta_{\mathrm{s}}^{k}\eta_{\mathrm{s}}\frac{\left(\mu_{\mathrm{M,s}}+\dfrac{\mu_{\mathrm{M,s}}^{\mathrm{t}}}{\sigma_k}\right)}{(\eta_{\mathrm{P}}-\eta_{\mathrm{S}})} +$$
$$\frac{4\pi\Delta\chi\mu_{\mathrm{M,P}}\eta_{\mathrm{P}}}{\Delta\eta_{\mathrm{P}}}\left[\left(1-\sqrt{\frac{k_{\mathrm{M,n}}^{\mathrm{o}}}{k_{\mathrm{M,s}}^{\mathrm{o}}}}\right)\left(RSP-\alpha_{\mathrm{s}}^{k}\right)+\left(1-\sqrt{\frac{k_{\mathrm{M,s}}^{\mathrm{o}}}{k_{\mathrm{M,n}}^{\mathrm{o}}}}\right)\left(RNP+\alpha_{\mathrm{n}}^{k}\right)\right]$$
$$+\frac{0.18\pi\Delta\chi\Delta\eta_{\mathrm{P}}\eta_{\mathrm{P}}(r_{\mathrm{o}}-\delta_{\mathrm{P}})^2\rho_{\mathrm{M,P}}{}^{2}}{\mu_{\mathrm{M,P}}^{\mathrm{t}}}\left[\begin{array}{l}\dfrac{\exp\left(\dfrac{-2.5}{1+\mathrm{Re}_{\mathrm{M}}^{\mathrm{t}}/50}\right)\rho_{\mathrm{M,P}}{}^{2}k_{\mathrm{M,P}}^{\mathrm{o}}{}^{3}}{10\mu_{\mathrm{M,P}}\varepsilon_{\mathrm{M,P}}\left(1+\mathrm{Re}_{\mathrm{M}}^{\mathrm{t}}/50\right)^2} \\ +2k_{\mathrm{M,P}}^{\mathrm{o}}\exp\left(\dfrac{-2.5}{1+\mathrm{Re}_{\mathrm{M}}^{\mathrm{t}}/50}\right)\end{array}\right]$$
$$+\frac{0.18\pi\Delta\chi\Delta\eta_{\mathrm{P}}\eta_{\mathrm{P}}(r_{\mathrm{o}}-\delta_{\mathrm{P}})^2\rho_{\mathrm{M,P}}{}^{2}k_{\mathrm{M,P}}^{\mathrm{o}}}{\mu_{\mathrm{M,P}}^{\mathrm{t}}}\exp\left(\frac{-2.5}{1+\mathrm{Re}_{\mathrm{M}}^{\mathrm{t}}/50}\right) \qquad \text{(C.9)}$$

$$b_{\mathrm{M,P}}^{k} = 2\pi\Delta\eta_{\mathrm{P}}\eta_{\mathrm{P}}(r_{\mathrm{o}}-\delta_{\mathrm{w}})^2\rho_{\mathrm{M,w}}u_{\mathrm{M,w}}k_{\mathrm{M,W}} + 2\pi\Delta\chi\Delta\eta_{\mathrm{P}}\eta_{\mathrm{P}}(r_{\mathrm{o}}-\delta_{\mathrm{P}})^2 G_{\mathrm{M,P}}$$
$$+\frac{0.18\pi\Delta\chi\Delta\eta_{\mathrm{P}}\eta_{\mathrm{P}}(r_{\mathrm{o}}-\delta_{\mathrm{P}})^2\rho_{\mathrm{M,P}}{}^{2}k_{\mathrm{M,P}}^{\mathrm{o}}}{\mu_{\mathrm{M,P}}^{\mathrm{t}}}\left[\begin{array}{l}\dfrac{\exp\left(\dfrac{-2.5}{1+\mathrm{Re}_{\mathrm{M}}^{\mathrm{t}}/50}\right)\rho_{\mathrm{M,P}}{}^{2}k_{\mathrm{M,P}}^{\mathrm{o}}{}^{3}}{10\mu_{\mathrm{M,P}}\varepsilon_{\mathrm{M,P}}\left(1+\mathrm{Re}_{\mathrm{M}}^{\mathrm{t}}/50\right)^2} \\ +2k_{\mathrm{M,P}}^{\mathrm{o}}\exp\left(\dfrac{-2.5}{1+\mathrm{Re}_{\mathrm{M}}^{\mathrm{t}}/50}\right)\end{array}\right] \qquad \text{(C.10)}$$

C.1 Discretized Dissipation Rate Equation

Liquid dissipation equation

$$a_{\mathrm{L,S}}^{\varepsilon\varepsilon}\varepsilon_{\mathrm{L,S}} + a_{\mathrm{L,N}}^{\varepsilon\varepsilon}\varepsilon_{\mathrm{L,N}} + a_{\mathrm{L,P}}^{\varepsilon\varepsilon}\varepsilon_{\mathrm{L,P}} = b_{\mathrm{L,P}}^{\varepsilon} \qquad \text{(C.11)}$$

$$a_{\mathrm{L,P}}^{\varepsilon\varepsilon} = 2\pi\Delta\eta_{\mathrm{P}}\left[\left(\delta_{\mathrm{e}}\left(\eta_{\mathrm{P}}-2\right)+r_o\right)\delta_{\mathrm{e}}\rho_{\mathrm{L,e}}u_{\mathrm{L,e}}\right]+J_{\mathrm{L,n}}\left(RNP+\alpha_{\mathrm{n}}^{\varepsilon}\right)$$

$$-J_{L,s}\left(RSP-\alpha_{\mathrm{s}}^{\varepsilon}\right)+2\pi\Delta\chi\beta_{\mathrm{n}}^{\varepsilon}\left(\delta_{\mathrm{P}}\left(\eta_{\mathrm{n}}-2\right)+r_{\mathrm{o}}\right)\frac{\left(\mu_{\mathrm{L,n}}+\dfrac{\mu_{\mathrm{L,n}}^{\mathrm{t}}}{\sigma_{\varepsilon}}\right)}{\delta_{\mathrm{P}}\left(\eta_{\mathrm{N}}-\eta_{\mathrm{P}}\right)}$$

$$-2\pi\Delta\chi\beta_{\mathrm{s}}^{\varepsilon}\left(\delta_{\mathrm{P}}\left(\eta_{\mathrm{s}}-2\right)+r_{\mathrm{o}}\right)\frac{\left(\mu_{\mathrm{L,s}}+\dfrac{\mu_{\mathrm{L,s}}^{\mathrm{t}}}{\sigma_{\varepsilon}}\right)}{\delta_{\mathrm{P}}\left(\eta_{\mathrm{P}}-\eta_{\mathrm{S}}\right)}$$

$$+\frac{0.6\pi\Delta\chi\Delta\eta_{\mathrm{P}}\left(\delta_{\mathrm{P}}\left(\eta_{\mathrm{P}}-2\right)+r_{\mathrm{o}}\right)\delta_{\mathrm{P}}{\rho_{\mathrm{M,P}}}^{2}C_{\varepsilon 2}}{\sqrt{\mu_{\mathrm{L,P}}^{\mathrm{t}}}}\times$$

$$\left[\begin{array}{l}\left(1-0.3\exp\left(-{\mathrm{Re}_{\mathrm{L}}^{\mathrm{t}}}^{2}\right)\right)\left(1.5\exp\left(\dfrac{-2.5}{1+\mathrm{Re}_{\mathrm{L}}^{\mathrm{t}}}\right)\right)^{0.5}\sqrt{\varepsilon_{\mathrm{L,P}}^{\mathrm{o}}}- \\ \dfrac{\left(\exp\left(\dfrac{-2.5}{1+\mathrm{Re}_{\mathrm{L}}^{\mathrm{t}}/50}\right)\right)^{0.5}{k_{\mathrm{L,P}}}^{2}\rho_{\mathrm{L,P}}}{40\mu_{\mathrm{L,P}}\sqrt{\varepsilon_{\mathrm{L,P}}^{\mathrm{o}}}\left(1+\mathrm{Re}_{\mathrm{L}}^{\mathrm{t}}/50\right)^{2}} \\ -0.6\left(\exp\left(\dfrac{-2.5}{1+\mathrm{Re}_{\mathrm{L}}^{\mathrm{t}}/50}\right)\right)^{0.5}\exp\left(-{\mathrm{Re}_{\mathrm{L}}^{\mathrm{t}}}^{2}\right)\end{array}\right]$$

$$+\frac{0.6\pi\Delta\chi\Delta\eta_{\mathrm{P}}\left(\delta_{\mathrm{P}}\left(\eta_{\mathrm{P}}-2\right)+r_{\mathrm{o}}\right)\delta_{\mathrm{P}}{\rho_{\mathrm{L,P}}}^{3/2}C_{\varepsilon 2}}{\sqrt{\mu_{\mathrm{L,P}}^{\mathrm{t}}}}\times$$

$$\left[\left(1-0.3\exp\left(-{\mathrm{Re}_{\mathrm{L}}^{\mathrm{t}}}^{2}\right)\right)\left(1.5\exp\left(\frac{-2.5}{1+\mathrm{Re}_{\mathrm{L}}^{\mathrm{t}}}\right)\right)^{0.5}\sqrt{\varepsilon_{\mathrm{L,P}}^{\mathrm{o}}}\right] \qquad \text{(C.12)}$$

$$a_{\mathrm{L,S}}^{\varepsilon\varepsilon} = -J_{\mathrm{L,s}}\left(RSS+\alpha_{\mathrm{s}}^{\varepsilon}\right)-2\pi\Delta\chi\beta_{\mathrm{s}}^{\varepsilon}\left(\delta_{\mathrm{P}}\left(\eta_{\mathrm{s}}-2\right)+r_{\mathrm{o}}\right)\frac{\left(\mu_{\mathrm{L,s}}+\dfrac{\mu_{\mathrm{L,s}}^{\mathrm{t}}}{\sigma_{\varepsilon}}\right)}{\delta_{\mathrm{P}}\left(\eta_{\mathrm{P}}-\eta_{\mathrm{S}}\right)} \qquad \text{(C.13)}$$

$$a_{\mathrm{L,N}}^{\varepsilon\varepsilon} = J_{\mathrm{L,n}}\left(RNN-\alpha_{\mathrm{n}}^{\varepsilon}\right)-2\pi\Delta\chi\beta_{\mathrm{n}}^{\varepsilon}\left(\delta_{\mathrm{P}}\left(\eta_{\mathrm{n}}-2\right)+r_{\mathrm{o}}\right)\frac{\left(\mu_{\mathrm{L,n}}+\dfrac{\mu_{\mathrm{L,n}}^{\mathrm{t}}}{\sigma_{\varepsilon}}\right)}{\delta_{\mathrm{P}}\left(\eta_{\mathrm{N}}-\eta_{\mathrm{P}}\right)} \qquad \text{(C.14)}$$

$$b_{\mathrm{L,P}}^{\varepsilon} = 2\pi\Delta\eta_{\mathrm{P}}\left(\delta_{\mathrm{w}}\left(\eta_{\mathrm{P}}-2\right)+r_{\mathrm{o}}\right)\delta_{\mathrm{w}}\rho_{\mathrm{L,w}}u_{\mathrm{L,W}}\varepsilon_{\mathrm{L,W}}$$
$$+\frac{0.6\pi\Delta\chi\Delta\eta_{\mathrm{P}}\left(\delta_{\mathrm{P}}\left(\eta_{\mathrm{P}}-2\right)+r_{\mathrm{o}}\right)\delta_{\mathrm{P}}{\rho_{\mathrm{L,P}}}^{2}\varepsilon_{\mathrm{L,P}}^{\mathrm{o}}C_{\varepsilon 2}}{\sqrt{\mu_{\mathrm{L,P}}^{\mathrm{t}}}}\times$$
$$\left[\begin{array}{l}\left(1-0.3\exp(-\mathrm{Re}_{\mathrm{L}}^{\mathrm{t}\,2})\right)\left(1.5\exp\left(\frac{-2.5}{1+\mathrm{Re}_{\mathrm{L}}^{\mathrm{t}}}\right)\right)^{0.5}\sqrt{\varepsilon_{\mathrm{L,P}}^{\mathrm{o}}}- \\ \frac{\left(\exp\left(\frac{-2.5}{1+\mathrm{Re}_{\mathrm{L}}^{\mathrm{t}}/50}\right)\right)^{0.5}{k_{\mathrm{L,P}}^{\mathrm{o}}}^{2}\rho_{\mathrm{L,P}}}{40\mu_{L,P}\sqrt{\varepsilon_{\mathrm{L,P}}^{\mathrm{o}}}\left(1+\mathrm{Re}_{\mathrm{L}}^{\mathrm{t}}/50\right)^{2}}- \\ 0.6\left(\exp\left(\frac{-2.5}{1+\mathrm{Re}_{L}^{t}/50}\right)\right)^{0.5}\exp(-\mathrm{Re}_{\mathrm{L}}^{\mathrm{t}\,2})\end{array}\right]$$
$$0.6\pi\Delta\chi\Delta\eta_{\mathrm{P}}\left(\delta_{\mathrm{P}}\left(\eta_{\mathrm{P}}-2\right)+r_{\mathrm{o}}\right)\delta_{\mathrm{P}}G_{\mathrm{L,P}}C_{\varepsilon 1}f_{1}\sqrt{\frac{\rho_{\mathrm{L,P}}\varepsilon_{\mathrm{L,P}}^{\mathrm{o}}}{\mu_{\mathrm{L,P}}^{\mathrm{t}}}\exp\left(\frac{-2.5}{1+\mathrm{Re}_{\mathrm{L}}^{\mathrm{t}}/50}\right)}$$
$$+4\pi\Delta\eta_{\mathrm{P}}\Delta\chi\left(\delta_{\mathrm{P}}\left(\eta_{\mathrm{P}}-2\right)+r_{\mathrm{o}}\right)\frac{\delta_{\mathrm{P}}\mu_{\mathrm{L,P}}\mu_{\mathrm{L,P}}^{\mathrm{t}}}{\rho_{\mathrm{L,P}}{\delta_{\mathrm{P}}}^{4}}\left[\left.\frac{\partial^{2}u_{L}}{\partial\eta^{2}}\right|_{\mathrm{P}}\right] \qquad \text{(C.15)}$$

Mixture dissipation equation

$$a_{\mathrm{M,S}}^{\varepsilon\varepsilon}\varepsilon_{\mathrm{M,S}}+a_{\mathrm{M,N}}^{\varepsilon\varepsilon}\varepsilon_{\mathrm{M,N}}+a_{\mathrm{M,P}}^{\varepsilon\varepsilon}\varepsilon_{\mathrm{M,P}}=b_{\mathrm{M,P}}^{\varepsilon}$$

$$a_{M,P}^{\varepsilon\varepsilon} = 2\pi\Delta\eta_P\left[\eta_P\left(r_o-\delta_e\right)^2\rho_{M,e}u_{M,e}\right]+J_{M,n}\left(RNP+\alpha_n^{\varepsilon}\right)-J_{M,s}\left(RSP-\alpha_s^{\varepsilon}\right)+$$

$$2\pi\Delta\chi\beta_n^{\varepsilon}\eta_n\frac{\left(\mu_{M,n}+\dfrac{\mu_{M,n}^t}{\sigma_\varepsilon}\right)}{\left(\eta_N-\eta_P\right)}-2\pi\Delta\chi\beta_s^{\varepsilon}\eta_s\frac{\left(\mu_{M,s}+\dfrac{\mu_{M,s}^t}{\sigma_\varepsilon}\right)}{\left(\eta_P-\eta_S\right)}$$

$$+\frac{0.6\pi\Delta\chi\Delta\eta_P\eta_P\left(r_o-\delta_P\right)^2{\rho_{M,P}}^2C_{\varepsilon 2}}{\sqrt{\mu_{M,P}^t}}\times$$

$$\left[\begin{array}{l}\left(1-0.3\exp(-{\mathrm{Re}_M^t}^2)\right)\left(1.5\exp\left(\dfrac{-2.5}{1+\mathrm{Re}_M^t}\right)\right)^{0.5}\sqrt{\varepsilon_{M,P}^o}- \\ \dfrac{\left(\exp\left(\dfrac{-2.5}{1+\mathrm{Re}_M^t/50}\right)\right)^{0.5}{k_{M,P}}^2\rho_{M,P}}{40\mu_{M,P}\sqrt{\varepsilon_{M,P}^o}\left(1+\mathrm{Re}_M^t/50\right)^2}- \\ 0.6\left(\exp\left(\dfrac{-2.5}{1+\mathrm{Re}_M^t/50}\right)\right)^{0.5}\exp(-{\mathrm{Re}_M^t}^2)\end{array}\right]$$

$$+\frac{0.6\pi\Delta\chi\Delta\eta_P\eta_P\left(r_o-\delta_P\right)^2{\rho_{M,P}}^{3/2}C_{\varepsilon 2}}{\sqrt{\mu_{M,P}^t}}\times \qquad \text{(C.16)}$$

$$\left[\left(1-0.3\exp(-{\mathrm{Re}_M^t}^2)\right)\left(1.5\exp\left(\frac{-2.5}{1+\mathrm{Re}_M^t}\right)\right)^{0.5}\sqrt{\varepsilon_{M,P}^o}\right]$$

$$a_{M,S}^{\varepsilon\varepsilon} = -J_{M,s}\left(RSS+\alpha_s^{\varepsilon}\right)-2\pi\Delta\chi\beta_s^{\varepsilon}\eta_s\frac{\left(\mu_{M,s}+\dfrac{\mu_{M,s}^t}{\sigma_\varepsilon}\right)}{\left(\eta_P-\eta_S\right)} \qquad \text{(C.17)}$$

$$a_{M,N}^{\varepsilon\varepsilon} = J_{M,n}\left(RNN-\alpha_n^{\varepsilon}\right)-2\pi\Delta\chi\beta_n^{\varepsilon}\eta_n\frac{\left(\mu_{M,n}+\dfrac{\mu_{M,n}^t}{\sigma_\varepsilon}\right)}{\left(\eta_N-\eta_P\right)} \qquad \text{(C.18)}$$

$$b^{\varepsilon}_{\mathrm{M,P}} = 2\pi\Delta\eta_{\mathrm{P}}\eta_{\mathrm{P}}(r_{\mathrm{o}}-\delta_{\mathrm{w}})^{2}\rho_{\mathrm{M,w}}u_{\mathrm{M,W}}\varepsilon_{\mathrm{M,W}} -$$

$$+\frac{0.6\pi\Delta\chi\Delta\eta_{\mathrm{P}}\eta_{\mathrm{P}}(r_{\mathrm{o}}-\delta_{\mathrm{P}})^{2}\rho_{\mathrm{M,P}}{}^{2}\varepsilon^{\mathrm{o}}_{\mathrm{M,P}}C_{\varepsilon 2}}{\sqrt{\mu^{\mathrm{t}}_{\mathrm{M,P}}}}\times$$

$$\left[\begin{array}{l}(1-0.3\exp(-\mathrm{Re}^{\mathrm{t}}_{\mathrm{M}}{}^{2}))\left(1.5\exp\left(\frac{-2.5}{1+\mathrm{Re}^{\mathrm{t}}_{\mathrm{M}}}\right)\right)^{0.5}\sqrt{\varepsilon^{\mathrm{o}}_{\mathrm{M,P}}}- \\ \frac{\left(\exp\left(\frac{-2.5}{1+\mathrm{Re}^{\mathrm{t}}_{\mathrm{M}}/50}\right)\right)^{0.5}k_{\mathrm{M,P}}{}^{2}\rho_{\mathrm{M,P}}}{40\mu_{\mathrm{M,P}}\sqrt{\varepsilon^{\mathrm{o}}_{\mathrm{M,P}}}\left(1+\mathrm{Re}^{\mathrm{t}}_{\mathrm{M}}/50\right)^{2}}- \\ 0.6\left(\exp\left(\frac{-2.5}{1+\mathrm{Re}^{\mathrm{t}}_{\mathrm{M}}/50}\right)\right)^{0.5}\exp(-\mathrm{Re}^{\mathrm{t}}_{\mathrm{M}}{}^{2})\end{array}\right]$$

$$+4\pi\Delta\eta_{\mathrm{P}}\Delta\chi\eta_{\mathrm{P}}\frac{\mu_{\mathrm{M,P}}\mu^{\mathrm{t}}_{\mathrm{M,P}}}{\rho_{\mathrm{M,P}}(r_{\mathrm{o}}-\delta_{\mathrm{P}})^{2}}\left[\left.\frac{\partial^{2}u_{\mathrm{M}}}{\partial\eta^{2}}\right|_{\mathrm{P}}\right]+$$

$$0.6\pi\Delta\chi\Delta\eta_{\mathrm{P}}\eta_{\mathrm{P}}(r_{\mathrm{o}}-\delta_{\mathrm{P}})^{2}G_{\mathrm{M,P}}C_{\varepsilon 1}f_{1}\sqrt{\frac{\rho_{\mathrm{M,P}}\varepsilon^{\mathrm{o}}_{\mathrm{M,P}}}{\mu^{\mathrm{t}}_{\mathrm{M,P}}}\exp\left(\frac{-2.5}{1+\mathrm{Re}^{\mathrm{t}}_{\mathrm{M}}/50}\right)} \qquad \text{(C.19)}$$

APPENDIX D

Discretization of Boundary Conditions

D.1 Boundary Conditions at the Tube Wall ($\eta = 2$)

Liquid Boundary Continuity Equation

- $J''_{\mathrm{L}} = 0$

$$J_{\mathrm{L,P}} = 0 \qquad [D.1]$$

$$a^{JJ}_{\mathrm{L,S}} J_{\mathrm{L,S}} + a^{Ju}_{\mathrm{L,P}} u_{\mathrm{L,P}} + a^{JJ}_{\mathrm{L,P}} J_{\mathrm{L,P}} + a^{J\delta}_{\mathrm{L,P}} \delta_{\mathrm{P}} = b^{J}_{\mathrm{L,P}} \qquad [D.2]$$

where, $a^{JJ}_{\mathrm{L,P}} = 1$ [D.3]

$$a^{JJ}_{\mathrm{L,S}} = a^{Ju}_{\mathrm{L,P}} = a^{J\delta}_{\mathrm{L,P}} = b^{J}_{\mathrm{L,P}} = 0 \qquad [D.4]$$

Liquid Boundary Momentum Equation

- $u_{\mathrm{L}} = 0$

$$u_{\mathrm{L,P}} = 0 \qquad [D.5]$$

$$a^{uu}_{\mathrm{L,S}} u_{\mathrm{L,S}} + a^{uJ}_{\mathrm{L,S}} J_{\mathrm{L,S}} + a^{uu}_{\mathrm{L,P}} u_{\mathrm{L,P}} + a^{uJ}_{\mathrm{L,P}} J_{\mathrm{L,P}} + a^{uu}_{\mathrm{L,N}} u_{\mathrm{L,N}} + a^{u\delta}_{\mathrm{L,P}} \delta_{\mathrm{P}} + a^{uP}_{\mathrm{L,P}} P'_{\mathrm{P}} = b^{u}_{\mathrm{L,P}} \qquad [D.6]$$

where, $a^{uu}_{\mathrm{L,P}} = 1$ [D.7]

$$a^{uu}_{\mathrm{L,S}} = a^{uJ}_{\mathrm{L,S}} = a^{uJ}_{\mathrm{L,P}} = a^{uu}_{\mathrm{L,N}} = a^{u\delta}_{\mathrm{L,P}} = a^{up}_{\mathrm{L,P}} = b^{u}_{\mathrm{L,P}} = 0 \qquad [D.8]$$

Liquid Boundary Energy Equation

- $T_{\mathrm{L}} = T_{\mathrm{wall}}$

$$T_{\mathrm{L,P}} = T_{\mathrm{wall}} \qquad [D.9]$$

$$a^{TJ}_{\mathrm{L,S}} J_{\mathrm{L,S}} + a^{TT}_{\mathrm{L,S}} T_{\mathrm{L,S}} + a^{Tu}_{\mathrm{L,P}} u_{\mathrm{L,P}} + a^{TJ}_{\mathrm{L,P}} J_{\mathrm{L,P}} + a^{TT}_{\mathrm{L,P}} T_{\mathrm{L,P}} + a^{TT}_{\mathrm{L,N}} T_{\mathrm{L,N}} + a^{T\delta}_{\mathrm{L,P}} \delta_{\mathrm{P}} = b^{T}_{\mathrm{L,P}} \qquad [D.10]$$

where, $a_{\mathrm{L,P}}^{TT} = 1$ [D.11]

$$b_{\mathrm{L,P}}^{T} = T_{\mathrm{wall}} \quad [D.12]$$

$$a_{\mathrm{L,S}}^{TJ} = a_{\mathrm{L,S}}^{TT} = a_{\mathrm{L,P}}^{Tu} = a_{\mathrm{L,P}}^{TJ} = a_{\mathrm{L,N}}^{TT} = a_{\mathrm{L,P}}^{T\delta} = 0 \quad [D.13]$$

D.2 Boundary Conditions at the Center Line ($\eta = 0$):

Mixture Boundary Continuity Equation

- $J_{\mathrm{M}}'' = 0$

$$J_{\mathrm{M,P}} = 0 \quad [D.14]$$

$$a_{\mathrm{M,S}}^{JJ} J_{\mathrm{M,S}} + a_{\mathrm{M,P}}^{Ju} u_{\mathrm{M,P}} + a_{\mathrm{M,P}}^{JJ} J_{\mathrm{M,P}} + a_{\mathrm{M,P}}^{J\delta} \delta_{\mathrm{P}} = b_{\mathrm{M,P}}^{J} \quad [D.15]$$

where, $a_{\mathrm{M,P}}^{JJ} = 1$ [D.16]

$$a_{\mathrm{M,S}}^{JJ} = a_{\mathrm{M,P}}^{Ju} = a_{\mathrm{M,P}}^{J\delta} = b_{\mathrm{M,P}}^{J} = 0 \quad [D.17]$$

Mixture Boundary Momentum Equation

- $\dfrac{\partial u_{\mathrm{M}}}{\partial \eta} = 0$

$$u_{\mathrm{M,N}} = u_{\mathrm{M,P}} \quad [D.18]$$

$$a_{\mathrm{M,S}}^{uu} u_{\mathrm{M,S}} + a_{\mathrm{M,S}}^{uJ} J_{\mathrm{M,S}} + a_{\mathrm{M,P}}^{uu} u_{\mathrm{M,P}} + a_{\mathrm{M,P}}^{uJ} J_{\mathrm{M,P}} + a_{\mathrm{M,N}}^{uu} u_{\mathrm{M,N}} + a_{\mathrm{M,P}}^{u\delta} \delta_{\mathrm{P}} + a_{\mathrm{M,P}}^{uP} P_{\mathrm{P}}' = b_{\mathrm{M,P}}^{u} \quad [D.19]$$

where, $a_{\mathrm{M,N}}^{uu} = -1$ [D.20]

$$a_{\mathrm{M,P}}^{uu} = 1 \quad [D.21]$$

$$a_{\mathrm{M,S}}^{uu} = a_{\mathrm{M,S}}^{uJ} = a_{\mathrm{M,P}}^{uJ} = a_{\mathrm{M,P}}^{u\delta} = a_{\mathrm{M,P}}^{up} = b_{\mathrm{M,P}}^{u} = 0 \quad [D.22]$$

Mixture Boundary Energy Equation

- $\dfrac{\partial T_{\mathrm{M}}}{\partial \eta} = 0$

$$T_{\mathrm{M,N}} = T_{\mathrm{M,P}} \qquad [D.23]$$

$$a^{TJ}_{\mathrm{M,S}} J_{\mathrm{M,S}} + a^{TT}_{\mathrm{M,S}} T_{\mathrm{M,S}} + a^{TW}_{\mathrm{M,S}} W_{\mathrm{S}} + a^{Tu}_{\mathrm{M,P}} u_{\mathrm{M,P}} + a^{TJ}_{\mathrm{M,P}} J_{\mathrm{M,P}} + a^{TT}_{\mathrm{M,P}} T_{\mathrm{M,P}} + a^{TW}_{\mathrm{M,P}} W_{\mathrm{P}} + a^{TT}_{\mathrm{M,N}} T_{\mathrm{M,N}} + a^{TW}_{\mathrm{M,N}} W_{\mathrm{N}} + a^{T\delta}_{\mathrm{M,P}} \delta_{\mathrm{P}} = b^{T}_{\mathrm{M,P}} \qquad [D.24]$$

where, $a^{TT}_{\mathrm{M,N}} = -1$ [D.25]

$$a^{TT}_{\mathrm{M,P}} = 1 \qquad [D.26]$$

$$a^{TJ}_{\mathrm{M,S}} = a^{TT}_{\mathrm{M,S}} = a^{TW}_{\mathrm{M,S}} = a^{Tu}_{\mathrm{M,P}} = a^{TJ}_{\mathrm{M,P}} = a^{TW}_{\mathrm{M,P}} = a^{TW}_{\mathrm{M,N}} = a^{T\delta}_{\mathrm{M,P}} = b^{T}_{\mathrm{M,P}} = 0 \qquad [D.27]$$

Mixture Boundary Mass Diffusion Equation

- $\dfrac{\partial W}{\partial \eta} = 0$

$$W_{\mathrm{N}} = W_{\mathrm{P}} \qquad [D.28]$$

$$a^{WJ}_{\mathrm{M,S}} J_{\mathrm{M,S}} + a^{WW}_{\mathrm{M,S}} W_{\mathrm{S}} + a^{Wu}_{\mathrm{M,P}} u_{\mathrm{M,P}} + a^{WJ}_{\mathrm{M,P}} J_{\mathrm{M,P}} + a^{WW}_{\mathrm{M,P}} W_{\mathrm{N}} + a^{W\delta}_{\mathrm{M,P}} \delta_{\mathrm{P}} = b^{W}_{\mathrm{M,P}} \qquad [D.29]$$

where, $a^{WW}_{\mathrm{M,N}} = -1$ [D.30]

$$a^{WW}_{\mathrm{M,P}} = 1 \qquad [D.31]$$

$$a^{WJ}_{\mathrm{M,S}} = a^{WW}_{\mathrm{M,S}} = a^{Wu}_{\mathrm{M,P}} = a^{WJ}_{\mathrm{M,P}} = a^{W\delta}_{\mathrm{M,P}} = b^{W}_{\mathrm{M,P}} = 0 \qquad [D.32]$$

D.3 Boundary Conditions at the Interface ($\eta = 1$)

Continuity Equation at the Interface

- $J''_{\mathrm{L}} = J''_{\mathrm{M}}$

$$J_{\mathrm{L,P}} = J_{\mathrm{M,S}} \qquad [D.33]$$

$$a_{\mathrm{I,S}}^{JJ} J_{\mathrm{M,S}} + a_{\mathrm{I,P}}^{JJ} J_{\mathrm{L,P}} = b_{\mathrm{I,P}}^{J} \qquad [D.34]$$

where, $a_{\mathrm{I,S}}^{JJ} = -1$ [D.35]

$$a_{\mathrm{I,P}}^{JJ} = 1 \qquad [D.36]$$

$$b_{\mathrm{I,P}}^{J} = 0 \qquad [D.37]$$

Momentum Equation at the Interface

- $$\left.\begin{aligned} u_{\mathrm{L}} &= u_{\mathrm{M}} \\ \frac{\mu_{\mathrm{L}}}{\delta}\frac{\partial u_{\mathrm{L}}}{\partial \eta} &= \frac{\mu_{\mathrm{M}}}{(r_{\mathrm{o}} - \delta)}\frac{\partial u_{\mathrm{M}}}{\partial \eta} \end{aligned}\right\}$$

$$\frac{\beta_{\mathrm{n}}^{u}\mu_{\mathrm{L,P,eff}}}{\delta_{P}}\left(\frac{u_{\mathrm{L,N}} - u_{\mathrm{L,P}}}{\eta_{\mathrm{N}} - \eta_{\mathrm{P}}}\right) = \frac{\beta_{\mathrm{s}}^{u}\mu_{\mathrm{M,P,eff}}}{(r_{o} - \delta_{\mathrm{P}})}\left(\frac{u_{\mathrm{L,P}} - u_{\mathrm{M,S}}}{\eta_{\mathrm{P}} - \eta_{\mathrm{S}}}\right) \qquad [D.38]$$

Applying Newton Raphson linearization results in the following:

$$\begin{aligned} &\frac{\beta_{\mathrm{n}}^{u}\mu_{\mathrm{L,P,eff}}}{(\eta_{\mathrm{N}} - \eta_{\mathrm{P}})}\left(\frac{u_{\mathrm{L,N}}^{\mathrm{n}} - u_{\mathrm{L,P}}^{\mathrm{n}}}{\delta_{\mathrm{P}}^{\,o}} - \frac{u_{\mathrm{L,N}}^{\mathrm{o}} - u_{\mathrm{L,P}}^{\mathrm{n}}}{\delta_{\mathrm{P}}^{\,\mathrm{o}2}}\delta_{\mathrm{P}}^{\mathrm{n}} + \frac{u_{\mathrm{L,N}}^{\mathrm{o}} - u_{\mathrm{L,P}}^{\mathrm{o}}}{\delta_{\mathrm{P}}^{\mathrm{o}}}\right) \\ &= \frac{\beta_{\mathrm{s}}^{u}\mu_{\mathrm{M,P,eff}}}{(\eta_{\mathrm{P}} - \eta_{\mathrm{S}})}\left(\frac{u_{\mathrm{L,P}}^{\mathrm{n}} - u_{\mathrm{M,S}}^{\mathrm{n}}}{(r_{\mathrm{o}} - \delta_{\mathrm{P}}^{\mathrm{o}})} - \frac{u_{L,P}^{o} - u_{\mathrm{M,S}}^{\mathrm{o}}}{(r_{o} - \delta_{\mathrm{P}}^{\mathrm{o}})^{2}}\delta_{\mathrm{P}}^{\mathrm{n}} + \frac{u_{\mathrm{L,P}}^{\mathrm{o}} - u_{\mathrm{M,S}}^{\mathrm{o}}}{(r_{o} - \delta_{\mathrm{P}}^{\mathrm{o}})^{2}}\delta_{\mathrm{P}}^{\mathrm{o}}\right) \end{aligned} \qquad [D.39]$$

$$a_{\mathrm{I,S}}^{uu} u_{\mathrm{M,S}} + a_{\mathrm{I,P}}^{uu} u_{\mathrm{L,P}} + a_{\mathrm{I,N}}^{uu} u_{\mathrm{L,N}} + a_{\mathrm{I,P}}^{u\delta}\delta_{\mathrm{P}} = b_{\mathrm{I,P}}^{u} \qquad [D.40]$$

where, $a_{\mathrm{I,S}}^{uu} = -\dfrac{\beta_{\mathrm{s}}^{u}\mu_{\mathrm{M,P,eff}}}{(\eta_{\mathrm{P}} - \eta_{\mathrm{S}})(r_{\mathrm{o}} - \delta_{\mathrm{P}}^{\mathrm{o}})}$ [D.41]

$$a_{\mathrm{I,P}}^{uu} = \frac{\beta_s^u \mu_{\mathrm{M,P,eff}}}{(\eta_\mathrm{P} - \eta_\mathrm{S})(r_\mathrm{o} - \delta_\mathrm{P}^\mathrm{o})} + \frac{\beta_\mathrm{n}^u \mu_{\mathrm{L,P,eff}}}{(\eta_\mathrm{N} - \eta_\mathrm{P})\delta_\mathrm{P}^\mathrm{o}} \qquad [D.42]$$

$$a_{\mathrm{I,N}}^{uu} = -\frac{\beta_\mathrm{n}^u \mu_{\mathrm{L,P,eff}}}{(\eta_\mathrm{N} - \eta_\mathrm{P})\delta_\mathrm{P}^\mathrm{o}} \qquad [D.43]$$

$$a_{\mathrm{IP}}^{u\delta} = \frac{\beta_\mathrm{s}^u \mu_{\mathrm{M,P,eff}} \left(u_{\mathrm{L,P}}^\mathrm{o} - u_{\mathrm{M,S}}^\mathrm{o}\right)}{(\eta_\mathrm{P} - \eta_\mathrm{S})(r_\mathrm{o} - \delta_\mathrm{P}^\mathrm{o})^2} + \frac{\beta_\mathrm{n}^u \mu_{\mathrm{L,P,eff}} \left(u_{\mathrm{L,N}}^\mathrm{o} - u_{\mathrm{L,P}}^\mathrm{o}\right)}{(\eta_\mathrm{N} - \eta_\mathrm{P})\delta_\mathrm{P}^{\mathrm{o}2}} \qquad [D.44]$$

$$b_{\mathrm{I,P}}^{u} = \frac{\beta_\mathrm{s}^u \mu_{\mathrm{M,P,eff}} \left(u_{\mathrm{L,P}}^\mathrm{o} - u_{\mathrm{M,S}}^\mathrm{o}\right)}{(\eta_\mathrm{P} - \eta_\mathrm{S})(r_\mathrm{o} - \delta_\mathrm{P}^\mathrm{o})^2}\delta_\mathrm{P}^\mathrm{o} + \frac{\beta_\mathrm{n}^u \mu_{\mathrm{L,P,eff}} \left(u_{\mathrm{L,N}}^\mathrm{o} - \mathrm{u}_{\mathrm{L,P}}^\mathrm{o}\right)}{(\eta_\mathrm{N} - \eta_\mathrm{P})\delta_\mathrm{P}^\mathrm{o}} \qquad [D.45]$$

Temperature Equation at the Interface

- $T_\mathrm{L} = T_\mathrm{M} = T_{\mathrm{sat@P_v}}$

$$T_{\mathrm{L,P}} = T_{\mathrm{sat}}(W, P') \qquad [D.46]$$

$$T_{\mathrm{L,P}} = T_{\mathrm{L,P}}^\mathrm{o} + \left.\frac{\partial T_{\mathrm{sat}}(W,P')}{\partial W}\right|_\mathrm{P}^\mathrm{o} (W_\mathrm{P} - W_\mathrm{P}^\mathrm{o}) + \left.\frac{\partial T_{\mathrm{sat}}(W,P')}{\partial P'}\right|_\mathrm{P}^\mathrm{o} \left(P_\mathrm{P}' - P_\mathrm{P}'^\mathrm{o}\right) \qquad [D.47]$$

$$a_{\mathrm{I,P}}^{TT} T_{\mathrm{M,P}} + a_{\mathrm{I,P}}^{TW} W_\mathrm{P} + a_{\mathrm{I,P}}^{TP} P_\mathrm{P}^{'} = b_{\mathrm{I,P}}^{T} \qquad [D.48]$$

where, $a_{\mathrm{I,P}}^{TT} = 1$ [D.49]

$$a_{\mathrm{I,P}}^{TW} = -\left.\frac{\partial T_{\mathrm{sat}}(W,P')}{\partial W}\right|_\mathrm{P}^\mathrm{o} \qquad [D.50]$$

$$a_{\mathrm{I,P}}^{Tp} = -\left.\frac{\partial T_{\mathrm{sat}}(W,P')}{\partial P'}\right|_\mathrm{P}^\mathrm{o} \qquad [D.51]$$

$$b_{\mathrm{I,P}}^{T} = T_{\mathrm{L,P}}^\mathrm{o} - \left.\frac{\partial T_{\mathrm{sat}}(W,P')}{\partial W}\right|_\mathrm{P}^\mathrm{o} W_\mathrm{P}^\mathrm{o} - \left.\frac{\partial T_{\mathrm{sat}}(W,P')}{\partial P'}\right|_\mathrm{P}^\mathrm{o} P_\mathrm{P}'^\mathrm{o} \qquad [D.52]$$

Mass Diffusion Equation at the Interface

- $J''_{M} W - \dfrac{\rho_{M} D_{eff}}{(r_o - \delta)} \dfrac{\partial W}{\partial \eta} = 0$

$$\frac{J_{M,S} W_P}{2\pi\eta_P (r_o - \delta_P)\Delta\chi} - \frac{\beta_s^W \rho_{M,P} D_{P,eff}}{(r_o - \delta_P)} \left(\frac{W_P - W_S}{\eta_P - \eta_S} \right) = 0 \qquad [D.53]$$

$$\left(J^{o}_{M,S} W^{o}_{P} + J''_{M,S} W^{o}_{P} - J^{o}_{M,S} W^{o}_{P} \right) - 2\pi\eta_P \beta_s^W \rho_{M,P} D_{P,eff} \Delta\chi \left(\frac{W_P - W_S}{\eta_P - \eta_S} \right) \qquad [D.54]$$

$$a^{WJ}_{I,S} J_{M,S} + a^{WW}_{I,P} W_P + a^{WW}_{I,S} W_S + a^{u\delta}_{I,P} \delta_P = b^{W}_{I,P} \qquad [D.55]$$

where, $a^{WJ}_{I,S} = W^{o}_{P}$ [D.56]

$$a^{WW}_{I,P} = J^{o}_{M,S} - 2\pi\eta_P \frac{\beta_s^W \rho_{M,P} D_{P,eff} \Delta\chi}{(\eta_P - \eta_S)} \qquad [D.57]$$

$$a^{WW}_{I,S} = 2\pi\eta_P \frac{\beta_s^W \rho_{M,P} D_{P,eff} \Delta\chi}{(\eta_P - \eta_S)} \qquad [D.58]$$

$$a^{u\delta}_{I,P} = 0 \qquad [D.59]$$

$$b^{W}_{I,P} = J^{o}_{M,S} W^{o}_{P} \qquad [D.60]$$

Energy Conservation Equation at the Interface

- $\left.\begin{aligned} & T_L = T_M \\ & \frac{\lambda_{L,eff}}{\delta} \frac{\partial T_L}{\partial \eta} = \frac{\lambda_{M,eff}}{(r_o - \delta)} \frac{\partial T_M}{\partial \eta} - J''_{M} h_{fg} \end{aligned}\right\}$

$$2\pi\eta_{\mathrm{P}}(r_o-\delta_{\mathrm{P}})\frac{\beta_{\mathrm{n}}^{T}\lambda_{\mathrm{L,P,eff}}\Delta\chi}{\delta_{\mathrm{P}}}\left(\frac{T_{\mathrm{L,N}}-T_{\mathrm{L,P}}}{\eta_{\mathrm{N}}-\eta_{\mathrm{P}}}\right)= 2\pi\beta_{\mathrm{n}}^{T}\lambda_{\mathrm{M,P,eff}}\Delta\chi\left(\frac{T_{\mathrm{L,P}}-T_{\mathrm{M,S}}}{\eta_{\mathrm{P}}-\eta_{\mathrm{S}}}\right)-J_{\mathrm{L,P}}h_{\mathrm{fg}} \quad [D.61]$$

$$2\pi\eta_{\mathrm{P}}r_{\mathrm{o}}\frac{\beta_{\mathrm{n}}^{T}\lambda_{\mathrm{L,P,eff}}\Delta\chi}{(\eta_{\mathrm{N}}-\eta_{\mathrm{P}})}\left(\frac{T_{\mathrm{L,N}}^{\mathrm{n}}-T_{\mathrm{L,P}}^{\mathrm{n}}}{\delta_{\mathrm{P}}^{\mathrm{o}}}-\frac{T_{\mathrm{L,N}}^{\mathrm{o}}-T_{\mathrm{L,P}}^{\mathrm{o}}}{\delta_{\mathrm{P}}^{\mathrm{o}2}}\delta_{\mathrm{P}}^{\mathrm{n}}+\frac{T_{\mathrm{L,N}}^{\mathrm{o}}-T_{\mathrm{L,P}}^{\mathrm{o}}}{\delta_{\mathrm{P}}^{\mathrm{o}}}\right) = 2\pi\beta_{\mathrm{s}}^{T}\lambda_{\mathrm{M,P,eff}}\Delta\chi\left(\frac{T_{\mathrm{L,P}}-T_{\mathrm{M,S}}}{\eta_{\mathrm{P}}-\eta_{\mathrm{S}}}\right)-J_{\mathrm{L,P}}h_{\mathrm{fg}} \quad [D.62]$$

$$a_{\mathrm{I,S}}^{\delta T}T_{M,S}+a_{\mathrm{I,P}}^{\delta J}J_{\mathrm{L,P}}+a_{\mathrm{I,P}}^{\delta T}T_{\mathrm{L,P}}+a_{\mathrm{I,N}}^{\delta T}T_{\mathrm{L,N}}+a_{\mathrm{I,P}}^{\delta\delta}\delta_{\mathrm{P}}=b_{\mathrm{I,P}}^{\delta} \quad [D.63]$$

where, $a_{\mathrm{I,S}}^{\delta T}=2\pi\eta_{\mathrm{P}}\frac{\beta_{\mathrm{s}}^{T}\lambda_{\mathrm{M,P,eff}}\Delta\chi}{(\eta_{\mathrm{P}}-\eta_{\mathrm{S}})}$ [D.64]

$$a_{\mathrm{I,P}}^{\delta J}=h_{\mathrm{fg}} \quad [D.65]$$

$$a_{\mathrm{I,P}}^{\delta J}=-2\pi\eta_{\mathrm{P}}\frac{\beta_{\mathrm{n}}^{T}\lambda_{\mathrm{L,P,eff}}\Delta\chi(r_{\mathrm{o}}-\delta_{\mathrm{P}}^{\mathrm{o}})}{\delta_{\mathrm{P}}^{\mathrm{o}}(\eta_{\mathrm{N}}-\eta_{\mathrm{P}})}-2\pi\eta_{\mathrm{P}}\frac{\beta_{\mathrm{s}}^{T}\lambda_{\mathrm{M,P,eff}}\Delta\chi}{(\eta_{\mathrm{P}}-\eta_{\mathrm{S}})} \quad [D.66]$$

$$a_{\mathrm{I,N}}^{\delta T}=2\pi\eta_{\mathrm{P}}\frac{\beta_{\mathrm{n}}^{T}\lambda_{\mathrm{L,P,eff}}\Delta\chi(r_{\mathrm{o}}-\delta_{\mathrm{P}}^{\mathrm{o}})}{\delta_{\mathrm{P}}^{\mathrm{o}}(\eta_{\mathrm{N}}-\eta_{P})} \quad [D.67]$$

$$a_{\mathrm{I,P}}^{\delta\delta}=-2\pi\eta_{\mathrm{P}}\frac{\beta_{\mathrm{n}}^{\mathrm{o}}\lambda_{\mathrm{L,P,eff}}\Delta\chi(T_{\mathrm{L,N}}^{\mathrm{o}}-T_{\mathrm{L,P}}^{\mathrm{o}})}{\delta_{\mathrm{P}}^{\mathrm{o}2}(\eta_{\mathrm{N}}-\eta_{\mathrm{P}})} \quad [D.68]$$

$$b_{\mathrm{I,P}}^{\delta}=-2\pi r_{\mathrm{o}}\eta_{\mathrm{P}}\frac{\beta_{\mathrm{n}}^{T}\lambda_{\mathrm{L,P,eff}}\Delta\chi(T_{\mathrm{L,N}}^{\mathrm{o}}-T_{\mathrm{L,P}}^{\mathrm{o}})}{\delta_{\mathrm{P}}^{\mathrm{o}}(\eta_{\mathrm{N}}-\eta_{\mathrm{P}})} \quad [D.69]$$

D.4 Global Mass Balance Equation

- $\int_0^1 \rho_M u_M \eta (r_o - \delta)^2 \, d\eta + \int_1^2 \rho_L u_L \delta (\delta(\eta - 2) + r_o) d\eta = \frac{\dot{m}_{in}}{2\pi}$

$$\sum_{jm-1}^{NM-1} \rho_{M,e} u_{M,e} \eta_P (r_o - \delta_e)^2 (\Delta\eta)_{jm} + \sum_{jl-1}^{NL} \rho_{L,e} u_{L,e} \delta_e (\delta_e(\eta - 2) + r_o)(\Delta\eta)_{jl} = \frac{\dot{m}_{in}}{2\pi} \quad [D.70]$$

$$\sum_{jm-1}^{NM-1} a_{M,jm}^{Pu} u_{M,jm} + \sum_{jl-1}^{NL} a_{L,jl}^{Pu} u_{L,jl} + a_P^{P\delta} \delta_P = b_P^P \quad [D.71]$$

where, $a_{M,jm}^{pu} = \rho_{M,jm} \eta_{jm} \Delta\eta_{jm} (r_o - \delta_e^o)^2$ [D.72]

$$a_{L,jl}^{pu} = \rho_{L,jl} \eta_{jl} \delta_e^o ((\eta_{jl} - 2)\delta_e^o + r_o) \quad [D.73]$$

$$a_P^{p\delta} = \sum_{jm-1}^{NM-1} -4\rho_{M,jm} \eta_{jm} \Delta\eta_{jm} u_{M,jm}^o (r_o - \delta_e^o) + \sum_{jl-1}^{NL} \rho_{L,jl} \Delta\eta_{jl} u_{L,jl}^o (8\delta_P^o(\eta - 2) - 4\delta_w(\eta - 2) + 2r_o) \quad [D.74]$$

$$b_P^p = \sum_{jm-1}^{NM-1} -4\rho_{M,jm} \eta_{jm} \Delta\eta_{jm} u_{M,jm}^o \delta_P^o (r_o - 2\delta_P^o + \delta_w) + \sum_{jl-1}^{NL} \rho_{L,jl} \Delta\eta_{jl,} u_{L,jl}^o \delta_P^o [(\eta_{jl} - 2)(8\delta_P^o - 4\delta_w) + 2r_o] + \frac{\dot{m}_{in}}{2\pi} \quad [D.75]$$

APPENDIX E

Bordered Block Matrix

E.1 Full Matrix Equation

$$\begin{bmatrix} A_{\underset{1}{\mathrm{M,P}}} & A_{\underset{1}{\mathrm{M,N}}} & & & & & & & \vdots \\ A_{\underset{2}{\mathrm{M,S}}} & A_{\underset{2}{\mathrm{M,P}}} & A_{\underset{2}{\mathrm{M,N}}} & & & & & & \\ & \ddots & \ddots & \ddots & & & O & & \\ & & A_{\underset{NM-1}{\mathrm{M,S}}} & A_{\underset{NM-1}{\mathrm{M,P}}} & A_{\underset{NM-1}{\mathrm{M,N}}} & & & & \\ & & & A_{\mathrm{I,S}} & A_{\mathrm{I,P}} & A_{\mathrm{I,N}} & & & E_2 \\ & & & & A_{\underset{2}{\mathrm{L,S}}} & A_{\underset{2}{\mathrm{L,P}}} & A_{\underset{2}{\mathrm{L,N}}} & & \\ & & & & & \ddots & \ddots & \ddots & \\ & & O & & & & A_{\underset{NL-1}{\mathrm{L,S}}} & A_{\underset{NL-1}{\mathrm{L,P}}} & A_{\underset{NL-1}{\mathrm{L,N}}} \\ & & & & & & & A_{\underset{NL}{\mathrm{L,S}}} & A_{\underset{NL}{\mathrm{L,P}}} \\ \cdots & & & & E_1 & & & \cdots & E_3 \end{bmatrix} \begin{bmatrix} \vdots \\ X_1 \\ \vdots \\ X_2 \end{bmatrix} = \begin{bmatrix} \vdots \\ B_1 \\ \vdots \\ B_2 \end{bmatrix} \tag{E.1}$$

E.2 Block Entries

For $j_{\mathrm{L}} = 1, 2, \ldots, NM\text{-}1$:

$$A_{\underset{j_{\mathrm{M}}}{\mathrm{M,P}}} = \begin{bmatrix} a^{uu}_{\mathrm{M,P}} & a^{uJ}_{\mathrm{M,P}} & 0 & 0 \\ a^{Ju}_{\mathrm{M,P}} & a^{JJ}_{\mathrm{M,P}} & 0 & 0 \\ a^{Tu}_{\mathrm{M,P}} & a^{TJ}_{\mathrm{M,P}} & a^{TT}_{\mathrm{M,P}} & a^{TW}_{\mathrm{M,P}} \\ a^{Wu}_{\mathrm{M,P}} & a^{WJ}_{\mathrm{M,P}} & 0 & a^{WW}_{\mathrm{M,P}} \end{bmatrix}_{j_{\mathrm{M}}} \tag{E.2}$$

$$A_{\underset{j_{\mathrm{M}}}{\mathrm{M,N}}} = \begin{bmatrix} a^{uu}_{\mathrm{M,N}} & 0 & 0 & 0 \\ 0 & 0 & 0 & 0 \\ 0 & 0 & a^{TT}_{\mathrm{M,N}} & a^{TW}_{\mathrm{M,N}} \\ 0 & 0 & 0 & a^{WW}_{\mathrm{M,N}} \end{bmatrix}_{j_{\mathrm{M}}} \tag{E.3}$$

$$A_{\underset{j_{\mathrm{M}}}{\mathrm{M,S}}} = \begin{bmatrix} a^{uu}_{\mathrm{M,S}} & a^{uJ}_{\mathrm{M,S}} & 0 & 0 \\ 0 & a^{JJ}_{\mathrm{M,S}} & 0 & 0 \\ 0 & a^{TJ}_{\mathrm{M,S}} & a^{TT}_{\mathrm{M,S}} & a^{TW}_{\mathrm{M,S}} \\ 0 & a^{WJ}_{\mathrm{M,S}} & 0 & a^{WW}_{\mathrm{M,S}} \end{bmatrix}_{j_{\mathrm{M}}} \tag{E.4}$$

$$A_{\mathrm{I,P}} = \begin{bmatrix} a_{\mathrm{I,P}}^{uu} & 0 & 0 & 0 \\ 0 & a_{\mathrm{I,P}}^{JJ} & 0 & 0 \\ 0 & 0 & a_{\mathrm{I,P}}^{TT} & a_{\mathrm{I,P}}^{TW} \\ 0 & a_{\mathrm{I,P}}^{WJ} & 0 & a_{\mathrm{I,P}}^{WW} \end{bmatrix} \tag{E.5}$$

$$A_{\mathrm{I,N}} = \begin{bmatrix} a_{\mathrm{I,N}}^{uu} & 0 & 0 & 0 \\ 0 & 0 & 0 & 0 \\ 0 & 0 & 0 & 0 \\ 0 & 0 & 0 & a_{\mathrm{I,N}}^{WW} \end{bmatrix} \tag{E.6}$$

$$A_{\mathrm{I,S}} = \begin{bmatrix} a_{\mathrm{I,S}}^{uu} & 0 & 0 & 0 \\ 0 & a_{\mathrm{I,S}}^{JJ} & 0 & 0 \\ 0 & 0 & 0 & 0 \\ 0 & 0 & 0 & 0 \end{bmatrix} \tag{E.7}$$

For $j_{\mathrm{L}} = 2, 3, \ldots, NL$

$$\underset{j_{\mathrm{L}}}{A_{\mathrm{L,P}}} = \begin{bmatrix} a_{\mathrm{L,P}}^{uu} & a_{\mathrm{L,P}}^{uJ} & 0 & 0 \\ a_{\mathrm{L,P}}^{Ju} & a_{\mathrm{L,P}}^{JJ} & 0 & 0 \\ a_{\mathrm{L,P}}^{Tu} & a_{\mathrm{L,P}}^{TJ} & a_{\mathrm{L,P}}^{TT} & 0 \\ 0 & 0 & 0 & 1 \end{bmatrix}_{j_{\mathrm{L}}} \tag{E.8}$$

$$\underset{j_{\mathrm{L}}}{A_{\mathrm{L,N}}} = \begin{bmatrix} a_{\mathrm{L,N}}^{uu} & 0 & 0 & 0 \\ 0 & 0 & 0 & 0 \\ 0 & 0 & a_{\mathrm{L,N}}^{TT} & 0 \\ 0 & 0 & 0 & 0 \end{bmatrix}_{j_{\mathrm{L}}} \tag{E.9}$$

$$\underset{j_{\mathrm{L}}}{A_{\mathrm{L,S}}} = \begin{bmatrix} a_{\mathrm{L,S}}^{uu} & a_{\mathrm{L,S}}^{uJ} & 0 & 0 \\ 0 & a_{\mathrm{L,S}}^{JJ} & 0 & 0 \\ 0 & a_{\mathrm{L,S}}^{TJ} & a_{\mathrm{L,S}}^{TT} & 0 \\ 0 & 0 & 0 & 0 \end{bmatrix}_{j_{\mathrm{L}}} \tag{E.10}$$

$$E_1 = \begin{bmatrix} (0 \quad 0 \quad 0 \quad 0)_1 (0 \quad 0 \quad 0 \quad 0)_2 \cdots (0 \quad 0 \quad 0 \quad 0)_{j_M} \cdots (0 \quad 0 \quad a_{I,S}^{\delta T} \quad 0) \\ (a_M^{pu} \quad 0 \quad 0 \quad 0)_1 (a_M^{pu} \quad 0 \quad 0 \quad 0)_2 \cdots (a_M^{pu} \quad 0 \quad 0 \quad 0)_{j_M} \cdots (a_M^{pu} \quad 0 \quad 0 \quad 0)_{NM-1} \end{bmatrix}$$

$$\begin{matrix} (0 \quad a_{I,P}^{\delta J} \quad a_{I,P}^{\delta I'} \quad 0) \quad (0 \quad 0 \quad a_{I,N}^{\delta T} \quad 0) \quad \cdots \quad (0 \quad 0 \quad 0 \quad 0)_{j_L} \\ (a_L^{pu} \quad 0 \quad 0 \quad 0)_1 \quad (a_L^{pu} \quad 0 \quad 0 \quad 0)_2 \quad \cdots \quad (a_L^{pu} \quad 0 \quad 0 \quad 0)_{j_L} \end{matrix}$$

$$\begin{matrix} \cdots \quad (0 \quad 0 \quad 0 \quad 0) \\ \cdots \quad (a_L^{pu} \quad 0 \quad 0 \quad 0)_{NL} \end{matrix} \Bigg] \qquad \text{(E.11)}$$

$$E_2 = \begin{bmatrix} (a_{M,P}^{u\delta} \quad a_{M,P}^{J\delta} \quad a_{M,P}^{T\delta} \quad a_{M,P}^{W\delta})_1 (a_{M,P}^{u\delta} \quad a_{M,P}^{J\delta} \quad a_{M,P}^{T\delta} \quad a_{M,P}^{W\delta})_2 \cdots (a_{M,P}^{u\delta} \quad a_{M,P}^{J\delta} \quad a_{M,P}^{T\delta} \quad a_{M,P}^{W\delta})_{j_M} \\ (a_{M,P}^{up} \quad 0 \quad 0 \quad 0)_1 (a_{M,P}^{up} \quad 0 \quad 0 \quad 0)_2 \cdots (a_{M,P}^{up} \quad 0 \quad 0 \quad 0)_{j_M} \end{bmatrix}$$

$$\begin{matrix} \cdots (a_{M,P}^{u\delta} \quad a_{M,P}^{J\delta} \quad a_{M,P}^{T\delta} \quad a_{M,P}^{W\delta})_{NM-1} (a_{I,P}^{u\delta} \quad 0 \quad 0 \quad a_{I,P}^{W\delta}) (a_{L,P}^{u\delta} \quad a_{L,P}^{J\delta} \quad a_{L,P}^{T\delta} \quad 0)_2 \\ \cdots (a_{L,P}^{up} \quad 0 \quad 0 \quad 0)_{NM-1} (0 \quad 0 \quad a_{I,P}^{Tp} \quad 0) (a_{M,P}^{up} \quad 0 \quad 0 \quad 0)_2 \end{matrix}$$

$$\begin{matrix} \cdots (a_{L,P}^{u\delta} \quad a_{L,P}^{J\delta} \quad a_{L,P}^{T\delta} \quad 0)_{j_L} \cdots (a_{L,P}^{u\delta} \quad a_{L,P}^{J\delta} \quad a_{L,P}^{T\delta} \quad 0)_{NL} \\ \cdots (a_{L,P}^{up} \quad 0 \quad 0 \quad 0)_{j_L} \cdots (a_{L,P}^{up} \quad 0 \quad 0 \quad 0)_{NL} \end{matrix} \Bigg]^T \qquad \text{(E.12)}$$

$$E_3 = \begin{bmatrix} a_{I,P}^{\delta\delta} & 0 \\ a_P^{p\delta} & 0 \end{bmatrix} \qquad \text{(E.13)}$$

$$B_1 = \Big[(b_{M,P}^u \quad b_{M,P}^J \quad b_{M,P}^T \quad b_{M,P}^W)_1 (b_{M,P}^u \quad b_{M,P}^J \quad b_{M,P}^T \quad b_{M,P}^W)_2 \cdots (b_{M,P}^u \quad b_{M,P}^J \quad b_{M,P}^T \quad b_{M,P}^W)_{j_M}$$
$$\cdots (b_{M,P}^u \quad b_{M,P}^J \quad b_{M,P}^T \quad b_{M,P}^W)_{NM-1} (b_{I,P}^u \quad b_{I,P}^J \quad b_{I,P}^T \quad b_{I,P}^W) (b_{L,P}^u \quad b_{L,P}^J \quad b_{L,P}^T \quad 0)_2$$

$$\cdots (b_{L,P}^u \quad b_{L,P}^J \quad b_{L,P}^T \quad 0)_{j_L} \cdots (b_{L,P}^u \quad b_{L,P}^J \quad b_{L,P}^T \quad 0)_{NL} \Big]^T \qquad \text{(E.14)}$$

$$B_2 = \begin{bmatrix} b_{\mathrm{I,P}}^{\delta} \\ b_{\mathrm{P}}^{p} \end{bmatrix} \tag{E.15}$$

$$\begin{aligned} X_1 = [&(u_{\mathrm{M}} \quad J_{\mathrm{M}} \quad T_{\mathrm{M}} \quad W)_1 (u_{\mathrm{M}} \quad J_{\mathrm{M}} \quad T_{\mathrm{M}} \quad W)_2 \cdots (u_{\mathrm{M}} \quad J_{\mathrm{M}} \quad T_{\mathrm{M}} \quad W)_{j_{\mathrm{M}}} \\ &\cdots (u_{\mathrm{M}} \quad J_{\mathrm{M}} \quad T_{\mathrm{M}} \quad W)_{NM-1} (u_{\mathrm{L}} \quad J_{\mathrm{L}} \quad T_{\mathrm{L}} \quad W_{\mathrm{dummy}})_1 (u_{\mathrm{L}} \quad J_{\mathrm{L}} \quad T_{\mathrm{L}} \quad W_{\mathrm{dummy}})_2 \\ &\cdots (u_{\mathrm{L}} \quad J_{\mathrm{L}} \quad T_{\mathrm{L}} \quad W_{\mathrm{dummy}})_{j_{\mathrm{L}}} \cdots (u_{\mathrm{L}} \quad J_{\mathrm{L}} \quad T_{\mathrm{L}} \quad W_{\mathrm{dummy}})_{NL}]^T \end{aligned} \tag{E.16}$$

$$\mathbf{X}_2 = \begin{bmatrix} \delta \\ \dfrac{dP}{d\chi} \end{bmatrix} \tag{E.17}$$